INVESTIGATION OF PERFORMANCE OF PROTON EXCHANGE MEMBRANE ELECTROLYSIS WITH PHOTOVOLTAIC SYSTEMS

PROTON DEĞİŞİM MEMBRAN ELEKTROLİZİN FOTOVOLTAİK SİSTEMLER İLE BİRLİKTE İNCELENMESİ

CEMRE KADIOĞLU

PROF. DR. MURAT KÖKSAL
Supervisor

Submitted to
Graduate School of Science and Engineering of Hacettepe University
As Partial Fulfillment to the Requirements
for the Award of the Degree of Master of Science
in Mechanical Engineering

2023

ÖZET

PROTON DEĞİŞİM MEMBRAN ELEKTROLİZİN FOTOVOLTAİK SİSTEMLER İLE BİRLİKTE İNCELENMESİ

Cemre KADIOĞLU

Yüksek Lisans, Makine Mühendisliği Bölümü
Tez Danışmanı: Prof. Dr. Murat KÖKSAL
Haziran 2023, 183 sayfa

Son zamanlarda küresel ısınma ve enerji bağımlılığıyla ilgili endişeler nedeniyle yeşil hidrojen üretimine olan ilgi artmıştır. Yeşil hidrojen üretimi, sanayi, ulaşım, ısınma veya enerji depolama alternatifleri gibi çeşitli uygulamalar için yenilenebilir enerji kaynaklarını kullanarak hidrojen üretimine dayanmaktadır. Proton elektrolit membran (PEM) elektrolizörleri, yakın gelecekte ölçeklendirilebilme potansiyeli olan iki ticari olarak kullanılabilir elektrolizör tiplerinden biri olduğu ve daha hızlı tepki verme özelliğine sahip olduğu için bu tür uygulamalar için uygun bir seçenektir.

Bu tez, yenilenebilir kaynaklardan değişken yük koşulları altında, tesis bileşenlerinin hidrojen üretimi ve sistem verimliliği üzerindeki etkisini incelemek için PEM elektrolizör sistemlerinin tasarım ve modellemesine odaklanmaktadır. Elektrolizör ve sistem bileşenlerinin modellemesi MATLAB kullanılarak gerçekleştirilmiş ve tasarım parametreleri tasarim hesap çizelgeleri ile beslenmiştir. Modeli besleyen güç üretim verileri, System Advisory Model (SAM) tarafından gerçekleştirilen güneş PV santrali modellemesi verilerinden elde edilmiştir.

Farklı konumlar için 1 MW ila 1 GW arasında değişen sistem kapasiteleri tasarlandı ve simüle edilmiştir, bu da kapasite faktörü, hava koşulları, sistem boyut ve tasarımının sistem performansı üzerindeki etkilerinin gözlemlenmesine olanak sağlamıştır. Sonuçlar, daha büyük bir sistemin tasarlanmasının hidrojen üretimi verimliliği üzerindeki etkisinin neredeyse olmadığı ve kapasite faktörlerinin sistemin hıdrojen uretimi ve verimliliği üzerinde daha büyük bir etkiye sahip olduğunu göstermektedir.

Sistemle ilgili belirsizlikler belirlenmiştir ve hidrojen üretimini etkileyen faktörlerin PEM I-V eğrisi, DC-DC dönüştürücü kayıpları ve hidrojen kurutucu/saflaştırıcı kayıpları olduğu belirlenmiştir. En iyi ve en kötü senaryolar incelenmiş ve çalışma, tasarım ve ekipman kalitesine bağlı olarak hidrojen üretiminin yaklaşık % -2,5 ila +% 4,5 arasında, ortalama sistem verimliliğinin de yaklaşık olarak -2,5 ila +% 1,5 kWh/kg arasında değişebileceği gösterilmiştir.

Anahtar kelimeler: Polimer Elektrolit Membran Elektrolizi, Fotovoltaik Sistemler, Soğutma, Saatlik Analiz, Tasarım, Yeşil Hidrojen.

ABSTRACT

INVESTIGATION OF PERFORMANCE OF PROTON EXCHANGE MEMBRANE ELECTROLYSIS WITH PHOTOVOLTAIC SYSTEMS

Cemre KADIOĞLU

Master of Science, Department of Mechanical Engineering
Supervisor: Murat KÖKSAL
June 2023, 183 pages

Attention towards green hydrogen production has recently risen due to global warming and energy dependency concerns. Green hydrogen production relies on renewable energy sources to generate hydrogen for various applications, such as industry, transport, heating, or energy storage alternatives. Proton electrolyte membrane (PEM) electrolyzers are well-suited for such applications as it is one of the two commercially available electrolyzer types that could be scalable in the near future and also could be operated at varying loads due to its ability of quicker response.

This thesis focuses on the design and steady-state modeling of PEM electrolyzer systems to investigate the impact of balance of plant (BoP) components on the overall system efficiency and hydrogen production under varying power supply conditions from renewable sources. The modeling of the electrolyzer and system components were performed in MATLAB and design parameters were fed by spreadsheets. Power supply data fed to the model was generated from solar PV plant modeling data performed in System Advisory Model (SAM).

System capacities ranging from 1 MW to 1 GW were designed and simulated for different locations, allowing for the observation of the effects of capacity factor, weather conditions, system scale and design on system performance. The results show that the effect of designing a larger system has negligible impact, and that capacity factors have larger impact on hydrogen production and efficiency of the system.

Uncertainties regarding the system were determined and it was observed that the factors affecting the hydrogen production and system efficiency where the PEM stack I-V curve, DC-DC converter losses and the hydrogen dryer/purifier losses. Best and worst case scenarios were studied and it showed that hydrogen production can vary about -2.5% and +4.5% the average system efficiency can also vary around -2.5 and +1.5 kWh/kg depending on design and equipment quality.

Keywords: Polymer Electrolyte Membrane Electrolysis, Photovoltaic Systems, Cooling, Hourly Analysis, Design, Green Hydrogen.

ACKNOWLEDGEMENTS

I want to thank my supervisor, Prof. Dr. Murat Köksal for his great understanding, support, and patience as I completed my Master's thesis. I sincerely appreciate his commitment and faith in my abilities.

For the knowledge I have acquired during my studies, I would like to thank Hacettepe University and the Department of Mechanical Engineering.

I am incredibly appreciative of my family's unwavering love, patience, and support throughout my academic journey. I have been continuously motivated by their support.

I would like to dedicate my thesis to those who have been affected by the catastrophic earthquake that struck Turkey in the year 2023, honoring the lives lost and the individuals impacted by this devastating event.

Cemre Kadıoğlu
June 2023, Ankara

TABLE OF CONTENTS

LIST OF TABLES

LIST OF FIGURES

1. INTRODUCTION

The increase in global warming has led societies to take action on carbon emissions. The demand for renewable energy systems is at rise, and the most significant challenge is that it cannot be utilized on demand which is the greatest obstacle in converting to 100 % renewable. One of the arising solutions to the problem is to store energy in the form of hydrogen and use it as fuel for industry applications or to generate electricity on demand. Green hydrogen is the production of hydrogen from renewable energy systems (RESs) thus having zero emissions. Other advantages of hydrogen is that it can be stored not only daily but seasonally and can also be transported by tanks and pipelines which opens roads to exporting green energy.

Hydrogen is currently mostly obtained by hydrocarbon reforming which involves the separation of hydrogen from fossil fuels also having CO_2 as a byproduct. Green Hydrogen however, is produced by electrolysis of water. Alkaline, Proton Exchange Membrane and Solid Oxide Electrolyzers are three main technologies, though the latter is still not mature. PEM electrolyzers have the advantage of operating on a wider capacity (5 - 10 % minimum load) (International Renewable Energy Agency, 2020a) range and have a quicker response time to changing energy input whereas Alkaline Electrolyzers work with a minimum load of 20 – 40 % and slower response (Schiebahn et al., 2015). This makes it a better option to use with RESs which provides a fluctuating energy source.

In this study, the PEM electrolyzer system is modeled to calculate the production and efficiency of the system when fed with solar PV energy production. The main reason for focusing on PEMEL is that RESs provide partial energy for most of the operation duration. PEMELs are able to perform electrolysis at partial loads with a wider range. The efficiency of hydrogen production at partial loads will be investigated using renewable energy as an input. The power consumption of other system components can not be ignored while calculating the efficiency of the operation and thus have to be included in calculations.

1.1. Literature Review on PEM Systems and Modeling

Although PEM electrolysis was developed in the 1960s by General Electric, it has gained more attention after to 2000s with its ability to work under an unstable power supply.

Literature on the modeling of PEM electrolysis has significantly increased after 2010. Numerous publications are available focused on modeling the PEM cell/ stack. But only very few publications consider the modeling of the BoP (Balance of Plant) which consists of pumps, fans, chillers, power converters and compressors.

Hamdan's (2013) study on low-cost membrane incorporation to PEM electrolyzers included an experimental study of system efficiency with a stack capacity of 25 kW.

Yigit and Selamet (2016) modeled a PEM electrolysis system including a water pump, cooling fan, hydrogen storage tank and power controller. The percentages of energy losses of the components were observed at different current densities. The system's dynamic response at the startup with constant power was also observed. The system was designed for a stack consisting of 5 cells of 100 cm^2 active area. This is considered rather low capacity and is a laboratory scale system.

Olivier (2017a) performed dynamic modeling of the PEM stack and components such as power converters, pumps, gas seperators, purification systems and cooling. The dynamic behaviour of the system was investigated in terms of power consumption, pressure buildup, hydrogen production and temperature. The model in this study was validated with experimental data of a 25 kW PEM electrolysis system. As also mentioned in the study, the power consumption behaviour of the cooling system and including the scalability was open to improvement. Sood (2020) also used a similar approach and modeled a PEM electrolysis system validated with data from laboratory scale electrolyzers.

Mancera (2020) experimentally investigated the dynamic behavior of the PEM electrolysis system of a 10 kW stack. Parameters investigated included pressure, temperature, hydrogen production rate, stack voltage, and system efficiency.

Joseph (2022) performed modeling of the PEM electrolyzer, compressor and power electronics in order to observe optimal operation considering. efficiency, storage and costs. Although the capacity of the system was 100 MW it should be noted that a model of the cooling system was not incorporated in this study.

Egeland-Eriksen (2023) simulated offshore hydrogen production with PEM electrolyzers from a 2.3 MW wind turbine. The BoP components where a battery stack, desalination of sea water, hydrogen compression and storage.

The H2A program carried out by the National Renewable Energy Laboratory (NREL) include estimated efficiencies of MW scale electrolysis systems including BoP components consumptions (National Renewable Energy Laboratory, 2020).

A later program carried out by the NREL called H2NEW include graphs of partial loading of PEM system showing the efficiency losses in categories of electrical, mechanical and hydrogen losses (Pivovar et al., 2021, 2022).

1.2. Commercial PEM Systems

Systems provided in commercial catalogues range from laboratory scale to up to 20MW modules that could be connected with each other to form a larger plant. The catalogues indicate the average and nominal stack efficiencies at a range of 48 – 53 kWh/kg and when maximum stack efficiency of 56 kWh/kg. The total system efficiencies are not clearly stated in all catalogues and range between 54.5 – 59 kWh/kg depending on maximum or total efficiency. Catalogues used to observe these are provided in Appendix 1.

1.3. Objectives of the Thesis

As can be seen by the previously mentioned literature review, studies from literature are mostly carried out on small scale electrolyzers and not much

emphasis has been given to the cooling systems except for recent studies carried out by the NREL. It is important to be able to predict the performance of a designed utility scale PEM system obtaining realistic results.

Therefore, the first objective of this study is to develop a pseudo steady-state hourly analysis model of PEM electrolyzer and required system components including design sheet to set up simulations.

After comparing system efficiency values with available literature and validating the model, the second objective of this study is to compare simulation results performed at different locations and observe how much the weather and energy yields affect the efficiency and annual production of the system.

1.4. Scope and Methodology

The system design is carried out by observations of manufacturer containerized designs and do not include water supply system booster pump consumption and hydrogen pressurization with storage as these two systems are subjective to availability of municipality water supply and end use of hydrogen. System capacities ranging from 1 MW to 1 GW are simulated and investigated. The renewable energy source for the system is provided by solar PV simulations.

The resulting model is able to work with any energy input data thus can be used for different energy sources. The efficiency values utilized in design and simulation stages are referenced to standards such as ASHRAE and ARI which provides a baseline. Energy models of cooling equipment are incorporated from available energy models that are already used in building energy simulation programs such as EnergyPlus.

The results obtained from the model are compared with graphs provided in recent NREL studies. On top of that, the model can carry out yearly analysis based on different locations and the effect of weather data and energy input can be observed. This enables the program to predict the systems efficiency at any planned location and also foresee the parameters such as annual hydrogen production and water consumption.

2. PEM ELECTROLYSIS AND LITERATURE

Electrolysis is the process applying electric current to water causing electron transfer between electrodes resulting in the formation of oxygen at the anode and hydrogen at the cathode side.

(Overall Reaction) $$H_2O \rightarrow H_2 + \frac{1}{2}O_2 \quad (2.1)$$

The main principle of electrolysis is the same across all systems. The minimum amount of energy needed to initiate the process is calculated by Gibbs free energy. At standard conditions the resulting enthalpy, entropy and Gibbs free energy can be calculated from Table 2.1.

Table 2.1 Enthalpy and entropy of values at standard state (Haynes et al., 2014)

Substance	ΔH^0 (kJ/mol)	ΔS^0 (J/mol.K)
H_2O (l)	-285.8	70
H_2 (g)	0	130.7
O_2 (g)	0	205.2

$$\Delta G = \Delta H - T.\Delta S \quad (2.2)$$

$$\Delta G^0 = 0 – (-285.8) – 298 \text{ x } (130.7 + 205.2/2 - 70)/1000 = 237.1 \text{ kJ/mol}$$

The voltage required to supply the minimum energy needed is called the reversible voltage V^0_{rev}, which can be calculated by the following relation between Gibbs free energy:

$$V^0_{rev@298K,1atm} = \frac{\Delta G^0}{z.F} = \frac{237.1 \text{ kJ/mol}}{2 \text{ x } 96485 \text{ C/mol}} = 1.229V \quad (2.3)$$

where F=96,485 C/mol is the Faraday's constant and z=2 is the number of electrons transferred during reaction.

As stated in Equation 2.3, V^0_{rev} is calculated from Gibbs energy. The potential calculated using enthalpy is called the thermoneutral voltage V^0_{tn}. The thermoneutral voltage expresses the voltage needed in order to provide not only the reversible Gibbs energy but also the heat needed to undergo the reaction.

$$V^0_{tn@298K,1atm} = \frac{\Delta H^0}{z.F} = \frac{285.8 \text{ kJ/mol}}{2 \text{ x } 96485 \text{ C/mol}} = 1.481V \quad (2.4)$$

The cell voltage V_{cell} is usually greater than V^0_{tn} because of factors affecting its efficiency. Thus, V^0_{tn} is used to calculate the excess heat while the electrolyzers undergo the reaction.

2.1. PEM Electolyzer

PEM electrolyzers use pure water and electric current to produce oxygen at the anode and hydrogen at the cathode. They can operate in a temperature range of 20 - 100°C (Carmo et al., 2013) and pressures ranging between atmospheric and 85 bar (Bessarabov et al., 2016).

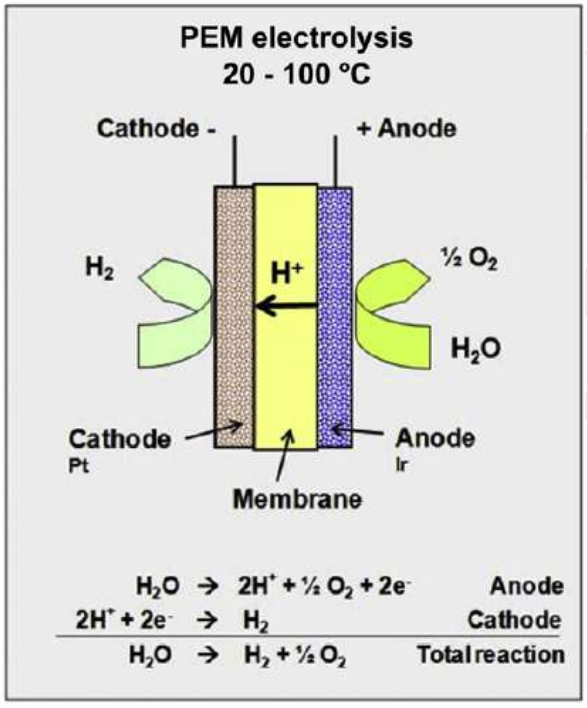

Figure 2.1 Schematic of the operating principle of PEM water electrolysis cell (Carmo et al., 2013).

As could be seen in Figure 2.1, oxidation occurs at the anode and the H^+ protons pass through the membrane and form H_2 by the electrons provided by the outer circuit to the cathode.

2.1.1. Components of PEM Electrolyzer

The PEM electrolyzer consists of 4 layers sandwiched together. The first layer is the polymer electrolyte membrane (PEM) also called solid electrolyte membrane (SEM), which only conduct the protons. The membrane is coated with porous

catalyst layers on each side. These components together are called the membrane electrode assembly (MEA) and are responsible for the reaction taking place. The next layer is the gas diffusion layer (GDL), also called the current collector (CC), which conducts the current as well as provides flow of reactants and products from the electrodes to the end plates and vice versa. The titanium end plates are responsible for the encloser of the cell assembly and provide the electric connection between the cell and the outer circuit. The end plates, also called the bipolar plates in case of a stack assembly with multiple cells, generally have grooved channels for the transportation of water, oxygen and hydrogen in the system. The transport of materials can also be provided by adding an extra spacer layer between the GDLs and end plates instead of grooves (Bessarabov et al., 2016).

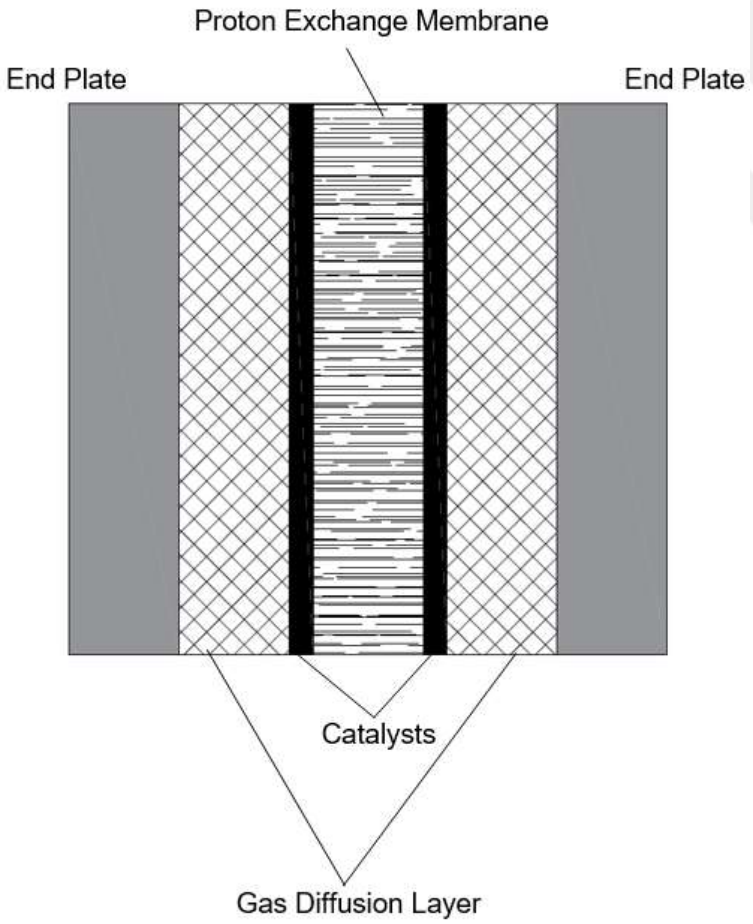

Figure 2.2 Proton Exchange Membrane electrolyzer assembly

2.1.2. Working principle of PEM Electrolyzer

The water enters from the anode channels on the end plate (or bipolar plate) of the cell which then soaks the GDL. As current is supplied to the cell, the water atoms split on the anode catalyst surface. The PEM conducts H^+ to the cathode side leaving O_2 bubbles on the anode catalyst surface which then exit from the same channels used to supply water. The H^+ atoms form H_2 on the cathode catalyst layer which exit from the channels of their endplate. The water feed to the cathode side is optional as it is only there to facilitate the efficient removal of the hydrogen (Sood et al., 2020).

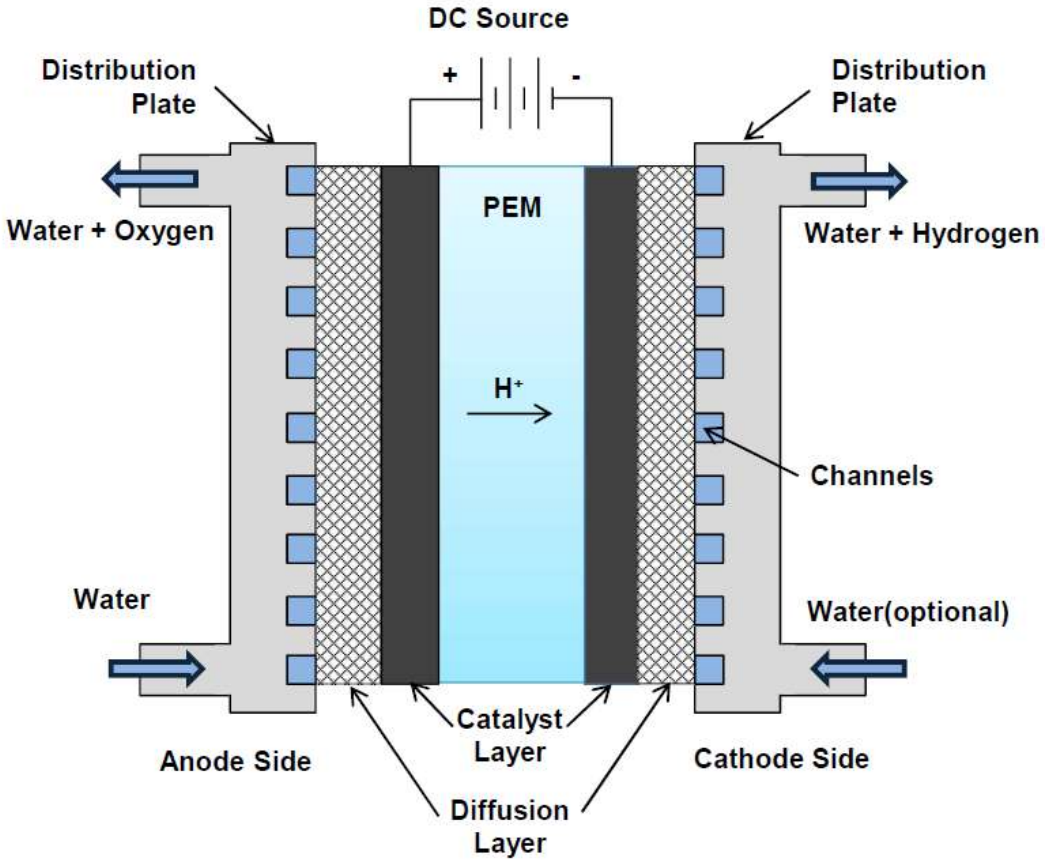

Figure 2.3 Schematics of PEM electrolyzer cell (Sood et al., 2020).

2.2. PEM Electrolyzer Cell Voltage

The PEM electrolyzer cell voltage consists of the open circuit voltage and the irreversible losses. The open circuit voltage is the required potential of the cell to initiate the reaction which is dependent on temperature and pressure. As current starts passing through the cell, the cell undergoes irreversible voltage losses which contribute to the total cell voltage.

$$V_{cell}=V_{ocv}+V_{act}+V_{ohm}+V_{dif} \quad (2.5)$$

2.2.1. Open Circuit Voltage

As stated earlier, temperature and pressure both affect V_{ocv} and can be calculated by the Nernst equation.

$$V_{ocv}=V_{rev}-\frac{R.T}{2.F}.\ln\left(\frac{a\{H_2O\}}{a\{H_2\}.a\{O_2\}^{1/2}}\right) \quad (2.6)$$

where activities are replaced with pressures.

$$V_{ocv} = V_{rev} - \frac{R.T}{2.F}.\ln\left(\frac{p_{H_2O}/p_{op}}{(p_{H_2}/p_{op}).(p_{O_2}/p_{op})^{1/2}}\right)$$

$$= V_{rev} - \frac{R.T}{2.F}.\ln\left(\frac{1}{(p_{H_2}/p_{op}).(p_{O_2}/p_{op})^{1/2}}\right) \quad (2.7)$$

The operation pressure mentioned in the equation p_{op} may differ between the cathode and the anode depending on the design of the electrolyzer. So the formula maybe in written in the form of anode and cathode pressures as.

$$V_{ocv}= V_{rev} - \frac{R.T}{2.F}.\ln\left(\frac{1}{(p_{H_2}/p_C).(p_{O_2}/p_A)^{1/2}}\right) \quad (2.8)$$

The vapour pressure affects the partial pressures of hydrogen and oxygen with the change in temperature ($p_A=p_{O2}+p^0_{H2O}$, $p_C=p_{H2}+p^0_{H2O}$) and the partial pressure can be expressed as a function of temperature by the following formulas stated below Equation 2.9 (Bessarabov et al., 2016) and Equation 2.10 (Biaku et al., 2008).

$$p^0_{H_2O} =\exp\left(11.676-\frac{3816.44}{T-46.13}\right) \quad (T=K, P=atm) \quad (2.9)$$

$$p^0_{H_2O}=6.10\ .10^{-3}\ .\ \exp\left(\frac{T}{T+238.3}\ .\ 17.2694\right) \quad (T=°C, P=atm) \quad (2.10)$$

Both equations seem appropriate to use as they have very low error when compared to textbook data (Lange, 1999) in Table 2.2.

Table 2.2 Comparison table of partial pressure of water vapor data with equations from literature

	Lange (1999) (data)		Bessarabov (2016) eq 2.9		Biaku (2007) eq 2.10	
T(C)	ph2o(mmHg)	ph2o (atm)	ph2o (atm)	error (%)	ph2o (atm)	error(%)
10	9.209	0.0121	0.0118	-2.3%	0.0122	0.9%
15	12.788	0.0168	0.0165	-1.8%	0.0170	0.8%
20	17.535	0.0231	0.0227	-1.4%	0.0232	0.7%
25	23.756	0.0313	0.0309	-1.1%	0.0314	0.6%
30	31.824	0.0419	0.0415	-0.8%	0.0421	0.5%
35	42.175	0.0555	0.0551	-0.6%	0.0557	0.4%
40	55.324	0.0728	0.0725	-0.5%	0.0730	0.3%
45	71.88	0.0946	0.0943	-0.3%	0.0948	0.2%
50	92.51	0.1217	0.1215	-0.2%	0.1219	0.2%
55	118.04	0.1553	0.1551	-0.1%	0.1555	0.1%
60	149.38	0.1966	0.1964	-0.1%	0.1967	0.1%
65	187.54	0.2468	0.2466	0.0%	0.2470	0.1%
70	233.7	0.3075	0.3074	0.0%	0.3078	0.1%
75	289.1	0.3804	0.3804	0.0%	0.3808	0.1%
80	355.1	0.4672	0.4674	0.0%	0.4681	0.2%
85	433.6	0.5705	0.5705	0.0%	0.5717	0.2%
90	525.76	0.6918	0.6920	0.0%	0.6940	0.3%
95	633.9	0.8341	0.8344	0.0%	0.8376	0.4%
100	760	1.0000	1.0003	0.0%	1.0053	0.5%

V_{rev} is also affected by temperature and is calculated by calculating the change in Gibbs energy. If it is assumed that enthalpy and entropy of the reaction is constant, the result will be the following Equation 2.11.

$$\Delta G = \Delta H - T.\Delta S$$

$$\Delta G^{0}_{298K,1atm} = \Delta H^{0}_{298K,1atm} - 298.\Delta S^{0}_{289K,1atm}$$

$$\Delta G - \Delta G^{0}_{298K,1atm} = -(T - 298).\Delta S^{0}$$

$$V_{rev} = \frac{\Delta G}{2.F} = \frac{\Delta G^{0}_{298K,1atm}}{2.F} - \frac{(T\text{-}298).\Delta S^{0}}{2.F}$$

$$V_{rev} = \frac{\Delta G}{2.F} = V^{0}_{rev@298K,1atm} - \frac{(T\text{-}298).\Delta S^{0}}{2.F}$$

$$V_{ocv} = V^{0}_{rev@298K,1atm} - \frac{(T\text{-}298).\Delta S^{0}}{2.F} - \frac{R.T}{2.F}.\ln\left(\frac{1}{(p_{H_2}/p_C).(p_{O_2}/p_A)^{1/2}}\right)$$

$$V_{ocv} = 1.229 - 8.46x10^{-4}(T\text{-}298) + \frac{R.T}{2.F}.\ln\left(\frac{p_{H_2}}{p_C}\right)\sqrt{\frac{p_{O_2}}{p_A}} \qquad (2.11)$$

The resulting equation is also given in (Bessarabov et al., 2016). In literature, there are other equations that were used to determine the open circuit voltages. Two empirical equations that were derived to determine V_{rev} are mentioned by Equation 2.12 and 2.13.

$$V_{rev}=1.5184 - 1.5421x10^{-3}T + 9.523x10^{-5}TxlnT + 9.84x10^{-8}T^{2} \qquad (2.12)$$

(Roy et al., 2006)

$$V_{rev}=1.52-1.22x10^{-3}T+1.18x10^{-5}TxlnT+5.66x10^{-7}T^{2} \qquad (2.13)$$

(Dale, 2009)

The maximum deviation between the results of V_{rev} between these three equations are 0.4% as shown in Table 2.3.

Table 2.3 Comparision table of V_{rev} values calculated from equations in literature.

T(K)	Vrev			Maximum deviation
	(Bessarabov et al., 2016)	(Roy et al., 2006)	(Dale, 2009)	
283	1.242	1.242	1.239	-0.2%
288	1.237	1.238	1.235	-0.2%
293	1.233	1.233	1.231	-0.2%
298	1.229	1.229	1.227	-0.2%
303	1.225	1.225	1.223	-0.2%
308	1.221	1.221	1.219	-0.2%
313	1.216	1.217	1.215	-0.1%
318	1.212	1.212	1.211	-0.1%

T(K)	Vrev			Maximum deviation
	(Bessarabov et al., 2016)	(Roy et al., 2006)	(Dale, 2009)	
323	1.208	1.208	1.207	-0.1%
328	1.204	1.204	1.203	-0.1%
333	1.199	1.200	1.199	0.0%
338	1.195	1.196	1.196	-0.1%
343	1.191	1.192	1.192	-0.1%
348	1.187	1.188	1.188	-0.1%
353	1.182	1.183	1.184	-0.2%
358	1.178	1.179	1.181	-0.2%
363	1.174	1.175	1.177	-0.3%
368	1.170	1.171	1.173	-0.3%
373	1.166	1.167	1.170	-0.4%

The effect of pressure and temperature on the open circuit voltage can be seen in Figure 2.4.

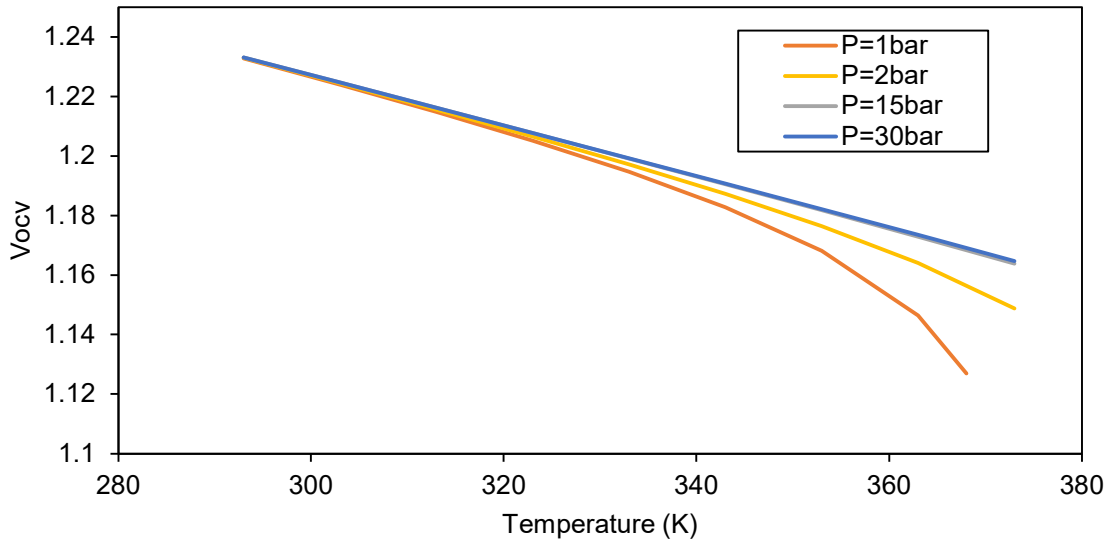

Figure 2.4 V_{ocv} – Variation of open circuit voltage with temperature for different pressures

As can be seen, the open circuit voltage increases with increasing pressure, whereas the increase in temperature decreases the V_{ocv}.

2.2.2. Activation voltage

The activation voltage is the required voltage to overcome the half reactions on the catalyst surfaces of cell. It is mostly dependent on the catalyst material on the anode and cathode catalyst material. Figure 2.5 is a representation diagram showing the increase in cell voltage due to activation potentials.

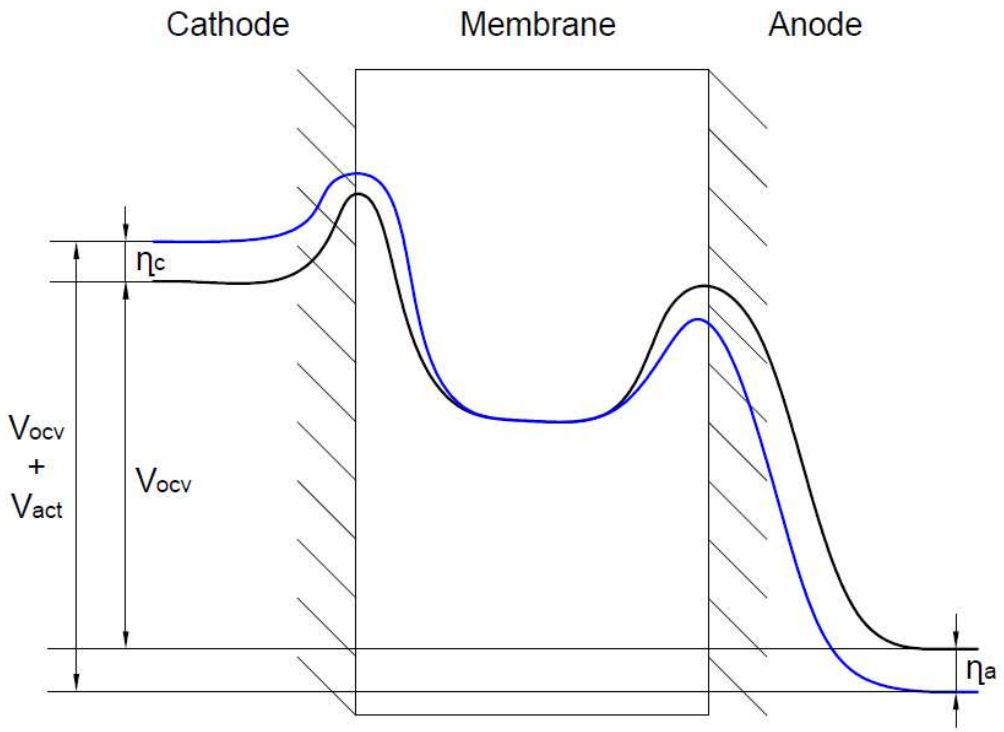

Figure 2.5 Representation of energy barrier on a PEM cell

Making use of the Faraday's law to relate reaction activity with current.

$$Q=n.z.F \tag{2.14}$$

where Q is the electric charge in coulombs and n is the amount of material in mols. Current is the amount of electric charge flow, therefore

$$I = \frac{dQ}{dt} = z.F.\frac{dn}{dt} = z.F.\dot{n} \tag{2.15}$$

where $\dot{n}$ is the rate of reaction in mol/s. The current density is i=I/A and the reaction rate per unit area is expressed by $r=\dot{n}/A$ mol/s.cm^2.

$$i = \frac{I}{A} = z.F.\frac{\dot{n}}{A} = z.F.r \tag{2.16}$$

Examining the half reaction on the cathode side (Figure 2.6), the forwards and backwards reaction rate can be expressed as the following.

$$r_f = k_f . C_r$$
$$r_b = k_b . C_b \quad (2.17)$$

where k is the reaction rate constant, and C is the surface concentration. The reaction rate constant can be expressed by the Arrhenius equation.

$$k = \Lambda . e^{\frac{-\Delta G^{\neq}}{RT}} \quad (2.18)$$

where Λ is the pre-exponential factor.

At the point of equilibrium, the forward and backward reaction rates are equal therefore expressed as the following.

$$r_f = r_b \quad (2.19)$$

$$\Lambda_f . C_r . \exp\left[\frac{-E_f}{RT}\right] = \Lambda_b . C_o . \exp\left[\frac{-E_b}{RT}\right] \quad (2.20)$$

At equilibrium there is no current, therefore

$$i_f - i_b = 0 \quad (2.21)$$

$$z.F.r_f = z.F.r_b \quad (2.22)$$

$$z.F.\Lambda_f . C_r . \exp\left[\frac{-E_f}{RT}\right] = z.F.\Lambda_b . C_o . \exp\left[\frac{-E_b}{RT}\right] = i_0 \quad (2.23)$$

i_0 is called the exchange current density and depends on the catalyst material and reaction medium.

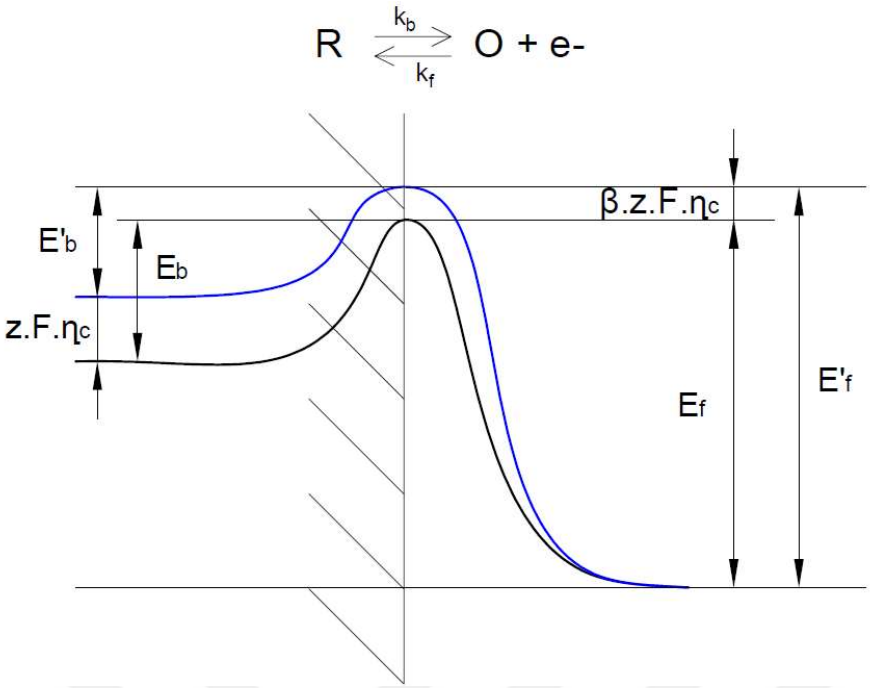

Figure 2.6 Energy barrier diagram for cathode half reaction of PEM cell

The increase of the energy barrier is a fraction of the activation potential known as the symmetry parameter β. Forming a balance equation for the forward reaction from the diagram results in the following Equation 2.25.

$$E'_f = E_f + \beta.z.F.\eta_c \tag{2.24}$$

$$i_f = z.F.\Lambda_f.C_r.\exp\left[\frac{-E'_f}{RT}\right] = \underbrace{z.F.\Lambda_f.C_r.\exp\left[\frac{-E_f}{RT}\right]}_{i_0}.\exp\left[\frac{-\beta.z.F.\eta_c}{RT}\right]$$

$$i_f = i_0.\exp\left[\frac{-\beta.z.F.\eta_c}{RT}\right] \tag{2.25}$$

Executing the same process for the backward reaction results as the following Equation 2.27.

$$E'_b = E_b + \beta.z.F.\eta_c - z.F.\eta_c \tag{2.26}$$

$$i_b = z.F.\Lambda_b.C_o.\exp\left[\frac{-E'_b}{RT}\right] = \underbrace{z.F.\Lambda_b.C_o.\exp\left[\frac{-E_b}{RT}\right]}_{i_0}.\exp\left[\frac{-(\beta-1).z.F.\eta_c}{RT}\right]$$

$$i_b = i_0.\exp\left[\frac{-(\beta-1).z.F.\eta_c}{RT}\right] \tag{2.27}$$

Since the electron flow is to the opposite of the forward reaction we can calculate the current density as Equation 2.28 to obtain a positive result.

$$i = i_b - i_f = i_0 . \left\{ \exp\left[\frac{-(\beta-1).z.F.\eta_c}{RT}\right] - \exp\left[\frac{-\beta.z.F.\eta_c}{RT}\right] \right\} \quad (2.28)$$

The symmetry parameter can be written in terms of charge transfer coefficient as the following Butler-Volmer equation (2.30).

$$\alpha = 1-\beta \quad (2.29)$$

$$i = i_b - i_f = i_0 . \left\{ \exp\left[\frac{\alpha.z.F.\eta_c}{RT}\right] - \exp\left[\frac{-(1-\alpha).z.F.\eta_c}{RT}\right] \right\} \quad (2.30)$$

The Butler-Volmer equation can be further simplified in the following conditions.

- When η_{act} is considered very small or more fundamentally when $i << i_0$, the Taylor series expansion of exponential terms can be performed with powers higher than 1 neglected ($e^x \approx 1+x$ for small x) (O'Hayre et al., 2016). Thus, the equation simplifies to Equation 2.31.

$$i = i_0 . \left[\frac{z.F.\eta_{act}}{RT}\right] \quad (2.31)$$

Figure 2.7 is a plot example to visualize this simplification where it can be observed that the values are very close between η_{act} -0.02 and 0.02.

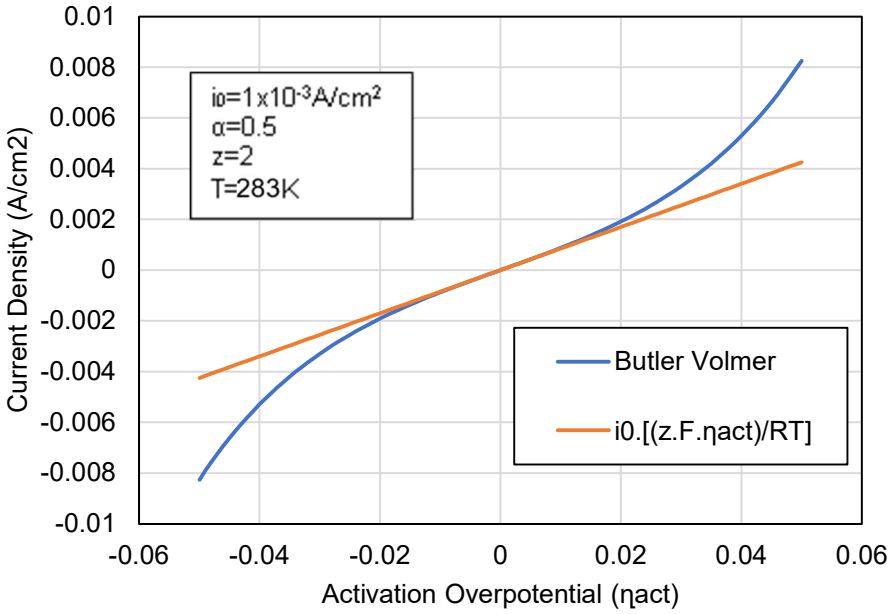

Figure 2.7 Variation of current density with activation overpotential using Equation 2.31 Butler-Volmer equation.

- For cases where α=0.5 the Butler Volmer equation can be represented using the hyperbolic sine function.

$$\sinh(x) = \frac{1}{2}(e^{x} - e^{-x}) \tag{2.32}$$

$$i = i_0 . \left\{ \exp\left[\frac{0.5.z.F.\eta_{act}}{RT}\right] - \exp\left[\frac{-0.5.z.F.\eta_{act}}{RT}\right] \right\} \tag{2.33}$$

$$i = 2.i_0 . \sinh\left(\frac{0.5.z.F.\eta_{act}}{RT}\right) \tag{2.34}$$

- When η_{act} is large (or more fundamentally, when $i >> i_0$), the second exponential term in the Butler–Volmer equation becomes negligible (O'Hayre et al., 2016).

$$i = i_0 . \exp\left[\frac{\alpha.z.F.\eta_{act}}{RT}\right] \tag{2.35}$$

Figure 2.8 is a plot example showing that both equations are converging.

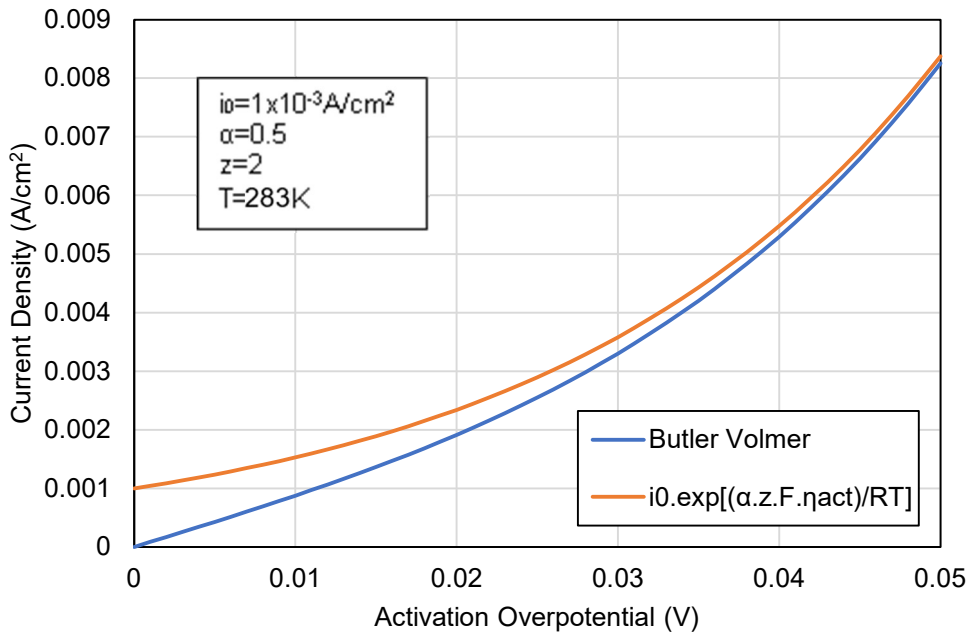

Figure 2.8 Variation of current density with activation overpotential using Equation 2.35 and Butler-Volmer equation

Solving this equation to find η_{act} for any given current will result in the following Tafel equation (2.39).

$$\eta_{act} = -\left[\frac{RT}{\alpha.z.F}\right] \ln i_0 + \left[\frac{RT}{\alpha.z.F}\right] \ln i \quad (2.36)$$

$$a = -\left[\frac{RT}{\alpha.z.F}\right] \ln i_0 , \qquad b = \left[\frac{RT}{\alpha.z.F}\right] \quad (2.37, 2.38)$$

$$\eta_{act} = a + b \ln i \quad (2.39)$$

Writing this expression with base 10 logarithms and plotting as the following.

$$\frac{\ln x}{\log x} = 2.3 \quad (2.40)$$

$$\eta_{act} = a + 2.3b \log i \quad (2.41)$$

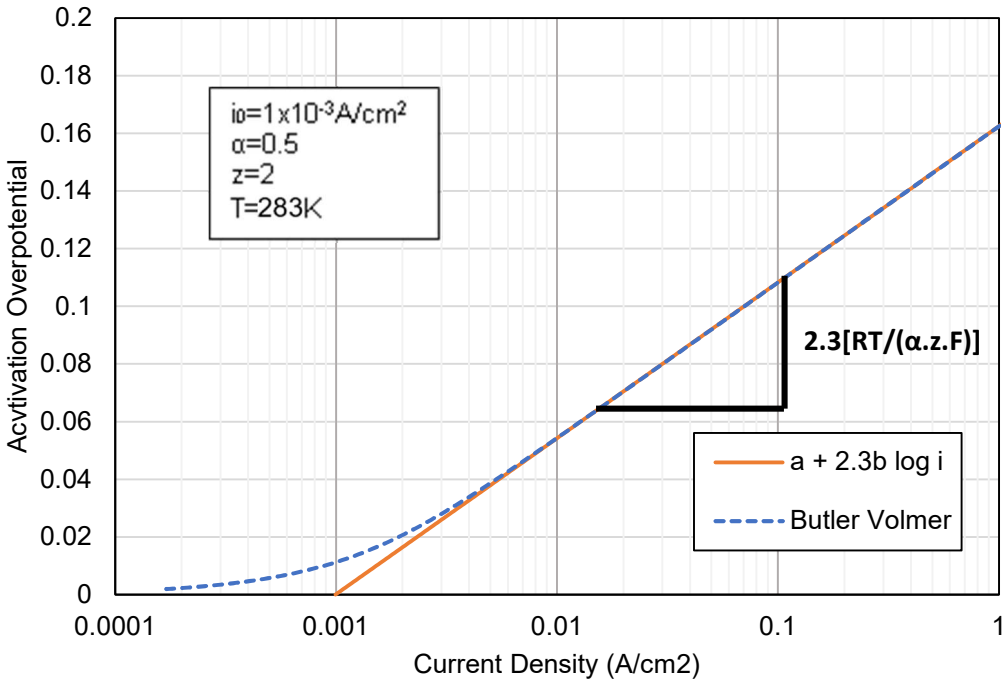

Figure 2.9 Semi-logarithmic plot of variation of activation overpotential with current density using Equation 2.41 and Butler-Volmer equation and

The Tafel equation as shown in Figure 2.9 can be used to determine the activation overvoltage at higher current densities. The point where the logarithmic slope intersects the x axis is equal to the exchange current density. This graph shows that the Tafel equation is dependent on exchange current density and charge transfer coefficient.

It is important to notice the magnitude of the effect of certain parameters that affect the voltage. The effect of exchange current density on the activation voltage is expressed in Figure 2.10 for the anode side. It could be observed that as the exchange current density increases by 10 times, the activation voltage decreases about 0.05 V. The effect of the charge transfer coefficient could also be observed from Figure 2.11. The effect of CTC in an exchange current density of 10^{-5} A/cm^2 is around a 0.1 V decrease for every 0.1 increase. Whereas in an exchange current density of 10^{-12} A/cm^2, a decrease of 0.1 of CTC contributes to an increase of 0.2 V.

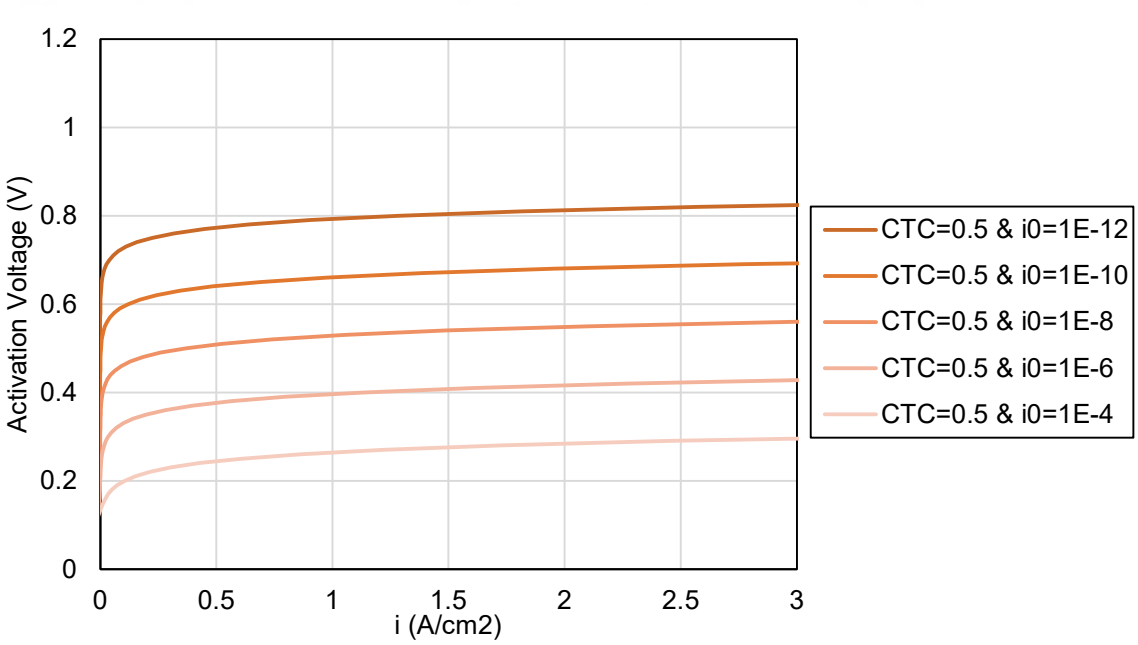

Figure 2.10 Activation voltage – Current density graph demonstrating the effect of exchange current density on voltage losses

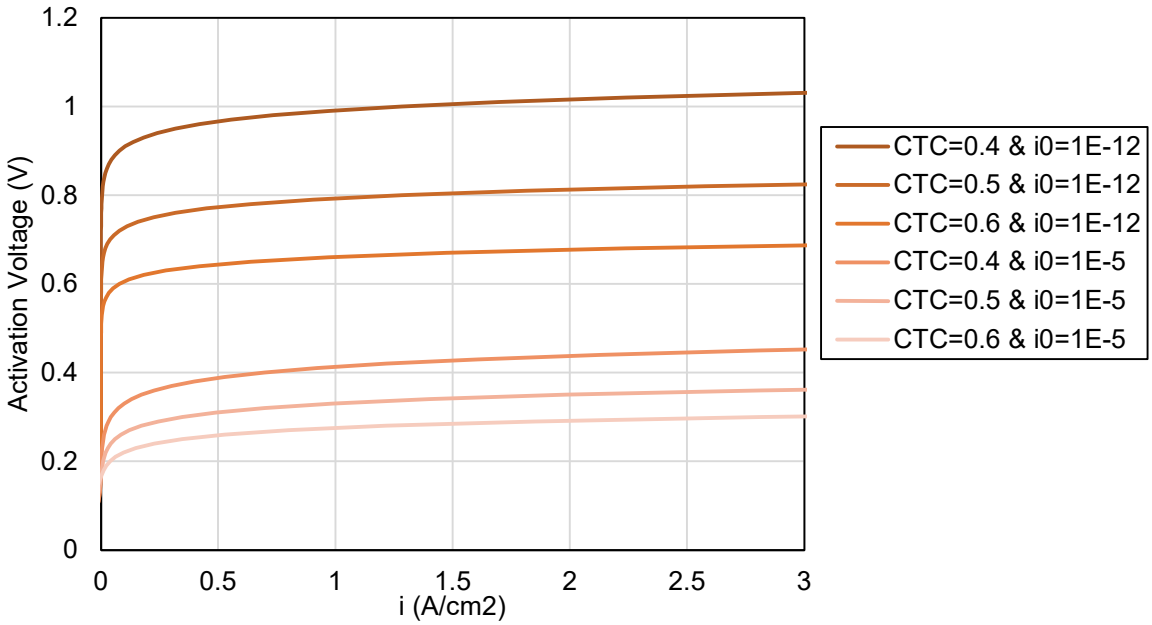

Figure 2.11 Activation voltage – Current density graph demonstrating the effect of CTC on voltage losses for different exchange current densities.

In literature about PEM electrolysis there are uses of Butler Volmer and the simplified equations mentioned above.

2.2.3. Ohmic voltage

The ohmic voltage is the electric potential loss occurring due to the electric resistance of the cell components such as the membrane, catalyst, gas diffusion layer, and bipolar plates. The ohmic potential can be interpreted as the following Equation 2.43.

$$V_{ohm}=I.(R_{plt}+R_{GDL}+R_{ct}+R_{mem}) \tag{2.42}$$

$$V_{ohm}=I.(R_{total}+R_{mem}) \tag{2.43}$$

The resistance of the membrane can be calculated by an equation initially proposed by Springer (1991) for PEM fuel cells and then utilized for modeling PEM electrolyzers in various literature (Ni et al., 2008; Brown et al., 2008; Marangio et al., 2009; Lebbal and Lecœuche, 2009; Awasthi et al., 2011; Zhang et al., 2012; Kim et al., 2013; Abdin et al., 2015; Yigit and Selamet, 2016; Tiktak, 2019).

$$R_{mem}=\frac{\delta_m}{A.\sigma_m} \tag{2.44}$$

$$\sigma_m=(0.005139\lambda-0.00326).\exp\left[1268.\left(\frac{1}{303}-\frac{1}{T_{cell}}\right)\right] \quad (2.45)$$

In Equations 2.44 and 2.45, δ_m, σ_m, λ are the membrane thickness, conductivity and water uptake coefficient respectively. For electrolysis λ is assumed to be in the range of 14 - 25 in fully hydrated membranes (Santarelli and Torchio, 2007; Bessarabov et al., 2016).

Harrison (2006) and Dale (2009) calculated empirical equations based on experimental data of an electrolyzer with Nafion117 membrane listed in Table 2.4.

Table 2.4 Other Equations used for membrane resistance.

Literature	Membrane	Membrane Thickness	Equation
(Harrison, 2006)	Nafion117	178 μm	$\sigma=0.001.T_c+0.03$ (2.46)
(Dale, 2009)	Nafion117	178 μm	$\sigma=0.048+8.15x10^{-4}T_c+5.11x10^{-7}T_c^2$ (2.47)

Figure 2.12 is a representation graph of conductivity with respect to temperature making use of Equation 2.45 for different λ values and Equation 2.46 and 2.47.

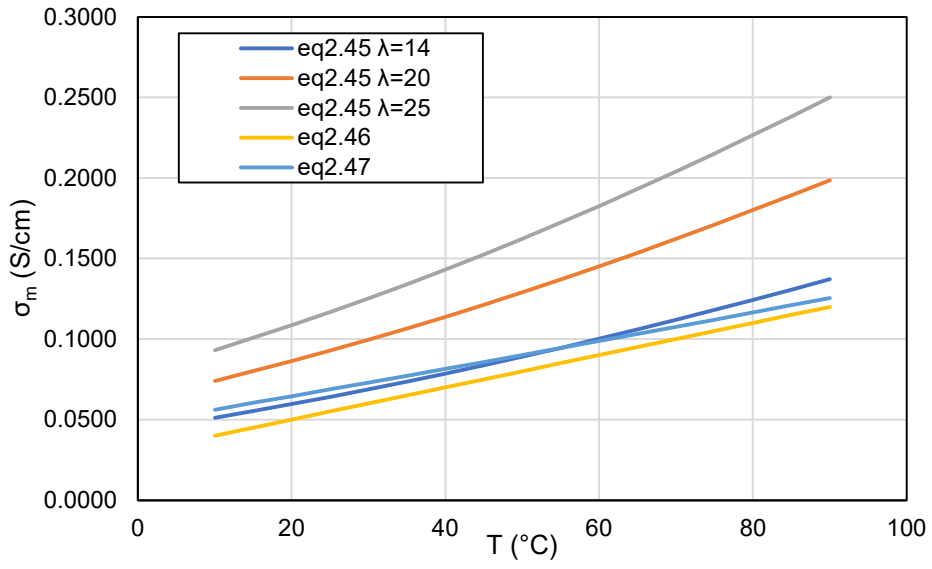

Figure 2.12 Variation of membrane conductivity with respect to temperature for Equations 2.45, 2.46 and 2.47.

As could be observed by the graph the change between different eq and λ contributes to a range of upto 50% difference. The maximum and minimum potential range at T=80°C and i=1.5 A/cm^2 according to the above would be 0.157 - 0.324 V considering the membrane thickness of 178 μm. The effect of λ can be observed from this graph as an increase of 1 contributes to an increase of around 0.01 S/cm which effects the voltage by decreasing about 0.01 V. The thickness of the membrane also effects the voltage significantly, as an increase of 1 μm in thickness, increases the voltage by around 0.015.

R_{total} can be calculated from the electric resistance of the other layers of the cell or estimated from experimental data by calculating the slope of the I-V curve where it is close to linear (over 1 A/cm^2) and subtracting R_{mem}. It is suggested by Marr and Li (1998) and mentioned by Marangio (2009) that the resistivity of the electrode and plate to be $60x10^{-6}$ Ω.m and $130x10^{-6}$ Ω.m respectively. Rozain (2014) mentions that the resistance of the membrane was approximately 100 - 130 mΩ.cm^2 and the resistance of the other cell components would be 120 - 150 mΩ.cm^2 after experimenting with Nafion117 (178 μm).

2.2.4. Diffusion Voltage

The diffusion voltage, also known as the concentration voltage, resembles the potential loss that occurs due to the high current densities. At high enough current densities, the oxygen bubbles forming on the anode catalyst surface increase thus, lessening the contact between the reactant, water, with the anode surface.

The diffusion voltage can be determined by integrating a limit current density with the simplified Butler-Volmer equation (2.31). (Grigoriev et al., 2001), (García-Valverde et al., 2012).

$$i = i_0 . \left(1 - \frac{i}{i_{lim}}\right) . \exp\left[\frac{\alpha . z . F . V_{act+dif}}{RT}\right] \qquad (2.48)$$

$$V_{act+dif}= \frac{R.T}{\alpha.z.F}\ln\left(\frac{\frac{i}{i_0}}{1-\frac{i}{i_{lim}}}\right)=\underbrace{\frac{R.T}{\alpha.z.F}\ln\left(\frac{i}{i_0}\right)}_{V_{act}}\underbrace{-\frac{R.T}{\alpha.z.F}\ln\left(1-\frac{i}{i_{lim}}\right)}_{V_{dif}} \quad (2.49)$$

$$V_{dif}=-\frac{R.T}{\alpha.z.F}\ln\left(1-\frac{i}{i_{lim}}\right) \quad (2.50)$$

The sinh simplification of the Butler-Volmer equation can also be used in the same sense (Bessarabov et al., 2016).

$$V_{dif}= -\frac{R.T}{\alpha.z.F}\sinh^{-1}\left(\frac{1}{2}\left\{1-\frac{i}{i_{lim}}\right\}\right) \quad (2.51)$$

As stated by (Bessarabov et al., 2016), i_{lim}, the limit current density for fuel cells is generally around 2 A/cm^2. As for the PEM electrolyzer it is stated that it can be as high as 5 A/cm^2 depending on the water flow and is neglected in most literature studies due to the fact that commercial PEM electrolyzers do not operate at as high of a current density range.

2.3. I-V Curves and Limits

The cell voltage consists of loss potential added on top of V_{ocv} as shown by Equation 2.52.

$$V_{cell}= V_{ocv}+V_{loss}=V_{ocv}+V_{act,a}+V_{act,c}+V_{ohm}+V_{diff} \quad (2.52)$$

As mentioned earlier diffusion (concentration) voltage can be neglected in PEMEL because the feed water is circulated for the purpose of cooling which is discussed later in this paper. This minimizes the effect of bubbles and is one of the main reasons the effect of concentration losses are negligible up to high current densities. Therefore, Equation 2.52 can be written as:

$$V_{cell}=V_{ocv}+V_{act,a}+V_{act,c}+V_{ohm} \quad (2.53)$$

Figure 2.13 is a generic I-V plot visualizing the effect of voltage losses on the cell voltage.

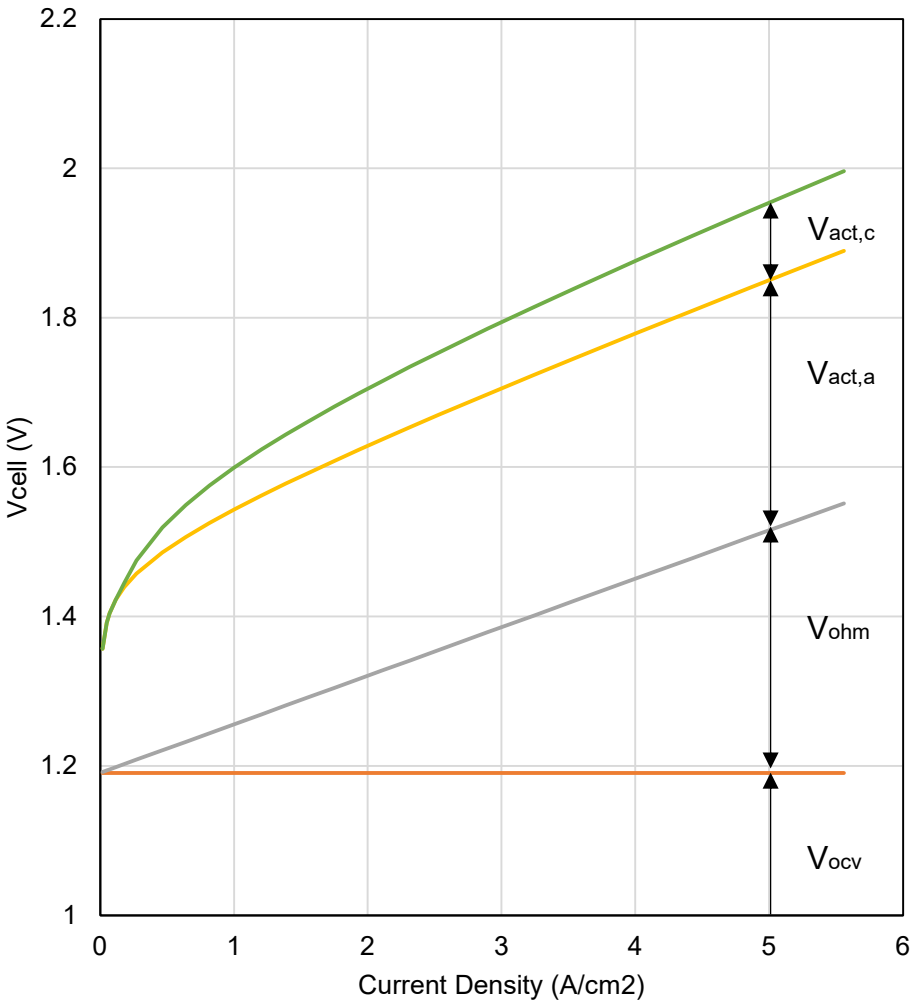

Figure 2.13 I-V curve representation of variation in cell voltage and losses with respect to current density.

As visualized above, the effect of activation voltages almost constant after a current density of 1 A/cm^2 and the effect of anode side is significantly greater than the cathode side. The ohmic voltage losses however increase linearly with increasing current density which decreases the efficiency of the cell when operating at higher current densities. The open circuit voltage on the other hand remains constant at constant temperature and pressure.

It is important to analyze the I-V curves provided by experimental studies in literature in order to develop a realistic model. Figure 2.14 is a plot of I-V data from experimental studies in literature.

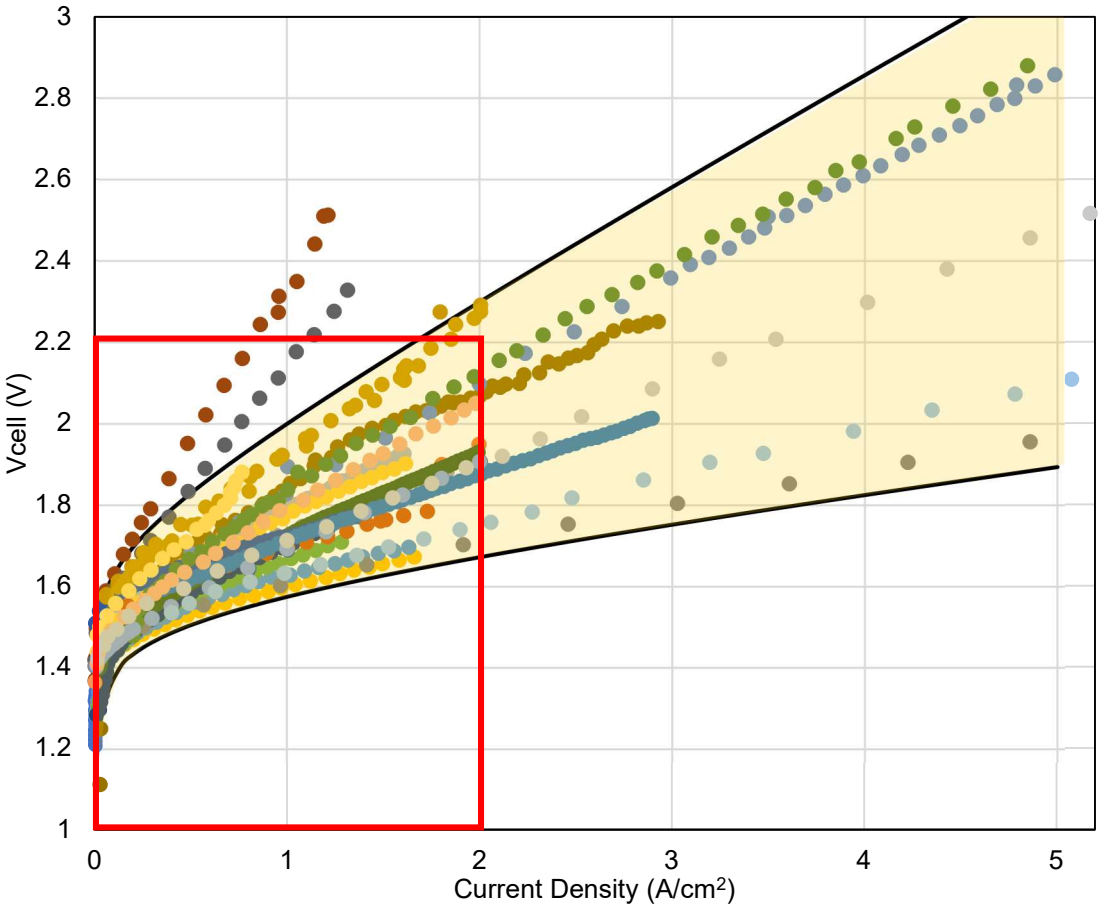
3
2.8
2.6
2.4
2.2
2
1.8
1.6
1.4
1.2
1
Vcell (V)
0
1
2
3
4
5
Current Density (A/cm2)

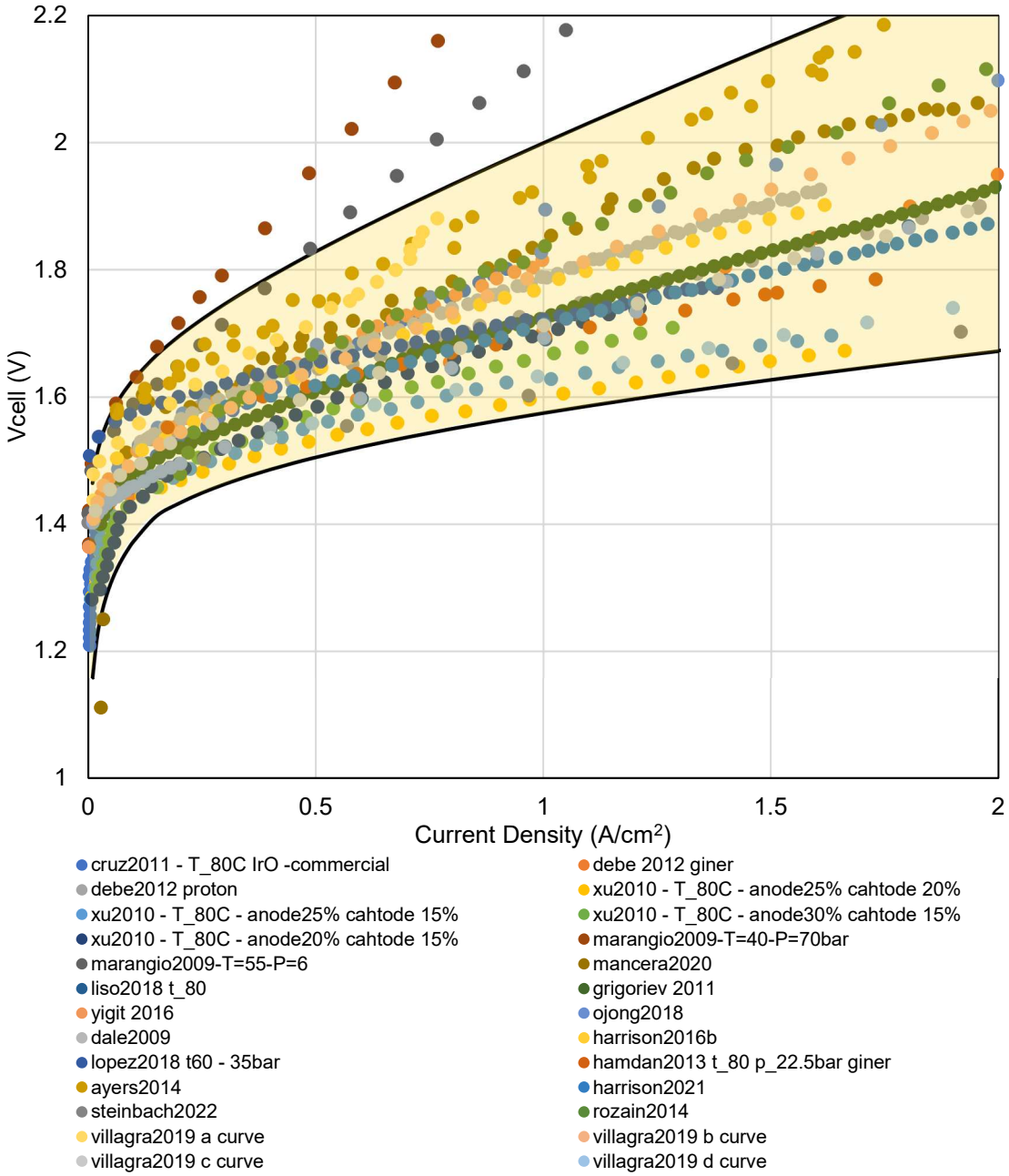

Figure 2.14 Collected experimental I-V curve data from literature (Ayers et al., 2014; Cruz et al., 2011; Dale, 2009; Debe et al., 2012; Grigoriev et al., 2011; Hamdan, 2013; Harrison, 2006, 2021; Liso et al., 2018; Mancera et al., 2020; Marangio et al., 2009; Ojong, 2018; Rozain and Millet, 2014; Steinbach et al., 2022; Villagra and Millet, 2019; Xu and Scott, 2010; Yigit and Selamet, 2016).

It is important to be able to examine the operating range of commercial electrolyzers. It is mentioned in the study (Villagra and Millet, 2019) that 2 V is considered a limit for the oxidation of titanium in common practice. Although the conducted experiments in literature can be found exceeding up to 3 V, it could be seen that most are limited to around 2 V which could also be observed as the

voltage level on nominal capacity for commercial electrolyzers. However, it can also be seen that 1.75 V can be considered the nominal voltage and 2 V could be considered the maximum operating voltage of the cell. Since there is such a potential limit, to be able to increase the capacity of a cell without increasing the voltage would require a decrease in activation voltage and also more importantly the ohmic voltage. The decrease in the activation voltage would not be as effective as the decrease in ohmic voltage. This is due to the fact that the effect of the activation voltage is near constant over 1 A/cm^2 as mentioned earlier. Whereas the increase in membrane conductivity will decrease the slope of the close to linear curve observed after 1 A/cm^2 which leads to a larger decrease in higher current densities.

The IRENA and FHC JU have reports indicating state of the art data and future targets of certain key performance indicators (KPIs) for the performance of PEM electrolysis (Davies et al., 2021; International Renewable Energy Agency, 2020a).

Table 2.5 Target KPI parameters affecting cell performance stated by EU Comission and IRENA

	FCH 2 JU					IRENA	
Parameter and Unit	SoA 2012	SoA 2017	Target 2020	Target 2024	Target 2030	SoA 2020	Target 2050
Electricity Consumption @ Nominal Capacity (kWh/kg)	60	58	55	52	50	50-83	<45
Current Density (A/cm2)	1.7	2	2.2	2.4	2.5	1-2	4-6
Voltage range limits (V)	-	-	-	-	-	1.4-2.5	<1.7
Stack unit size	-	-	-	-	-	1 MW	5 MW
Electrode Area (cm2)	-	-	-	-	-	1500	>10000

The cell voltages are not clearly specified for FCH JU and are assumed to be 2 V. The state of the art and target current densities on the other hand are provided and have been represented in Figure 2.15 to visualize the I-V curve regions on Figure 2.16 and compared with I-V curves found in literature of this study.

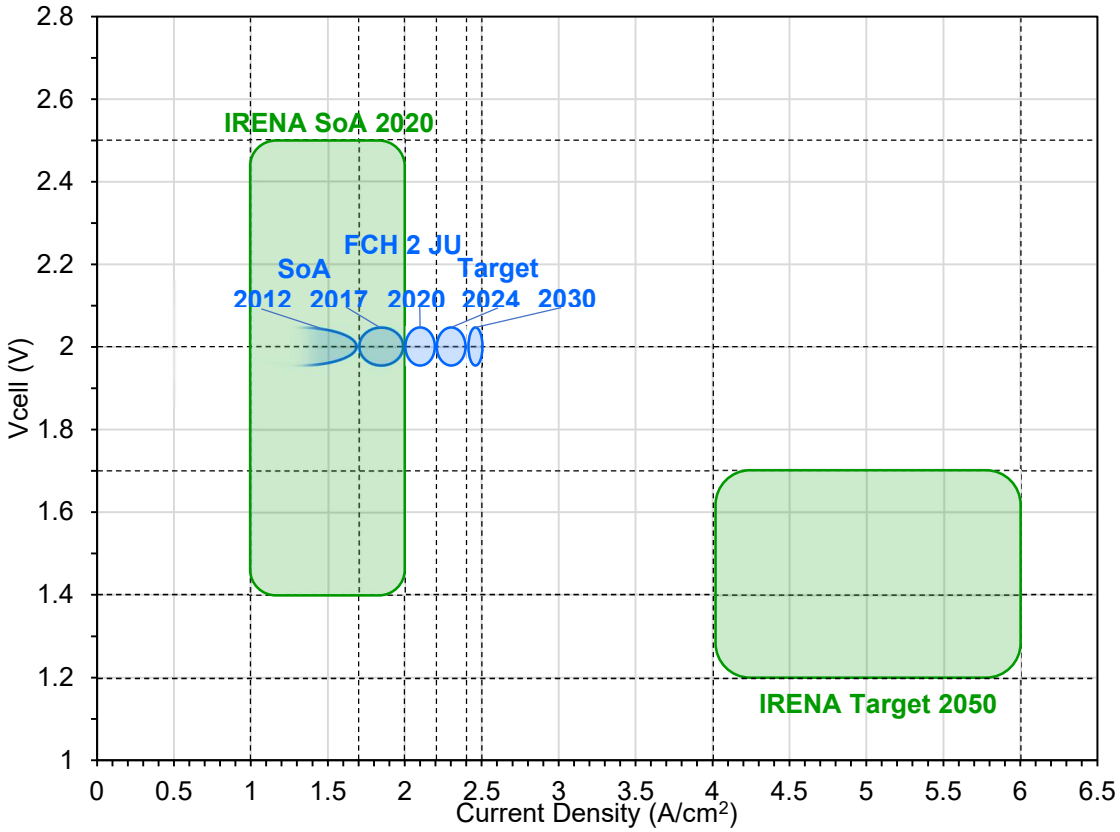

Figure 2.15 Representation of target KPI parameters mentioned in Table 2.5.

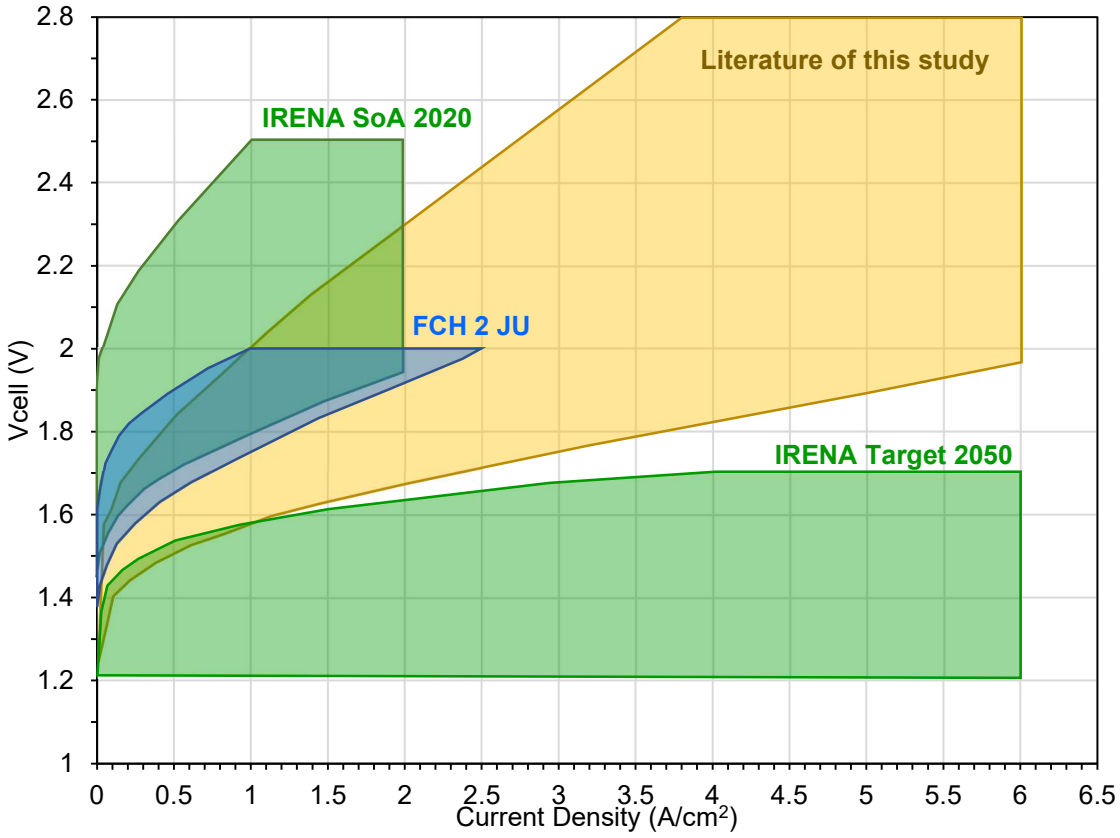

Figure 2.16 Graphical I-V representation of literature and targets

It is mentioned in the European Commission JRC Technical Report (Davies et al., 2021) that the mentioned targets on the table for 2030 have already been met. This is seen in Figure 2.16 where the curves provided by literature in the yellow region have lower voltage values at higher current densities than of the blue region.

2.4. PEM Electrolyzer Permeation Loss

Hydrogen losses occur due to permeation from cathode to anode side by the effect of pressure difference. Equation 2.54 could be utilized to calculate the hydrogen loss due to permeation (Grigoriev et al., 2011).

$$\dot{n}_{H_2loss} = \frac{D_{H2}}{H_{H2}} . \frac{P_c - P_a}{L} . A_{cell} \tag{2.54}$$

D_{H2} and H_{H2} are diffusion coefficient and Henry's Law constant of hydrogen respectively.

2.5. PEM Electrolyzer Cell and System Efficiency

The efficiency of the PEM cell is calculated using the lower heating value (LHV) or higher heating value (HHV). The efficiency related to the LHV is calculated using the reversible voltage of 1.23 V and is expressed in Equation 2.55.

$$\eta_{cell,LHV} = \frac{V_{rev}}{V_{cell}} = \frac{1.23V}{V_{cell}} \tag{2.55}$$

The efficiency related to the HHV is calculated using the thermos neutral voltage of 1.48V and is expressed in Equation 2.56.

$$\eta_{cell,HHV} = \frac{V_{tn}}{V_{cell}} = \frac{1.48V}{V_{cell}} \tag{2.56}$$

Electrolysis is an endothermic reaction. Therefore, as discussed by Bessarabov and Millet (2018a), when the cell voltage is between 1.23 – 1.48 V the heat flux is towards the cell. At 1.48 V there is no heat flux and after exceeding 1.48 the heat flux is at an outwards direction from the cell to the environment.

The system efficiency also includes the energy consumption of the auxiliaries such as pumps, compressors, cooling units etc. Therefore, the system efficiency

is calculated by dividing the power of the hydrogen produced by the total energy consumption.

$$\eta_{sys,LHV} = \frac{P_{H_2}}{P_{stacks}+P_{aux}} = \frac{LHV.\dot{n}_{H_2}}{N_{stack}.N_{cell}.V_{cell}.I+P_{aux}} \quad (2.57)$$

$$\eta_{sys,HHV} = \frac{P_{H_2}}{P_{stacks}+P_{aux}} = \frac{HHV.\dot{n}_{H_2}}{N_{stack}.N_{cell}.V_{cell}.I+P_{aux}} \quad (2.58)$$

$$\dot{n}_{H_2} = N_{cell}.\frac{I}{z.F} \quad (2.59)$$

Most manufacturer catalogues and KPIs mentioned in related reports also express efficiency in terms of kWh energy consumed per kg or m^3/h H_2 produced on stack and system level.

$$\eta_{stack,kWh/kg} = \frac{P_{stack}}{\dot{m}_{H_2}} = \frac{N_{cell}.V_{cell}.I}{1000\ .\ 3600\ .\ M_{H_2}.N_{cell}.I/z.F} = \frac{V_{cell}}{3600000\ .\ M_{H_2}/z.F} \quad (2.60)$$

When Equation 2.60 is simplified, it could be observed that the stack kWh/kg efficiency only depends on the cell voltage. Having obtained this conclusion, the commercial PEMEL companies provide kWh/kg stack efficiencies of their products in their catalogues for average or nominal operations which could be used to calculate the nominal cell voltage. Some companies provide kWh/Nm^3 which could be converted by multiplying it by 11.126 Nm^3/kg. In Table 2.6 cell voltages for maximum capacities and nominal capacities are calculated from manufacturer data where catalogues are available in Appendix 1.

Table 2.6 Parameter evaluation of manufacturer catalogue data

Company	System Model Name	Max. Stack Capacity (MW)	No. of Stacks	H2 Production Rate		Calculated Stack Efficiency		Vcell Acc. to Calc. Eff. (V)	Average/Nominal Stack Efficiency Stated in Catalogue		Vcell Acc. to Catalogue Eff. (V)
				(Nm3/h)	(kg/h)	(kWh/Nm3)	(kWh/kg)		(kWh/Nm3)	(kWh/kg)	
Plug Power (Giner ELX)	EX-425D	1	1	200	17.98	5.00	55.63	2.08	-	49.9	1.86
Nel Hydrogen	MC250	1.25	1	246	22.11	5.08	56.53	2.11	-	50.4	1.88
Proton Onsite	M400	2.1	-	417	37.48	5.04	56.03	2.09	-	-	-
Cummins	HyLYZER - 4000	-	-	4000	359.52	-	-	-	4.30	48.00	1.79
H2B2	EL200N	-	1	200	17.98	-	-	-	4.7	52.92	1.97
Elogen	E200	1	-	200	17.98	5.00	55.63	2.08	4.4	49.54	1.85

Note: Blue cells are manufacturer data, other values are calculated.

It is shown that manufacturer data sheets express the nominal cell voltage in a range of 1.79 V - 1.97 V despite the maximum cell voltage being calculated around 2.10 V which means that the actual hydrogen production rate mentioned

in the catalogues could not be achieved in nominal voltage values but only in maximum voltage. There is no certain standard for determining the nominal voltage but for maximum voltage, it could be seen that manufacturers have limited to 2.10 V in order to prevent degradation.

It is important to note that stack efficiency values are not dictated by I-V curve characteristics. I-V curves determine the size of the cell and stack which affects capital costs. The efficiency of the stack however has been shown to be related to the partial loading of the stack. It seems that the kWh/kg efficiencies stated in manufacturer catalogues could not be used to compare other brand models. The competition between stacks is actually related to the stack size but not the efficiency as all stacks have the same efficiency at full load.

$$\eta_{sys,kWh/kg} = \frac{P_{stack}+P_{aux}}{\dot{m}_{H_2}} = \frac{N_{cell}.V_{cell}.I+P_{aux}}{3600.M_{H_2}.N_{cell}.I/z.F} \tag{2.61}$$

2.6. PEM Electrolyzer Cooling and Water Flow

The water supplied to the electrolyzer does not only consist of the amount of water needed to carry out the electrolysis reaction but also consists of an amount that is circulated for heat management reasons. For this reason, most PEM electrolyzers operate with a circulation line which contains a heat exchanger to absorb the heat generated from the stack.

The water flow through the cell could be expressed in a non-dimensional form as expressed by Equation 2.62 (Bessarabov and Millet, 2018).

$$\lambda_{H_2O} = \frac{\dot{m}_{H_2O}.2F}{M_{H_2O}.i.A} \tag{2.62}$$

The required water mass flow rate in order to remove the excess heat could be calculated by Equation 2.63.

$$\dot{m}_{H_2O}.c^{p}_{H_2O}.\Delta T = i.A.(V_{cell}-V_{tn}) \tag{2.63}$$

By using Equation 2.62 and 2.63 the non-dimensional ratio of flow could be expressed as Equation 2.64.

$$\lambda_{H_2O} = \frac{2F}{M_{H_2O}.c^{p}_{H_2O}.\Delta T}(V_{cell}-V_{tn}) \tag{2.64}$$

The non-dimensional ratio is dependent on V_{cell} and ΔT. Figure 2.17 helps to visualize the change in λ_{H2O} for different values of V_{cell} at with respect to ΔT.

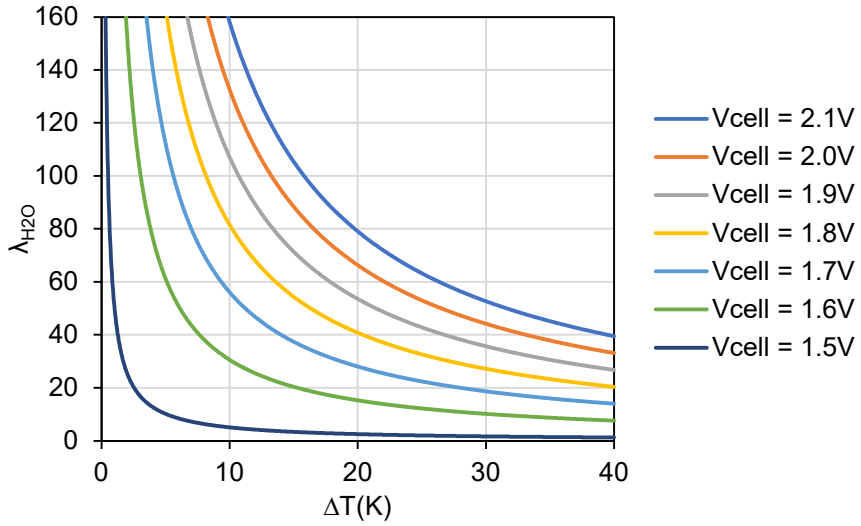

Figure 2.17 Non-dimensional flow water flow ratio graph with respect to temperature difference at different cell voltages

3. SYSTEM COMPONENTS AND LITERATURE

3.1. System Configurations

The electolyzer system consists of several components, which were observed from literature. There is a demand for water supply, cooling, and electric energy in order to operate the electrolyzer. Below are schematic diagrams of the common PEM electrolysis systems from literature and commercial catalogues.

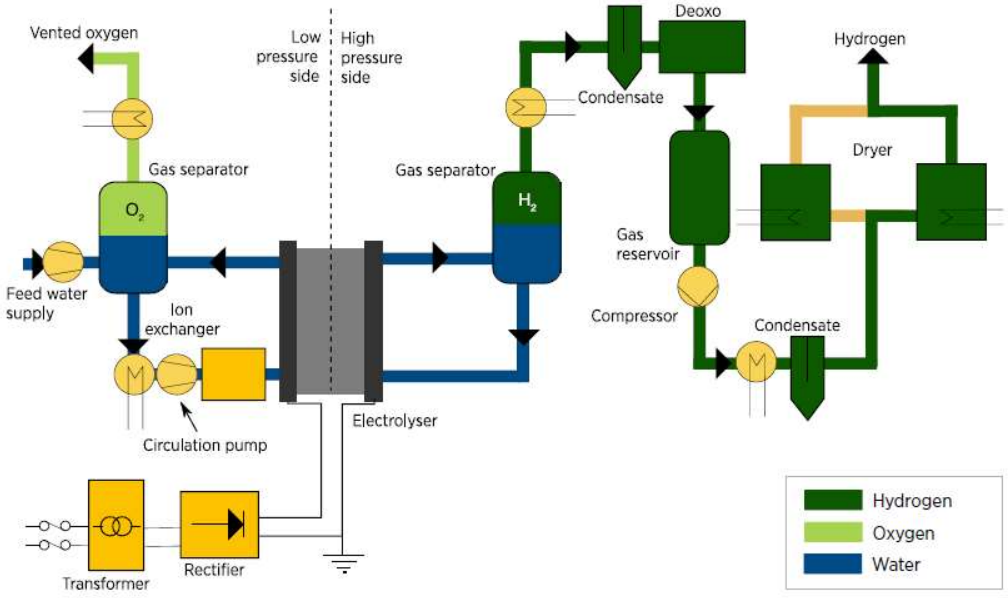

Figure 3.1 System configuration of IRENA (International Renewable Energy Agency, 2020a)

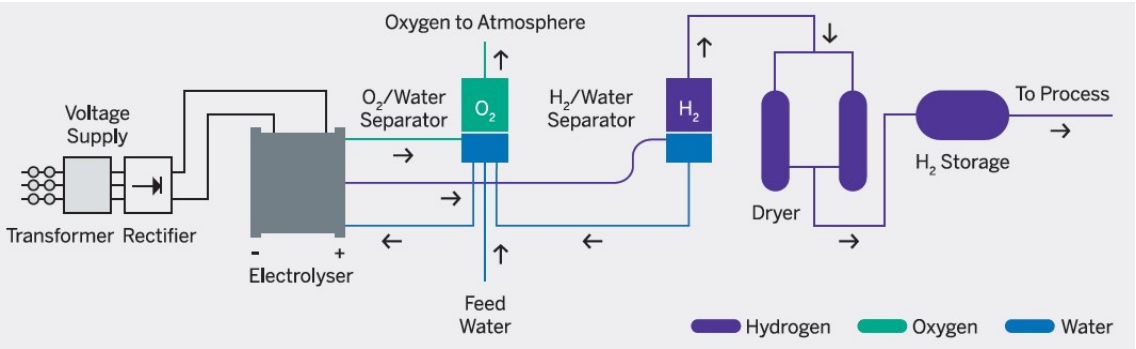

Figure 3.2 System configuration from Nel Hydrogen Brochure (Nel Hydrogen, 2023)

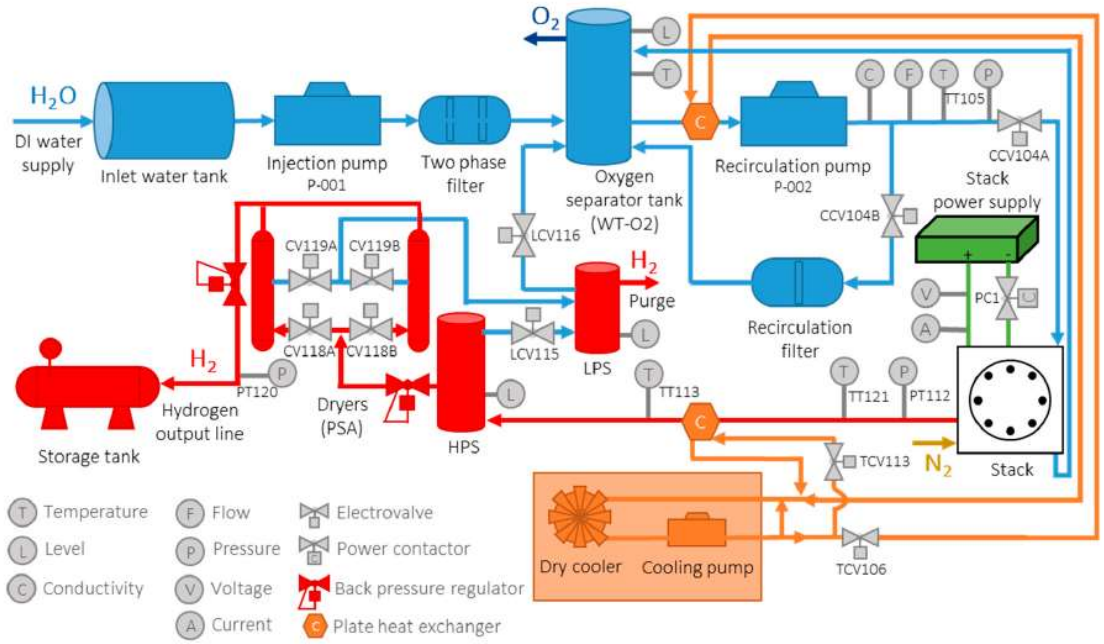

Figure 3.3 System Schematics of Mancera et al. (2020)

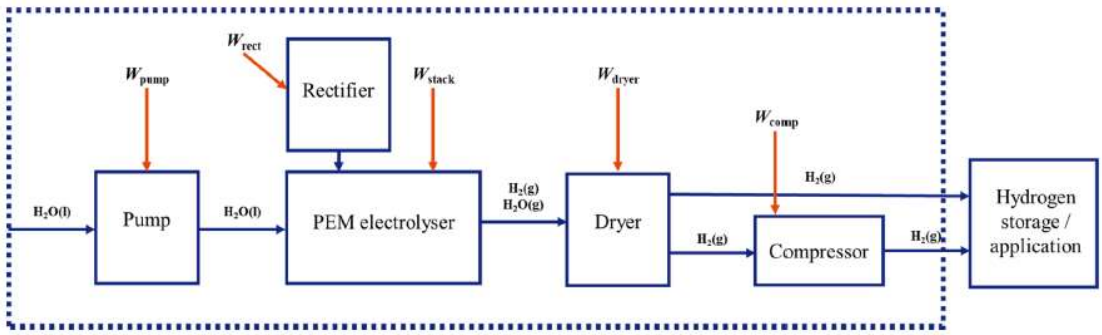

Figure 3.4 System Schematics of Ragnhild Hancke et al. (2022)

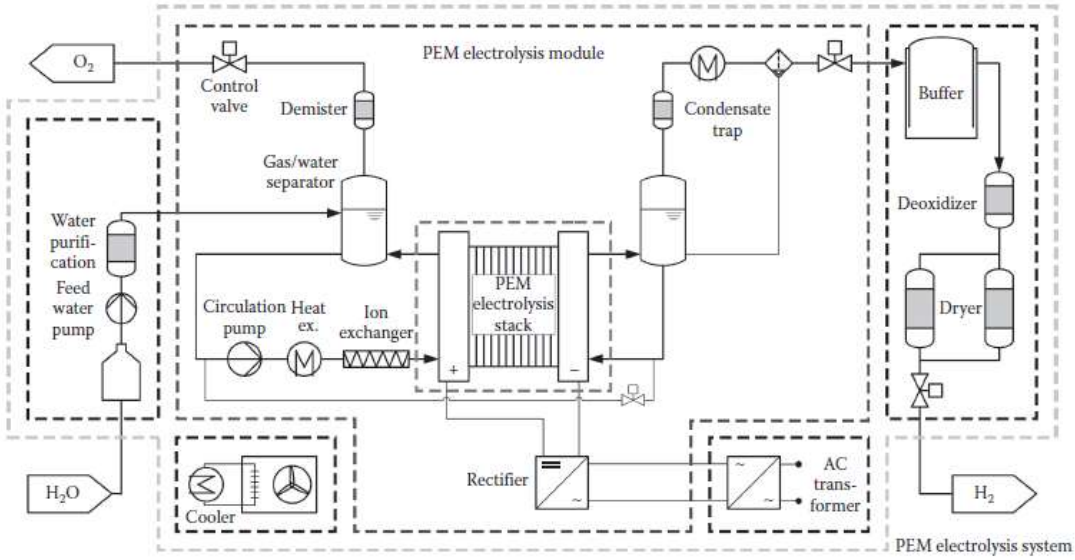

Figure 3.5 System Schematics of Bessarabov et al. (2016)

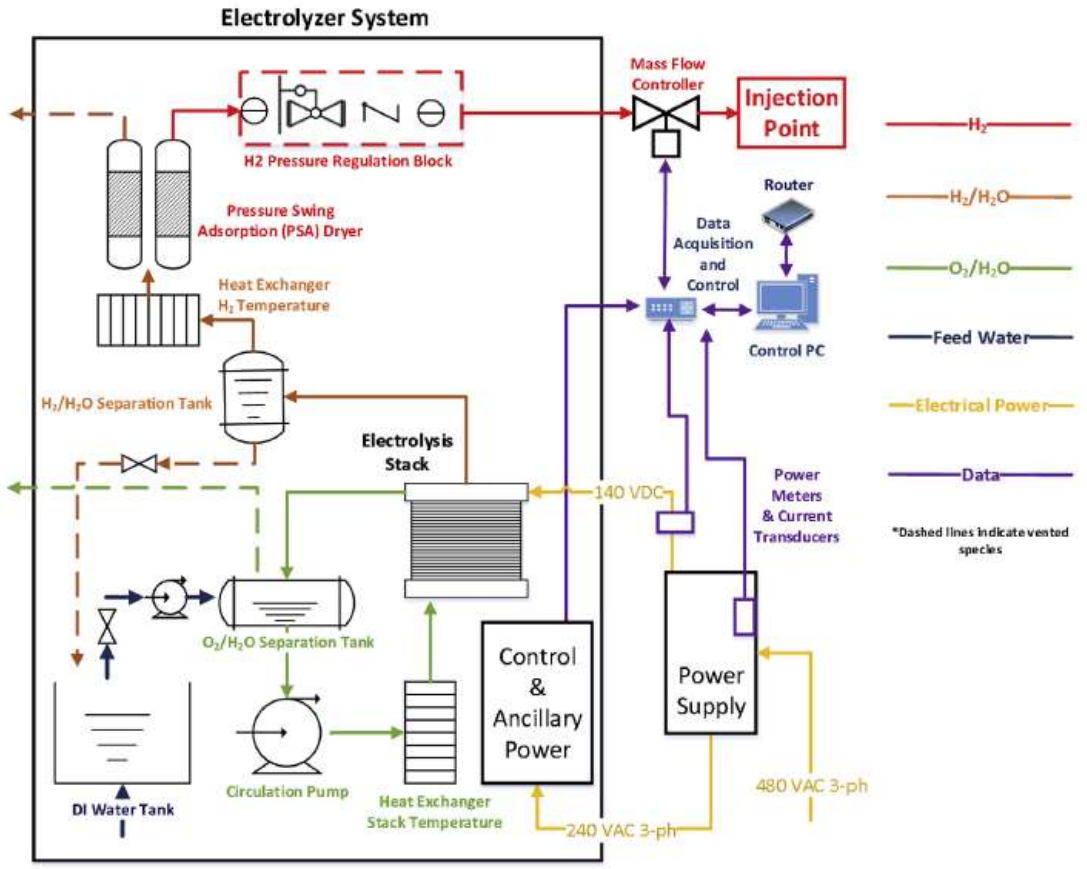

Figure 3.6 System Schematics of Stansberry and Brouwer (2020)

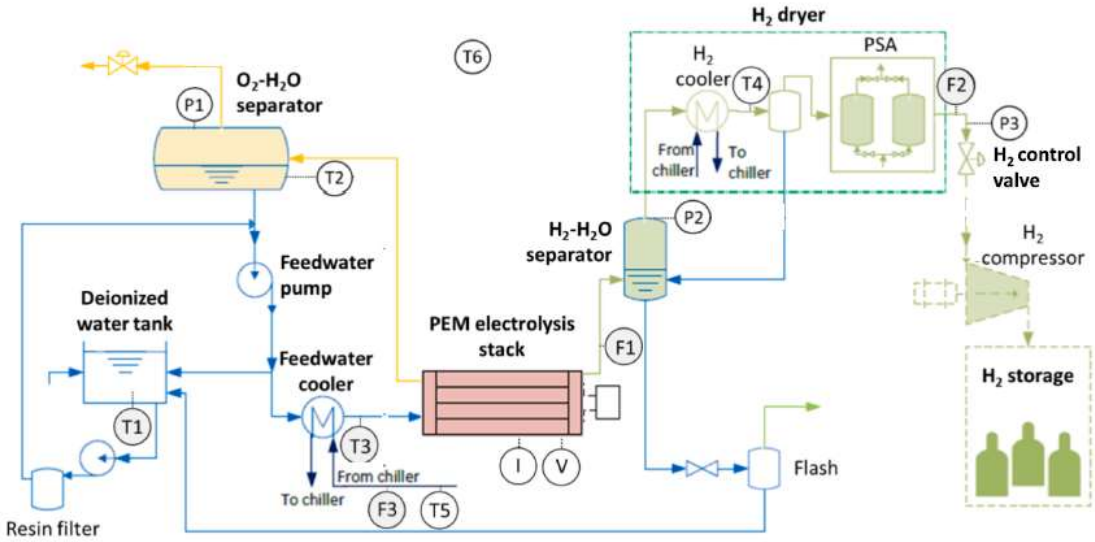

Figure 3.7 System Schematics of Crespi et al. (2023)

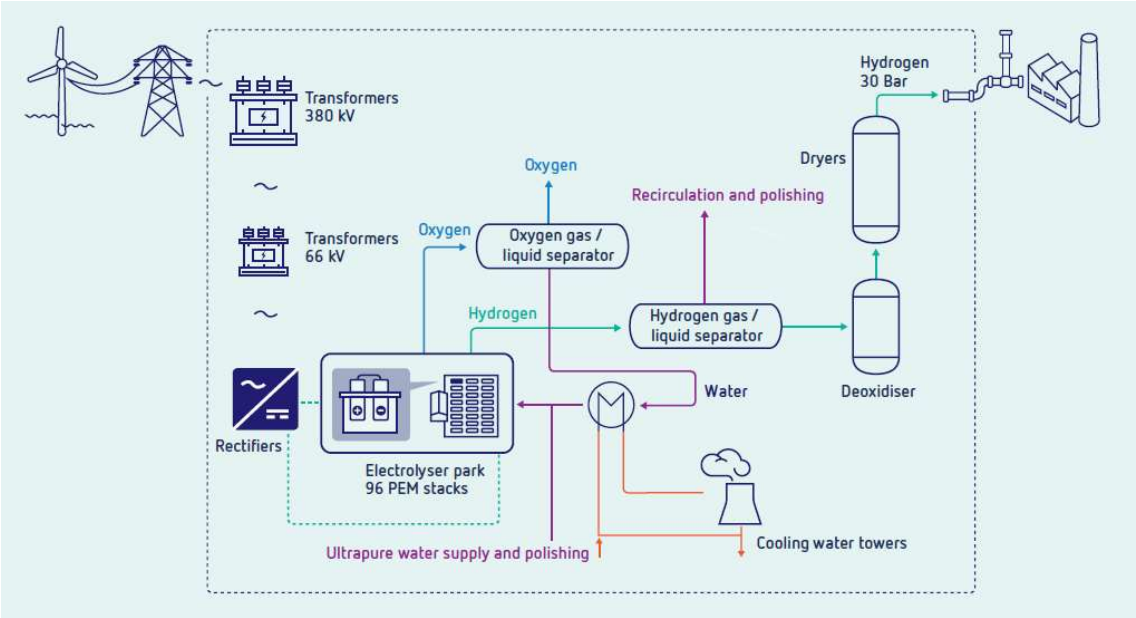

Figure 3.8 System Schematics of Noordende and Ripson (2022)

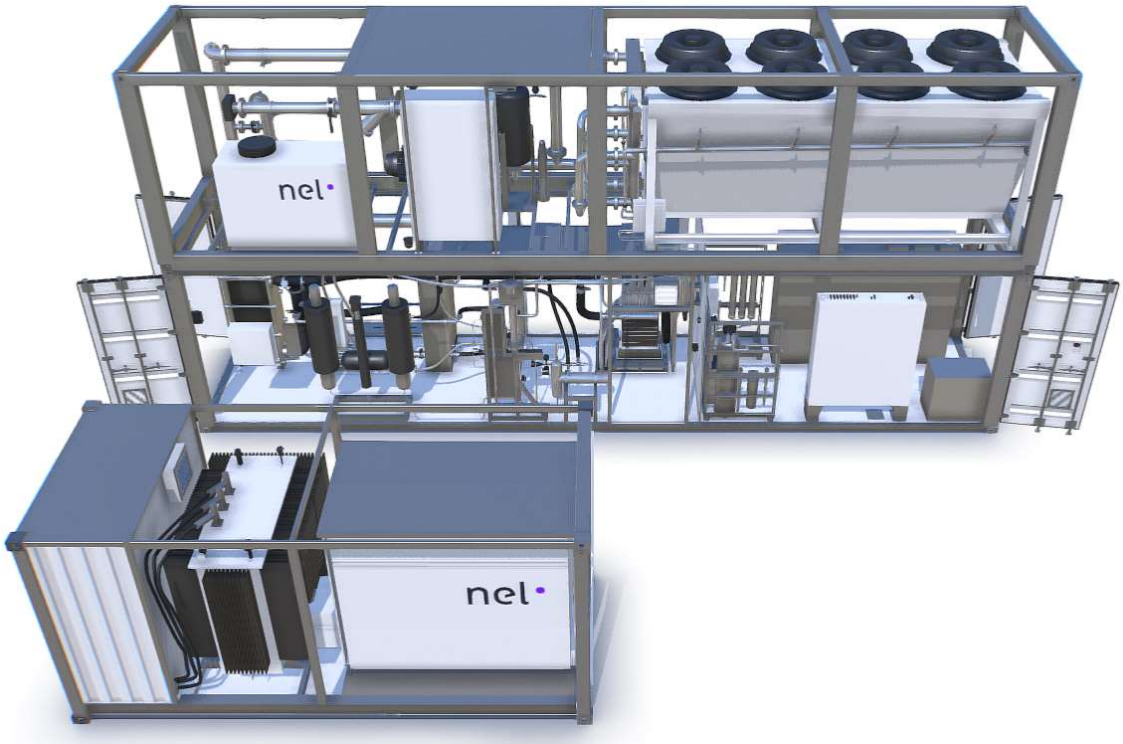

Figure 3.9 3D model of Nel Hydrogen Electrolyzer System (Nel Hydrogen, 2023)

Figure 3.10 3D model of H-Tec Electrolyzer System (H-Tec, 2023)

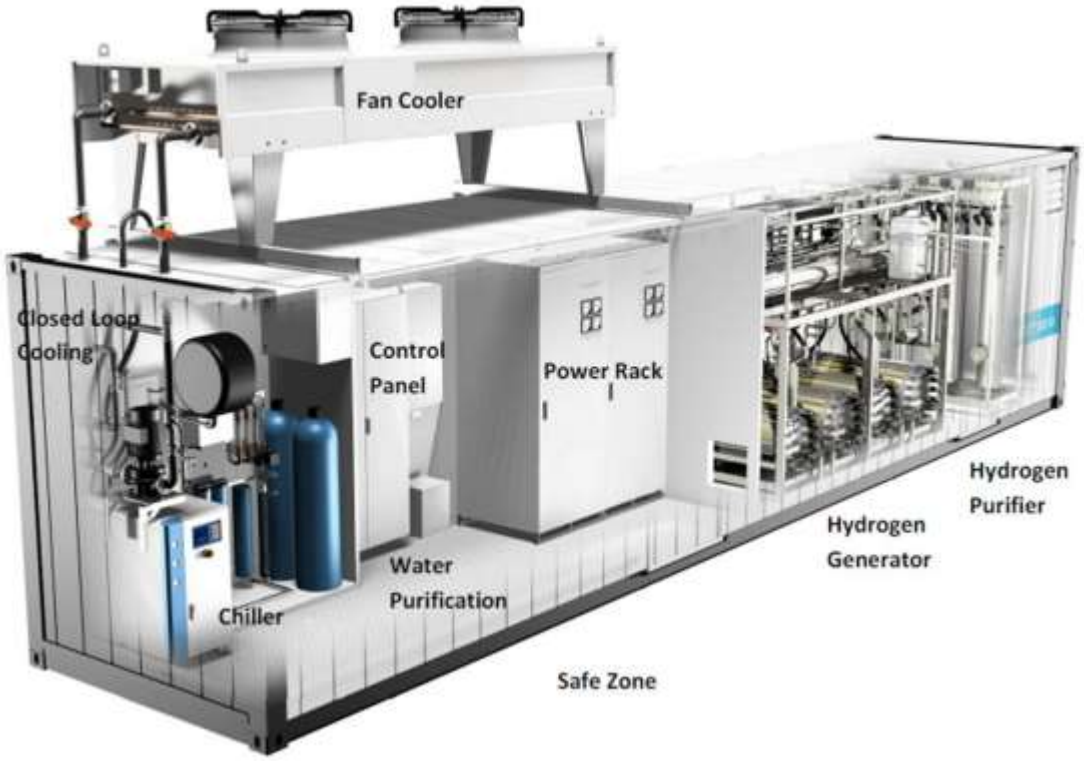

Figure 3.11 3D model of Hydrogenics Electrolyzer System (Verkoeyen, 2018)

It can be observed that PEM electrolyzer systems consist of 4 main subsystems which are as follows

- Feed water and filtration
- Cooling system
- Hydrogen drying/ purification system
- Electrical power supply system

Additional systems include

- Compression and hydrogen storage system
- Oxygen purification, compression and storage system

These are optional needs that differ with the specific need of the installation.

Figure 3.12 and Table 3.1 below show the pressure ranges required for various applications regarding hydrogen so that compressor pressure can be designed accordingly.

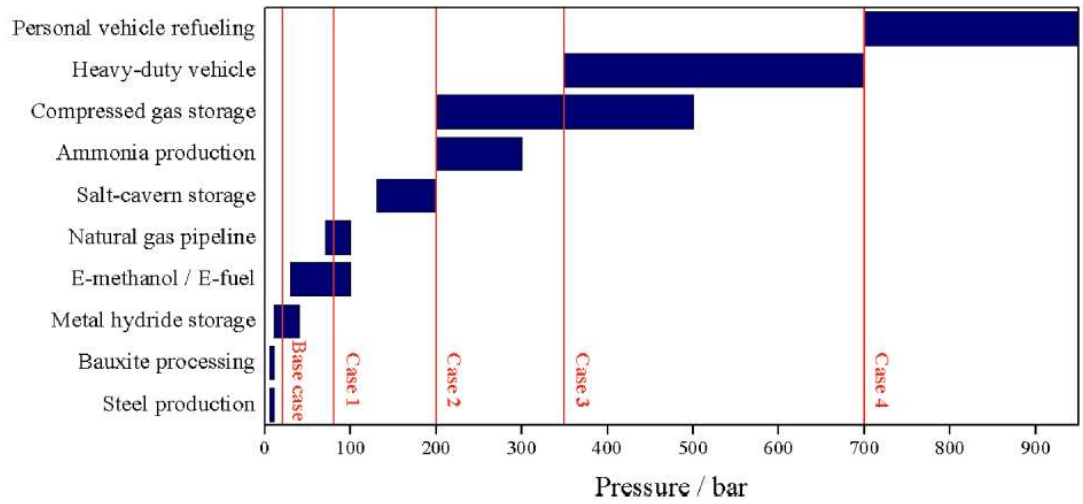

Figure 3.12 Pressure levels for possible applications of green hydrogen (Ragnhild Hancke et al., 2022)

Table 3.1 Summary of the use cases of green hydrogen with corresponding pressures (Ragnhild Hancke et al., 2022)

Case	Pressure (bar)	Application
1	80	E-methanol, e-fuels, natural gas pipeline
2	200	Salt-cavern storage, compressed gas storage, ammonia production
3	350	Compressed gas storage, heavy-duty vehicle
4	700	Personal vehicle refueling, heavy0duty vehicle

Compression of hydrogen will not be carried out in this study as it is optional and varies with many applications as previously mentioned.

3.2. Converters and Transformers

For this study the energy source of the stacks will be solar which means that the electrical input is DC and the stack will consume DC current, therefore DC-DC converters will be used for this application. DC-DC converters generally have a near to constant efficiency of 95-98% starting from around 20% partial load.

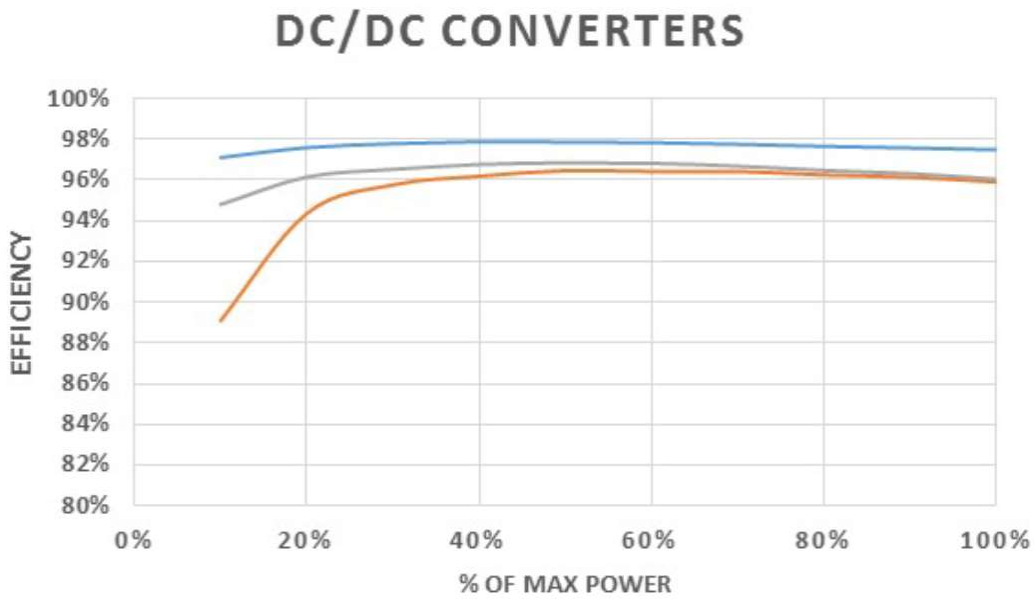

Figure 3.13 Sample efficiency variation with respect to partial load of DC-DC converters (Vossos et al., 2017)

The energy source for the system operations and other equipment will be supplied by utility electricity as it has to be uninterrupted. The efficiencies of AC-AC transformers lie in the range of 97 - 99.5 % and efficiency curve is as shown in Figure 3.14.

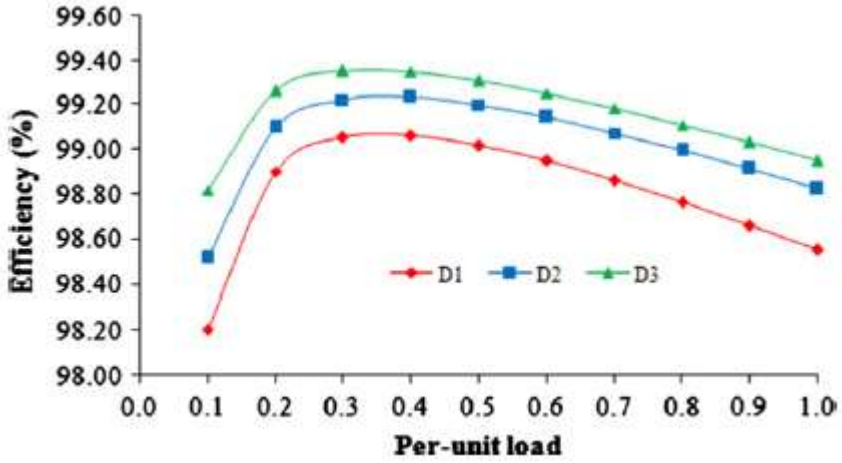

Figure 3.14 Sample efficiency variation with respect to partial load of AC-AC transformers (Georgilakis, 2011)

3.3. Gas Separators & Dryers

Having many ways of drying hydrogen, the most common methods for electrolysis are TSA and PSA. TSA requires low temperatures such as 5°C (Bessarabov et al., 2018) where PSA requires room temperature (T. Ohta and Veziroglu, 2007). Therefore, the hydrogen product containing water vapour is to be cooled down to 5°C by using chilled water.

3.4. Water Treatment and Supply

PEM electrolyzers need water at high purity to operate. Figure 3.15 is a schematic of a standard reverse osmosis (RO) system application.

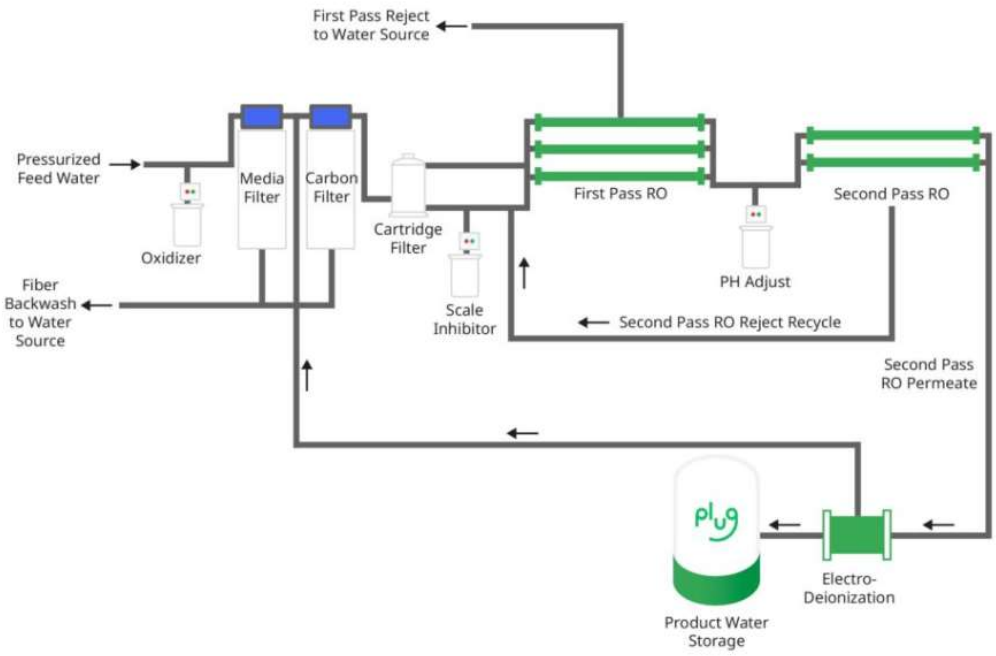

Figure 3.15 RO system schematic by Plug Power (Plug Power Inc., 2022a)

Once there is deionized water available within the system or from an external source, it is pumped into the system via a booster pump set. The booster pump also provides the pressure for the anode side and its flow rate is determined by the rate of reaction. The design capacity for the booster pump could be determined by the full loading conditions of the electrolyzer.

3.1. Cooling Circuit and Components

It was observed that the PEM stack is generally cooled by providing a heat exchanger on the anode circulation circuit where the temperature of the feed water is dropped in order to cool the stack. There are also examples of having another circulation circuit on the cathode side in order to decrease the velocity of cooling water or having separate cooling channels inside the stack (Tiktak, 2019). However, these are limited to modeling and laboratory studies and could not be observed in commercial plant schematics. Commercial PEM catalogues show that cooling is provided from the anode side only as previously mentioned.

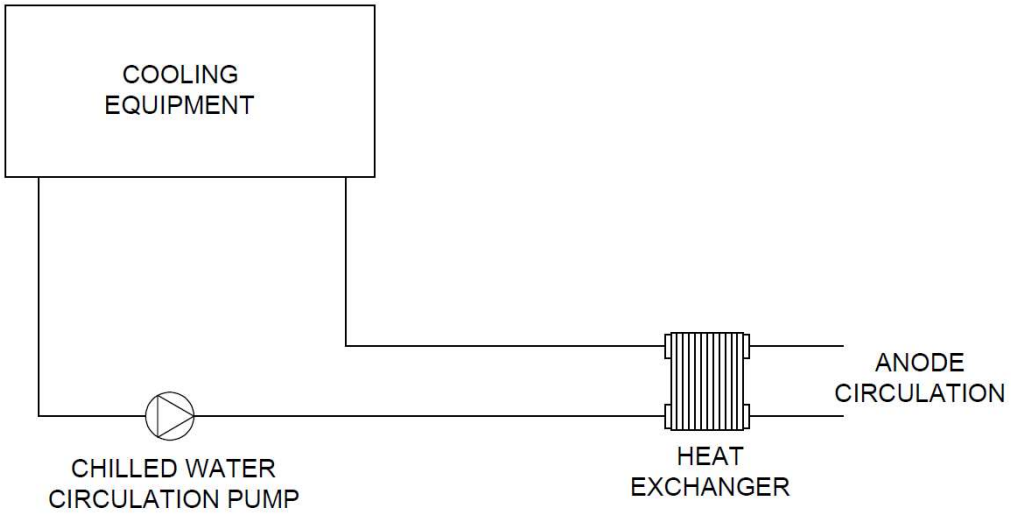

Figure 3.16 PEM stack heat rejection schematic

Commercial PEM systems generally use dry coolers for the heat rejection of the stacks. Dry coolers consist of water coils and fans that cool the water with ambient air.

Figure 3.17 Dry cooler by Refteco (REFTECO Srl, 2023)

In this study cooling towers will also be utilized for heat rejection of the stack in order to observe the difference between the two options in terms of total system efficiency.

Cooling towers consist of a box like closed steel case with air openings on certain places and a large fan. The cooling process is carried out by spraying water on fills and using outside air for cooling by using the effect of evaporation. Cooling towers could operate at lower loop temperatures as their performance is dictated by ambient air wet bulb temperature rather than dry bulb temperature.

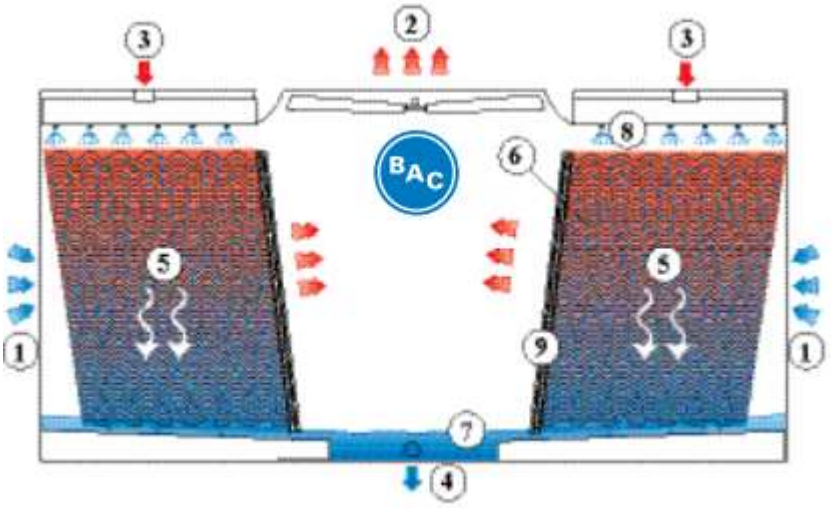

Figure 3.18 Cooling tower diagram by BAC (Baltimore Aircoil Company, 2023)

The cooling unit design capacity could be determined by the maximum operating voltage and capacity of the electrolyzer. For example, if the electrolyzer maximum voltage is determined to be 2.1 V, the HHV efficiency would be 70% which means that 30 % of the energy would be excess heat. If the electrolyzer capacity were to be 1 MW, that would result in having a design capacity of 300 kW cooling.

The stack cooling circulation pump flow is determined by the cooling capacity and ΔT.

$$\dot{m}_{stack,cooling} = \frac{\dot{Q}_{stack,\ cooling}}{c_p \cdot \Delta T_{stack\ cooling}} \tag{3.1}$$

For the anode circulation side, the flow and temperature difference required is determined by λ_{H2O} as mentioned in section 2.5. It is mentioned by Bessarabov and Millet (2018b) that λ_{H2O} ranges between 10 - 100 depending on the system. Considering it being 100 at maximum, the least ΔT required for the anode side would be around 15°C for a cell voltage of 2.1 V. The anode circulation pump capacity is determined by the maximum mass flow of the stack feed water.

$$\dot{m}_{anode\ circulation} = \dot{m}_{stack} \cdot \lambda_{H_2O} \quad (\lambda_{H_2O}=10\text{-}100) \tag{3.2}$$

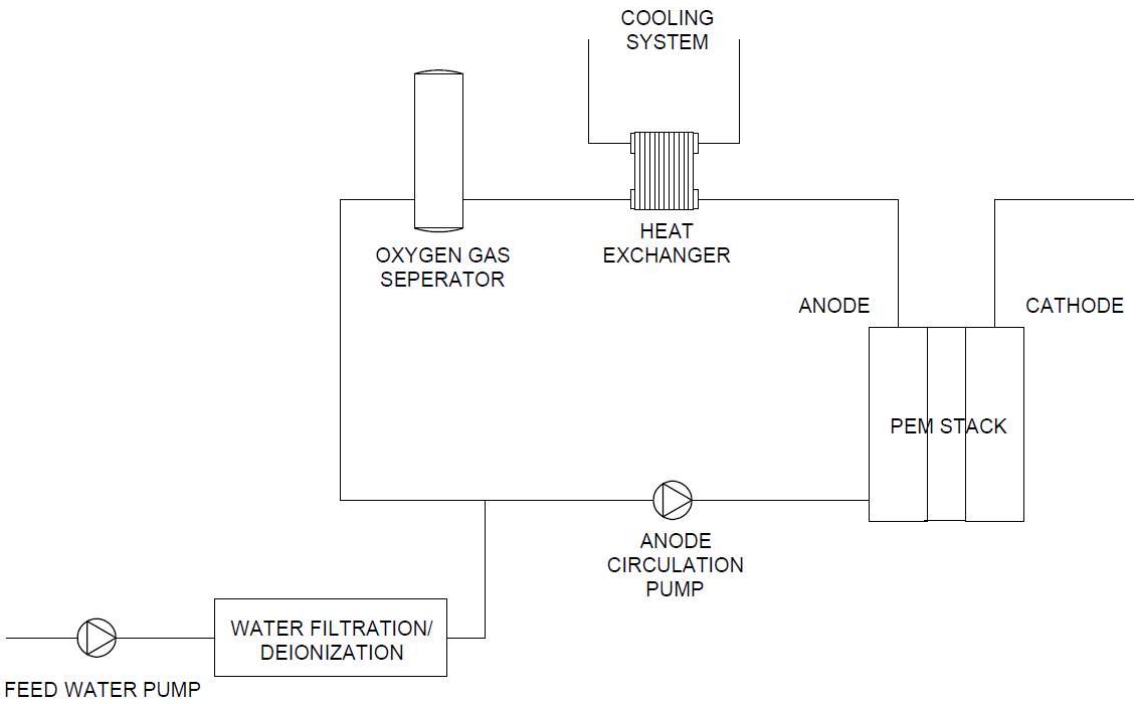

Figure 3.19 System anode side

As mentioned in previous sections, the hydrogen generated from the stack has to be cooled down to temperatures as low as 5°C for drying which would need to be carried out by air-cooled chillers for low to medium capacities and water-cooled chillers for medium to higher capacities. Chillers usually operate at a temperature range of 5-12°C with a ΔT of around 5-6°C. Air-cooled chillers are package units whereas water-cooled chillers require a cooling tower.

Table 3.2 Table of chiller types with approximate capacity ranges (images taken from(Daikin Airconditioning UK Limited, 2016; Carrier, 2023; Evapco .Inc, 2023))

 		Air-cooled chillers with scroll type compressors	< 700 kW
		Air-cooled chillers with screw type compressors	100 – 2000 kW
		Water-cooled chiller with scroll type compressors	< 200 kW
	+ 	Water-cooled chiller with screw type compressors	250 <> 1500 kW
		Water-cooled chiller with centrifugal type compressors	700 <> 20000 kW

Over a capacity of 2000kW, air-cooled chillers could be parallel connected in order to increase capacity or water-cooled chillers maybe used for greater capacities which includes the chiller, cooling tower, circulation pump and makeup water booster pump.

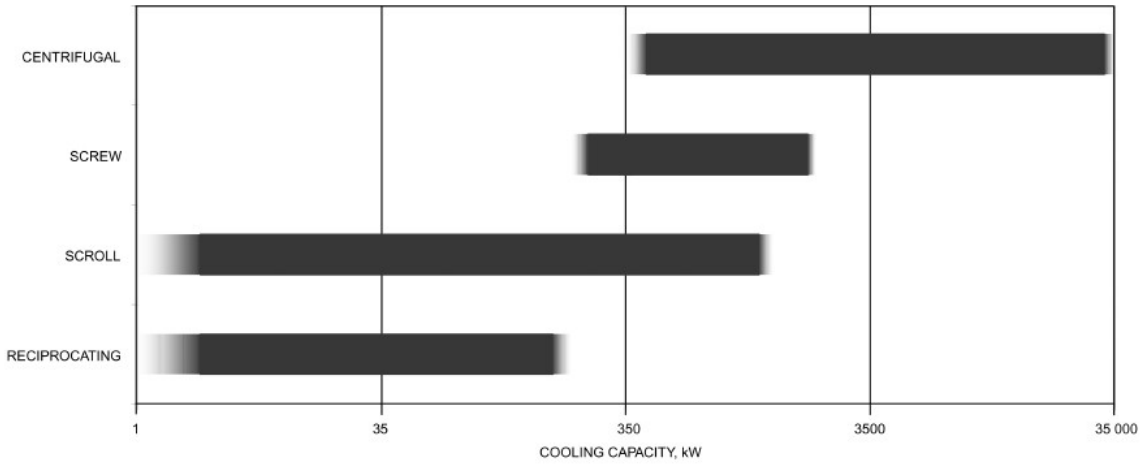

Figure 3.20 Water cooled chiller availability range according to compressor type. (American Society of Heating, Refrigerating and Air-Conditioning Engineers, 2020)

Table 3.3 Water chiller types. ASHRAE 90.1

Individual Chiller Plant Capacity	Electric Chiller Type
≤ 352 kW	Scroll
>352 kW, <1055 kW	Screw
≥1055 kW	Centrifugal

The hydrogen product containing water vapour is to be cooled from around 80°C to 5°C. In order to calculate the cooling load, the ratio of water vapour to gas should be calculated as follows:

$$\frac{\dot{m}_{H_2O}}{\dot{m}_{H_2}} = \frac{\dot{n}_{H_2O}.MM_{H_2O}}{\dot{n}_{H_2}.MM_{H_2}} \tag{3.3}$$

$$\frac{\dot{n}_{H_2O}}{\dot{n}_{H_2}} = \frac{p_{H_2O}}{p_{H_2}} = \frac{p^0_{H_2O}}{p_c - p^0_{H_2O}} \tag{3.4}$$

The molar ratio of water vapour to hydrogen can be calculated by using the vapour pressure of water at given temperature and the pressure of the cathode side. After finding the molar ratio, the mass ratio is calculated by multiplying the molar mass. The mass flow of hydrogen produced is already calculated in the

PEM model. Therefore, the mass flow of water vapour is determined and both mass flow rates are used in the Equation 3.5 by making use of their specific heats to cool them to 5°C.

$$\dot{Q}_{drying}=\left(\dot{m}_{H_2O}.c_{p,H_2O}+\dot{m}_{H_2}.c_{p,H_2}\right).\Delta T \tag{3.5}$$

3.2. PV Plant

The energy source for green hydrogen production can be provided by any renewable system. In this study, solar power is incorporated into the system.

The intensity of solar radiation determines the power produced by solar panels. The intensity is variable within the day because of the daily rotation of the sun and also differs throughout the year as the angle between the earth and sun's axis changes. The angle of the sun rays determines the length which light takes through the atmosphere. The lower the angle of incidence, the more length the rays have to travel in the atmosphere thus lowering the intensity of the incoming rays because of the absorption, scattering and reflection in the atmosphere.

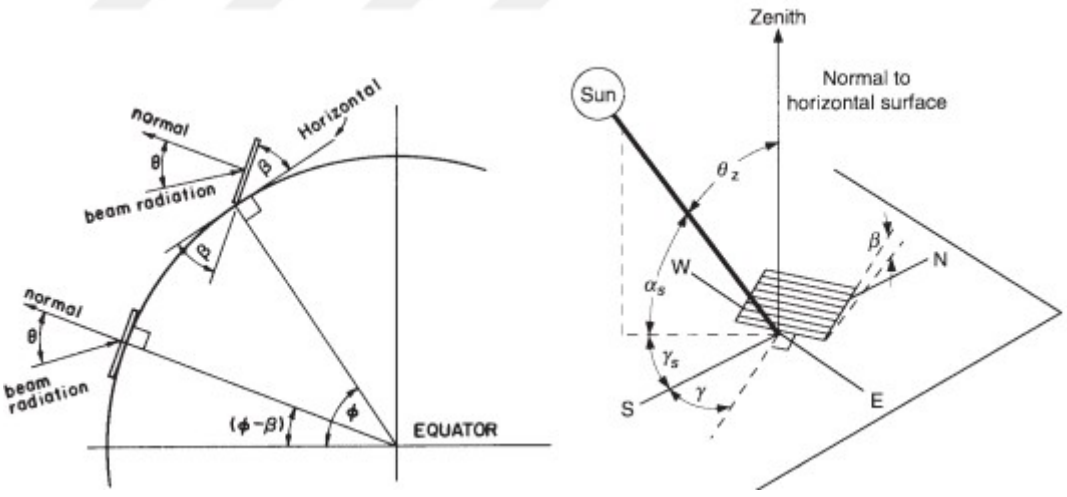

Figure 3.21 Visualization of solar incident angles (Duffie and Beckman, 2013)

The weather conditions also effect the power production on solar plants as cloudiness, rain and snow affect solar radiation.

In this study, energy yield data from PV panels is utilized for the PEM system simulation. The angle of the panel also affects the power production as rays coming at a perpendicular direction to the panel surface will result in more power generation.

The PV plant simulation in this study is conducted on System Advisory Model program which is a freely available program developed by the NREL. The design parameters to be used for the simulations will be collector selection, system capacity, angle of collector, distance between collector rows and location. Further details related to PV plants are provided in Chapters 4 and 5.

4. SYSTEM MODELING

The modeling and simulation of the system is carried out as shown in the schematic Figure 4.1.

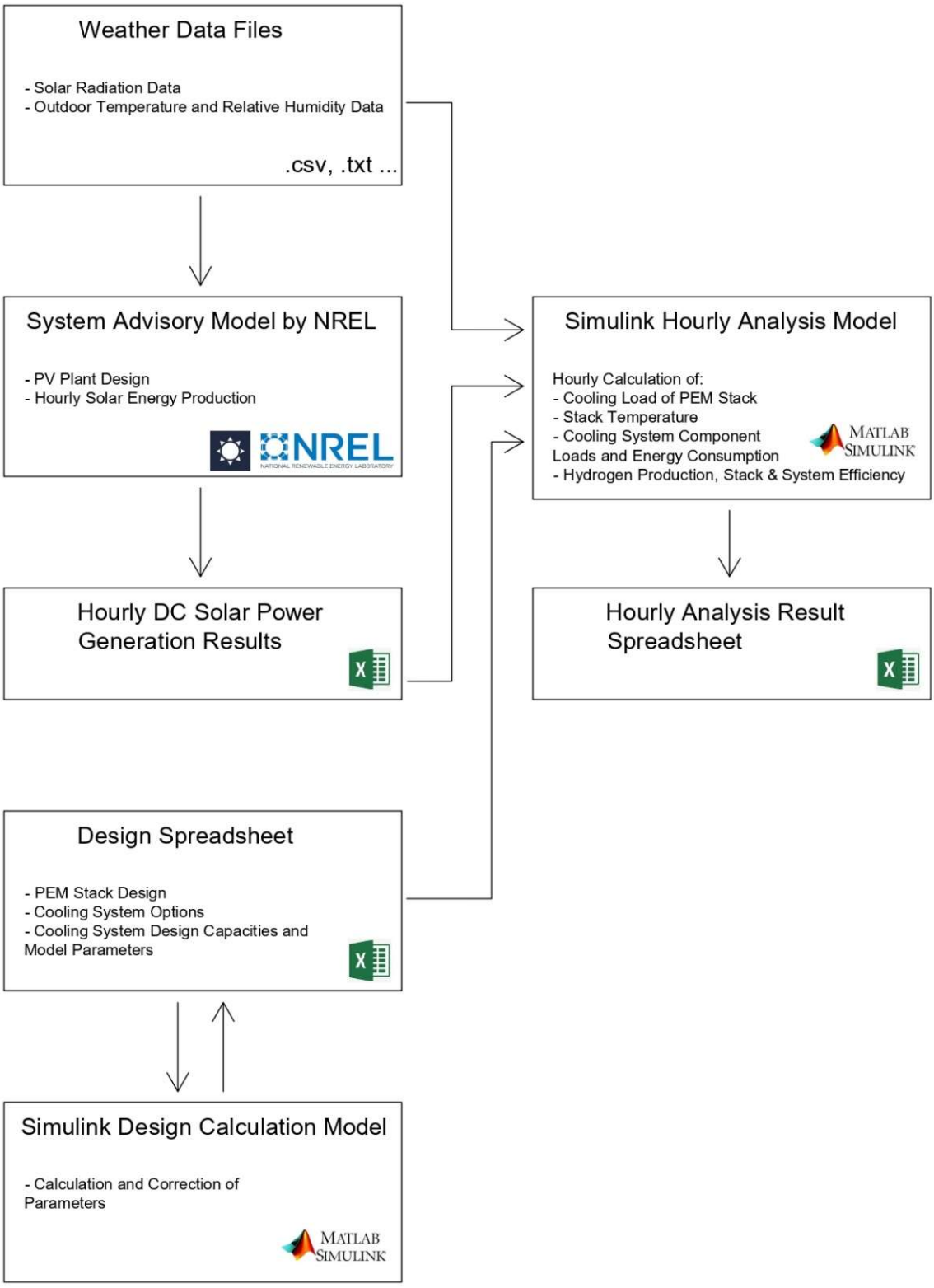

Figure 4.1 Modeling configuration and operation schematic

The plant design is carried out in a spreadsheet and parameters that need to be calculated or corrected by empirical models are implemented by a Simulink model which the results are transferred back to the spreadsheet. This spreadsheet provides the system parameters for a separate hourly analysis Simulink model.

The PV design and simulation is carried out in System Advisory Model environment which results in hourly DC power gain from solar as hourly data stored in a spreadsheet and then fed to the hourly analysis Simulink model.

The weather data file is utilized in SAM for PV plant simulation and in the hourly analysis Simulink model for the performances of cooling devices.

After the Simulink model is run, hourly data related to the PEM stack, cooling equipment, hydrogen production and water consumption are exported to a final spreadsheet to be reviewed and visualized by plots.

4.1. PEM Electrolyzer Modeling

In order to determine the efficiency of the electrolyzer, the I-V curve should be modeled and fitted with experimental data from the literature. Table 4.1 is the list of equations used for the I-V model.

Table 4.1 List of equations used for modeling of PEM stack

I-V Curve Modelling Equations	
Open Circuit Voltage	$V_{ocv} = 1.229 - 8.46x10^{-4}(T-298) + \frac{R.T}{2.F}.\ln\left(\frac{p_{H_2}}{p_C}\right)\sqrt{\frac{p_{O_2}}{p_A}}$
	$p^0_{H_2O} = \exp\left(11.676 - \frac{3816.44}{T-46.13}\right)$
	$p_{H_2} = p_C - p^0_{H_2O}$
	$p_{O_2} = p_A - p^0_{H_2O}$
	$V_{act,a} = \frac{RT}{\alpha_a.z.F}.\text{arcsinh}\left(\frac{i}{2.i_{0,a}}\right)$

Activation Voltage	$V_{act,c}=\frac{RT}{\alpha_c.z.F}.\text{arcsinh}\left(\frac{i}{2.i_{0,c}}\right)$
Ohmic Voltage	$V_{ohm}=i.(r_{total}+r_{mem})$
	$r_{mem}=\frac{\delta_m}{\sigma_m}$
	$\sigma_m=(0.005139\lambda-0.00326).\exp\left[1268.\left(\frac{1}{303}-\frac{1}{T}\right)\right]$

Table 4.2 List of the variables used in the determination of the I-V curve

I-V Curve Determining Variables	
T_{cell}	Cell Temperature
p_A	Anode Pressure
p_C	Cathode Pressure
$i_{0,a}$	Anode Exchange Current Density
$i_{0,c}$	Cathode Exchange Current Density
α_a	Anode Charge Transfer Coefficient
α_c	Cathode Charge Transfer Coefficient
λ	Water Constant
δ_m	Membrane Thickness
r_{total}	Other Cell Resistance

The first I-V curve model was determined for a commercial 225 kW electrolyzer from GinerX (Acquired by PlugPower in 2020) where experimental data were taken from Harrison (2021). Electrolyzer information is listed below.

- Cell Active Area: 1,250 cm^2
- Stack contains 29 cells
- Operating Pressure: 40 bar
- Operating Temperature: 70°C
- Nominal Operating Current: 3,750 A (Current density 3 A/cm^2)

The initial parameters for the I-V curve model are listed in Table 4.3.

Table 4.3 List of I-V curve model parameters

I-V Curve Model Parameters	
T_{cell}	70°C
p_A	40 bar
p_C	40 bar
$i_{0,a}$	$1x10^{-6}$ A/cm^2
$i_{0,c}$	$1x10^{-3}$ A/cm^2
α_a	0.5
α_c	0.5
λ	24
δ_m	5 mils (127 μm)
r_{total}	0.090 Ω.cm^2

The exchange current densities were estimated from literature. The water factor for the calculation of membrane resistance was assumed 24 and the membrane thickness is already known. The r_{total} as mentioned in previous chapters consist of the electric resistance other than the membrane. The activation potential is almost constant after exceeding a current density of 1 A/cm^2. Therefore, it can be assumed that the slope of the I-V curve after 1 A/cm^2 indicated the resistance of the cell. Subtracting r_{mem} from the slope value would result in r_{total}. The slope is around 0.155 Ω.cm^2 and r_{mem} is calculated as 0.065 Ω.cm^2 resulting in 0.090 Ω.cm^2 for r_{total}.

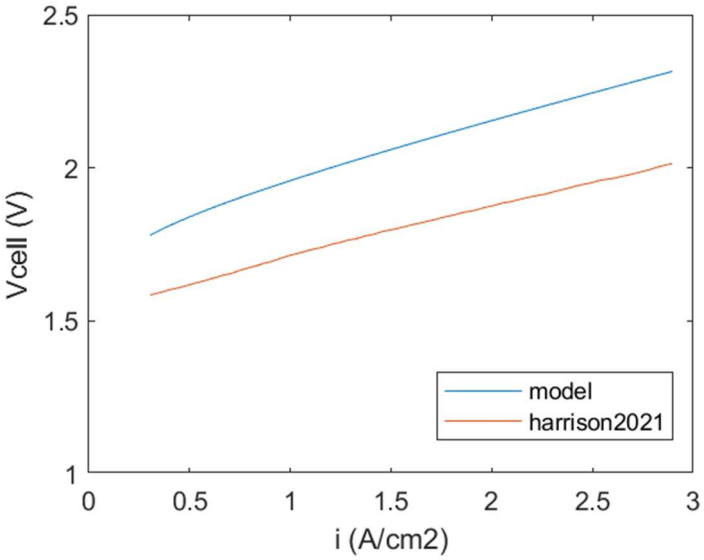

Figure 4.2 Initial I-V curve comparision of PEM model and (Harrison, 2021)

The resulting model needs correction as it has an error of abour 15%. It is observed that the effect of the activation voltage on the slope of the curve after 1A/cm^2 is around 0.022 Ω.cm^2 and there is an offset between the curves due to the activation voltage. Therefore, the model as improved by decreasing r_{total} to 0.068 Ω.cm^2 and increasing the exchange current densties of anode and cathode to 2x10^{-5} and 1x10^{-1} A/cm^2 resulting in a better fit with an average error of 0.5%.

Table 4.4 List of I-V curve model corrected parameters

Corrected I-V Curve Model Parameters	
T_{cell}	70 °C
p_A	40 bar
p_C	40 bar
$i_{0,a}$	2x10^{-5} A/cm^2
$i_{0,c}$	1x10^{-1} A/cm^2
α_a	0.5
α_c	0.5
λ	24
δ_m	5 mils (127μm)
r_{total}	0.068 Ω.cm^2

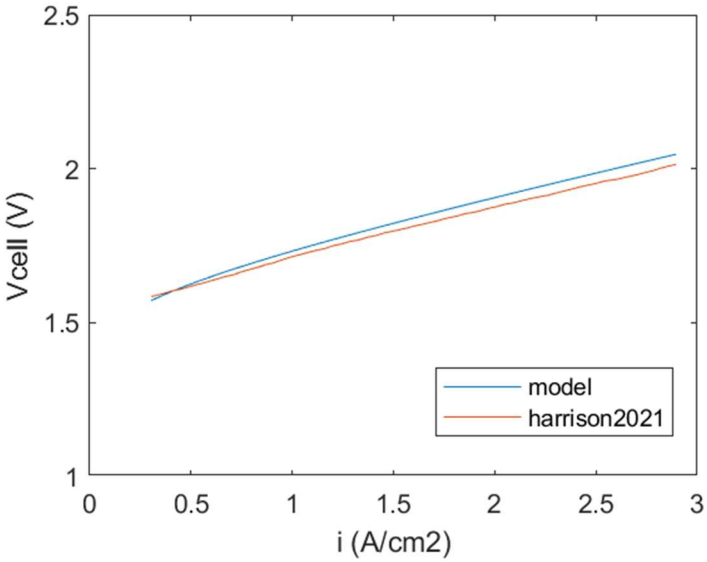

Figure 4.3 Final I-V curve comparision of PEM model and Harrison (2021)

Villagra (2019) performed experiments and modeling for different membrane thicknesses and taking into account the roughness of the membrane surface.

Table 4.5 Model parameters of (Villagra and Millet, 2019)

Table 1 – Fit parameters of the I–V curves of Fig. 8.

	Membrane dry thickness (μm)	Temperature (°C)	R_{cell} (mΩ cm^2)	j_0^a (A cm^{-2})	r_f^a (adim)	i_0^c (A cm^{-2})	r_f^c (adim)
Curve (a)	178	80	250	10^{-6}	5	10^{-3}	150
Curve (b)	178	80	210	10^{-6}	25	10^{-3}	150
Curve (c)	127	80	160	10^{-6}	60	10^{-3}	150
Curve (d)	51	80	92	10^{-6}	75	10^{-3}	150
Curve (e)	25	80	50	10^{-6}	75	10^{-3}	210

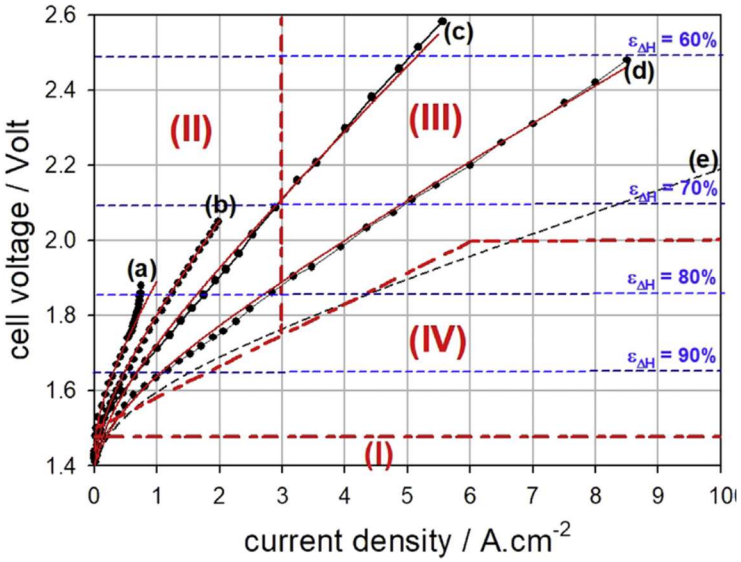

Figure 4.4 I-V plot of experimental values and model of Villagra and Millet (2019)

The current model was compared by only changing the thickness value of the membrane, temperature and pressure.

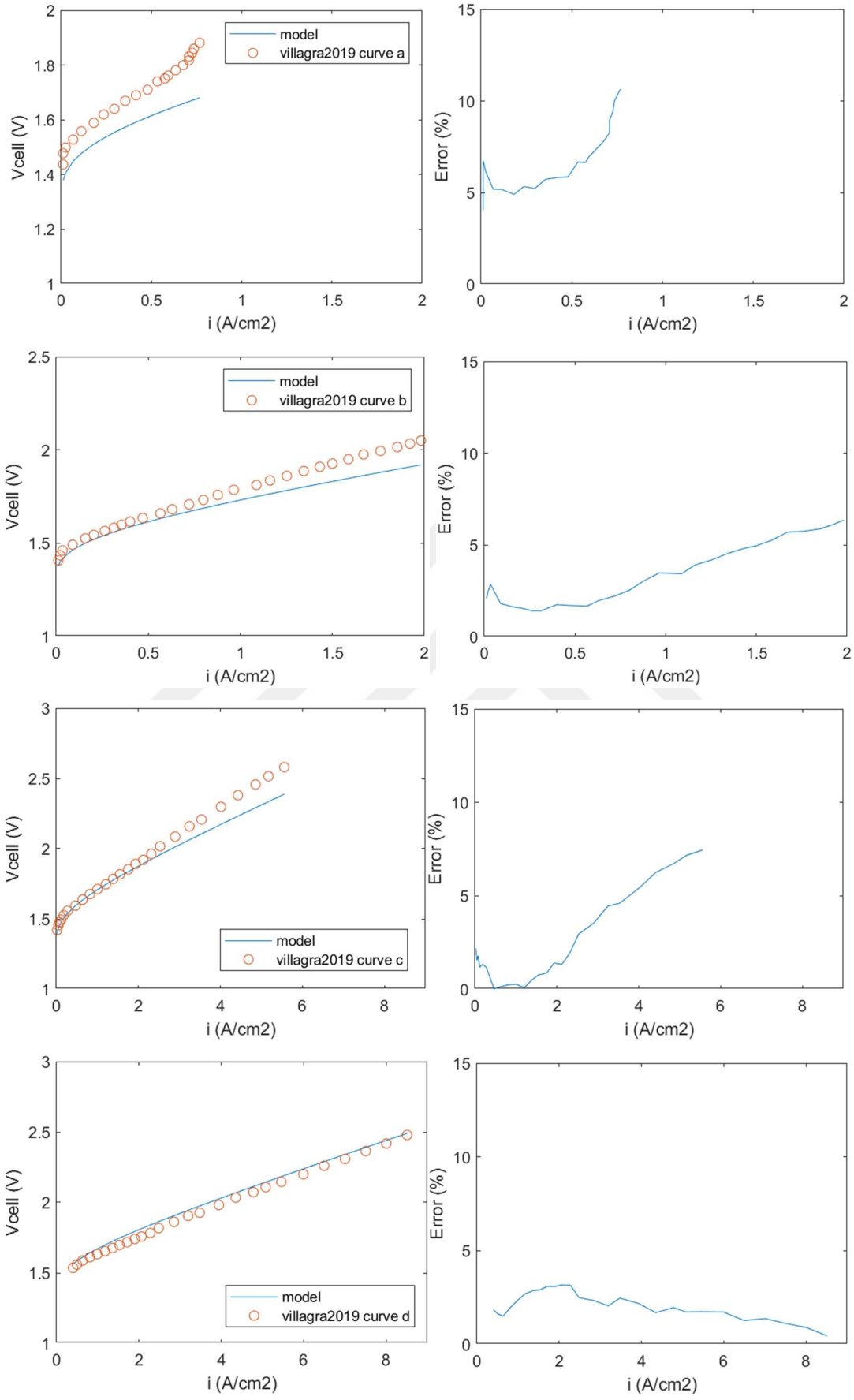

Figure 4.5 I-V and error plots of comparison between Villagra and Millet (2019) and final model

Table 4.6 Model parameters used in modeling for Villagra and Millet (2019) data

	Villagra2019 curve a	Villagra2019 curve b	Villagra2019 curve c	Villagra2019 curve b
T_{cell}	80°C	80°C	80°C	80°C
p_A	15 bar	15 bar	15 bar	15 bar
p_C	15 bar	15 bar	15 bar	15 bar
$i_{0,a}$	2x10^{-5} A/cm2	2x10^{-5} A/cm2	2x10^{-5} A/cm2	2x10^{-5} A/cm2
$i_{0,c}$	1x10^{-1} A/cm^2	1x10^{-1} A/cm^2	1x10^{-1} A/cm^2	1x10^{-1} A/cm^2
α_a	0.5	0.5	0.5	0.5
α_c	0.5	0.5	0.5	0.5
λ	24	24	24	24
δ_m	178 μm	178 μm	127 μm	51 μm
r_{total}	0.068 Ω.cm^2	0.068 Ω.cm^2	0.068 Ω.cm^2	0.068 Ω.cm^2
ε_{max}	10.6 %	6.4 %	7.5 %	3.2 %

The model seems acceptable when compared to experimental data and the difference can be due to the fact of having different resistance values for the components other than the membrane. As mentioned earlier, the electrolyzer tested Harrison (2021) is a commercial electrolyzer manufactured by Giner Inc. (Acquired by PlugPower in 2020) and had a capacity of 225 kW for the purpose of testing although it did perform at 217.8 kW @Vcell=2 V. The actual electrolyzers used in application are 1 MW as mentioned in PlugPower catalogues which is obtained by increasing the number of cells in the stack to 129. The model parameters are used from mentioned study and can be simulated for different temperature and pressure values.

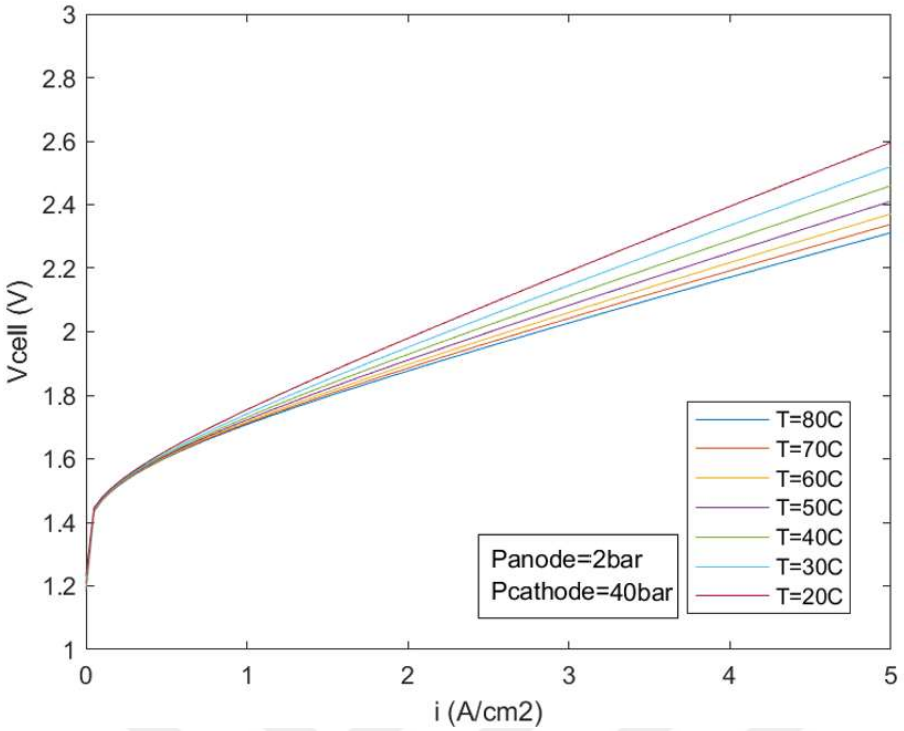

Figure 4.6 I-V curve variation of final model at different temperatures.

The nominal temperature to be used in the model is 80°C and the cathode and anode pressures are 40 and 2 - 3 bars respectfully. As commercial electrolyzers are able to withstand operation under differential pressure, keeping the anode at low pressure would decrease the head of the feed water pump thus decreasing the energy consumption. The cathode pressure is the maximum pressure the electrolyzer could operate as per PlugPower catalogues. The higher the pressure of hydrogen that is produced, the lesser energy consumption on the hydrogen compressor.

The stack voltage and power are calculated from Equations 4.1 to 4.3.

$$V_{stack} = V_{cell} \cdot N_{cell} \tag{4.1}$$

$$I_{stack} = i \cdot A \tag{4.2}$$

$$P_{stack}=V_{stack} \cdot I_{stack} \tag{4.3}$$

The Table 4.7 contains parameters of the electrolyzer to be used in model and its resulting curves.

Table 4.7 Electrolyzer stack model parameters to be used for simulations (1MW)

Electrolyzer Model Parameters	
A	1250 cm^2
n_{cell}	129
T_{cell}	80°C
p_A	40 bar
p_C	3 bar
$i_{0,a}$	$2x10^{-5}$ A/cm^2
$i_{0,c}$	$1x10^{-1}$ A/cm^2
α_a	0.5
α_c	0.5
λ	24
δ_m	5 mils (127 μm)
r_{total}	0.068 $\Omega.cm^2$

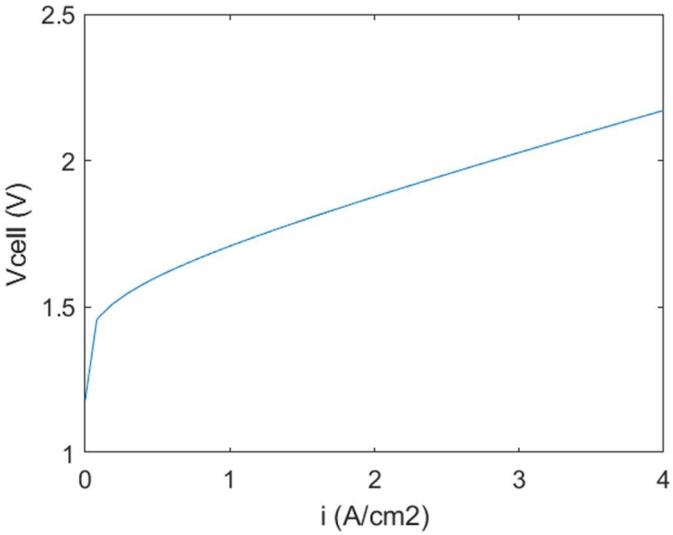

Figure 4.7 I-V curve plot of stack model

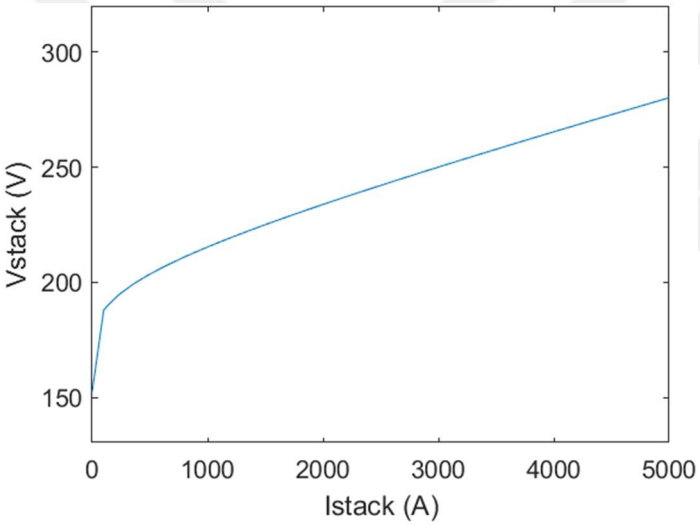

Figure 4.8 I-V curve plot of stack model

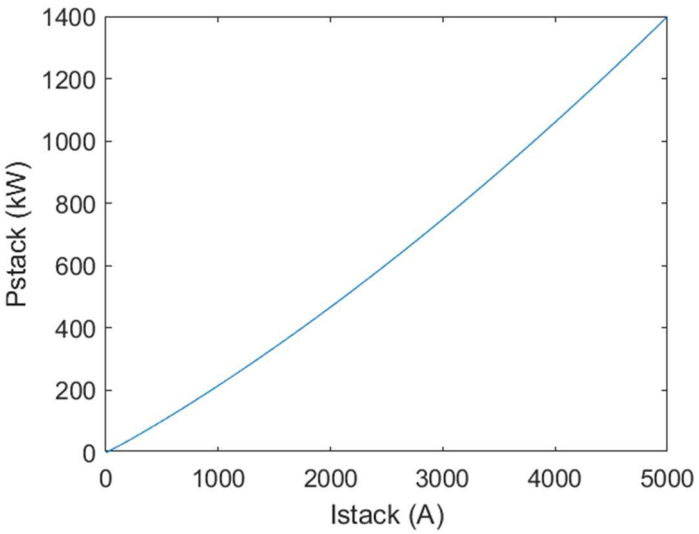

Figure 4.9 P-I curve plot of stack model

The HHV and LHV efficiency can be calculated as mentioned in previous chapters and Equations 4.4 and 4.5.

$$\eta_{cell,LHV} = \frac{V_{rev}}{V_{cell}} = \frac{1.23V}{V_{cell}} \tag{4.4}$$

$$\eta_{cell,HHV} = \frac{V_{tn}}{V_{cell}} = \frac{1.48V}{V_{cell}} \tag{4.5}$$

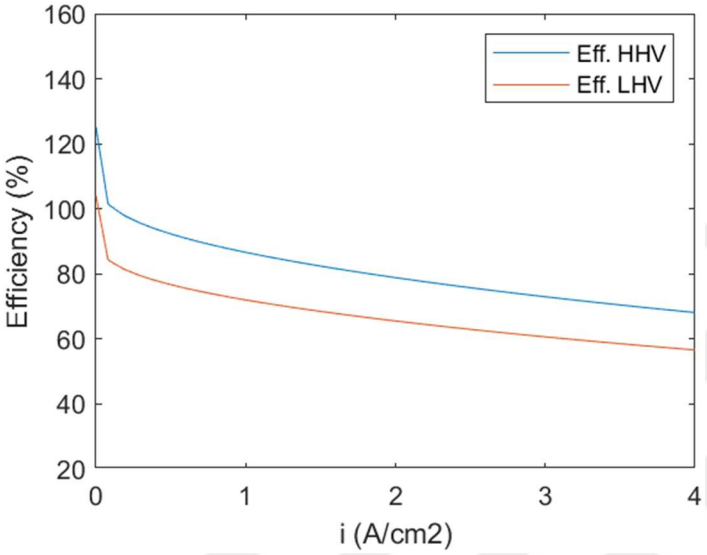

Figure 4.10 HHV and LHV efficiency curves of stack model

The HHV efficiency is seen to be over 100 % due to the fact that the electrical power is provided for the Gibbs energy, and the heat required for the endothermic reaction is provided by the heat generated by the voltage losses. When the heat generated due to voltage losses is lower than what is needed for the endothermic reaction, the HHV efficiency results over 100 %. This occurs at very low current densities and not at the electrolyzer's operating range of around 1.6 - 2.1 V.
The rate of hydrogen production is calculated from the current of the stack by Equations 4.6 and 4.7.

$$\dot{n}_{H_2,stack} = N_{cell} \cdot \frac{I_{stack}}{z.F} = N_{cell} \cdot \frac{I_{stack}}{2.F} \tag{4.6}$$

$$\dot{m}_{H_2,stack} = MM_{H_2} \cdot \dot{n}_{H_2,stack} = N_{cell} \frac{MM_{H_2} \cdot I_{stack}}{2.F} \tag{4.7}$$

where MM_{H2} is the molar mass of hydrogen ($2x10^{-3}$ kg/mol).

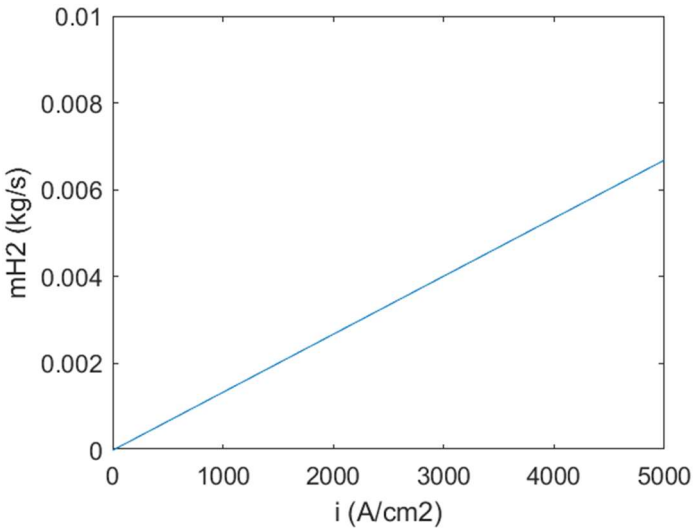

Figure 4.11 Plot of kg hydrogen production and current density

The consumption of water calculated and visualised as follows.

$$\dot{n}_{H_2O,stack} = \frac{1}{2}\dot{n}_{O_2,stack} = \dot{n}_{H_2,stack} \tag{4.8}$$

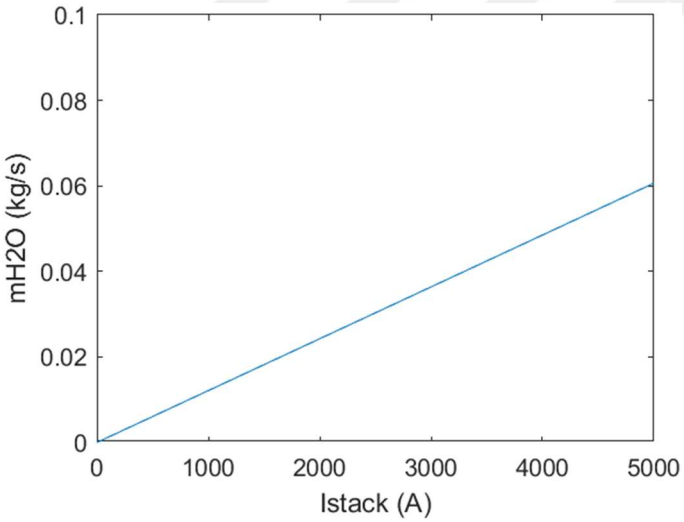

Figure 4.12 Plot of kg oxygen production and current

Since the PEM model operates on the I-V curve, the current density dictates the voltage of the PEM at partial loading. Therefore, since the analysis is carried out of renewable energy hourly data used as an input, the current density that satisfies the input power will be determined by iteration as power is the multiplication of current and voltage. This iteration will be performed for every time frame in order to produce correct data for real time temperature and energy input.

Hydrogen loss is calculated formula mentioned in Section 2.4

$$\dot{n}_{H_2loss} = \frac{D_{H2}}{H_{H2}} . \frac{P_c - P_a}{L} . A_{cell} . N_{cell} \quad (4.9)$$

where values of D_{H2} and H_{H2} are interpreted from (Grigoriev et al., 2011) for 80°C as $2.4x10^{-6}$ cm^2/s and 99129 $mol/cm^3.Pa$.

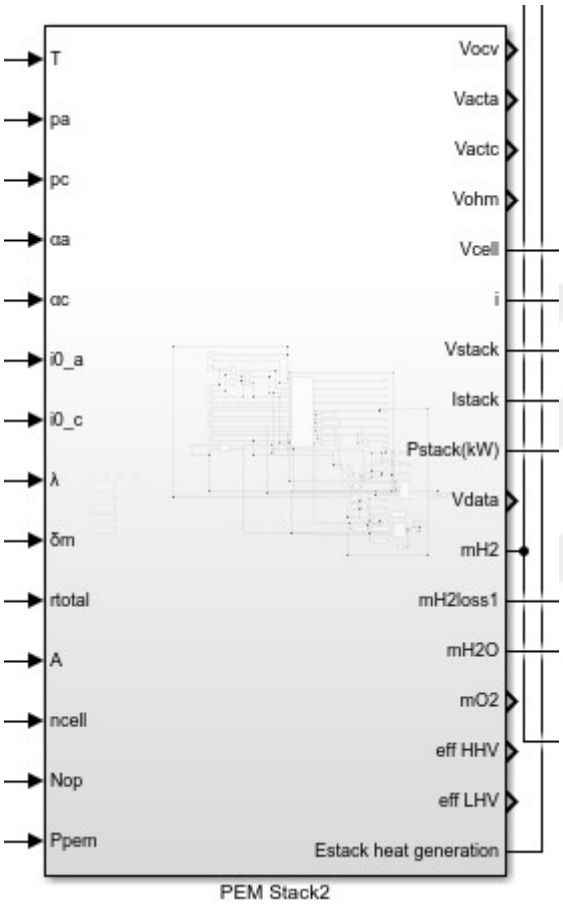

Figure 4.13 PEM stack model block

The model blocks in this study consist of Matlab function blocks or subsystems consisting of Matlab function blocks that perform the calculations by mentioned equations. As can be seen in the model block in Figure 4.13, the required cell parameters mentioned earlier are input to the left side of the model. The energy input comes from the DC-DC converter block that feeds the stack. All calculated parameters are available on the right side as the output for control and to be used for other blocks. The water consumption data is used in the booster pump block. The hydrogen produced is stored in the results spreadsheet and also used in the hydrogen purification block. The stack heat production data is used is adjusted in

the thermal model block and then used in the cooling system block to determine the performance of the dry cooler or cooling towers. The hydrogen loss data is stored in the results spread sheet and used in efficiency calculations.

There should also be a model to determine the stack temperature in varying operation capacities considering the thermal mass.
The thermal mass of a stack is to be calculated by the total mass and specific heat capacity as follows.

$$C_{th} = \sum c_{p,i} \cdot V_i \cdot \rho_i \qquad (4.10)$$

Tiktak (2019) states component thicknesses and properties for defining and could be used for reference in this calculation.

Table 4.8 PEM stack components and thermal capacity calculation from literature (Tiktak, 2019)

Layer/substance	Number of layers	Thickness	Specific heat $[kJ/kgK]$	Density $[g/cm^3]$	Thermal capacity $[kJ/K]$	Comment
Current collectors	200	1 mm	0.52	2.84	29.5	Titanium CC's Porosity: ϵ = 37 %
Bipolar plates	99	2 mm	0.52	4.51	29.0	Titanium BP's excluding channels for PW(flow distribution) and CW (62.5% titanium).
Process water	-		4.19	0.997	61.9	The amount of PW inside the stack at any given time. Equal to volume of pores of CC and flow distribution channels
MEA's	100	125 μm	-	-	-	Thin layer of Nafion 117 and electrodes of few micron thick
End plates	2	2 cm	0.46	8.00	14.7	Relatively thick stainless steel plates, mainly for support. Flow distribution channels not taken into account
Total					135.1	

Tiktak uses the membrane area to calculate the volume of all the components, however the actual area is greater than the membrane active area due to having borders for assembly and fluid flow channel connections. These borders could be on average of 20 % of the length of the active area which contributes to an increase of around 40 – 50 % of the component area. Tiktak has not included the water volume inside the stack for this calculation, however in this study, the circulation pump will be operating when the stack is operating even if there is no cooling in order to maintain the advantage of not producing diffusion resistance. Therefore, the water mass inside the circulation circuit should also be included in calculating the thermal mass.

For the model in this study, a 129 cell stack consumes a power of 1.186 MW @ V_{cell}=2.1 V. The thermal mass for such stack is calculated in Table 4.9.

Table 4.9 PEM stack components and thermal capacity calculation to be used in the simulations

Layer Substance	Number of layers	Active area (cm2)	Expected component area (+%50) (cm2)	Thickness (mm)	Material actaul volume factor	Volume (cm3)	Density (g/cm3)	Specific heat (kJ/kg.K)	Thermal capcaity (kJ/K)	Comment
Current collectors	258	1250	1875	1	0.63	30476.25	4.54	0.52	71.9	Titanium CC's Porosity: ε = 37 %
Bipolar plates	128	1250	1875	2	0.8	38400	4.54	0.52	90.7	Titanium material excluding chanels assumed to be %80 of plate volume
Process water (stack)	-	-	-	-	-	27498.75	0.997	4.19	114.9	The amount of water inside the stack
Process water (circuit piping)	-	-	-	-	-	43300	0.997	4.19	180.9	The amount of water estimated in the anode circuit piping. SCH40 2" pipe 20 m , 2.165 kg/m
MEA's	129	1250	1875	0.125	-	3023.438	-	-	-	Nafion 117
End plates	2	1250	1875	20	1	7500	8	0.46	27.6	Stainless steel end plates
Total									486.0	

The thermal mass of the stack results in 486 kJ/K. Operating the stack at maximum capacity at V_{cell}= 2.1 V will result in a heat production of 305.2 kW. This means that at constant operation at maximum capacity without the cooling system, the stack can raise its temperature from 20°C to 80°C at 83 s. Although it seems that the thermal mass is negligible since hourly analysis is conducted in this study, the time it takes to for the stack to warm up to 80°C at partial loads should also be investigated.

Table 4.10 PEM stack heating durations at low partial load operations

PEM stack partial load (%)	Vcell (V)	Power consumption (kW)	Heat generated (kW)	Time taken to increase temperature 20-80C at constant operation (min)
4.6%	1.52	54	1.4	347.1
5.2%	1.53	62	2	243.0
5.9%	1.54	70	2.7	180.0
6.6%	1.55	78	3.5	138.8
7.3%	1.56	86	4.4	110.4
8.2%	1.57	97	5.6	86.8
8.9%	1.58	105	6.6	73.6
10%	1.59	116	8	60.7
11%	1.60	127	9.5	51.2
12%	1.61	138	11.1	43.8
15%	1.64	175	17.1	28.4
20%	1.68	233	27.7	17.5
30%	1.75	350	54	9.0
40%	1.815	475	87.7	5.5
50%	1.87	592	123.5	3.9
60%	1.92	706	161.8	3.0
70%	1.97	833	207.3	2.3
80%	2.015	949	252	1.9
90%	2.06	1073	302.1	1.6
100%	2.10	1186	350.2	1.4

As mentioned earlier, since the analysis is carried out by calculating steady state formulas on hourly data, it seems that operating capacity of about 10 % and below will be affecting the analysis at start temperature of 20°C. This situation can only occur at the first start of the day. The heat loss of the PEM stack from the surface of the stack should be further investigated in order to predict if the PEM stack could cool down to temperatures as low as 20°C and also the time it takes to heat more accurately.

The heat loss consists of convection and radiative heat transfer.

$$Q_{loss} = Q_{conv} + Q_{rad} \quad (4.11)$$

Convective heat transfer from the surface of the stack to its surrounding is calculated by Equation 4.12.

$$Q_{conv} = h_c \cdot A_{st} \cdot (T_s - T_{amb}) \quad (4.12)$$

h_c: Convective heat transfer coefficient [W/(m^2K)]

A_{st}: Stack outer surface area [m^2]

T_s: Stack outer surface temperature is assumed as cell internal temperature [K]

T_{amb}: The temperature of surrounding air [K]

The surface area of the 1MW stack is around 1.28 m^2.

Nusslet number for forced convection is calculated using Equation 4.13.

$$\overline{Nu_f}=0.66Re_L^{0.675}Pr^{1/3} \quad (4.13)$$

For slow air moving at 0.2 m/s ReL=5000 and Pr=0.7, the heat transfer coefficient is obtained as:

$$h_c=\frac{\overline{Nu_f}.k}{L}=\frac{184 \text{ x } 0.025}{\sqrt{1250*1.5}/100}=10.6 \text{ Wm2/K} \quad (4.14)$$

Radiative heat transfer from stack surface to its surrounding is calculated by the Stefan Boltzmann Equation (4.15).

$$Q_{rad}=A_{st} .\epsilon.\sigma.\left(T_{st}^4 - T_{amb}^4\right) \quad (4.15)$$

ϵ : emissivity of the surface (assumed the value of stainless steel, 0.6)

σ : Boltzmann constant 5.67x10^{-8} W/m^2K^4

It can be assumed 80°C for stack surface temperature and 10°C for environment for the worst-case scenario which results in a convective heat transfer rate of Q_{con}=949.8 W and radiative heat transfer rate of Q_{rad}= 396.8 W.

As a result, Q_{loss} is 1347 W for the worst-case scenario. Therefore, after stopping the operation of the stack at 80°C, the required time for the stack to be cooled down to 20°C would be about 6 hours. This indicates that a model should be developed to calculate the cell temperature.

It should be noted that the effect of heating at the start of the operation will affect the first 5 hours of operation at worst case.

The model utilizes the hourly heat generation data of the stack subtracted by the heat loss of the stack to its environment. Then multiplying it by a period of 1 hour

and calculate the stack temperature without cooling involved. If the result is over 80°C, the cooling is activated and the stack temperature is set to 80°C. Otherwise, the cooling system will be on standby.

As can be seen in Figure 4.14, input values for calculating the thermal model are at the left of the block and the output values are on the right which are the stack temperature, and the adjusted cooling requirement is used in the cooling model block.

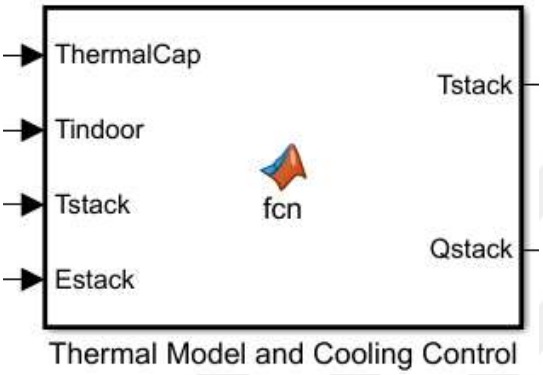

Figure 4.14 Thermal model block for PEM stack

4.2. System Component Modeling

It is important to model the system components in order to observe real time system efficiency.

4.2.1. Electrical Power Input Model

The electrical power input for the PEM stack is supplied by a DC-DC converter. And the BoP components will be powered by standard AC power supply from the grid. This application of the BoP is mentioned in PEM catalogues due to the need of having a constant power supply for the equipment.

4.2.1.1. DC-DC Converter Model

DC-DC converter model has a constant efficiency of 98 % for partial loads over 25 % and will have an efficiency decrease to 85 % at 5 % partial load.

The model is formed of a curve fit for the partial load range of 5 % - 25 %. The curve is a 3rd degree interpolating polynomial whose coefficients are calculated by the built in function “polyfit” in MATLAB.

$$\eta_{DC\text{-}DC}=\begin{cases} C1.PLR^4+C2.PLR^3+C3.PLR^2+C4.PLR+C5, & PLR\leq 0.25 \\ 0.96, & PLR>0.25 \end{cases} \quad (4.16)$$

C1	C2	C3	C4	C5
99.2912	-77.2829	18.6029	-1.0325	0.875

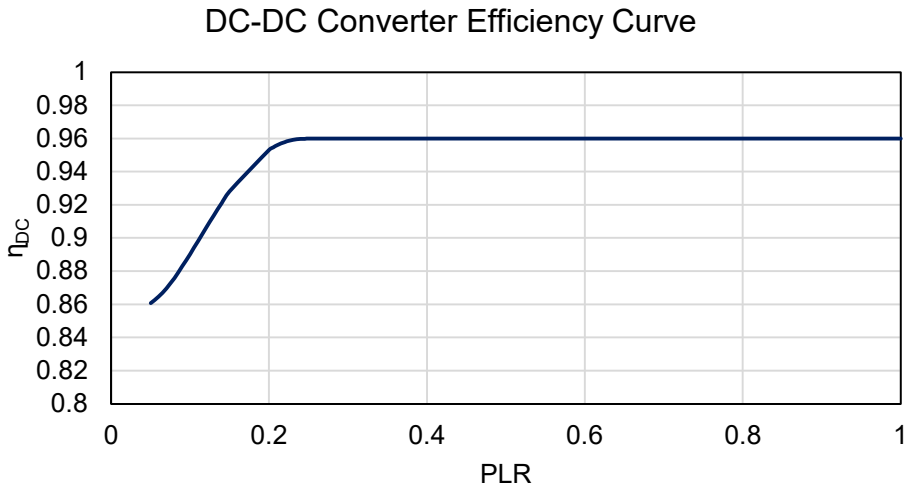

Figure 4.15 DC-DC efficiency graph

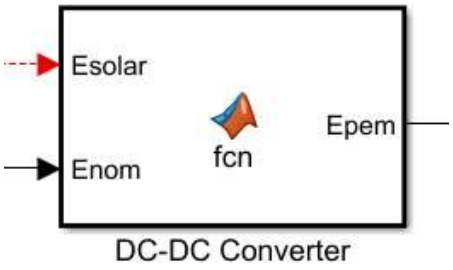

Figure 4.16 DC-DC converter model block

As shown in Figure 4.16, the DC converter block inputs are on the left of the model block. The incoming solar energy and nominal power design capacity are input to find the power supplied to the PEM stack after losses.

4.2.1.2. AC-AC Transformer Model

The AC-AC transformer model mentioned by Georgilakis (2011) could be utilized by Equation 4.17.

$$\eta_{AC} = \frac{PLR \,.\, P_{AC} \,.\, PR}{PLR \,.\, P_{AC} \,.\, PR + NLL + LL \,.\, PLR^2} \tag{4.17}$$

where,

P_{AC} : Rated Capacity of Transformer

PR : Power Ratio = 0.8

NLL : No-Load Loss

LL : Load Loss

NLL and LL values are taken from reference values provided in EN50464-1 standard.

Table 4.11 NLL and LL values mentioned in EN50464-1 standard.

Rated Voltage (kV)	Rated power (kVA)	No load losses Pb (W)	Load losses Py (W)
33	50	160	1050
	100	270	1650
	160	390	2150
	250	550	3000
	400	790	4150
	500	940	5000
	630	1100	5500
	800	1300	7000
	1000	1450	8900
	1250	1750	11500
	1600	2200	14500

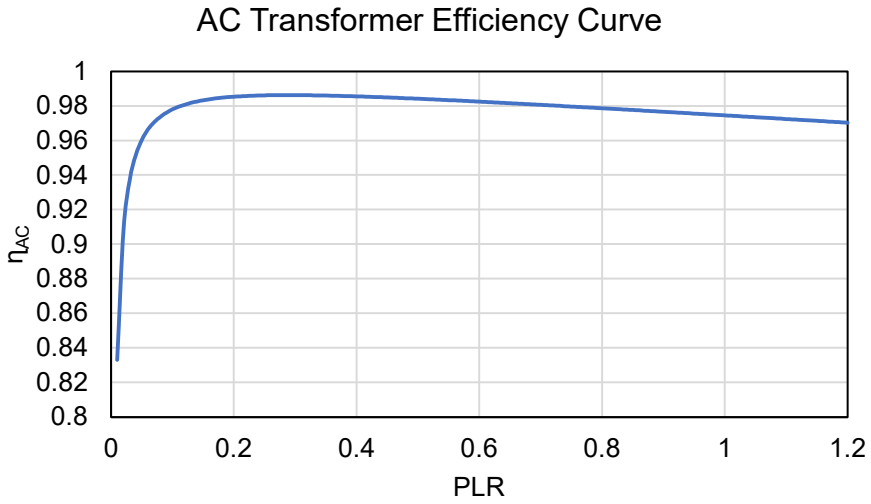

Figure 4.17 AC-AC transformer model sample efficiency curve

4.2.2. Cooling System Modeling

There are a few ways to design the cooling system. It should be noted that there are two locations in need for cooling. The first one is the anode circulation where the circuit is cooled for the purpose of cooling the PEM stack. The second place is the hydrogen cooling where the produced hydrogen should be cooled in order to condense and separate the water content. Stack cooling could be done in higher temperatures than chilled water as long as the required ΔT is ensured. On the hand lower tempertures are need for hydrogen separation where chilled water is needed. Therefore both needs can met by chilled water or the cooling systems could be segregated to dry/ evaporative cooler or cooling tower (high temperature cooling) for the PEM stack and chilled water for hydrogen seperation.

4.2.2.1. Chiller Model

The real time chiller COP is to be calculated by the “Electric Chiller Model Based on Condenser Entering Temperature” used by DOE-2.1 and EnergyPlus building energy simulation programs funded by the U.S. Department of Energy (COMNET, 2016; Pacific Northwest National Laboratory, 2016; U.S. Department of Energy, 2022). The same model is also used in other energy modeling programs.

The model includes three biquadratic performance curve functions which provide results at any given leaving chilled water temperature and condenser fluid entering temperature.

- Available cooling capacity - Temperature
- Energy input to cooling output - Temperature
- Energy input to cooling output ratio – Partial load

$$Q_{ch,available} = CAPFT \times Q_{ch,nominal} \quad (4.18)$$

$$CAPFT = a + b.T_{chws} + c.T_{chws}^2 + d.T_{cond} + e.T_{cond}^2 + f.T_{chws}.T_{cond} \quad (4.19)$$

$$EIRFT = a + b.T_{chws} + c.T_{chws}^2 + d.T_{cond} + e.T_{cond}^2 + f.T_{chws}.T_{cond} \quad (4.20)$$

$$EIRFPLR = a + b.PLR + c.PLR^2 \quad (4.21)$$

$$PLR = \frac{Q_{ch,operating}}{Q_{ch,available}} \quad (4.22)$$

$$P_{ch,operating} = P_{ch,nominal} \times EIRFPLR \times EIRFT \times CAPFT \quad (4.23)$$

where,

$Q_{ch,available}$ - chiller available capacity

$Q_{ch,operating}$ - present chiller load

T_{chws} – chilled water supply temperature

T_{cond} – condenser entering fluid temperature

$P_{ch,nominal}$ – rated power draw

$P_{ch,operating}$ – power drawn at operating conditions

$$COP_{ch,operating} = \frac{Q_{ch,operating}}{P_{ch,operating}} \quad (4.24)$$

It should be noted that T_{cond} is the temperature of the fluid entering the condenser where it is the temperature of the water supplied from the cooling tower for water-cooled chillers and the outdoor dry bulb temperature for air-cooled chillers. Coefficients used for calculating these functions could be found in EnergyPlus data sets which provide data of actual chiller models.

Sample coefficients that are to be used in the model are provided by (Pacific Northwest National Laboratory, 2016) as provided in Appendix 2. It should be

noted that coefficients provided are for calculations carried out in Fahrenheit. For this reason, the temperature values are converted to Fahrenheit inside the model block.

Chillers have a minimum unloading load ratio where the chiller cannot operate below that capacity. For situations where the required cooling capacity is less than the unloading ratio, the chiller will have to either operate at minimum unloading ratio (MUR) constantly or on an on/off cycle. It is required that the chiller does not operate at an on/off cycle for a long period (5-10 minutes the most). For this reason, there should be a separate limit for when the chiller must operate at an on/off cycle which is minimum partial load, PLR_{min}. PEM electrolyzers are to be operated to loads a low as 5 % therefore the PLR_{min} will be 0.05 for this study. Due to the fact that PLR_{min} is lower than MUR, the chiller will operate at MUR constantly when required load is between MUR and PLR_{min}, this causes false loading of the chiller. The chiller will start on/off cycling when the required load is below PLR_{min}.

For on/off cycling a cycling ratio CR will be calculated as the following.

$$CR = \min\left(\frac{PLR}{PLR_{min}}, 1\right) \tag{4.25}$$

And PLR will be revised as follows.

$$PLR = \max(PLR, MUR) \tag{4.26}$$

The false loading is calculated as by Equation 4.27.

$$Q_{false} = Q_{ch,available} \times PLR \times CR - Q_{ch,operating} \tag{4.27}$$

$P_{ch,operating}$ is also revised.

$$P_{ch,operating} = P_{ch,nominal} \times EIRFPLR \times EIRFT \times CAPFT \times CR \tag{4.28}$$

The condenser heat transfer rate is more than the evaporator as it is also responsible of the heat rejection of the compressor. The condenser load for the cooling tower is calculated by Equation 4.29.

$$Q_{cond} = Q_{ch,operating} + P_{ch,operating} + Q_{false} \tag{4.29}$$

As can be seen in Figure 4.18, the input parameters on the left are used to determine the power consumption, COP and condenser loop heat rejection requirement.

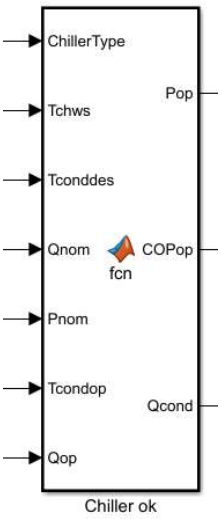

Figure 4.18 Chiller model block

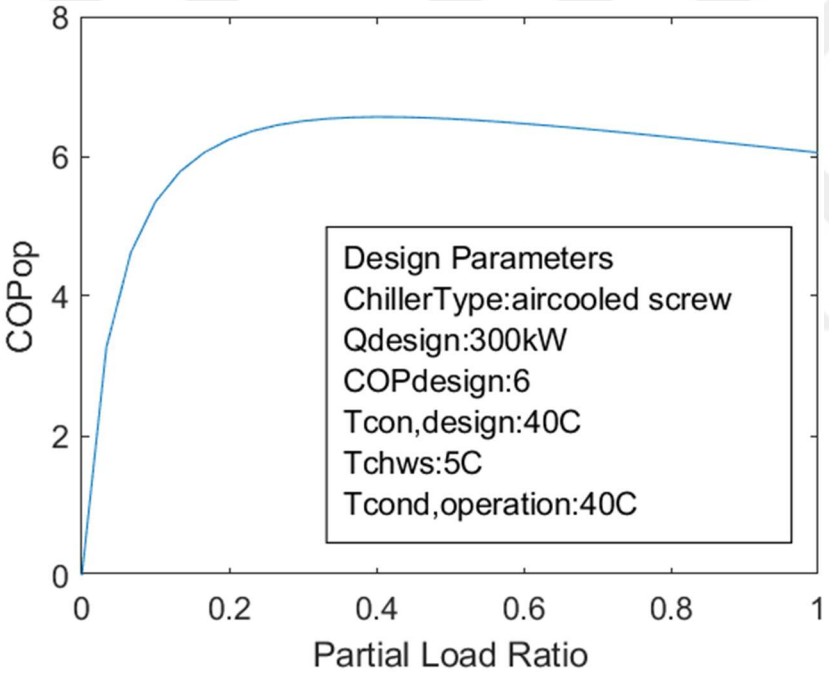

Figure 4.19 Chiller model sample efficiency curve

4.2.2.2. Cooling Tower Model

The cooling tower model from EnergyPlus is used in order to determine partial loads. Cooling towers operate according to outdoor wet bulb temperature, water inlet and outlet temperatures and capacity.

The range and approach of the cooling tower is the difference between water inlet - outlet temperature and water outlet – outdoor wet bulb temperature as illustrated by Figure 4.20.

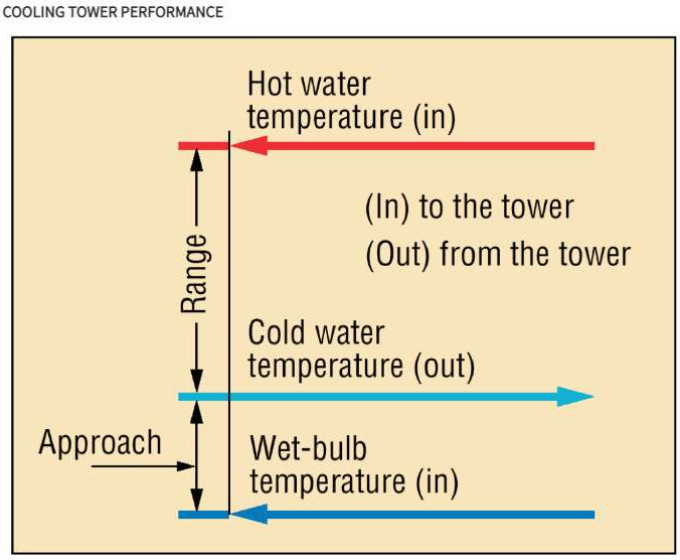

Figure 4.20 Cooling tower approach and range visualization (EnergyPurse, 2023)

The empirical YorkCalc model with 27 of its coefficients developed by York International Corp and used in EnergyPlus models which determine the approach of the cooling tower are shown in Equation 4.30 and Table 4.12.

$$\begin{aligned} \text{Approach} = {} & C1+C2.T_{wb}+C3.T_{wb}^2+C4.T_r+C5.T_{wb}.T_r+ \\ & C6.T_{wb}^2.T_r+ C7.T_r^2+C8.T_{wb}.T_r^2+C9.T_{wb}^2.T_r^2+ \\ & C10.\text{LGRatio}+C11.T_{wb}.\text{LGRatio}+C12.T_{wb}^2.\text{LGRatio}+ \\ & C13.T_r.\text{LGRatio}+C14.T_{wb}.T_r.\text{LGRatio}+ \\ & C15.T_{wb}^2.T_r.\text{LGRatio}+C16.T_r^2.\text{LGRatio}+ \\ & C17.T_{wb}.T_r^2.\text{LGRatio}+C18.T_{wb}^2.T_r^2.\text{LGRatio}+ \\ & C19.\text{LGRatio}^2+C20.T_{wb}.\text{LGRatio}^2+C21.T_{wb}^2.\text{LGRatio}^2 \\ & C22.T_r.\text{LGRatio}^2+C23.T_{wb}.T_r.\text{LGRatio}^2+ \\ & C24.T_{wb}^2.T_r.\text{LGRatio}^2+C25.T_r^2.\text{LGRatio}^2+ \\ & C26.T_{wb}.T_r^2.\text{LGRatio}^2+C27.T_{wb}^2.T_r^2.\text{LGRatio}^2 \end{aligned} \tag{4.30}$$

where

Twb – Outdoor wet bulb temperature

Tr – range

LGRatio – ratio of FRwater/FRair

FRwater – current water flow/ design water flow

FRair – current air flow / design air flow

Table 4.12 Cooling tower model coefficients provided by (U.S. Department of Energy, 2022)

Coefficient Number	Coefficient Value
C1	-0.35974120500000
C2	-0.05505360800000
C3	0.00238504320000
C4	0.17392687700000
C5	-0.02484737640000
C6	0.00048430224000
C7	-0.00558984945600
C8	0.00057700797120
C9	-0.00001342427256
C10	2.84765801111111
C11	-0.12176514900000
C12	0.00145992420000
C13	1.68042865100000
C14	-0.01669207860000
C15	-0.00071905320000
C16	-0.02548519444800
C17	0.00004874916960
C18	0.00002719234152
C19	-0.06537662555556
C20	-0.00227816700000
C21	0.00025002540000
C22	-0.09105654580000
C23	0.00318176316000
C24	0.00003862177200
C25	-0.00342853823520
C26	0.00000856589904
C27	-0.00000151682155

The approach temperature for the cooling tower operating at design conditions is calculated firstly calculated. The partial flow ratios FRair and FRwater will be set to 1 for this purpose. Design wet bulb temperature for summer is utilized from ASHRAE weather data and required design range is entered by the user which yields the design approach temperature. This determines the water outlet temperature which is also the condenser inlet design temperature for the chiller. The design capacity and nominal capacity of the cooling tower are different. Baseline nominal water flow according to ASHRAE 90.1 standard is 54 ml/s per 1/25 kW of nominal cooling at 25.6°C air wetbulb temperature, 35°C hot water and 29.4°C cold water outlet temperature. Therefore, the nominal capacity of the tower can be calculated by this correlation. At situations where the tower outlet water temperature is determined in design stage, such as when the cooling tower is coupled the stack directly with a heat exchanger at higher temperatures, the

FRwater is found by iteratively solving the model. The limits for FRwater is between 0.75 and 1.25 for this model. The FRwater acts a sizing factor for the cooling tower and the reference water flow is calculated by Equation 4.31 to find the nominal capacity of the tower.

$$\dot{V}_{reference} = \frac{\dot{V}_{reference}}{FR_{water,reference}} \quad (4.31)$$

After calculating the design approach temperature, the cooling tower water outlet design temperature is determined by adding the design wetbulb temperature and is used as a setpoint temperature to calculate the instant airflow ratio.

The original model calculates $T_{water,outlet,fanOFF}$ which is the outlet water temperature for when the cooling tower fan is off and there is free convection in the tower.

$$T_{water,outlet,fanOFF} = T_{water,inlet} - [Frac_{freeconv}(T_{water,inlet} - T_{water,oulet,fanMAX})] \quad (4.32)$$

where $Frac_{freeconv}$ is the fraction of tower capacity in free convection regime which could be in values from 0 to 0.2 but is 0.125 as default in modeling programs using this model. For this study the fractional capacity is neglected since there is no solid reference in literature to address a certain factor. Therefore there will be no cooling when the fan is off. $T_{water,outlet,fanMIN}$ is the water outlet temperature at the minimum speed of the VSD (Variable Speed Drive) fan where FRair is assumed 0.5 in the YorkCalc model. Therefore, if the calculated $T_{water,outlet}$ is lower than the design temperature then the fan speed can be lowered to a point where it is adequate. When the calculated $T_{water,outlet}$ is still lower than the setpoint even in minimum speed, the cooling tower operates on and off to meet the set point.

The fan power consumption at partial load is determined by Equation 4.33.

$$P_{fan} = (P_{fan,design})(FanPLR)(FR_{air})^3 \quad (4.33)$$

where $P_{fan,design}$ is the design/nominal fan power and FanPLR is the fan part-load ratio. FanPLR is determined as 0 when cooling tower is at free convection mode which is not the case in this study, and is determined as 1 for continues operation but is calculated when the cooling tower is working in on/off mode which actually expresses the ratio of on time for a certain period.

$$FanPLR = \left(\frac{T_{water,outlet,fanOFF} - T_{setpoint}}{T_{water,outlet,fanOFF} - T_{water,outlet,fanMIN}} \right) \quad (4.34)$$

where $T_{water,outlet,fanOFF}$ is actually $T_{water,inlet}$ since the it is assumed that there is no cooling when the fan is off. The other variable determining the instant fan power is FRair which is determined by iteration of the model.

The setpoint temperature value is not constant while operating. The cooling tower fans will run on maximum load until a minimum condenser water temperature is reached. The minimum limit setpoint temperature will be 19°C as also specified in the method used to calculate the NPLV of chillers as per AHRI 551/591 standard explained in the chiller sizing chapter of this study.

As shown in Figure 4.21, the parameters mentioned in calculations for the cooling tower are input on the left side of the block and the output parameters are the condenser water leaving temperature to be used by the chiller model, the fan consumption to be stored at the results spreadsheet for efficiency calculations and the makeup water requirement which is used in the booster pump block.

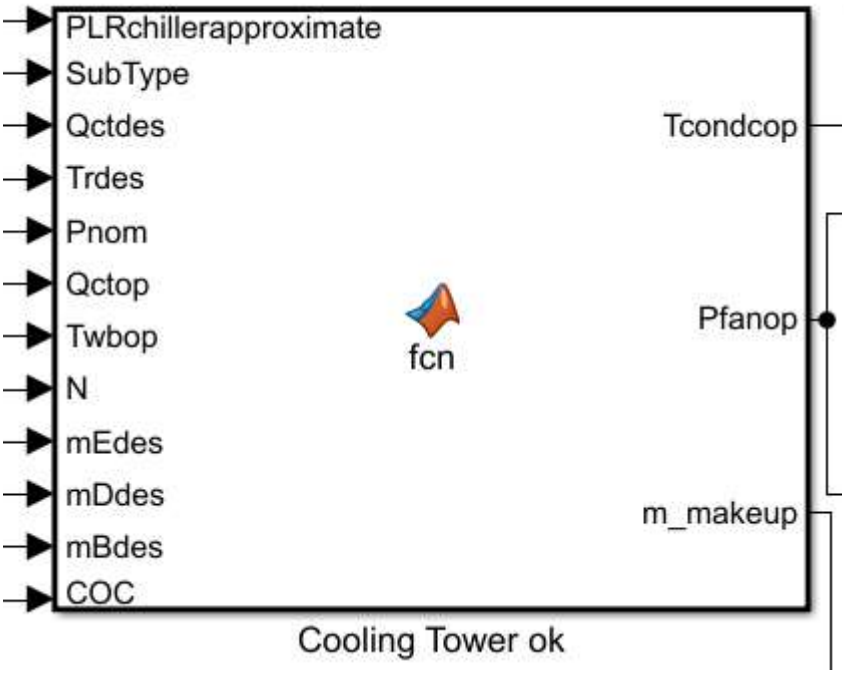

Figure 4.21 Cooling tower model block

Cooling towers require basin heaters in order to prevent freezing in cooling tower water when tower is not operating at ambient temperatures below 0°C.

The Equation 4.35 is used for the calculation.

$$P_{basin} = \max\left(0, CAP_{basin\ heater} \times \left(T_{setpoint} - T_{ambient}\right)\right) \quad (4.35)$$

where $CAP_{basin\ heater}$ is the basin heater capacity in W/K.

As shown by Figure 4.22, the input parameters of the basin heater are on the left of the block and the output parameters are on the right which are the power consumption of the basin heater and the temperature of the condenser loop after heating.

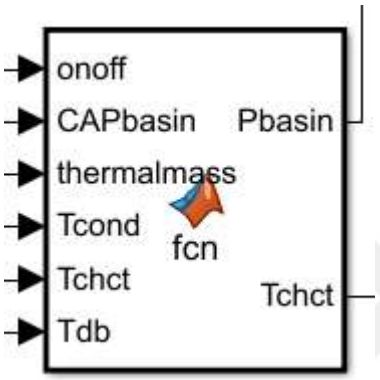

Figure 4.22 Cooling tower basin heater model block

The cooling tower requires makeup water as it is consumed in operation. Modeling of makeup water required for the cooling tower will be carried out by using design values calculated as mentioned in Section 5.3.2.

$$\dot{m}_{make\text{-}up} = \dot{m}_{evaporation} + \dot{m}_{drift} + \dot{m}_{blowdown} \quad (4.36)$$

The evaporation rate is calculated by the ratio of operation to design temperature difference of cooling tower water.

$$\dot{m}_{evaporation,operation} = \frac{\Delta T_{operation}}{\Delta T_{design}} \dot{m}_{evaporation,design} \quad (4.37)$$

The drift loss is modeled as mentioned in EnergyPlus Engineering Reference.

$$\dot{V}_{drift,makeup} = \dot{m}_{water,design} \left(\frac{PercentWaterDrift}{100}\right) FRair \quad (4.38)$$

The blowdown is calculated by same formula as used in design calculations (Section 5.3.2.).

$$\dot{m}_{blowdown} = \frac{\dot{m}_{evaporation} - (COC-1) \cdot \dot{m}_{drift}}{(COC-1)} \quad (4.39)$$

4.2.2.3. Dry Cooler Model

The dry cooler modeling is performed as per EnergyPlus by using the effectiveness-NTU relationship mentioned by below formulas. This method is explained in heat transfer text books (Incropera, 2007).

The heat capacity rates are calculated by Equations 4.40 and 4.41.

$$\dot{C}_a=\dot{m}_a c_{pa} \tag{4.40}$$

$$\dot{C}_w=\dot{m}_w c_{pw} \tag{4.41}$$

The maximum possible heat transfer rate is expressed by Equation 4.42.

$$\dot{Q}_{max}=\dot{C}_{min}\left(T_{w,in}-T_{db,out}\right) \tag{4.42}$$

$$\dot{C}_{max}=Max\left(\dot{C}_a,\dot{C}_w\right) \tag{4.43}$$

$$\dot{C}_{min}=Min\left(\dot{C}_a,\dot{C}_w\right) \tag{4.44}$$

Effectiveness is the ratio of the actual heat transfer rate for a heat exchanger to the maximum possible heat transfer rate (Incropera, 2007).

$$\varepsilon=\frac{\dot{Q}}{\dot{Q}_{max}} \tag{4.45}$$

Actual heat transfer rate is calculated by Equation 4.46.

$$\dot{Q}=\varepsilon.\dot{C}_{min}\left(T_{w,in}-T_{db,in}\right) \tag{4.47}$$

The effectiveness is calculated by the following formulas for cross flow where both fluids don't mix.

$$\varepsilon= 1-\exp\left\{\frac{\exp\left(\frac{-NTU.C_r}{\eta}\right)-1}{\frac{C_r}{\eta}}\right\} \tag{4.48}$$

$$\eta=NTU^{(-0.22)} \tag{4.49}$$

$$NTU=\frac{UA}{\dot{C}_{min}} \tag{4.50}$$

Lastly fluid outlet temperatures are calculated by Equations 4.51 and 4.52.

$$T_{db,out}=T_{db,in}+\frac{\dot{Q}}{\dot{C}_a} \tag{4.51}$$

$$T_{w,out}=T_{w,in}+\frac{\dot{Q}}{\dot{C}_w} \quad (4.52)$$

Firstly, the model is used for the design stage where the water inlet outlet temperatures, flowrate and dry-bulb outdoor temperature are determined beforehand. The model is iterated to find the required UA factor for design conditions.

The model is developed for dry coolers operating with two speed fans. Therefore, if the cooling requirement is between full fan speed capacity and low fan speed capacity the cooler will cycle on high and low speeds on a certain period. A coefficient ω, similar to the FanPLR of the cooling tower, is calculated to be used in the determination of the average fan power.

$$\omega=\frac{T_{set}-T_{wout,low}}{T_{wout,high}-T_{wout,low}} \quad (4.53)$$

$$P_{fan,avg}=\omega.P_{fan,high}+(1-\omega).P_{fan,low} \quad (4.54)$$

For cooling requirements lower than the low fanspeed capacity, the fans of the dry cooler operates on and off similarly and the same formulas are used (Equations 4.55 and 4.56).

$$\omega=\frac{T_{set}-T_{wout,off}}{T_{wout,on}-T_{wout,off}} \quad (4.55)$$

$$P_{fan}=\omega.P_{fan,low} \quad (4.56)$$

The leaving water temperature when the fans are off is the same as the entering water temperature as it is assumed that no cooling is carried out when the fans are off.

The stack cooling model for options of dry cooler and cooling model are inside the same block. The calculations for whichever is chosen for the system on the design sheet are carried out.

As shown in Figure 4.23, the parameters required for dry cooler calculation mentioned in this part are input on the left side of the model block. The output water leaving temperature data and power consumption of the dry cooler are on the right side of the block.

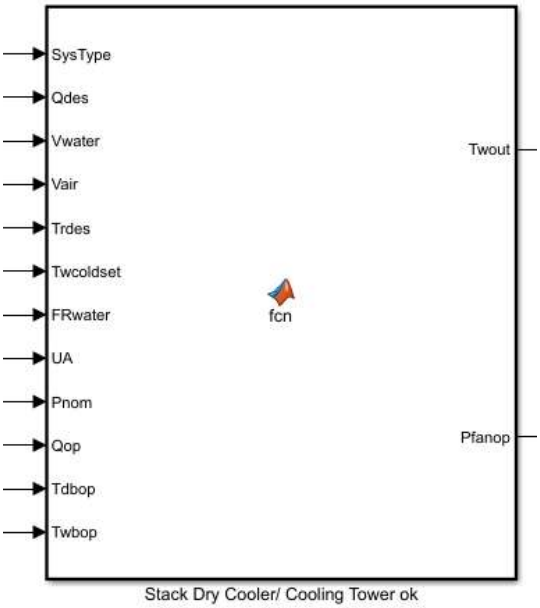

Figure 4.23 Dry cooler model block

4.2.3. Pump Modeling

The circulation pumps are used in the cooling system and anode circulation loop. For small systems with singular equipment these pumps operate on/off at constant flowrate. For larger systems, there is a shared pump for more than one equipment. In this situation the pump operates at partial loads and VSD controlled. For this situation, since the equipment are connected parallelly the system friction head does not differ majorly with changing pump flow rates because each equipment receives the full flow rate needed to operate.

In the situation of having a requirement of constant pressure and variable flowrate, the VSD controlled pump electric consumption increases on a close to linear trend with increasing flowrate.

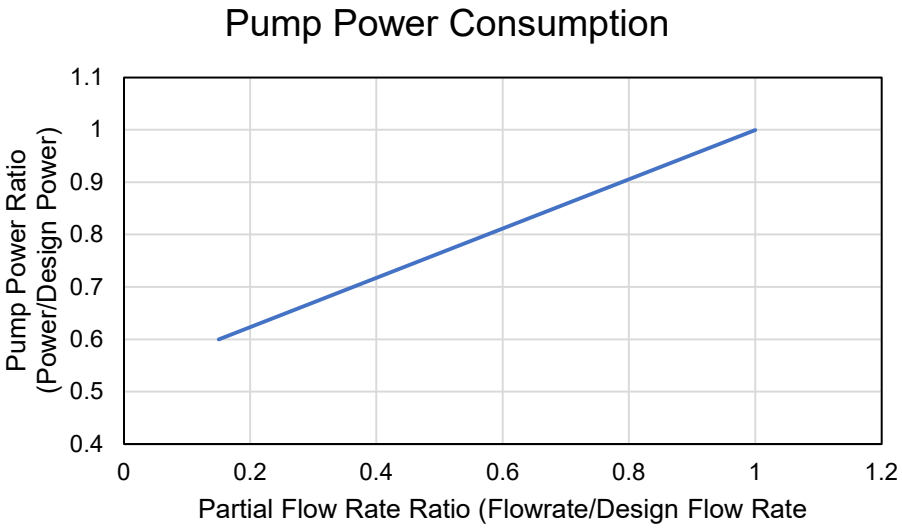

Figure 4.24 Pump power consumption curve

4.3. PV Plant Modeling

Modeling of PV plant is performed in System Advisory Model (SAM) which is a program developed by the NREL. The weather data files are utilized in the simulations. Figure 4.25 shows a typical screenshot of the location selection page.

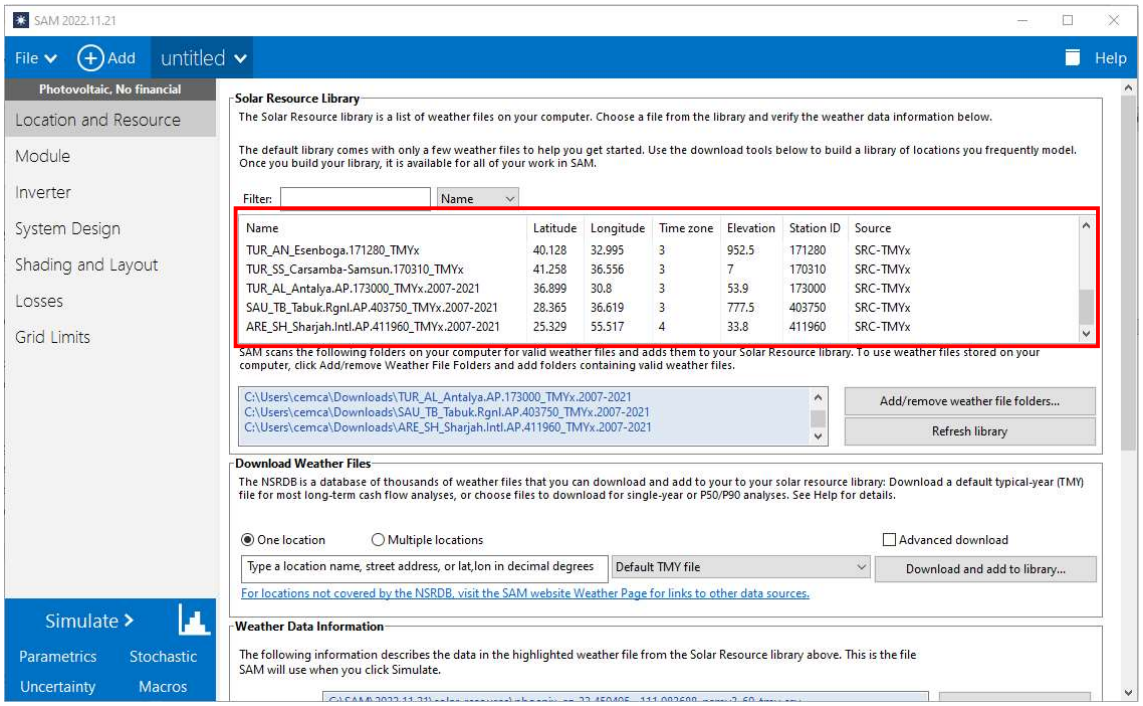

Figure 4.25 SAM location selection page

The program provides data for commercial PV modules of which most have an efficiency of around 17 – 20 % (Figure 4.26). The PV panel chosen for this study is SunPower-SPE-E19-310 which has an efficiency of 19 % also shown in Figure 4.26.

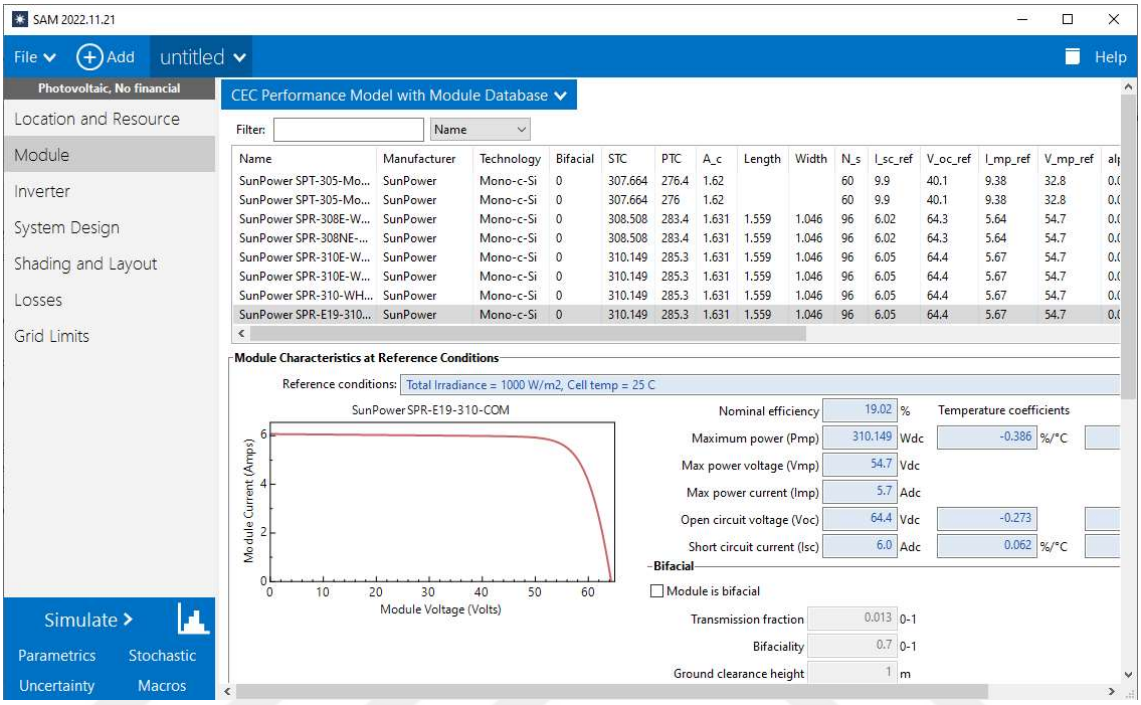

Figure 4.26 SAM PV module selection sheet

The invertor selection is not important for this study as DC to AC inverters are not used but directly coupled to the PEM systems. The system sizing can be carried out on the system design sheet by selecting the estimated sub array configuration continued by inputting desired array size in kW, tilt angle, azimuth angle and ground coverage ratio (GCR) (Figure 4.27). The ground coverage ratio is the ratio between row spacing and the edge length of the PV row. GCR affects the shading caused by the modules to each other which lowers the energy yield.

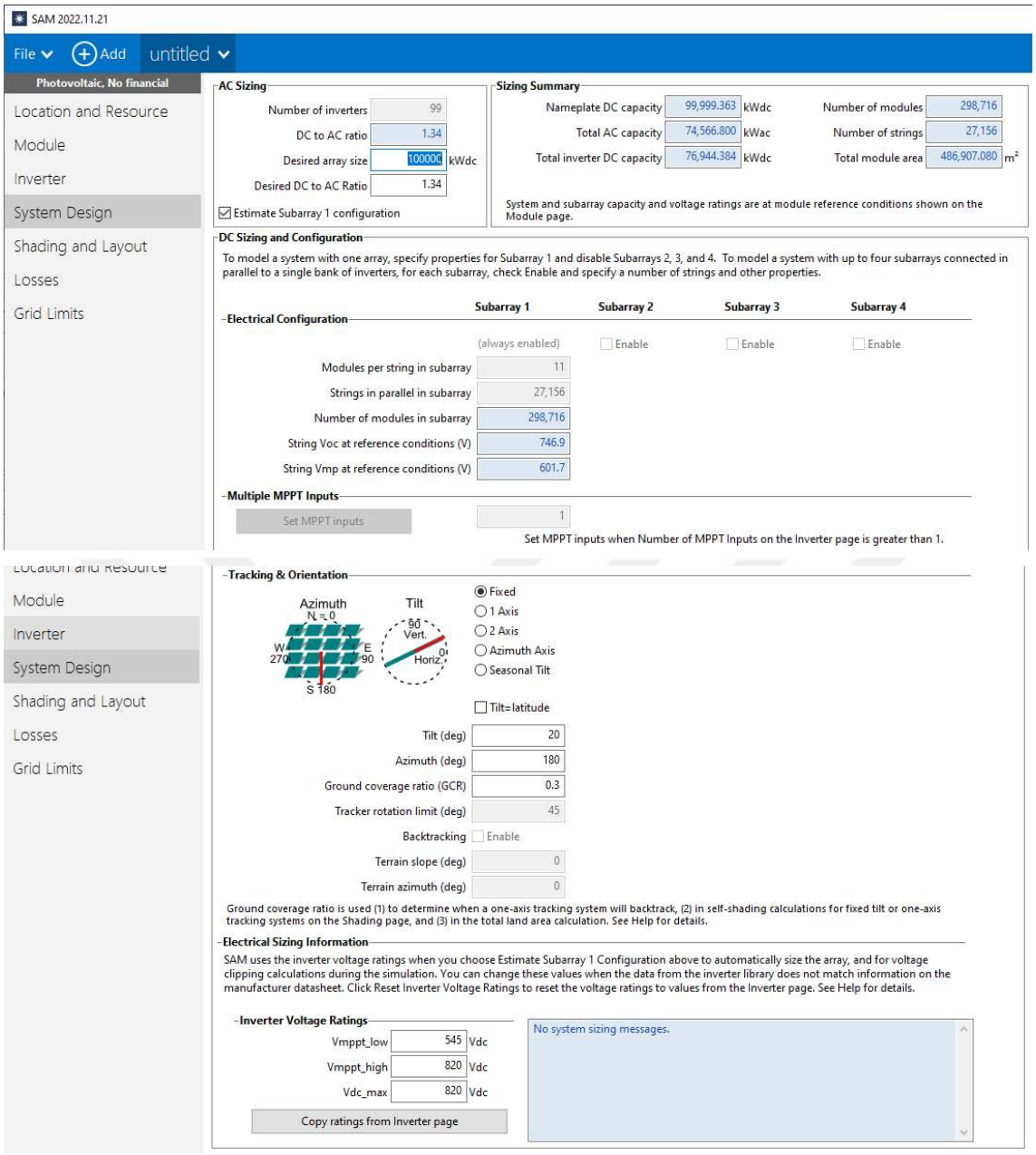

Figure 4.27 SAM system design sheet

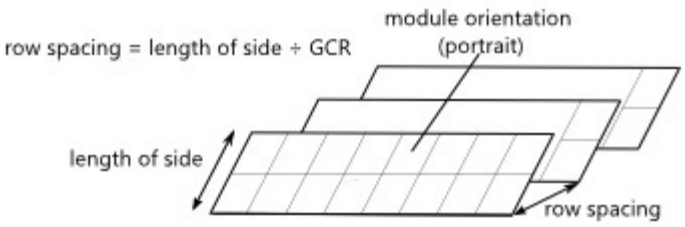

Figure 4.28 Ground coverage ratio (GCR) representation by SAM

Loss parameters related to DC power are carried out by default parameters in the program (Figure 4.29).

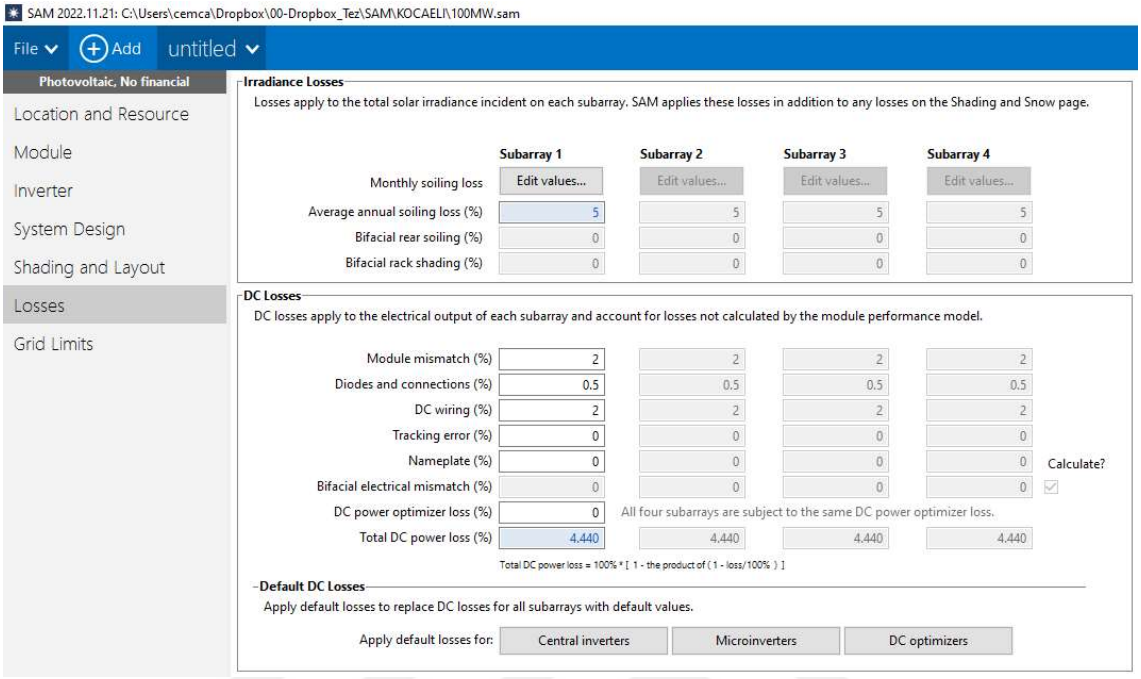

Figure 4.29 SAM losses sheet

The simulations result in hourly power generation data as shown in Figure 4.30 that are exported as spreadsheets and utilized in the MATLAB PEM system simulation.

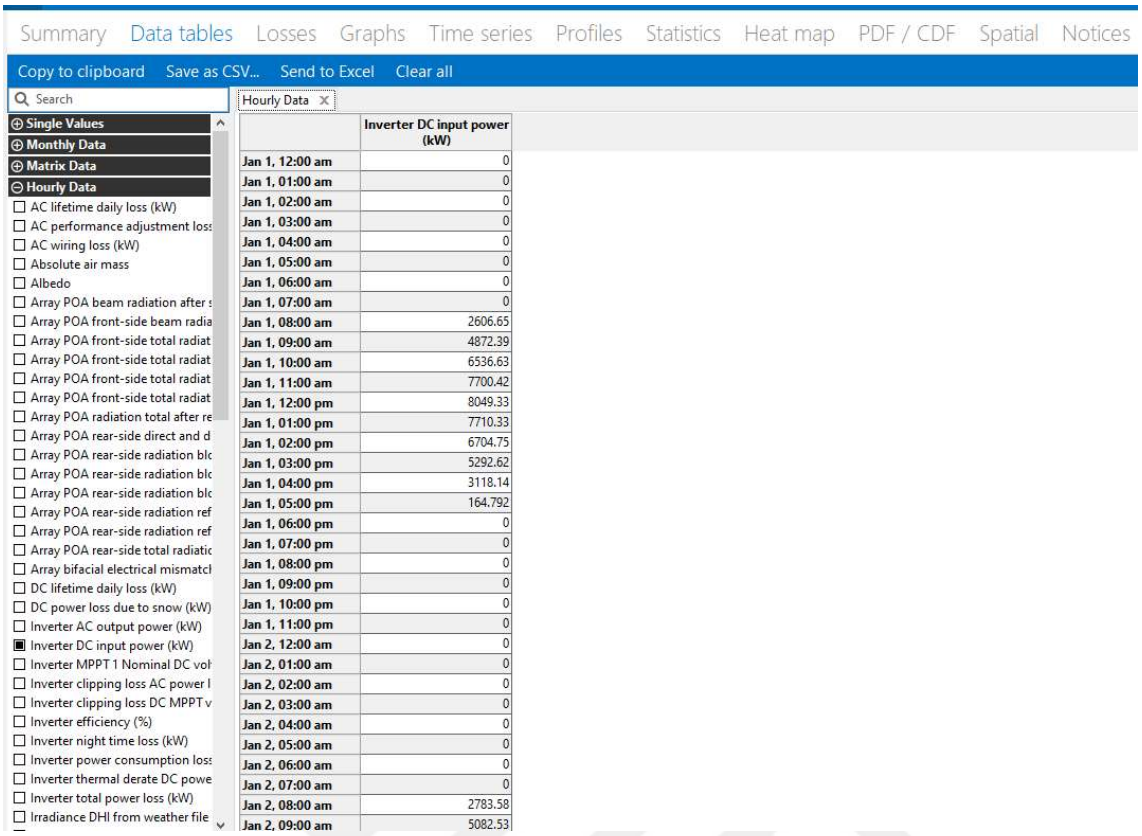

Figure 4.30 Typical hourly simulation results of a PV plant

The input and outputs of the SAM PV model are summarized in Table 4.13.

Table 4.13 Input and outputs of SAM PV model

Inputs	**Outputs**
Weather data file	Hourly DC energy production data
Location coordinates	
PV module selection for performance curves	
Desired plant capacity	
Tilt angle	
Azimuth angle	
GCR	

4.4. Weather Data

Weather data will be used for cooling tower calculations which affect the performance of the cooling system. The energy plus format weather data files are suitable for this application. Table 4.14 is a preview of the data that can be extracted from these files.

Table 4.14 Sample segment of data provided by .epw weather data file format.

Month	Day	Hour	Min	DryBulb {C}	DewPoint {C}	RelHum {%}	Atmos Pressure {Pa}
1	1	1	0	-12	-15	76	89582
1	1	2	0	-12	-15	76	89582
1	1	3	0	-11.3	-13.8	80	90536
1	1	4	0	-13	-15	83	89540
1	1	5	0	-15	-17	83	89456

There are a few free sources that these files could be accessed listed in Table 4.15.

Table 4.15 List of weather data file sources.(National Renewable Energy Laboratory, 2023)

Source	Region	Description
Climate.OneBuilding	Global	Typical-year hourly data from various sources. EPW format.
EnergyPlus	Global	Typical-year hourly data from various sources. EPW format.
European Commission PVGIS	Global	Typical-year hourly data from various sources. EPW format.

Although the weather data file does not provide wet bulb temperature data, it can be calculated by formulas expressed in ASHRAE Handbook: Fundamentals on Psychrometrics Chapter. The wet-bulb temperature will be used in the cooling tower model.

For temperatures below freezing point the following formula is used to calculate the saturation pressure (p_{ws}). The saturation pressure is calculated by equation 4.57 for temperatures below freezing point and Equation 4.58 for a temperature range 0 - 200°C.

$$\ln p_{ws} = C1/T_{db} + C2 + C3xT_{db} + C4xT_{db}^2 + C5xT_{db}^3 + C6xT_{db}^4 + \ln T_{db} \quad (4.57)$$

$$\ln p_{ws} = C8/T_{db} + C9 + C10xT_{db} + C11xT_{db}^2 + C12xT_{db}^3 + C13xT_{db}^4 + \ln T_{db} \quad (4.58)$$

Temperature values for these equations are in Kelvins. Coefficients for the Equations 4.57 and 4.58 are listed in Table 4.16.

Table 4.16 Coefficients of saturation pressure formula

Coefficients	
C1	-5.6745359E+03
C2	6.3925247E+00
C3	-9.6778430E-03
C4	6.2215701E-07
C5	2.0747825E-09
C6	-9.4840240E-13
C7	4.1635019E+00
C8	-5.8002206E+03
C9	1.3914993E+00
C10	-4.8640239E-02
C11	4.1764768E-05
C12	-1.4452093E-08
C13	6.5459673E+00

Vapour pressure ($p_{w)}$ could be calculated from p_{ws} and relative humidity (RH) by Equation 4.59.

$$p_w = p_{ws} \times RH/100 \tag{4.59}$$

After calculating p_w and p_{ws}, the humidity ratios could be calculated by the following Equations 4.60 and 4.61.

$$W = 0.621945 \cdot \frac{p_w}{p - p_w} \tag{4.60}$$

$$W_s = 0.621945 \cdot \frac{p_{ws}}{p - p_{ws}} \tag{4.61}$$

where W is the humidity ratio and W_s is the saturated humidity ratio. At this point, the following equations are used to calculate the humidity ratio for given dry and wet-bulb temperature. The wet bulb temperature is determined by iteration until the result is the same of what was calculated by Equation 4.60 in the first place. The temperature values used in this procedure are Celsius.

$$W = \frac{(2501 - 2.326.T_{wb}).W_s^{wb} - 1.006(T - T_{wb})}{2501 + 1.86.T - 4.186.T_{wb}} \tag{4.62}$$

Equation 4.63 is used for temperatures below freezing point.

$$W = \frac{(2830 - 0.24.T_{wb}).W_s^{wb} - 1.006(T - T_{wb})}{2830 + 1.86.T - 2.1.T_{wb}} \tag{4.63}$$

W_s^{wb} stated in the formulas are calculated by Equation 4.61.

The model solves the equations by first using graphical methods to find limits to be used in false-position method.

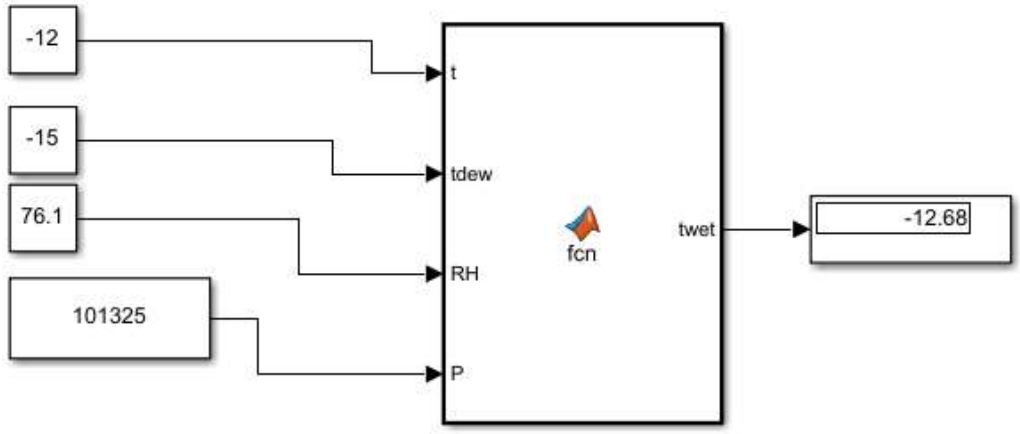

Figure 4.31 Wet bulb calculation model block

As shown in Figure 4.31 the wet bulb calculation input parameters are at the left side of the block and the calculated wet bulb temperature is output on the right side of the block.

4.5. Encloser Requirements

It is important to consider the energy need of the enclosed area that the system is placed. Closed areas where production or processing of explosive chemicals like hydrogen are carried out require ventilation in order to maintain safety. Table 4.17 states recommended ventilation rates by standards.

Table 4.17 List of ventilation requirements for hydrogen facilities according to different standards

Standard	Ventilation Requirement
EUR 9689, 1985	20 ACH
FMGlobal, 2000	10 ACH (25 ACH at leak detection for emergencies)
NSS 1740.16,1997	6 ACH
NFPA 2	0.0051 $m^3/s/m^2$

It is observed in manufacturer catalogues that the NFPA2 standard is met. By specifying the required flow from the volume of the closed space the fan capacity for ventilation could be determined.

4.6. Sequencing Operation

For situations with large capacities where there is more than one of each type of equipment, the equipment will operate in a certain sequence for better complete system efficiency.

4.6.1. PEM Stack Converter Sequence

The lower the partial load of the PEM stack, the higher the efficiency. Therefore, for situations where there is more than one stack the sequencing mentioned in Table 4.18 is carried out.

Table 4.18 Stack converter sequencing

Situation	Operation
$P_{solar} < 5\%.P_{stack}$	all stacks off
$P_{solar} < 5\%.P_{stack}.n_{stack}$	some stacks operating at 5% minimum partial load and one is operating above 5% to complete the difference n_{op5} (number of stacks operating at 5%)= rounddown($P_{solar}/5\%.P_{stack}$)-1 $P_{stack+1}$ (Power of stack not operating at 5%)=P_{solar}-(5%.$P_{stack}.n_{op5}$)
$P_{solar} > 5\%.P_{stack}.n_{stack}$	all stacks operate at same partial load $P_{stack}=P_{solar}/n_{stack}$

The higher the partial load, the less efficient the stack will operate as discussed in Section 5.1. Therefore, when there are more than one stack in the system, the power is shared to all of them at partial load instead of operating a few in full load. The reason the stacks are turned off at 5 % is because that is the lowest partial load it can operate (International Renewable Energy Agency, 2020a).

DC-DC converter operates according to mentioned stack sequencing.

4.6.2. Chiller Sequencing

Chiller sequencing is very similar to stack sequencing mentioned earlier, however instead of minimum load, the optimal load for highest COP will be used.

Table 4.19 Chiller sequencing

Situation	Operation
$Q_{cooling} < \%_{chiller,min}.Q_{chiller,av}$	one chiller operating on and off to meet required cooling load
$Q_{cooling} < \%_{chiller,opt}.Q_{chiller,av}$	one chiller operating at partial load required to meet cooling load
$Q_{cooling} < \%_{chiller,opt}.n_{chiller}.Q_{chiller,av}$	some chillers operating at optimal COP partial load and one is operating at higher load to complete the difference n_{opmin} (number of chillers operating at optimal COP load)= rounddown($Q_{cooling}/\%_{chiller,min}.Q_{chiller,av}$)-1 $Q_{chiller+1}$ (Load of chiller operating above optimal COP load)= $Q_{cooling}-(\%_{chiller,min}.Q_{chiller,av}.n_{opmin})$
$Q_{cooling} > \%_{chiller,opt}.n_{chiller}.Q_{chiller,av}$	all chillers operate at same partial load $Q_{chiller}=Q_{cooling}/n_{chiller}$

Table 4.20 PLR for highest COP

Chiller Type	PLR at Highest COP
aircooled scroll	40%
aircooled screw	40%
watercooled scroll	40%
watercooled screw	80%
watercooled centrifugal	80%

The optimum COP of the chillers were determined by the COP curves generated by the chiller model. COP curves for the five chiller types operating at different temperatures are shown in Figures 4.32 to 4.36.

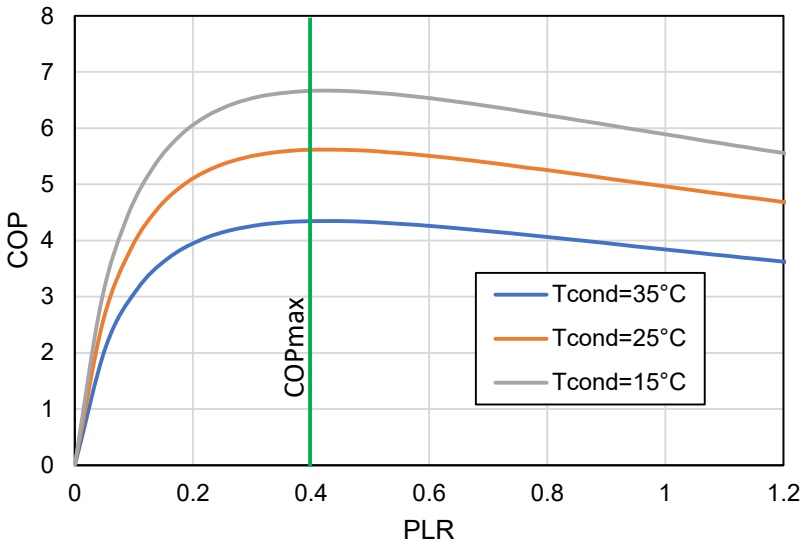

Figure 4.32 COP curve of air-cooled scroll chiller

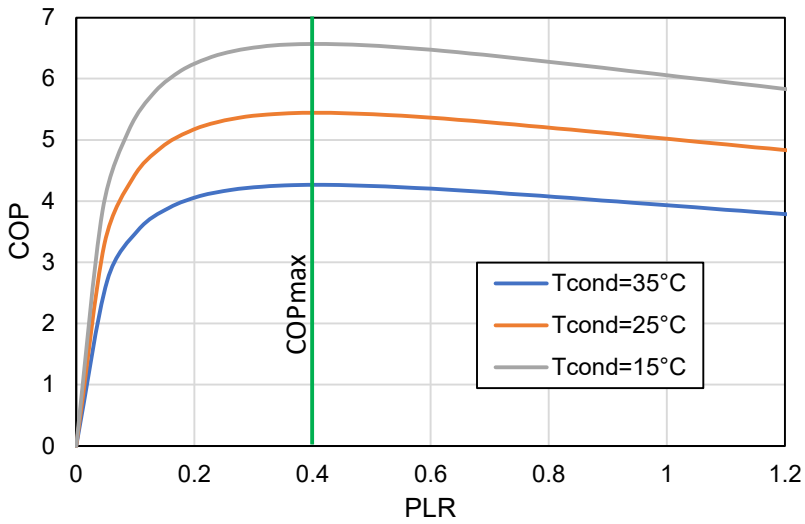

Figure 4.33 COP curve of air-cooled screw chiller

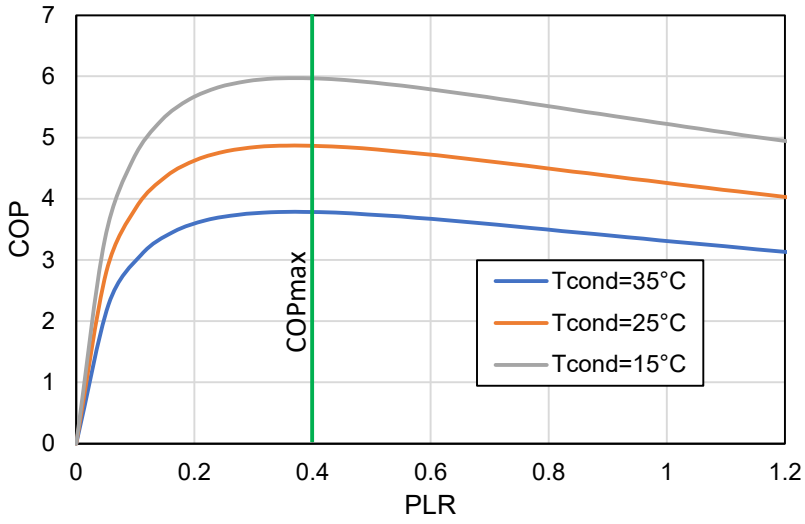

Figure 4.34 COP curve of water-cooled scroll chiller

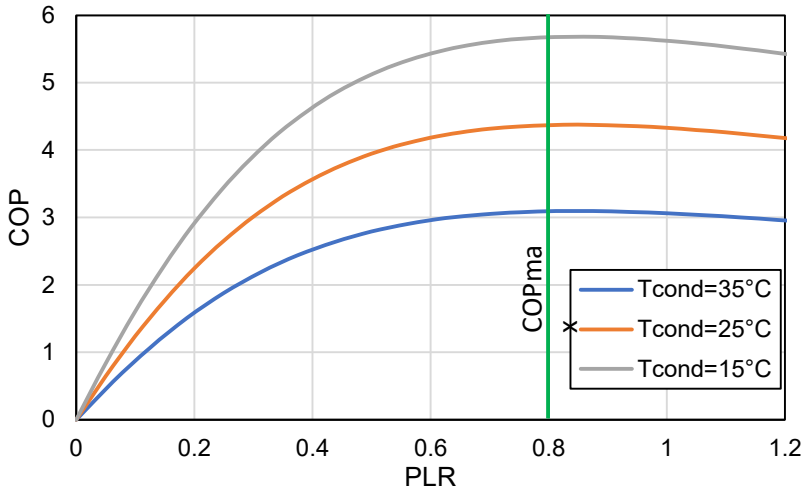

Figure 4.35 COP curve of water-cooled screw chiller

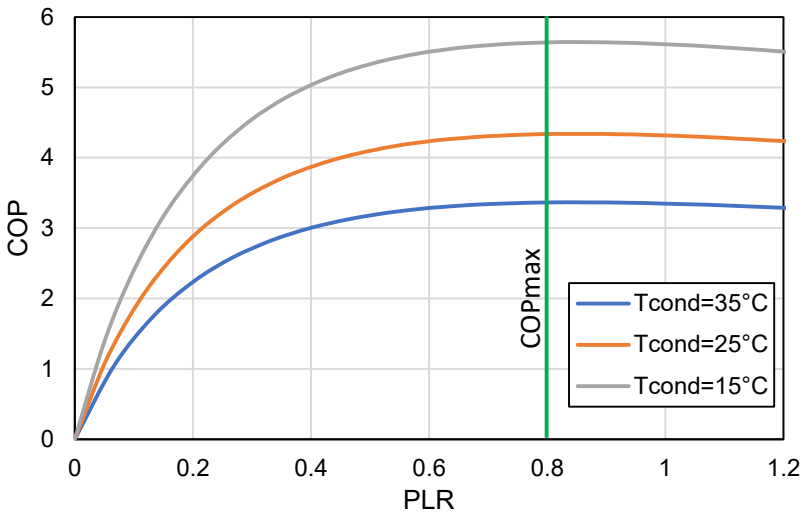

Figure 4.36 COP curve of water-cooled centrifugal chiller

4.6.3. Cooling Tower/ Dry Cooler Sequencing

The number of active stacks determines the number of active cooling towers or dry coolers. Similarly, the number of active chillers determines the number of active cooling towers dedicated to them.

Table 4.21 Cooling tower/ dry cooler sequencing

Situation	Operation
All times	All active cooling towers/drycoolers operate at same partial load $Q_{cooling}=Q_{cooling,total}/n_{op}$

In this situation, the condenser water temperature setpoint is set to the chiller with the lowest setpoint.

4.6.4. Pumps

The cooling system circulation pumps operate when the dedicated cooling equipment is active, and the anode circulation pump operates when the PEM stack is active. The flow rate of the pump is determined by the full load of the equipment multiplied by the number of equipment active. The number of stack and related dry cooler/ cooling tower equipment are not the same. Therefore, the pump operates on whichever needs the highest flowrate. For situations where there is a pump set consisting of more pumps, the amount of pumps that can meet the load at full load will operate and one other pump will operate at partial

load to meet the balance. Unlike the stack or chiller, the pumps start operating one by one as the load increases.

5. SYSTEM DESIGN/ SIZING

System design can vary depending on capacity. In this study design has been carried out for plant capacities of 1 MW, 5 MW, 10 MW, 50 MW, 100 MW ,1 GW. An example of the design sheet to be used for the sizing of the stack and cooling system is provided in Appendix 3.

5.1. PEM Stack Design

The PEM stack design is the same as the model parameters mentioned in the previous chapter which resembles Plug Power's Giner Allagash electrolyzer.
There will be one stack for each MW of plant capacity.

5.2. Electrical System Sizing

5.2.1. DC-DC Converter Sizing

The DC-DC converters are used to operate the stacks. Each stack has a dedicated converter. Therefore, the converter capacity is calculated by dividing the stack maximum power consumption at 2.1 V by the maximum efficiency of the converter which is 96 %.

$$P_{DC\text{-}converter} = \frac{P_{stack,max}}{\eta_{DC}} \tag{5.1}$$

The result is rounded up to the closest 5kW.

5.2.2. AC-AC Transformer Sizing

The AC-AC transformers are used to provide the BoP with the required power. Therefore, the total nominal electric consumption of all BoP equipment will be used to calculate the capacity of the transformer in terms of kVA by using the previously mentioned Equation 4.17 with partial load ratios set to 1.

5.2.3. Control Cabinet Sizing

The control cabinet is responsible for the automation of all the electric consuming components and will operate at all times. The control cabinet energy consumption is calculated as 5 % of the total nominal electric consumption of all components.

5.3. Cooling System Sizing

The cooling capacity is calculated by the heat generated by the stack at maximum cell voltage.

$$Q_{stack,cooling}=\left(1-\eta_{cell,HHV}\right) \text{ x } P_{stack,max} \quad (5.2)$$

ASHRAE 90.1 standard states efficiency values for cooling equipment which most products comply in the industry.

The shematics of two options created for the cooling system can be seen in Figure 5.1.

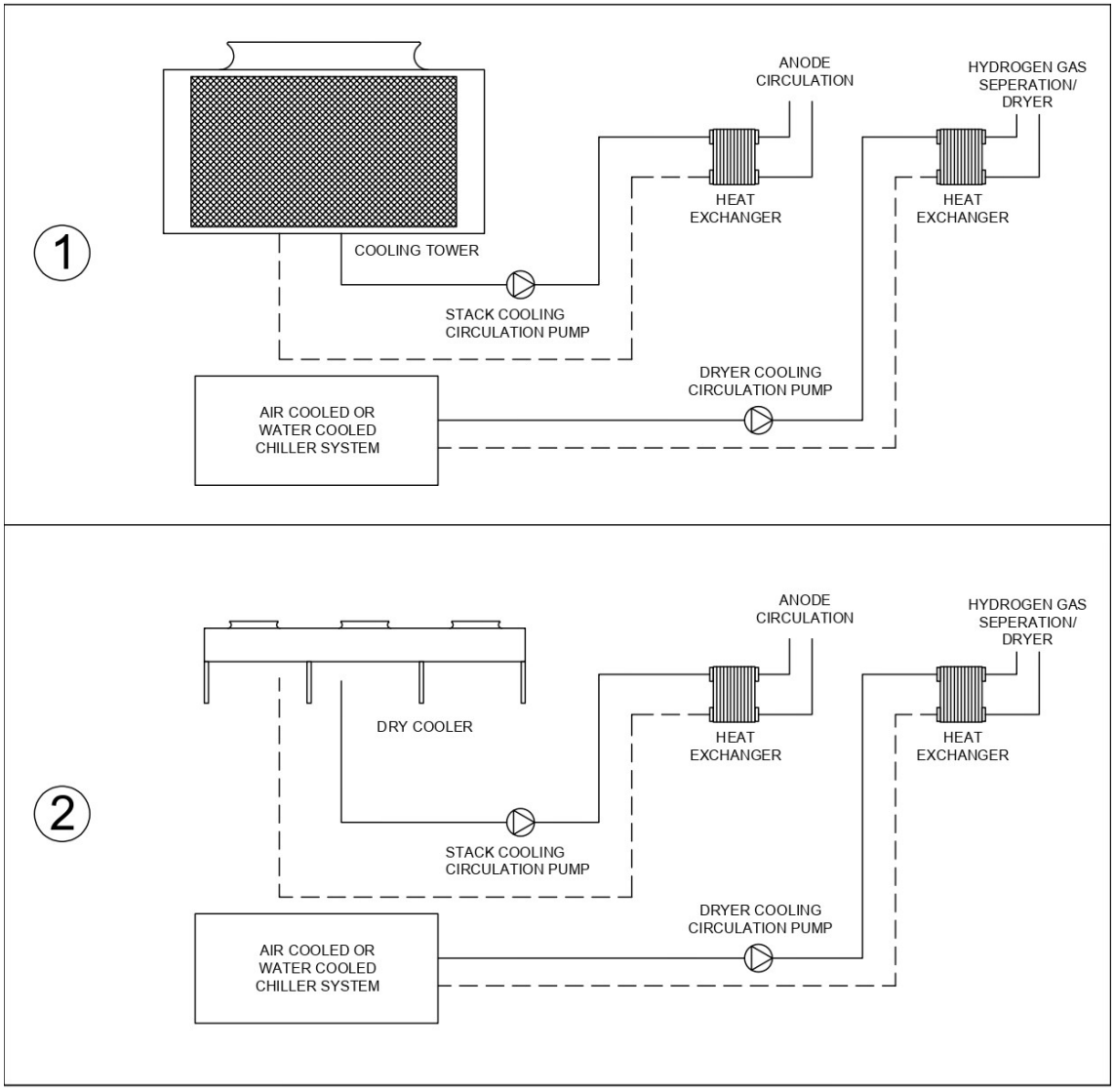

Figure 5.1 Cooling system design options.

As can be seen, there are two system types for this study. In both studies chillers are used for hydrogen drying process as it requires cooling to be performed in

temperatures as low as 5°C. The capacity required for the hydrogen dryer is relatively low. This could be observed from the sample design sheet where only 7.6 kW of cooling is needed for 350 kW of stack cooling. Since the stack ideally operates at around 80°C, the cooling of the stack could be carried out by a separate dry cooler (option1) or cooling tower (option2) at higher temperatures.

The chiller system could be water-cooled or air-cooled. Water cooled chillers also have a condenser circulation loop connected to a cooling tower to perform heat rejection. The air-cooled chillers are stand-alone equipment which perform heat rejection directly to the ambient air. These two chiller options are indicated as sub system types -1 and -2 as illustrated in Figure 5.2.

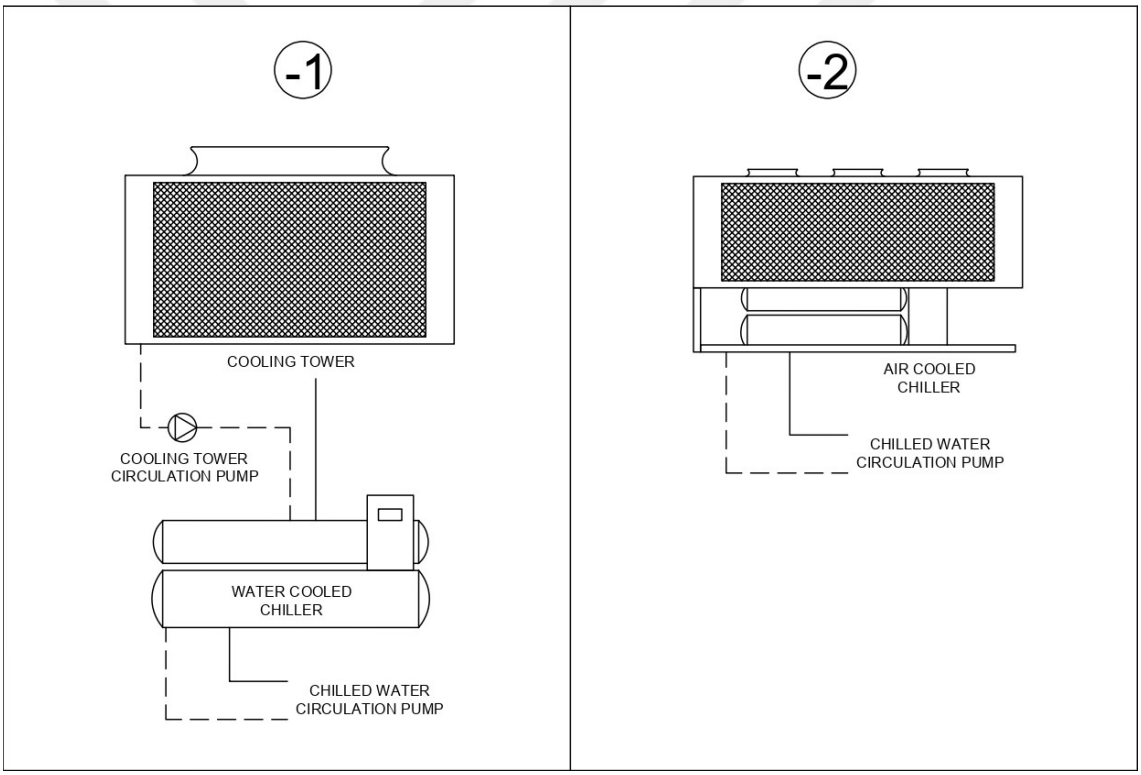

Figure 5.2 Chiller design options.

A separate Simulink model is formed for the design purpose of the cooling system in order to calculate the COP, fan nominal capacity and other design data required to be used in the partial load model. Table 4.25 summarizes the cooling system design options

Table 5.1 Summary of system cooling design options

System Number	Stack Cooling	H2 Purification
1.1	Dry Cooler	Air Cooled Chiller
1.2	Dry Cooler	Water Cooled Chiller
2.1	Cooling Tower	Air Cooled Chiller
2.2	Cooling Tower	Water Cooled Chiller

Table 5.2 lists of equipment that consumes power. The equipment mentioned on the list differs with system type options and also other details regarding infrastructure. More detailed schematics of the system including equipment codes are provided in Appendix 4 for clearer understanding.

Table 5.2 Energy consuming BoP component list

Energy Consuming BoP Components		
Code	**Description**	**Remarks**
PEM-001	PEM Stack	
Electrical Equipment		
DC-01	DC/DC Converter	For DC solar energy source
AC-01	AC/AC Transformer	For BoP equipment power supply
CTR-01	Control panel for system	System operation control & SCADA etc.
Cooling Equipment		
CH-001	Chiller	
CT-001	Cooling Tower	In case of water-cooled chiller
DC-001	Stack Dry Cooler	
CT-101	Stack Cooling Tower	
Pumps		
P-A-001	Anode Loop Circulation Pump	
P-S-001	Stack Cooling Circulation Pump	
P-H-001	Hydrogen Purifier Cooling Circulation Pump	
P-CT-001	Chiller Cooling Tower Circulation Pump	In case of water-cooled chiller
Booster Sets		
BS-001	System Booster Pump	
Ventilation		
EF-001	Exhaust Fan	Exhaust fans extracting required air for safety purpose

5.3.1. Chiller Sizing

The efficiency of chiller is expressed by COP and IPLV/NPLV. COP is the cooling capacity divided by electricity input. IPLV/NPLV is the integrated partial load value which expresses the weighted average of partial loading of the chiller. The IPLV/NPLV calculation is stated AHRI 551/591.

$$IPLV/NPLV=0.01.A+0.42.B+0.45.C+0.12.D \quad (5.3)$$

where the coefficients are as indicated in Table 5.3.

Table 5.3 Coefficients of IPLV/NPLV formula

Coefficients	
A	COP at 100% load
B	COP at 75% load
C	COP at 50% load
D	COP at 25% load

The partial load COPs are measured at different condenser entering water/ air temperatures determined by AHRI.

Table 5.4 NPLV conditions for rating

Partial Load Conditions for Rating	
Water-cooled Condenser	**NPLV**
100% load at Entering Tcond	User defined Entering Tcond
75% load at Entering Tcond	Equation 5.5
50% load at Entering Tcond	Equation 5.5
25% load at Entering Tcond	Equation 5.5
Air-cooled Condenser	
100% load at Entering Tdb	User defined Entering Tdb
75% load at Entering Tdb	Equation 6.3
50% load at Entering Tdb	Equation 6.3
25% load at Entering Tdb	Equation 6.3

Since our design temperature is determined by weather data, the NPLV calculation will be carried out. Formulas for determining the entering water/ air temperature are expressed below.

For an air-cooled condensers at NPLV.SI part load conditions, Equation 5.4 is used to determine the dry bulb temperature of the entering air (Entering T_{db}). Design temperature (Design T_{db}), is the entering dry-bulb temperature at 100% Load.

$$\text{Entering } T_{db} = \begin{cases} 16/11\ (\text{Design } T_{db} - 13)(\%\text{Load} - 0.3125)+13 & \text{for Load}>31.25\% \\ 13 & \text{for Load}\leq 31.25\% \end{cases} \quad (5.4)$$

for water-cooled chillers at NPLV.SI part load conditions, Equation 5.5 is used to determine the entering water temperature coming from the cooling tower

(Entering T_{cond}). Design temperature (Design T_{cond}), is the entering condenser temperature at 100% Load.

$$\text{Entering } T_{cond} = \begin{cases} 2.(\text{Design } T_{cond} - 19)(\%\text{Load} - 0.5) + 19 & \text{for Load} > 50.00\% \\ 19 & \text{for Load} \leq 50.00\% \end{cases} \quad (5.5)$$

The partial loads will be calculated by the model with the stated COP values mentioned in ASHRAE 90.1 stated in Table 5.5.

Table 5.5 Water-chilling packages minimum efficiency requirements

Equipment Type	**Equipment Size**	**Minimum Required COP at Full Load**	**Minimum Required COP for IPLV**
Air-cooled chillers	<528 kW	≥2.985 FL	≥4.048 NPLV/IPLV
	≥528 kW	≥2.985 FL	≥4.137 NPLV/IPLV
Water-cooled positive displacement chillers	<264 kW	≥4.694 FL	≥5.867 NPLV/IPLV
	≥264 kW and <528 kW	≥4.889 FL	≥6.286 NPLV/IPLV
	≥528 kW and <1055 kW	≥5.334 FL	≥6.519 NPLV/IPLV
	≥1055 kW and <2110 kW	≥5.771 FL	≥6.77 NPLV/IPLV
	≥2110 kW	≥6.286 FL	≥7.041 NPLV/IPLV
Water-cooled centrifugal chillers	<1055 kW	≥5.771 FL	≥6.401 NPLV/IPLV
	≥1055 kW and <1407 kW	≥6.286 FL	≥6.770 NPLV/IPLV
	≥1407 kW	≥6.286 FL	≥7.041 NPLV/IPLV

The IPVL value is calculated by the model mentioned in previous chapters and the COP will be increased if the IPVL is lower than mentioned in ASHRAE.
For centrifugal water-cooled chillers, the IPVL requirement is adjusted by a Path A calculation mentioned in ASHRAE, which is carried out for temperature values other than standard conditions.

$$FL_{adj} = FL \times K_{adj} \quad (5.6)$$

$$PLV_{adj} = IPLV \times K_{adj} \quad (5.7)$$

where FL is the full load COP value from Table 5.5, FL_{adj} is the adjusted value. Same applies for IPLV and PLV_{adj}.

K_{adj} multiplier is calculated by Equations 5.8 through 5.11.

$$K_{adj}=A \times B \tag{5.8}$$

$$A=0.00000153181 \times (LIFT)^4 - 0.000202076 \times (LIFT)^3 + 0.0101800 \times (LIFT)^2 - 0.264958 \times LIFT + 3.93073 \tag{5.9}$$

$$B=0.0027 \times T_{evap,leaving} \tag{5.10}$$

$$LIFT = T_{cond,leaving} - T_{evap,leaving} \tag{5.11}$$

$T_{cond,leaving}$ is the temperature of condenser water leaving the chiller and $T_{evap,leaving}$ is the temperature of the water exiting the evaporator of the chiller.

After the required design efficiency calculation is carried out the model will be simulated in the hourly analysis at patrial loads with varying temperature.

5.3.2. Cooling Tower Sizing

The sizing carried out for the cooling tower results in the cooling capacity of the tower, circulated water flow rate, circulation pump capacity, fan power and makeup water consumption. The model mentioned in previous chapters will be used to determine the leaving water temperature at design conditions.

For water cooled chiller systems the capacity of the cooling tower is 1.25 of the chiller cooling capacity which is based on the “assumption that at typical air conditioning conditions, for every kilowatt of heat picked up in the evaporator, the cooling tower must dissipate an additional 0.25 kW of compressor heat”. The nominal water flow rate is calculated by 54ml/s for every 1.25 kW rejected heat from 35°C to 29.4°C at a 25.6°C entering air wet-bulb temperature. (American Society of Heating, Refrigerating and Air-Conditioning Engineers, 2020). The temperature difference of the water regime could be determined differently which will change the design water flow rate which also changes the nominal tower capacity. The model results in the leaving water temperature which is the condenser entering temperature for the chiller model.

For situations where the cooling tower is directly coupled to the stack with a heat exchanger, the water outlet temperature will be determined as 35°C with a ΔT of

15°C. In this case the cooling tower model mentioned in the previous chapter will be utilized to iterate the required FRwater ratio which will be used to calculate the nominal capacity of the tower.

It is mentioned that the circulation pump capacity could be calculated as 300 W per l/s water flow as per ASHRAE 90.1 standard. The design fan power requirement is also mentioned in the same standard as water flow rate/ fan power ≥ 3.40 l/(s.kW).

The outdoor wet-bulb temperature is used as an input for the model for design calculations which is taken from 0.4 % summer wet-bulb temperature from ASHRAE which is specified for various locations in the Fundamentals Handbook or also ASHRAE climatic design website (American Society of Heating, Refrigerating and Air-Conditioning Engineers, 2021a, 2021b).

Cooling towers lose water during operation. Makeup water design flowrate as mentioned in most references are calculated as follows (Perry et al., 2007)

$$\dot{m}_{makeup}=\dot{m}_{evaporation}+\dot{m}_{drift}+\dot{m}_{blowdown} \tag{5.12}$$

The evaporation loss ($\dot{m}_{evaporation}$) is calculated by Equation 5.13.

$$\dot{m}_{evaporation}= 0.00085 \cdot \dot{m}_{cond} \cdot \Delta T_{cond} \cdot 5/9 \tag{5.13}$$

And can also be calculated by Equation 5.14.

$$\dot{m}_{evaporation}= \frac{Q_{coolingtower}}{h_{fg}}=\frac{\dot{m}_{cond} \cdot c_p \cdot \Delta T_{cond}}{h_{fg}} \tag{5.14}$$

$$=\dot{m}_{cond} \cdot \Delta T_{cond} \cdot \frac{4.2 \text{ kj/kg}}{2400 \text{ kj/kg}} = \dot{m}_{cond} \cdot \Delta T_{cond} \cdot 0.00175$$

Drift is entrained water in the tower discharge vapors and is calculated by Equation 5.15.

$$\dot{m}_{drift}=0.002 \text{ x } \dot{m}_{cond} \tag{5.15}$$

The system solids that are left behind as water is evaporated. Blowdown is the discharged portion of the circulating water in order to maintain water quality. The amount of blowdown can be calculated according to the number of cycles of concentration required to limit scale formation. “Cycles of concentration” is the

ratio of dissolved solids in the recirculating water to dissolved solids in the makeup water (Perry et al., 2007).

$$COC = \frac{\dot{m}_{evaporation} + \dot{m}_{drift} + \dot{m}_{blowdown}}{\dot{m}_{drift} + \dot{m}_{blowdown}} \quad (5.16)$$

Cycles of concentration (COC) must be below 3 and it is assumed 2.5 in this study. Thus, the Equation 5.16 could be adjusted to calculate the blowdown loss by Equation 5.17.

$$\dot{m}_{blowdown} = \frac{\dot{m}_{evaporation} - (COC-1)\dot{m}_{drift}}{(COC-1)} \quad (5.17)$$

Basin heaters are required for cold locations to prevent freezing, Basin heater design capacity is calculated by BAC manufacturer recommendation of 50 W/in^2 to prevent freezing at $T_{setpoint}$ of 5°C and $T_{ambient}$ of -18°C. Therefore, manufacturer data sheets were observed to form a table determining the basin area of cooling towers with regards to their capacity. Dividing the capacity of the heater by the temperature difference of 23°C will result in capacity in terms of W/K.

Table 5.6 Cooling tower basin heater estimation.

Cooling Tower kW	m2	Basin Heater Capacity kW	Basin Heater Capacity W/K
400-700	8	16	695
700-1400	12	24	1043
1400-2500	24	48	2087
2500-5000	30	60	2608
5000-10000	60	120	5217

50 W/in2 as per BAC manufacturer recommendations for setpoint 5C and outdoor -18C

5.3.3. Dry Cooler Sizing

Dry cooler sizing results in the design air flow rate and fan power. The water regime will be 70 - 55°C and the outdoor dry-bulb temperature will be taken from 0.4 % summer dry-bulb temperature from ASHRAE. The design air flow rate for the dry cooler proposed by EnergyPlus with Equation 5.18 could be used for design calculations.

$$\dot{V}_{fluidcoolere,air,des} = 4. \frac{\dot{Q}_{fluid\ cooler,nom}}{T_{in,water} - T_{in,air}} \quad (5.18)$$

Although when compared to commercial dry cooler product selection software, for ΔT = 15 values the multiplier lays in values between 4-11. Therefore, the

multiplier of the formula will be 6.5 for the model of this study. Where $V_{fluidcooler,air,des}$ is in m^3/h and $Q_{fluidcooler,nom}$ in Watts.

After the air flow rate is calculated, the model will start iterating to find the appropriate UA value that results in the same capacity. The dry cooler is considered to have a two-speed fan. The fraction of the low fan speed airflow and fan power is considered to be 0.5 and 0.16 respectively as also used in EnergyPlus as default values. The UA value also changes at low fan speed and is assumed to be a default fraction of 0.6 of what it is at full speed.

It is mentioned that the circulation pump capacity could be calculated as 300 W per l/s water flow as per ASHRAE 90.1 standard. The design fan power requirement is also mentioned in the same standard as water flow rate/ fan power ≥ 0.38 l/(s.kW).

5.4. Pump Sizing

The design flow of the circulation pumps are calculated by their dedicated equipment design heat capacity and the determined temperature regime. Later, the flowrates are used to determine the pump nominal power by ASHRAE 90.1 standard where it is suggested 140 W/L/s for chiller circulation pump and 300 W/L/s for other heat rejection circulation pumps.

The booster pump design capacity, however, is calculated by the pressure and flowrate. High pressure of 15 bars is determined for use with reverse osmosis systems. Water consumption flow rate are determined by maximum consumption of stacks and also of cooling towers if included. The design pump efficiency is determined 60 % for calculating the nominal power of the pump.

5.5. Fan Sizing

As mentioned in earlier chapters, constant ventilation is required for fire safety of the plant which its flow rate criteria is 0.0051 $m^3/s/m^2$ according to NFPA2. The fan power limit is calculated as advised in ASHRAE 90.1 by option 2 of constant flow fan power calculation.

$$P_{fan} = \dot{V}_{fan} x 0.0015 + A \quad (5.19)$$

$$A = PD \times \dot{V}_{fan}/650000 \quad (5.20)$$

Where V_{fan} is the flowrate in l/s and PD is applicable pressure drop adjustment for different elements to be used. As there is no physical designing of duct components in this study, for ease of use, a safe value of 300 Pa will be used as an average value considering hood exhaust could be used with dampers.

5.6. PV Plant Design

The simulation for PV plants were carried out for different locations. The parameters concerning design of PV plants are the plant capacity, azimuth angle, tilt angle and ground coverage ratio (GCR).

The azimuth angle for plants on the northern hemisphere will be 180° and the tilt angle will be determined according to parametric simulations carried out on SAM to find the angle which results in the most yield in increments of 5°.

The GCR depends on the edge length of the PV module and row spacing.

$$GCR = \frac{L}{R} \quad (5.21)$$

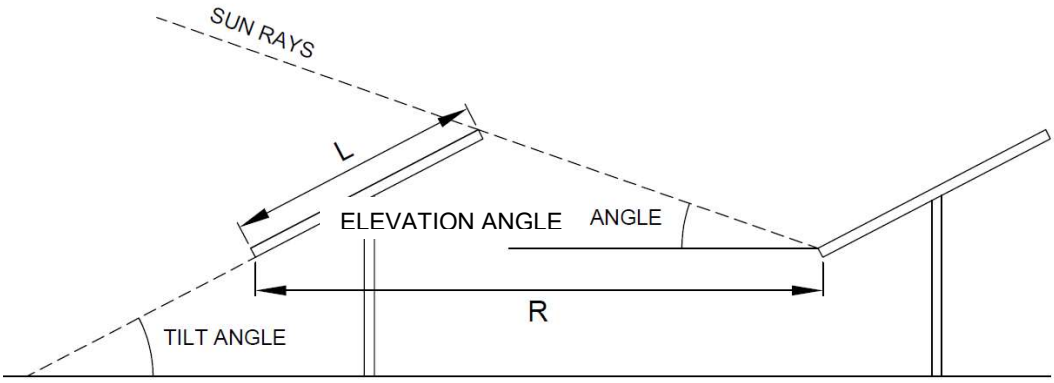

Figure 5.3 Visualization of angles required for GCR calculation.

$$R = L \cdot \cos(\text{Tilt Angle}) + L \cdot \frac{\sin(\text{Tilt Angle})}{\tan(\text{Elevation Angle})} \quad (5.22)$$

The row spacing is dependent on the tilt angle and the elevation angle. The elevation angle will be determined according to 9.00 am – 3.00 pm angles on 21 December of the specified location as mentioned in most resources.

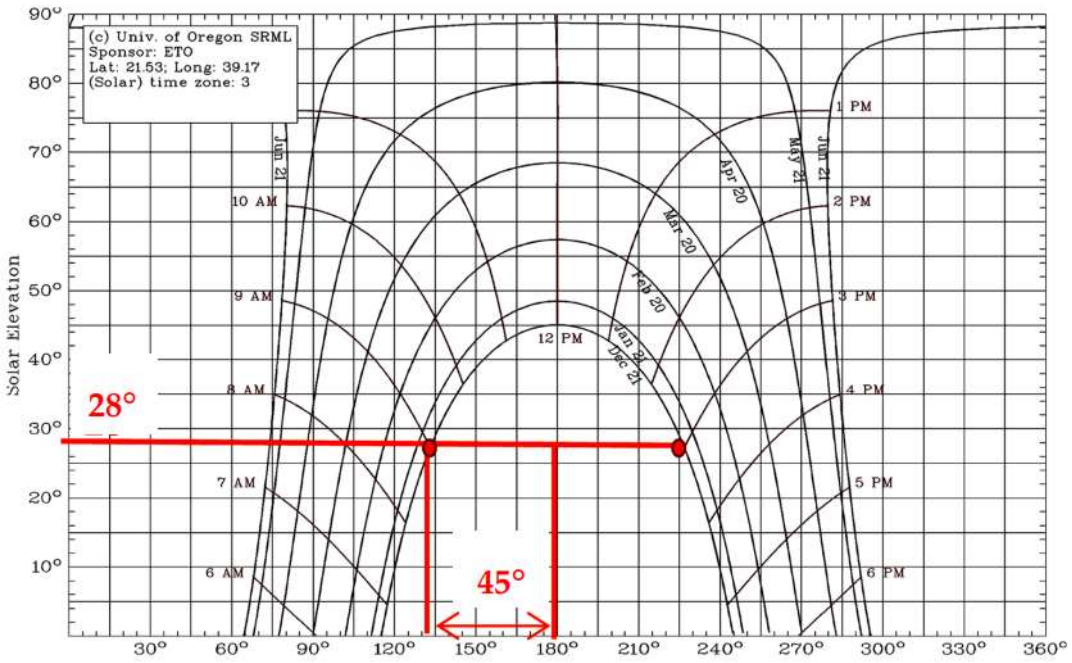

Figure 5.4 Example of a two-dimensional sun path, with angles (Al-Quraan et al., 2022)

5.7. Design Summary

A simulation is made to observe the performance and losses of the PEM plant operating from 5 to 100 % at constant outdoor weather values to be compared to few studies available in literature. The results and discussions are provided on Chapter 6. Further simulations are carried out as follows.

Locations to be simulated in Turkey is determined by the PV potential map provided by Solagris. “The PV potential is defined in the unit kWh/kWp and indicates the kWh of electricity that would be generated by a PV system with 1kW peak installed capacity” (Solagris, 2023).

Antalya was firstly simulated for all capacity design variations to observe effects in efficiencies. After the observations Sanliurfa and Kocaeli locations were to be simulated to compare the results with Antalya. Sanliurfa is a sample location that provides the one highest capacity factors of the country. Kocaeli is a sample location with lower capacity factor which is at the north of the country.

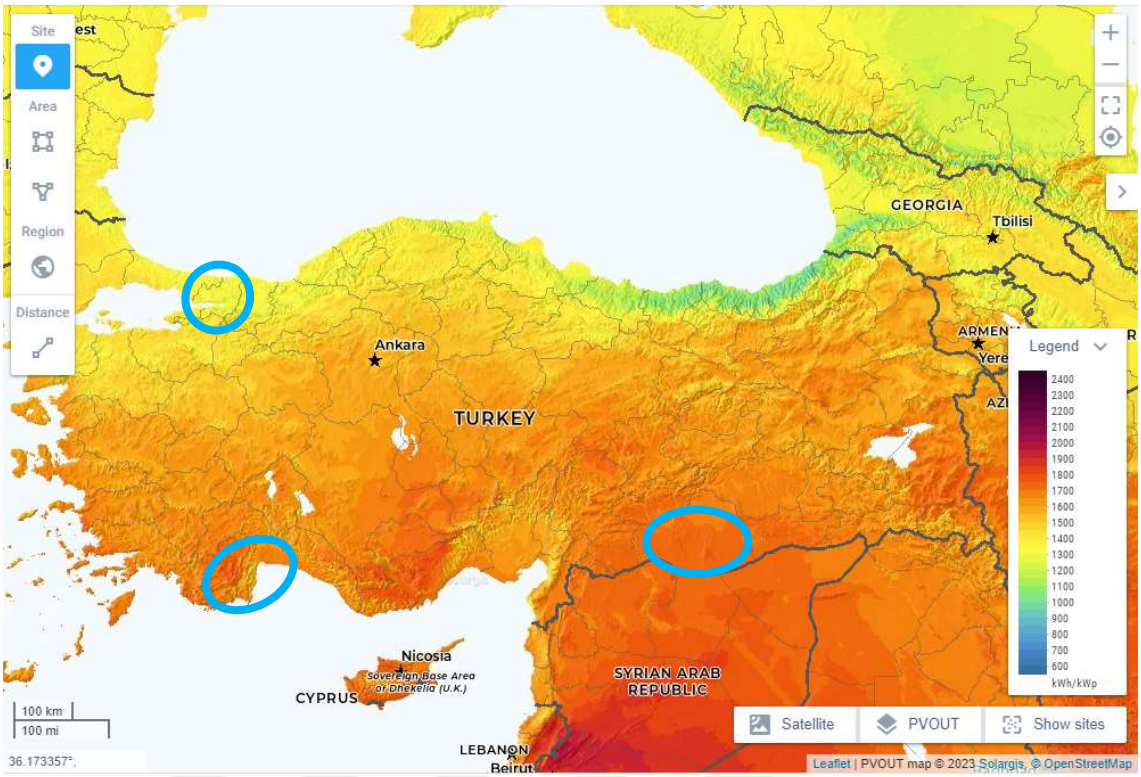

Figure 5.5 PV potential map of Turkey (Solagris, 2023)

Table 5.7 Summer design temperature data of considered cities from ASHRAE Fundamentals and PV plant design parameters.

Country	DB (°C)	WB (°C)	DESIGN ELEVATION ANGLE	TILT	GCR
Turkey - Kocaeli	33.2	24.7	14	35	0.321
Turkey-Antalya-Finike	37.1	27	16	35	0.355
Turkey - Sanliurfa	41.1	25.1	16	35	0.355

Locations to be simulated globally were determined by observing major GW scale PV projects across the globe Global Energy Monitor website provides location and capacities of all renewable energy projects.

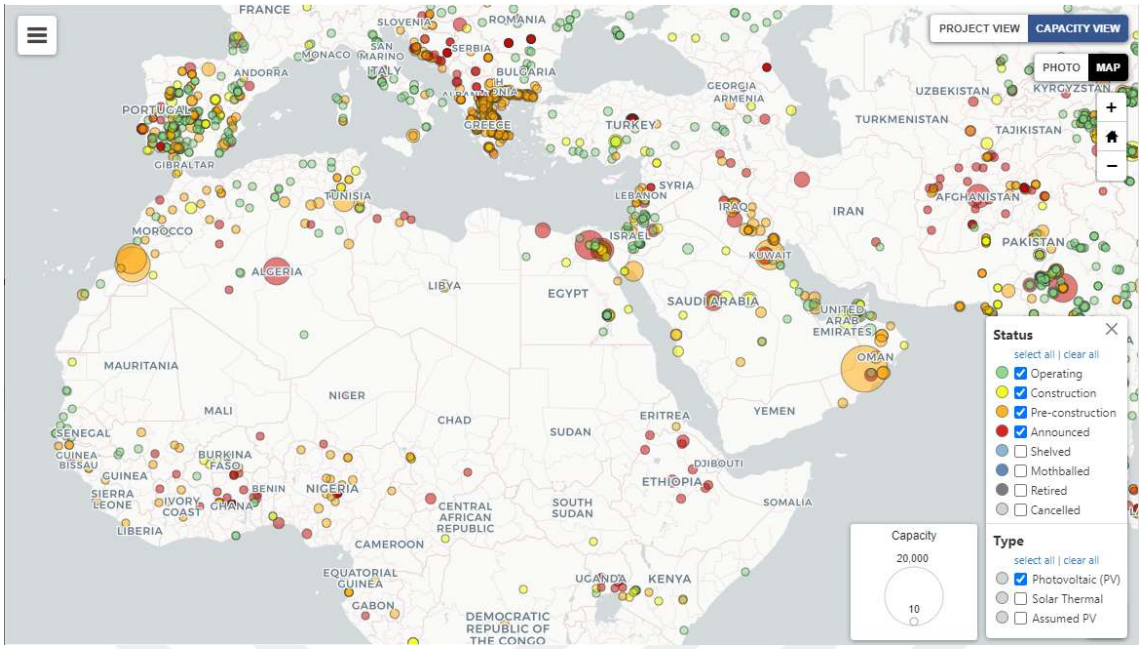
PROJECT VIEW
CAPACITY VIEW
PHOTO
MAP
FRANCE
SLOVENIA
ROMANIA
SAN MARINO
SERBIA
MONACO
ANDORRA
ITALY
BULGARIA
PORTUGAL
GREECE
GEORGIA
ARMENIA
UZBEKISTAN
KYRGYZSTAN
TURKEY
TURKMENISTAN
TAJIKISTAN
GIBRALTAR
TUNISIA
SYRIA
LEBANON
IRAQ
AFGHANISTAN
IRAN
MOROCCO
ISRAEL
KUWAIT
PAKISTAN
ALGERIA
LIBYA
EGYPT
SAUDI ARABIA
UNITED ARAB EMIRATES
OMAN
MAURITANIA
NIGER
MALI
CHAD
ERITREA
YEMEN
SENEGAL
SUDAN
GUINEA BISSAU
BURKINA FASO
GUINEA
DJIBOUTI
ETHIOPIA
SIERRA LEONE
BENIN
NIGERIA
IVORY COAST
GHANA
SOMALIA
CENTRAL AFRICAN REPUBLIC
SOUTH SUDAN
LIBERIA
CAMEROON
EQUATORIAL GUINEA
UGANDA
KENYA
GABON
DEMOCRATIC REPUBLIC OF THE CONGO
Status
select all | clear all
Operating
Construction
Pre-construction
Announced
Shelved
Mothballed
Retired
Cancelled
Type
select all | clear all
Photovoltaic (PV)
Solar Thermal
Assumed PV
Capacity
20,000
10

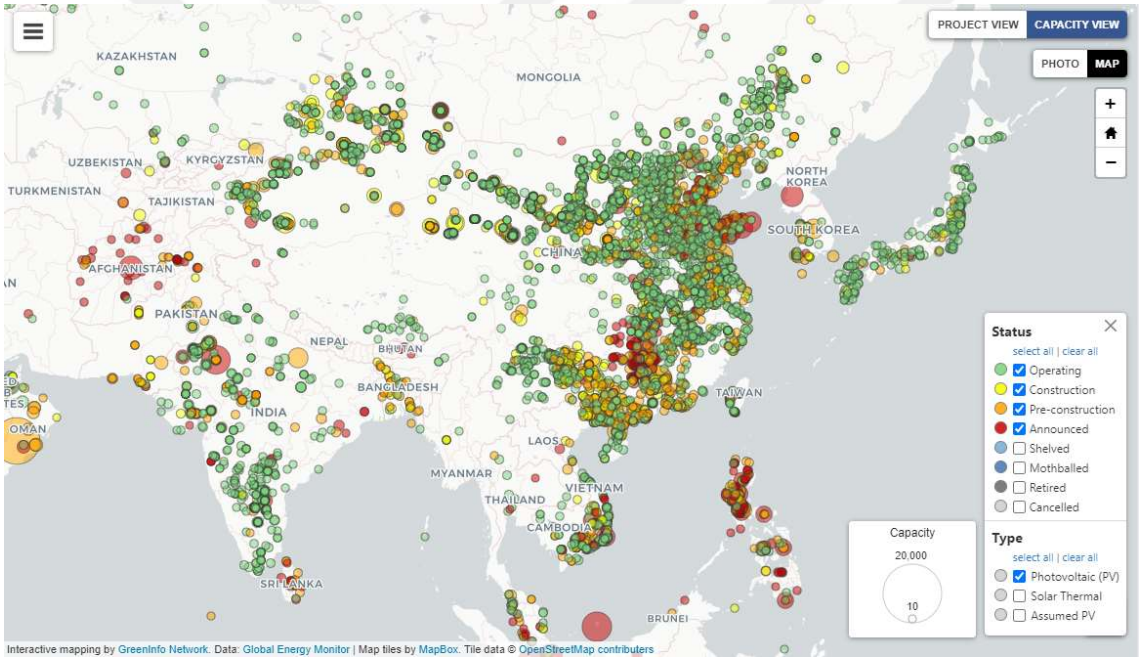
PROJECT VIEW
CAPACITY VIEW
PHOTO
MAP
KAZAKHSTAN
MONGOLIA
UZBEKISTAN
KYRGYZSTAN
NORTH KOREA
TURKMENISTAN
TAJIKISTAN
SOUTH KOREA
CHINA
AFGHANISTAN
PAKISTAN
NEPAL
BHUTAN
BANGLADESH
TAIWAN
INDIA
OMAN
LAOS
MYANMAR
VIETNAM
THAILAND
CAMBODIA
SRI LANKA
BRUNEI
Status
select all | clear all
Operating
Construction
Pre-construction
Announced
Shelved
Mothballed
Retired
Cancelled
Type
select all | clear all
Photovoltaic (PV)
Solar Thermal
Assumed PV
Capacity
20,000
10
Interactive mapping by GreenInfo Network. Data: Global Energy Monitor | Map tiles by MapBox. Tile data © OpenStreetMap contributors

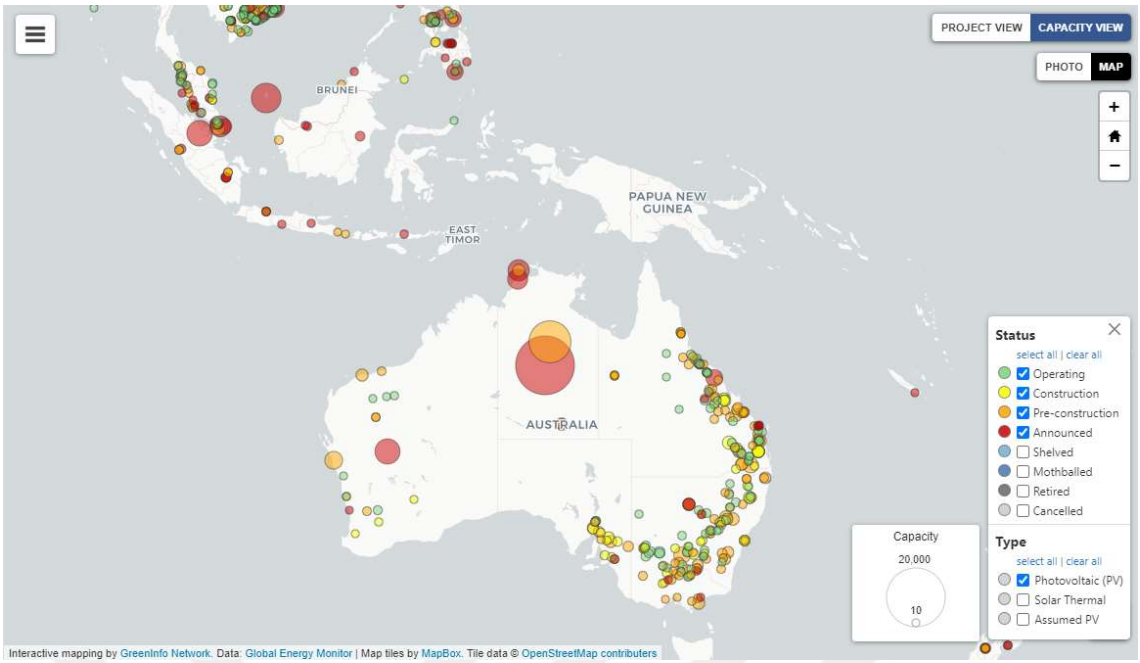

Figure 5.6 Mapped data of PV projects announced, in pre-construction, construction or operating stage phase (Global Energy Moniter, 2023).

Table 5.8 List of top 15 countries that have GW scale PV projects announced, in pre-construction, construction or operating phase (Global Energy Moniter, 2023).

Country	**MW**
China	51450
Australia	42733
India	31640
Egypt	13920
Oman	12500
Morocco	12000
Indonesia	11500
Philippines	11163
Brazil	7700
Kuwait	7700
Saudi Arabia	5050
Namibia	4750
United Arab Emirates	4677
United States	4500
Tunisia	4250

The top 15 countries with GW scale PV projects are listed in Table 5.8. These locations are simulated in the PEM model to compare for what the effect of difference in weather conditions and energy production could be.

Table 5.9 Weather file location, weather data and PV design parameters for worldwide analysis.

Country	Weather Data File Location	DB (°C)	WB (°C)	DESIGN ELEVATION ANGLE	TILT	GCR
China	SHAOGUAN, CHINA (WMO: 590820)	35.3	27.4	25	25	0.55
Australia	TENNANT CREEK, AUSTRALIA (WMO: 942380)	40.0	25.1	28	20	0.63
India	NGARI, CHINA (WMO: 552280)	22.7	9.7	20	40	0.4
Egypt	RAS SEDR, EGYPT (WMO: 624550)	38.3	25.1	22	30	0.48
Oman	MARMUL, OMAN (WMO: 413040)	44.0	25.2	30	20	0.65
Morocco	AGADIR AL MASSIRA INTL, MOROCCO (WMO: 602520)	38.9	22.5	22	30	0.48
Indonesia	RENGAT JAPURA, INDONESIA (WMO: 961710)	33.7	27.4	40	5	0.91
Philippines	TAYABAS, PHILIPPINES (WMO: 984270)	32.9	28.4	30	15	0.71
Brazil	PETROLINA, BRAZIL (WMO: 829840)	37.2	24.9	28	10	0.76
Kuwait	ALI AL SALEM AB, KUWAIT (WMO: 405736)	48.9	27.0	22	30	0.48
Saudi Arabia	AL WAJH, SAUDI ARABIA (WMO: 404000)	36.1	30.2	24	25	0.54
Namibia	ALEXANDER BAY, SOUTH AFRICA (WMO: 684030)	32.0	20.6	22	25	0.51
United Arab Emirates	AL DHAFRA, UNITED ARAB EMIRATES (WMO: 412162)	46.0	30.4	26	25	0.57
United States	TONOPAH, NV, USA (WMO: 724855)	35.3	17.3	26	40	0.48
Tunisia	TOZEUR NEFTA, TUNISIA (WMO: 607600)	44.0	24.7	18	35	0.39

6. RESULTS AND DISCUSSIONS

6.1. Simulation of 1 MW Electrolyzer System

A 1 MW electrolyzer system was simulated from 5 to 100 % to observe the efficiency of the system and the losses in the BoP. The design of 1MW-1.1 was used which resembles the containerized 1 MW models of various manufacturers. The results are compared to available literature (Hamdan, 2013; Colella et al., 2014; Pivovar et al., 2021, 2022).

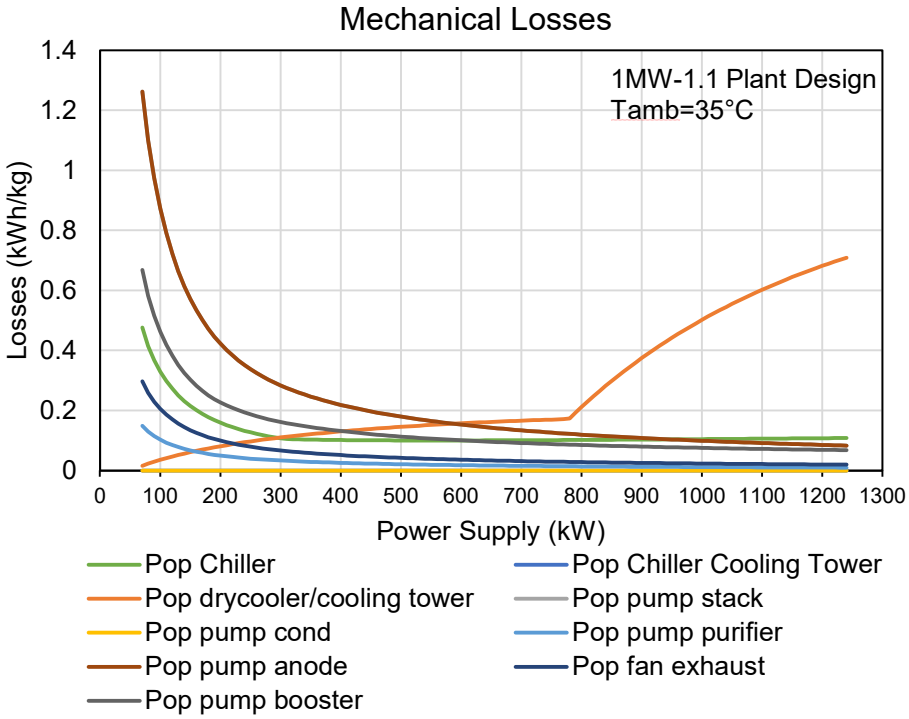

Figure 6.1 Mechanical component losses of PEM simulation

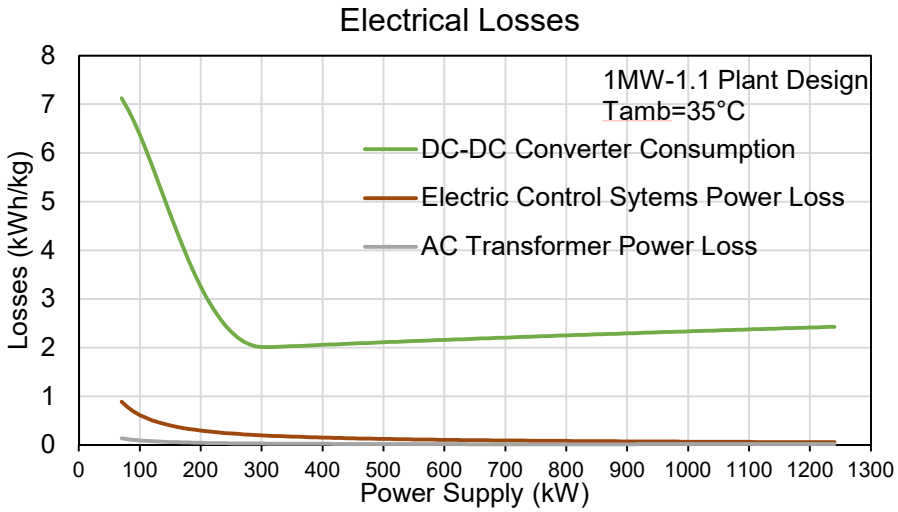

Figure 6.2 Electrical component losses of PEM simulation

As can be observed from the graphs, the system losses are high at very low loads and after meeting a low point it starts increasing as the dry cooler and the DC-DC converter efficiencies decrease at higher loads.

The graph shown by Figure 6.3 was compared to the chart provided by (Pivovar et al., 2022) in Figure 6.4 and proves to show similar characteristics. The mechanical losses in reference seem to converge to zero when this is not the case in this study's simulation. This has occurred because the flowrates of circulation loops are held constant and VSD pumps are used in larger systems for multiple equipment in this study. This is because of the thought that the anode circuit needs to maintain its design flowrate to prevent bubble concentration and that the cooling equipment were modeled for constant flow. Even if all flows were to be variable to adjust for optimal flow, the VSD pump power consumption would not converge to zero as the load approaches zero. This is because the fan and motor efficiencies decrease at low speeds and still has a significant consumption. The other effect of having higher mechanical losses at lower system loads is that the exhaust fan of the enclosure is also included in this model which operates at constant flowrate which will cause the kW/kg loss to diverge to infinity as the system load approaches zero. The graphs presented in (Pivovar et al., 2022) might not have included booster pumps and exhaust fans as booster pumps could be optional if high pressure water is readily available and exhaust fans might have not been included as part of BoP components as it is actually a ventilation component of the encloser but not directly of the PEM system.

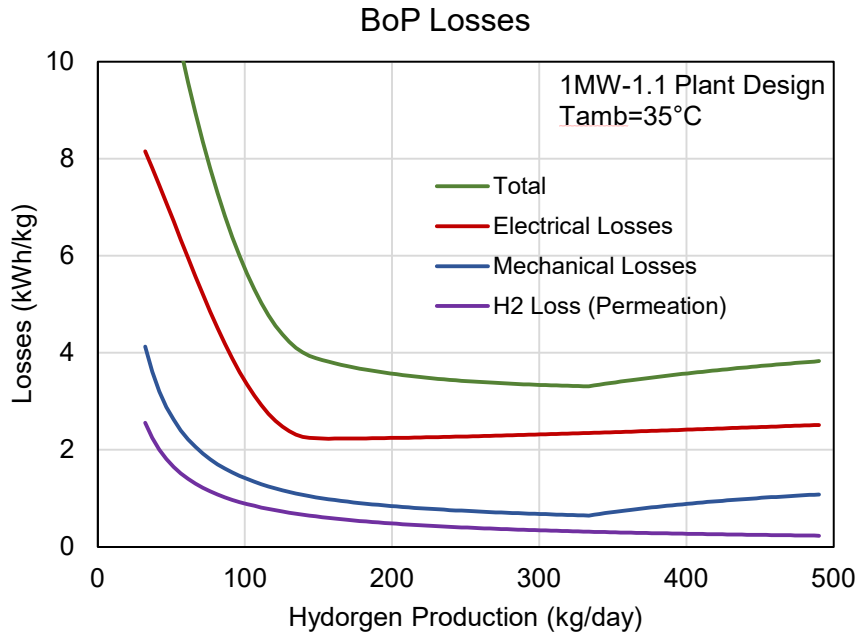

Figure 6.3 BoP losses of PEM simulation

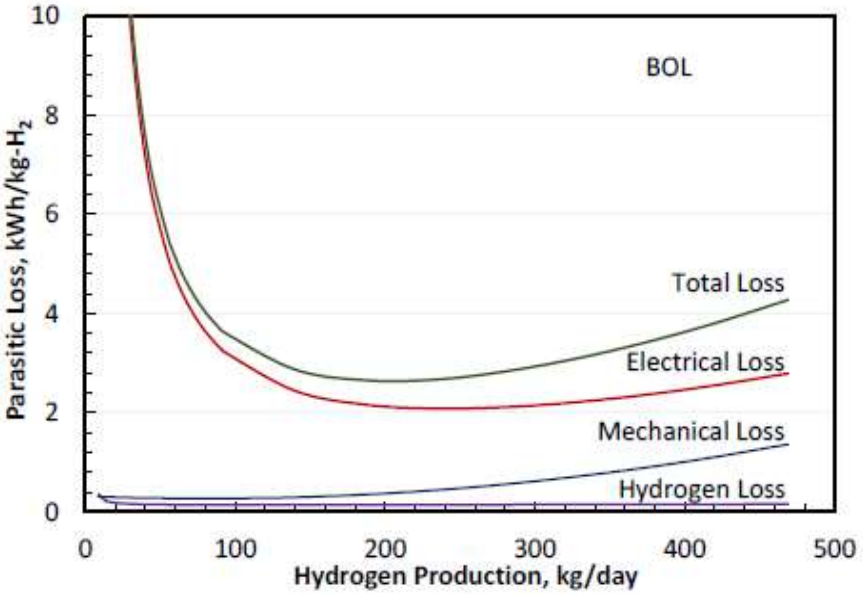

Figure 6.4 BoP losses from H2NEW report (Pivovar et al., 2022)

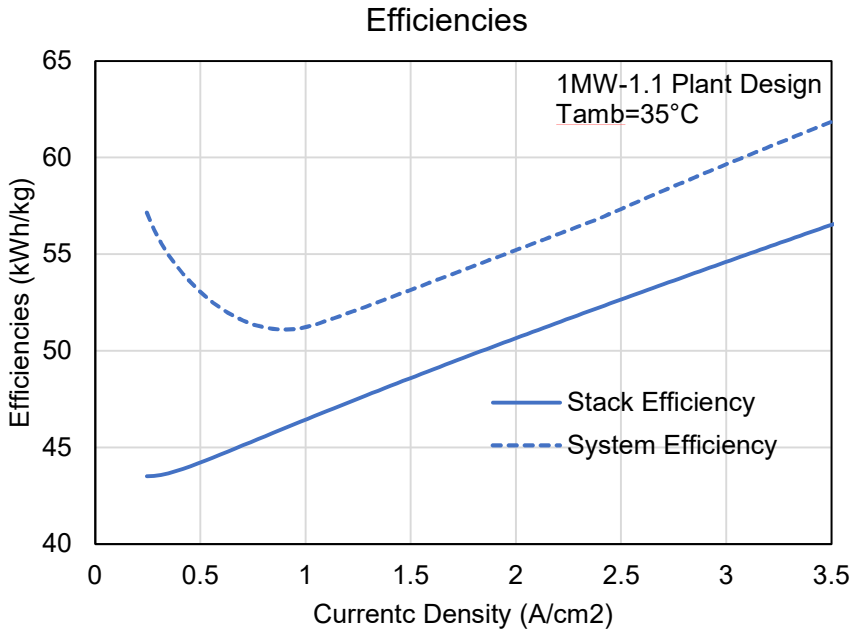

Figure 6.5 Efficiency curves of PEM simulation

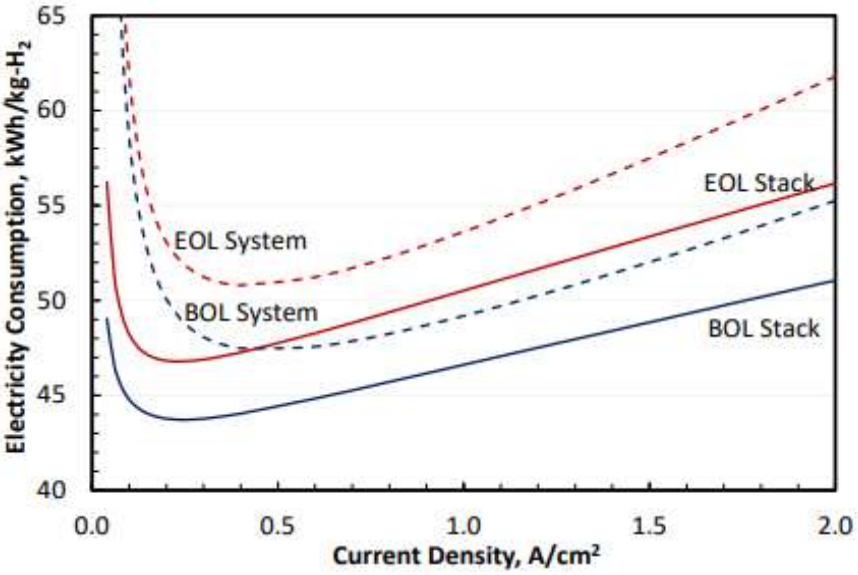

Figure 6.6 Efficiency curves from H2NEW report 2022 (Pivovar et al., 2022)

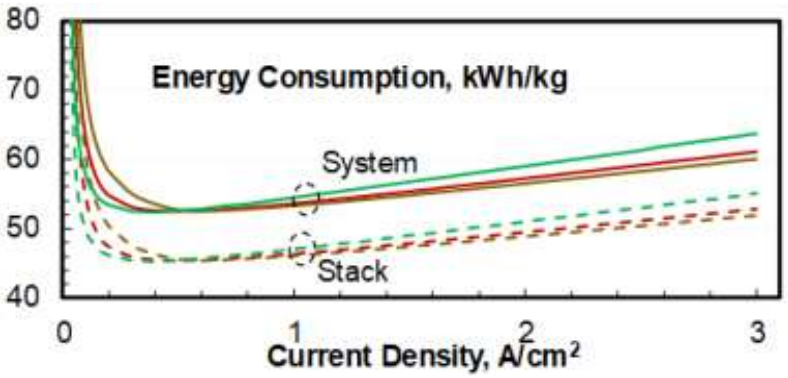

Figure 6.7 Efficiency curves from H2NEW report 2021 (Pivovar et al., 2021)

It can seen that there is a difference between the efficiency curves of the two reference Figures 6.6 and 6.7 (Pivovar et al., 2021, 2022). It is as thought the earlier study had assumed a constant kWh/kg consumption of BoP and not a variable consumption. The later seems more realistic as the stack and system curves are not parallel and this study's model provides very similar curve characteristics. The lowest consumption point of the system in this study is seems to lie on 0.9 A/cm^2 current density. The reference study seems to be around 0.5 A/cm^2 and this is mostly due to the effect of mechanical components mentioned earlier.

Table 6.1 Comparision of model simulation values and reference literature reports

	Simulation	H2NEW 2022 Report (Pivovar et al., 2022)	H2NEW 2021 Report (Pivovar et al., 2021)	Strategic Analysis Inc. Report 2014 (Colella et al., 2014) Vcell=1.75	(Hamdan, 2013) i=1900A/cm^2
	kWh/kg	kWh/kg	kWh/kg	kWh/kg	kWh/kg
@ BoP losses lowest point 333kg/day @Vcell=1.934V					
Electric BoP Consumption	2.35	2.2		3.79	
Mechanical Consumption	0.65	0.4		1.25	
H2 Loss (Permeation)	0.31	0.1		-	
Total	3.31	2.7		5.04	
Stack Efficiency	52.24				47.3
System Efficiency	56.85				64.8
@ System lowest point 125kg/day @Vcell=1.691V					
Stack Efficiency	46.04	43.7			
System Efficiency	51.11	47.5			
@ Maximum capacity point 488kg/day @Vcell=2.1V					
Electric BoP Consumption	2.51	2.8	3.69		
Mechanical Consumption	1.08	1.3	1.16		
H2 Loss (Permeation)	0.23	0.2	0.42		
Total	3.83	4.3	5.27		
Stack Efficiency	56.56	51.1			
System Efficiency	61.91	55.3			

The results are considered close to of Pivovar et al. (2022). The hydrogen losses were calculated for permeation at stack. The losses on the system side are actually part of the BoP losses so they are not indicated separately. Hydrogen losses seem to differ even in the two reports published by the same study team (Pivovar et al., 2021, 2022). This might be because of recent advances in membrane improvement or a difference in calculation of hydrogen loss in kWh/kg.

Hydrogen losses occur as permeation and losses due to dryer equipment. The effect of hydrogen losses accounts for a fraction inside stack, electrical and mechanical losses and is not a separate loss. The effect of hydrogen losses can be observed more clearly in Tables 6.2 to 6.4 summary sheets of efficiencies and is a more detailed way to observe the system performance. Figures 6.8 to 6.10 are visualizations of the energy consumption portions as pie charts to better comprehension. The pie charts do not segregate the hydrogen losses as in the table to prevent clusters.

Table 6.2 Detailed efficiency distribution evaluation table for point where BoP losses are at lowest

@ BoP losses lowest point 333kg/day @Vcell=1.934V

Hydrogen Production/ Loss	kg/s
H2Net	0.003862224
H2Dryer Loss	0.00011945
H2Permeation Loss	2.33625E-05

	Consumption			Efficiency	
	kW	%	%	kWh/kg	kWh/kg
Stack Consumption	722.099	91.35%	94.73%	51.935	53.85
H2Dryer Loss on Stack	22.333	2.83%		1.606	
H2Permeation Loss on Stack	4.368	0.55%		0.314	
Electric BoP Consumption	31.460	3.98%	4.13%	2.263	**2.35**
H2Dryer Loss on Electrical	0.973	0.12%		0.070	
H2Permeation Loss on Electrical	0.190	0.02%		0.014	
Mechanical Consumption	8.713	1.10%	1.14%	0.627	**0.65**
H2Dryer Loss on Mechanical	0.269	0.03%		0.019	
H2Permeation Loss on Mechanical	0.053	0.01%		0.004	
Total System	**790.459**				**56.85**
H2Dryer Loss Total	23.575	2.98%	3.57%	1.70	2.03
H2Permeation Loss Total	4.611	0.58%		0.33	

Note: Stack Efficiencies are not calculated by system net hydrogen production. Therefore the above calculation for the stack is not to be compared with literature or catalogues. The below calculation is made for this purpose.

Stack Efficency	kW	%	kWh/kg
Stack Consumption	744.298	99.40%	**52.24**
H2Permeation Loss on Stack	4.502	0.60%	

Note: Stack efficiencies are calculated excluding dryer losses by using (H2Net+H2Dryer Loss) in the denominator.

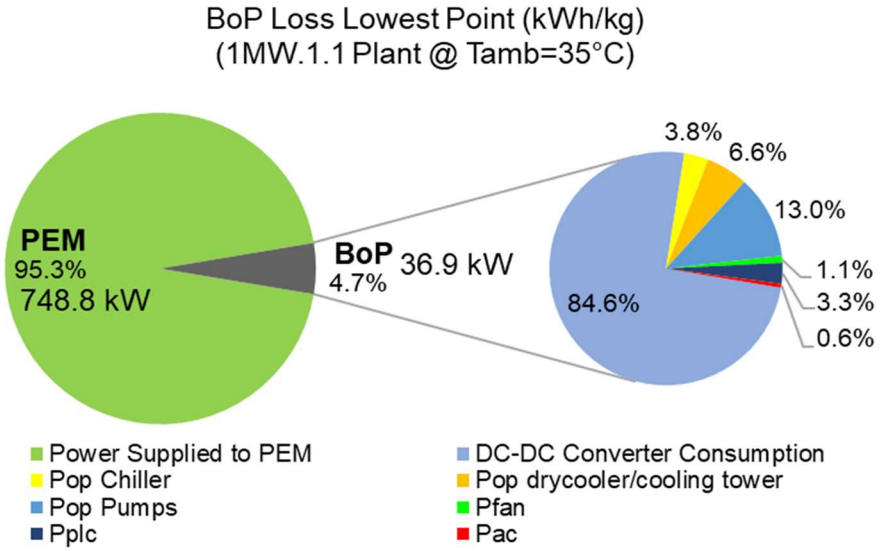

Figure 6.8 Efficiency distribution pie chart visualization for point where BoP losses are at lowest

Table 6.3 Detailed efficiency distribution evaluation table for point where system consumption is at lowest point

@ System lowest point 125kg/day @Vcell=1.691V

Hydrogen Production/ Loss	kg/s
H2Net	0.001453959
H2Dryer Loss	4.49678E-05
H2Permeation Loss	2.33625E-05

	Consumption			Efficiency	
	kW	%	%	kWh/kg	kWh/kg
Stack Consumption	237.270	88.70%	92.87%	45.330	47.46
H2Dryer Loss on Stack	7.338	2.74%		1.402	
H2Permeation Loss on Stack	3.813	1.43%		0.728	
Electric BoP Consumption	12.387	4.63%	4.85%	2.367	**2.48**
H2Dryer Loss on Electrical	0.383	0.14%		0.073	
H2Permeation Loss on Electrical	0.199	0.07%		0.038	
Mechanical Consumption	5.839	2.18%	2.29%	1.115	**1.17**
H2Dryer Loss on Mechanical	0.181	0.07%		0.034	
H2Permeation Loss on Mechanical	0.094	0.04%		0.018	
Total System	**267.503**				**51.11**
H2Dryer Loss Total	7.902	2.95%	4.49%	1.51	2.29
H2Permeation Loss Total	4.105	1.53%		0.78	

Note: Stack Efficiencies are not calculated by system net hydrogen production. Therefore the above calculation for the stack is not to be compared with literature or catalogues. The below calculation is made for this purpose.

Stack Efficency	kW	%	kWh/kg
Stack Consumption	244.492	98.42%	**46.04**
H2Permeation Loss on Stack	3.929	1.58%	

Note: Stack efficiencies are calculated excluding dryer losses by using (H2Net+H2Dryer Loss) in the denominator.

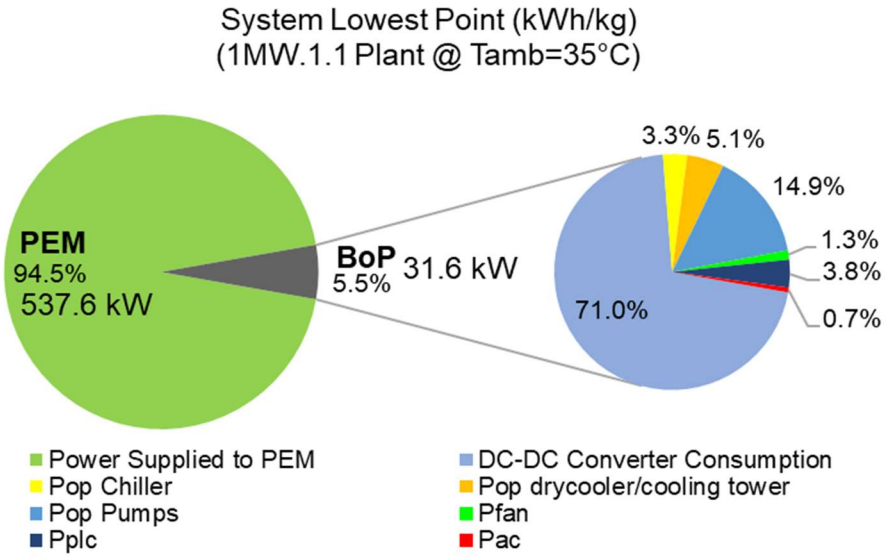

Figure 6.9 Efficiency distribution pie chart visualization for point where system losses are at lowest

Table 6.4 Detailed efficiency distribution evaluation table for point where system is at maximum capacity

@Maximum capacity point 488kg/day @Vcell=2.1V

Hydrogen Production/ Loss	kg/s
H2Net	0.00567059
H2Dryer Loss	0.000175379
H2Permeation Loss	2.33625E-05

	Consumption			Efficiency	
	kW	%	%	kWh/kg	kWh/kg
Stack Consumption	1150.092	91.00%	94.19%	56.338	58.31
H2Dryer Loss on Stack	35.570	2.81%		1.742	
H2Permeation Loss on Stack	4.738	0.37%		0.232	
Electric BoP Consumption	49.567	3.92%	4.06%	2.428	**2.51**
H2Dryer Loss on Electrical	1.533	0.12%		0.075	
H2Permeation Loss on Electrical	0.204	0.02%		0.010	
Mechanical Consumption	21.334	1.69%	1.75%	1.045	**1.08**
H2Dryer Loss on Mechanical	0.660	0.05%		0.032	
H2Permeation Loss on Mechanical	0.088	0.01%		0.004	
Total System	**1263.786**				**61.91**
H2Dryer Loss Total	37.763	2.99%	3.39%	1.85	2.10
H2Permeation Loss Total	5.030	0.40%		0.25	

Note: Stack Efficiencies are not calculated by system net hydrogen production. Therefore the above calculation for the stack is not to be compared with literature or catalogues. The below calculation is made for this purpose.

Stack Efficency	kW	%	kWh/kg
Stack Consumption	1185.516	99.59%	**56.56**
H2Permeation Loss on Stack	4.884	0.41%	

Note: Stack efficiencies are calculated excluding dryer losses by using (H2Net+H2Dryer Loss) in the denominator.

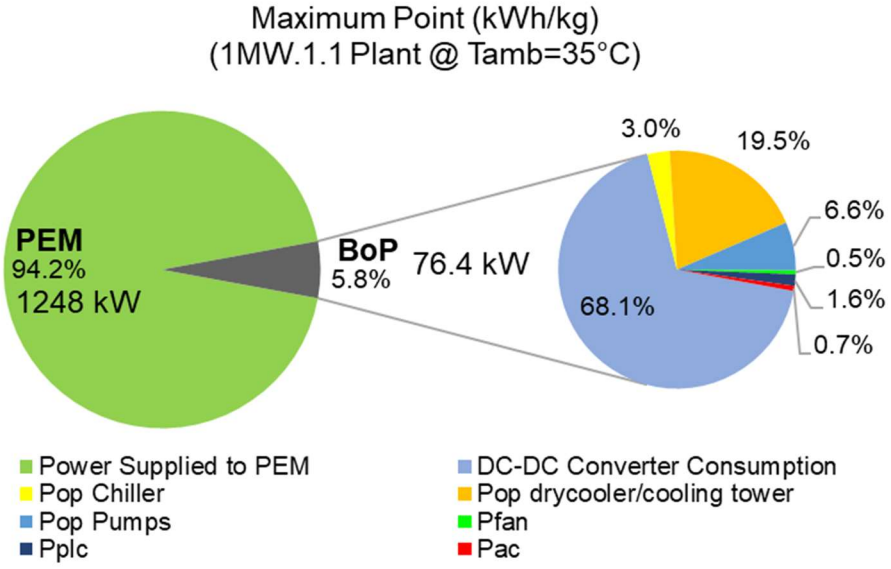

Figure 6.10 Efficiency distribution pie chart visualization for maximum operating point

It can be observed that hydrogen losses account for a range of 3.39 – 4.49 % of system power consumption contributing to an effect of 2.03 – 2.29 kWh/kg. The percentage of hydrogen loss due to dryers doesn't seem to change as significant (2.95 – 2.99 %) as permeation (0.40 – 1.53 %).

The factors affecting the system efficiency other than the electrochemical efficiency of the stack can be ordered from highest to lowest as Electrical Losses> Hydrogen Losses> Mechanical Losses.

It can be noted from the pie charts that the portion of consumption from the BoP is significantly lower compared to the stack. The change in portion of consumption of pumps and dry coolers could also be visually observed.

6.2. Simulations for selected locations in Turkey

A simulation for system capacities from 1 MW up to 1 GW was conducted in order to observe the difference between efficiencies and how much of an effect it would have. The simulation was carried out for Antalya-Finike location. The simulation carries out hourly calculations and results can be observed by plotting the results if intended. A sample is shown in Figure 6.11, where the first 96 hours of the year could be observed in terms of solar power production, stack consumption, cooling load, all equipment power consumption and also temperature of the stack.

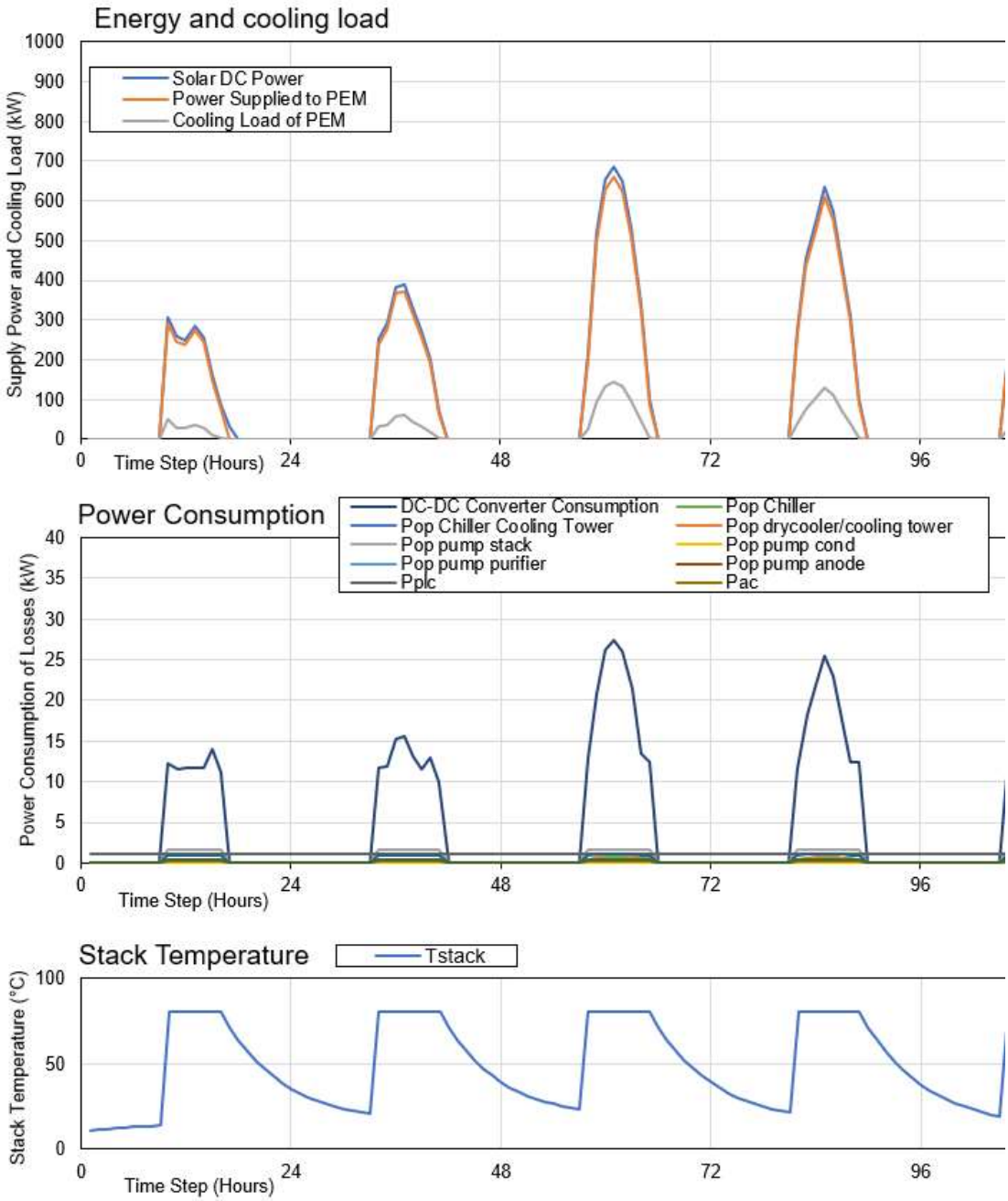

Figure 6.11 Snapshot of hourly simulation results evaluated for a 1MW-1.1. design for Antalya

The partial load profile of the location for year-round solar energy yield data simulated on SAM software is shown in Figure 6.12.

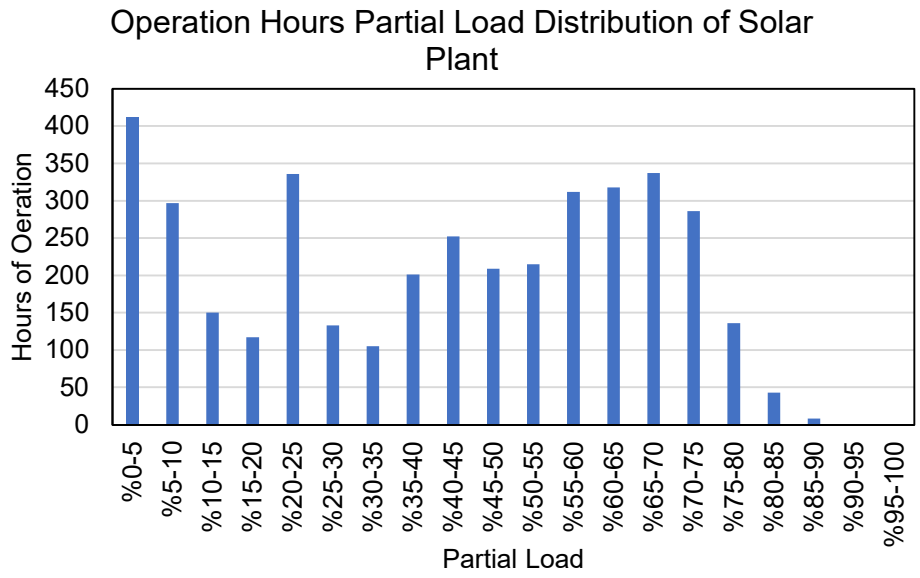

Figure 6.12 Partial load profile for year-round solar energy yield for Antalya-Finike

The stack efficiencies of systems with increasing capacities can be observed in Figure 6.13. It can be seen that the effect of sequencing in the situation where there is more than one stack is negligible.

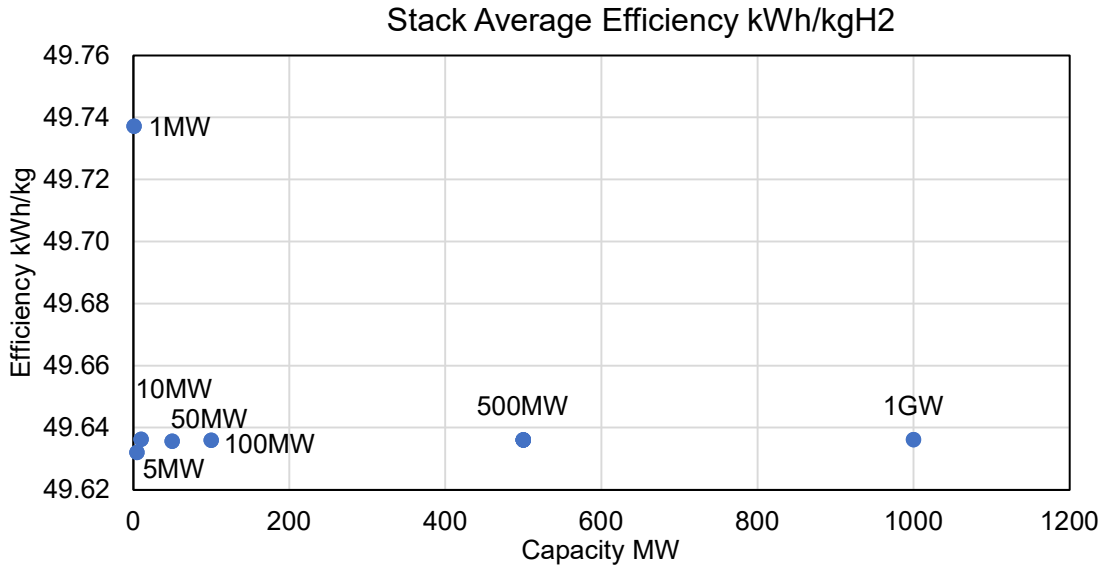

Figure 6.13 Average stack efficiency values for different system capacities simulated for Antalya-Finike

Each selected capacity has at least two different designs where stack cooling is performed by dry coolers in one design and cooling towers in the other. The effect of this design option could be observed in Figure 6.14 of complete system efficiency graphs.

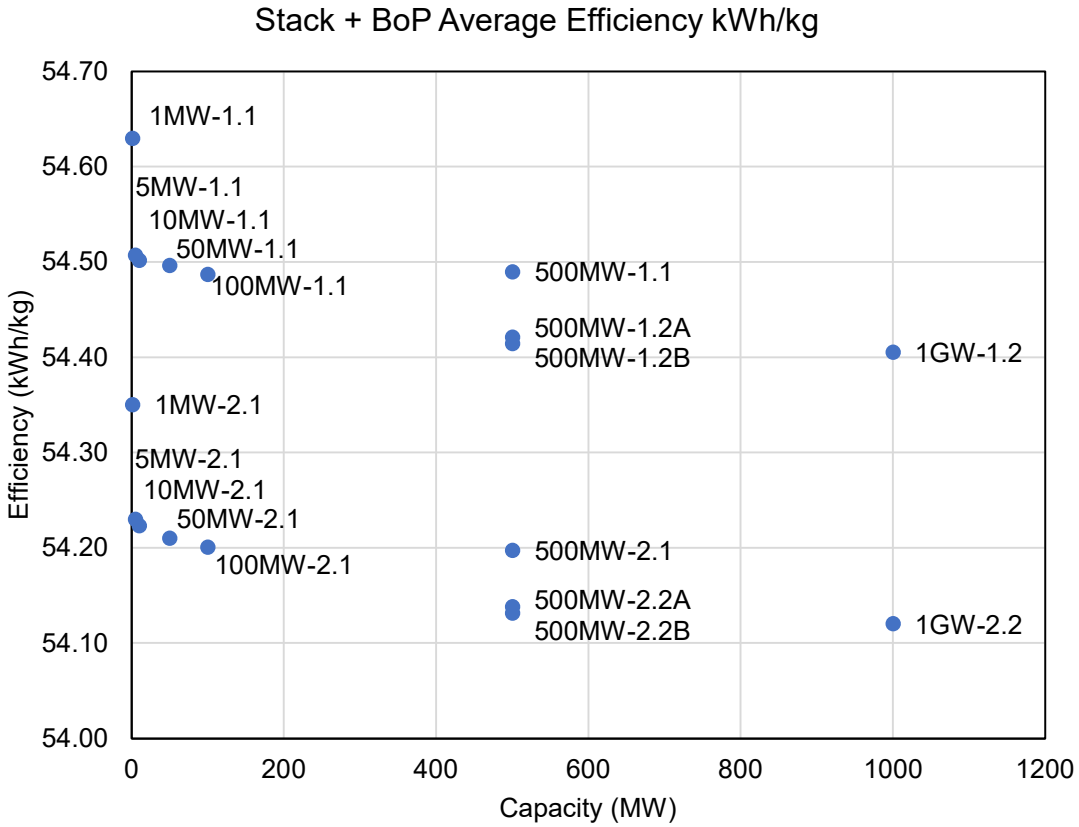

Figure 6.14 Average system efficiency values for different system capacities simulated for Antalya-Finike

It can be seen that increasing the system capacity from 1 MW to 1 GW has a negligible effect on efficiency. It should be kept in mind that the improvement in the stack efficiency mentioned previously is also included in this result.

The graph also shows that there is around a 0.3 kWh/kg constant difference between the systems with dry coolers and the cooling towers. The cooling towers have lower consumption in operation. This difference is about 0.55 % which seems to be not much of an advantage as cooling towers increase the system water consumption as shown in Figure 6.15.

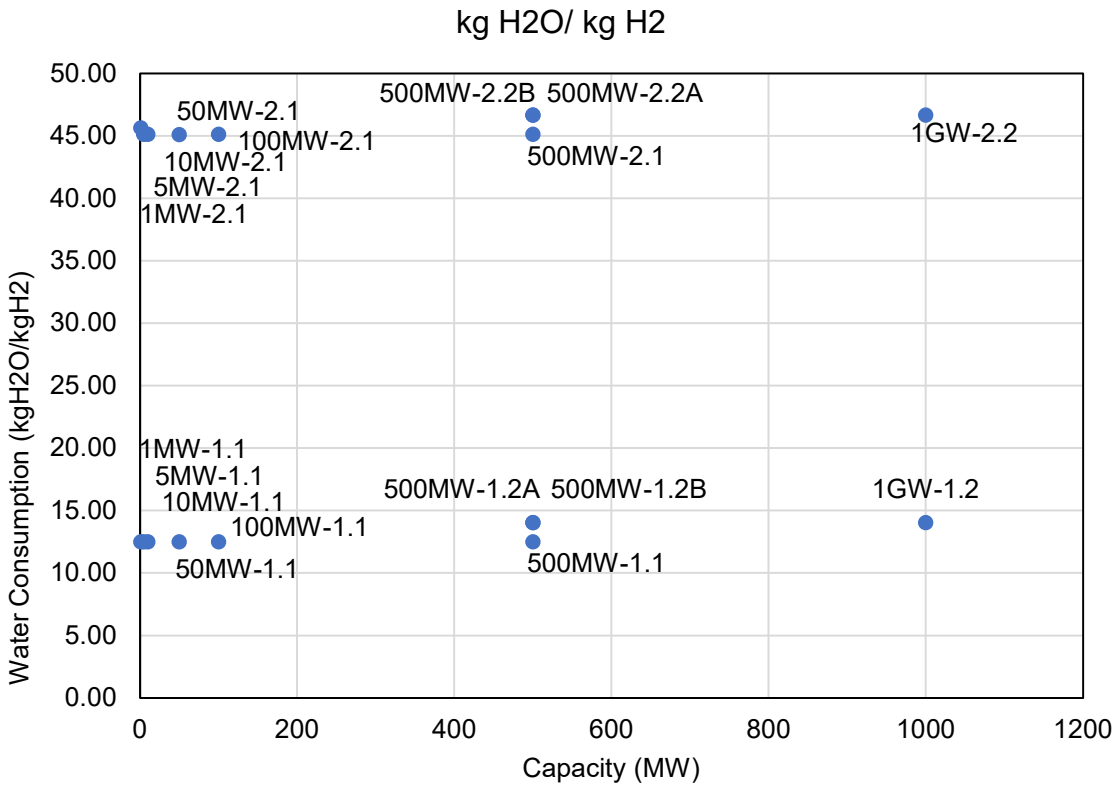

Figure 6.15 Average kg water consumption per kg hydrogen produced for different system capacities simulated for Antalya-Finike

The water consumption increases from a range of 12 - 15 kgH_2O/kgH_2 to around 45 kgH_2O/kgH_2 which proves to show that it is not worth using cooling towers for lowering energy consumption in these applications as it is responsible for a dramatic increase in water consumption.

It could also be concluded that the scale of the system does not make a major difference in the efficiency of the system. Thus, any one system capacity could be simulated for the other locations and results could be compared.

Comparison of different locations could be performed by four parameters: capacity factor of PV plant, yearly average temperature (or summer dry-bulb design temperature), average stack and system efficiency.

Sanliurfa and Kocaeli locations were simulated to compare the results with Antalya. Sanliurfa is a sample location that provides one of the highest capacity factors of the country. Kocaeli is a sample location with lower capacity factor

which is at the north of the country. Simulations were conducted for 100MW-1.1 design where stack cooling is performed by dry coolers. The simulation summary sheets are provided in Appendix 5.

Table 6.5 Simulation results summary for the three chosen cities in Turkey (100MW-1.1 design)

	Capacity Factor	Summer DB (C°)	Average Stack Efficiency (kWh/kg)	Average System Efficiency (kWh/kg)	Annual Hydrogen Production (kg)
Kocaeli	15.1%	33.2	48.97	53.99	2,503,769
Antalya	17.9%	37.1	49.64	54.49	2,926,909
Sanliurfa	19.8%	41.1	49.82	54.63	3,230,353

It can be observed that the difference between the lowest and highest point of average efficiency is 0.85 kWh/kg for the stack and 0.64 kWh/kg for the system and the hydrogen production is 29% higher for Sanliurfa than Kocaeli. Although average stack efficiencies are further apart, system efficiencies can be closer or even further either due to weather conditions or the partial load profile of the plant. This is later observed in the next section with more sample simulations.

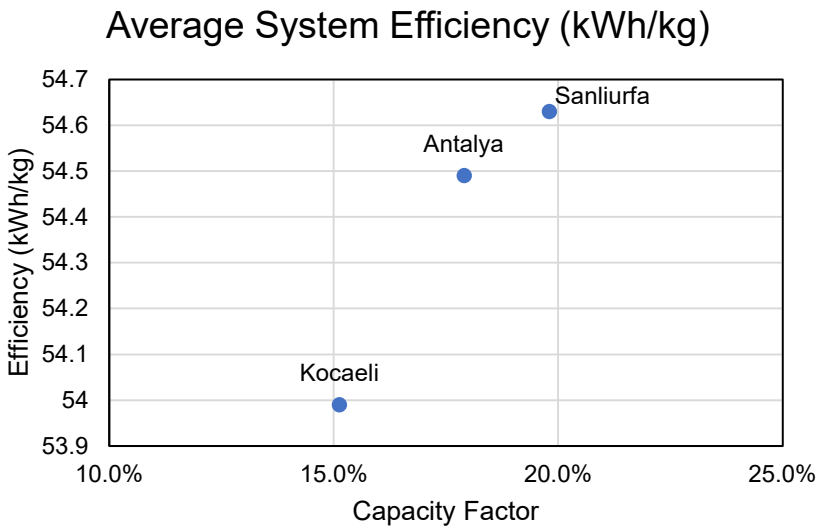

Figure 6.16 Average stack efficiencies with respect to capacity factor of selected locations in Turkey (100MW-1.1 design)

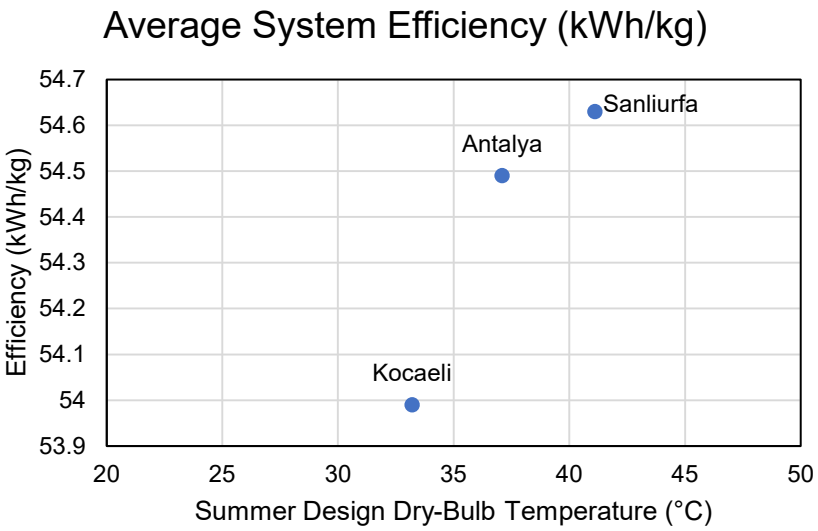

Figure 6.17 Average system efficiencies with respect to summer design dry-bulb temperature of selected locations in Turkey (100MW-1.1 design)

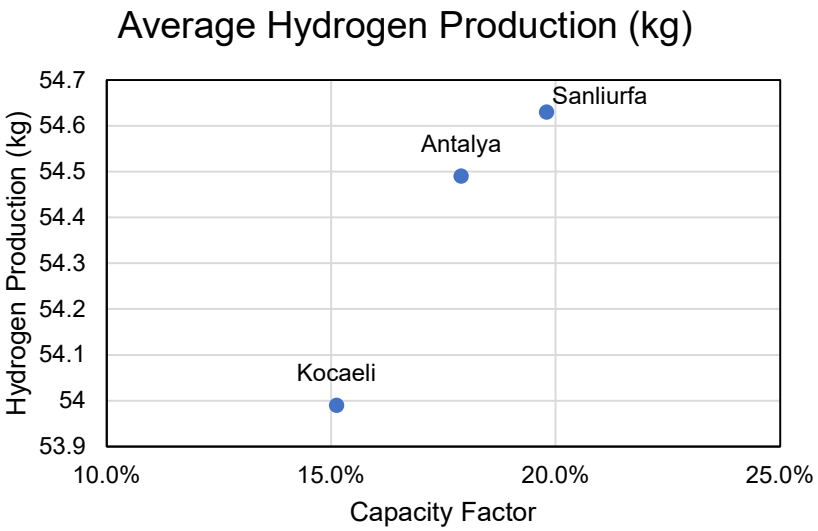

Figure 6.18 Annual hydrogen production with respect to capacity factor of selected locations in Turkey (100MW-1.1 design)

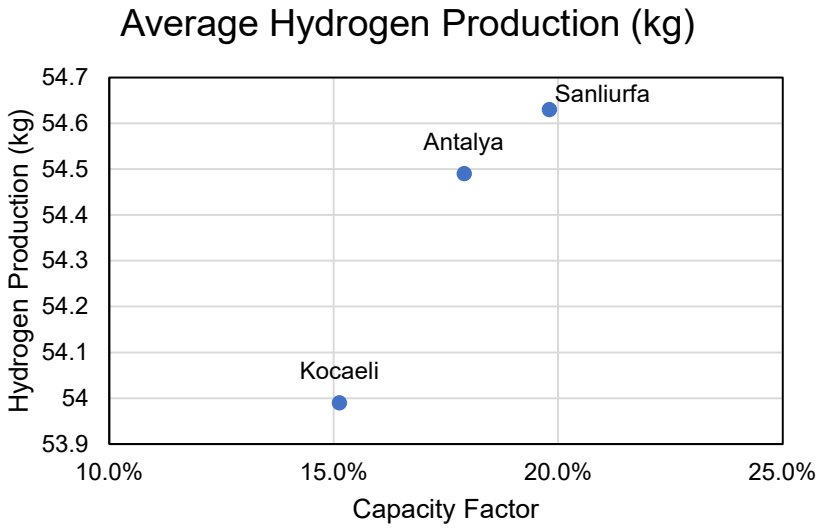

Figure 6.19 Annual hydrogen production with respect to summer design dry-bulb temperature of selected locations in Turkey (100MW-1.1 design)

6.3. Model uncertainty and system performance on worldwide results

6.3.1. Model Uncertainties

The aim of this section is to quantify the sensitivity of the model results to the data used in the model development. The uncertainties of models were determined by using available literature or product data in which the models were developed.

6.3.1.1. Uncertainty of PEM Electrolyzer

The PEM model in this study was formed to resemble the latest commercial electrolyzer technology. The parameters used for the electrolyzer resulted in ±0.5 % error in I-V curves when fitted with the Plug Power Allagash electrolyzer data provided by Harrison (2021) as mentioned in earlier chapters.

The electrolyzer was set to operate at 80°C but at first start up of the electrolyzer it may take up to 3 hours to warm up to the set point at low loads. The temperature tracking performed by taking into account the heat generated, thermal capacitance and heat transfer to surrounding can be considered to vary around ±5°C depending on the indoor conditioning.

These will affect the current as well as the voltage which then affects the stack efficiency at same power input. The change in efficiency will also change the amount of heat rejection which will affect the cooling system.

6.3.1.2. Uncertainty of DC-DC Converter

The uncertainty of DC-DC converter was determined by the Figure 3.13 showing a variation of three sample converters (Vossos et al., 2017).

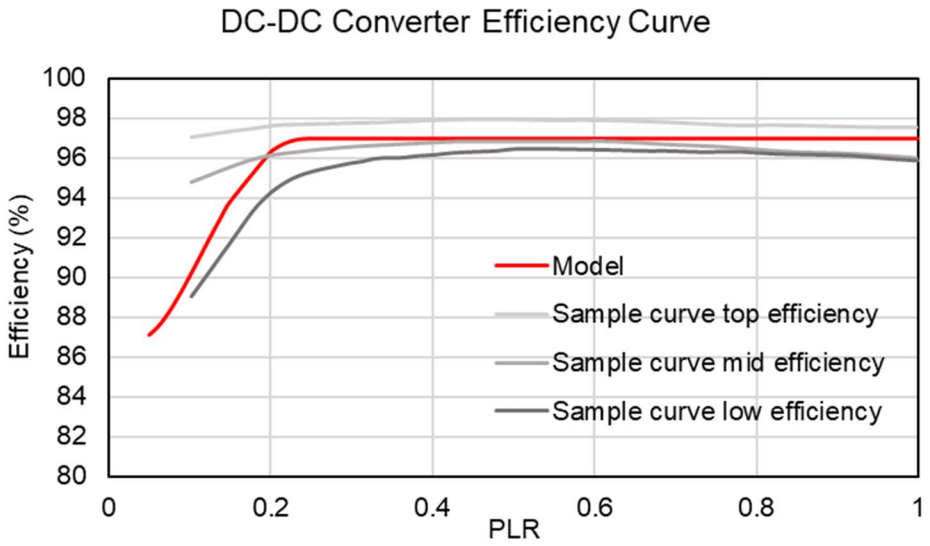

Figure 6.20 DC-DC converter efficiency curve comparision

As shown in Figure 6.20, the range of the efficiency that a possible selected DC-DC converter can be observed. To determine the power loss due to the DC-DC converter the percentage of power loss to full load can be calculated by subtracting the efficiency value by 100 resulting in Figure 6.21.

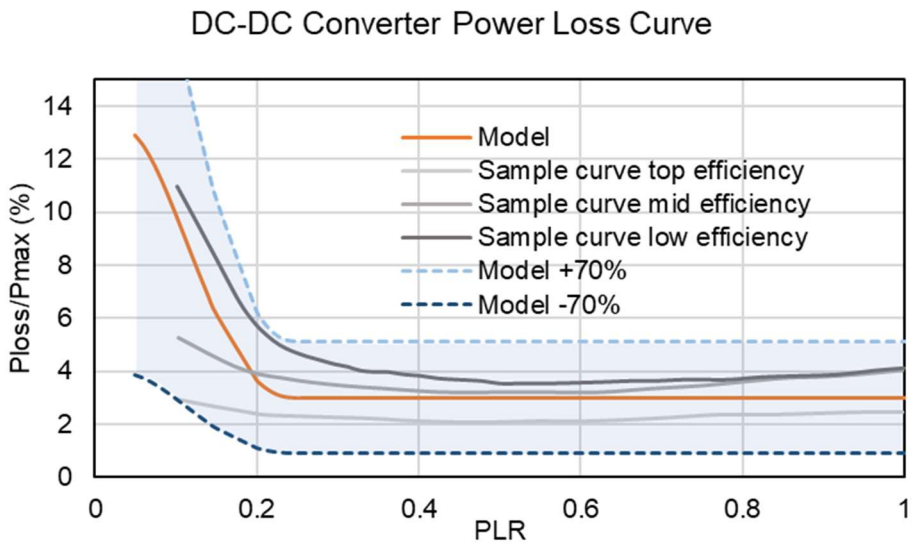

Figure 6.21 DC-DC converter power loss curve model uncertainty

Assuming the variance in power loss of a selected DC-DC converter to be ±70 % would be adequate when observing Figure 6.21.

6.3.1.3. Uncertainty of AC-AC Transformers

Unlike DC-DC transformers, AC-AC transformers are used in all utility power supply connections and is required to comply to standards. As mentioned in earlier chapters the EN50464-1 standard is taken as a baseline which most commercial transformers comply to operating at 50Hz frequency. The EU548/2014 directive indicates lower transformer loss criteria to reduce CO_2 pollution. The model curves were compared with the Tier1 (2015) and Tier2 (2022) criteria of EU548/2014 and also a manufacturer catalogue (also provided in Appendix 6) (EATON, 2021; MEKSAN, 2023) in Figure 6.22.

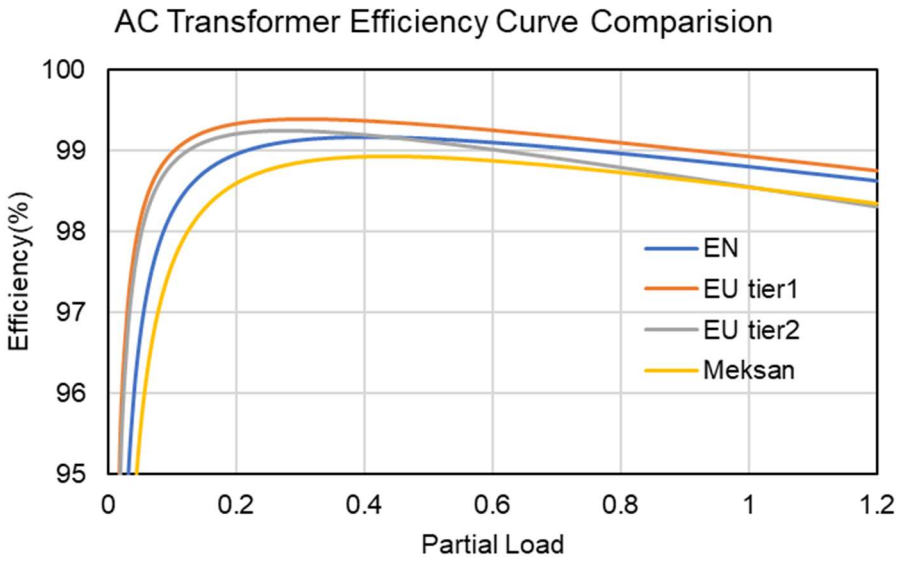

Figure 6.22 AC-AC converter efficiency curve model uncertainty

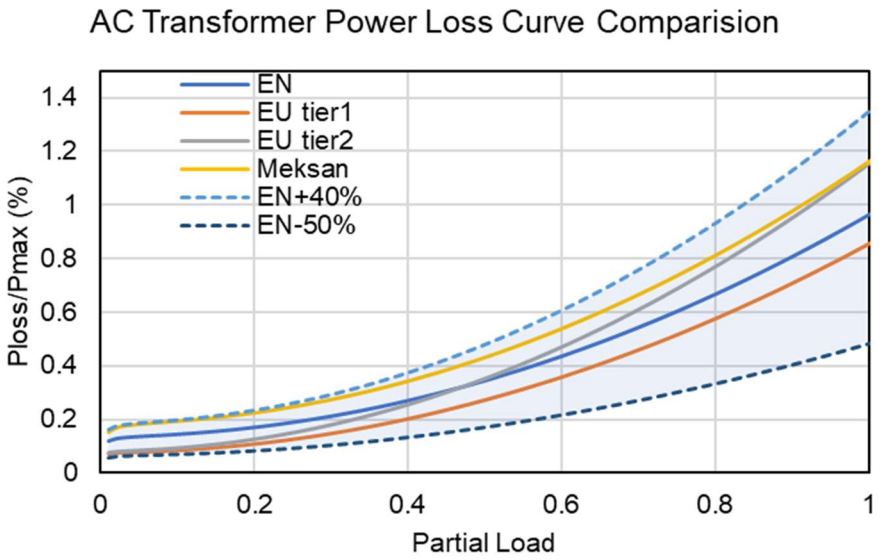

Figure 6.23 AC-AC converter power loss curve model uncertainty

Performing same approach as mentioned for DC-DC converters, assuming the variance in power loss of a selected DC-DC converter to be +40% -50% would be adequate when observing Figure 6.23.

6.3.1.4. Uncertainty of Chiller

The model in this study was from EnergyPlus engineering reference document with coefficients provided in a related PNNL report as mentioned in Chapter 4 (Pacific Northwest National Laboratory, 2016). The provided coefficients are meant to provide a baseline curve that is lower partial load COP than most of the

commercial chillers have to offer. A sample was studied with partial load data taken from a product selection of a commercial project. The data belongs to a water-cooled chiller with a centrifugal compressor that has a design capacity of 3200 kW at 33°C entering condenser water and 6°C leaving evaporator water temperature operating at a ΔT of 6°C of which are provided in Appendix 7. The comparison of COP values at different entering condenser water temperatures is given in Figure 6.24.

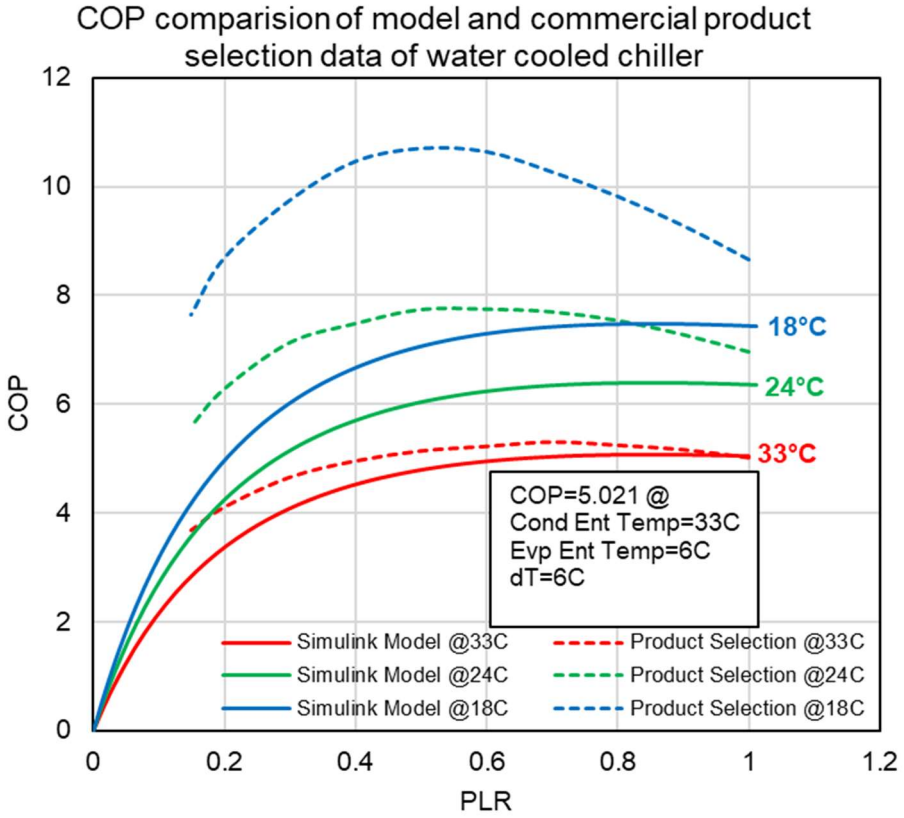

Figure 6.24 COP comparison of model and commercial product selection data of water-cooled chiller

As can be seen in Figure 6.24, the commercial COP values seem to lie significantly above the model values. Determining an uncertainty to this type of COP curve is challenging as most of the deviation occurs on the hunch of the curve but not very much on the full load point.

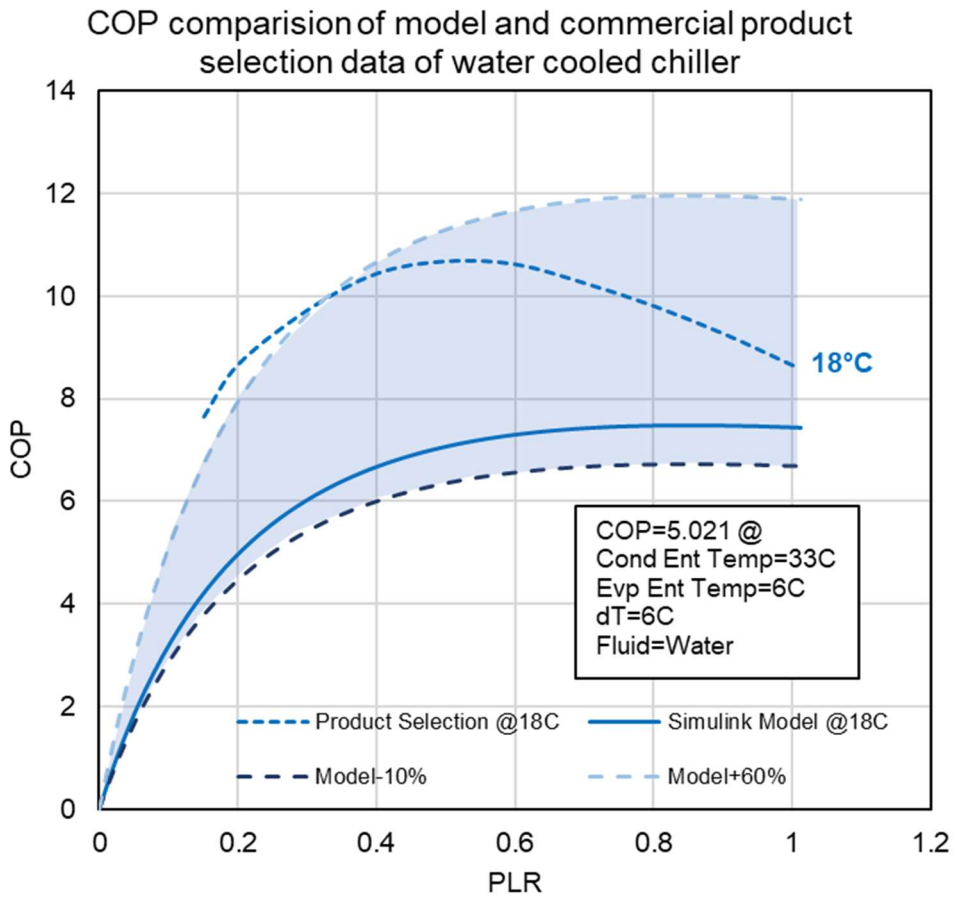

Figure 6.25 COP comparison of model and commercial product selection data of water-cooled chiller indicating variance

As seen in Figure 6.25, determining a the uncertainty of the chiller COP as +60 % and -10% causes an error as approaching full load. This is not necessarily a problem as the PEM system mostly operates at partial loads. The effect of the chiller on the system performance does also come out to be minimal at the end result so using this uncertainty range for the COP seems to be viable.

6.3.1.5. Uncertainty of Dry Cooler

Since there aren't partial load data openly available of commercial dry coolers the multiplier in Equation 5.18 was mentioned to be at a range of 4-11 with an average of 6.5 when compared with commercial dry cooler product selection software. This affects the AU factor which affects the performance of the chiller. Considering a ±1.5 variance would seem to be adequate for a possible commercial dry cooler selection.

6.3.1.6. Uncertainty of Pumps

The model used in this study has provided results higher than what commercial pump curves have to offer. Commercial pump power consumptions were around 15 to 30% lower than the model at low partial loads. A variance of +5% and -30% is considered.

6.3.1.7. Uncertainty of Fans

The fans used in this system are only for exhaust ventilation which operate at full load constantly. A variance of +10% can be considered for the possibility of having to acquire a larger fan due to manufacturers not having the exact capacity stated in design and having to choose a slightly larger fan.

6.3.2. Effect of Uncertainties

Table 6.6 summarizes the uncertainties discussed earlier.

Table 6.6 Summary of uncertainties of the PEM system

Model	Factor	Uncertainty	
		Lowest	Highest
PEM Stack	Tstack below 80°C	-5°C	+5°C
PEM Stack	Vstack	-0.5%	+0.5%
DC-DC Converter	Ploss/Pnom	-70%	+70%
AC-AC Transformer	Ploss/Pnom	-50%	+40%
Chiller	COPop	-10%	+60%
Dry Cooler	Mutlipier (Eq 5.18)	-1.5	+1.5
Pumps	Pop	-30%	+5%
Fans	Pop	-0%	+10%
Dryer	Dryer Losses	-1	+1

The effect of the uncertainties on the model results were studied for the location Saudi Arabia as a sample. Figure 6.26 shows the effect of mentioned factors where it could be observed that cell temperature, cell voltage, DC-DC converter and hydrogen dryers are the only factors affecting the hydrogen production. All the other factors only affect the AC energy consumption which is supplied separately from the utility grid for consistency.

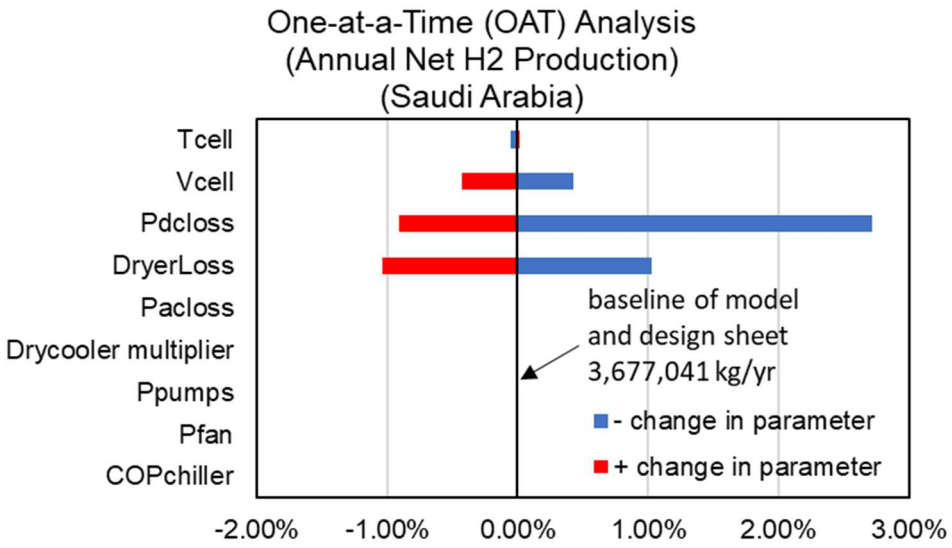

Figure 6.26 One at a time uncertainty analysis of annual hydrogen production of 100MW1.1 design for Saudi Arabia

The Figures 6.27 and 6.28 show the effects on kWh/kg efficiencies. The factors affecting the efficiency and the hydrogen production the most are the cell voltage, DC converter and the dryer losses. These three factors should be a priority to make significant improvements.

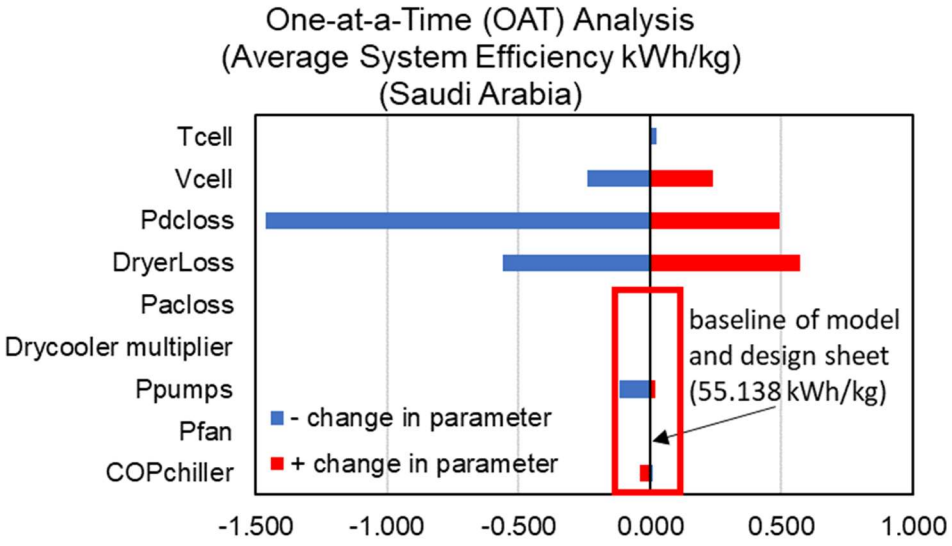

Figure 6.27 One at a time uncertainty analysis of average system efficiency of 100MW1.1 design for Saudi Arabia

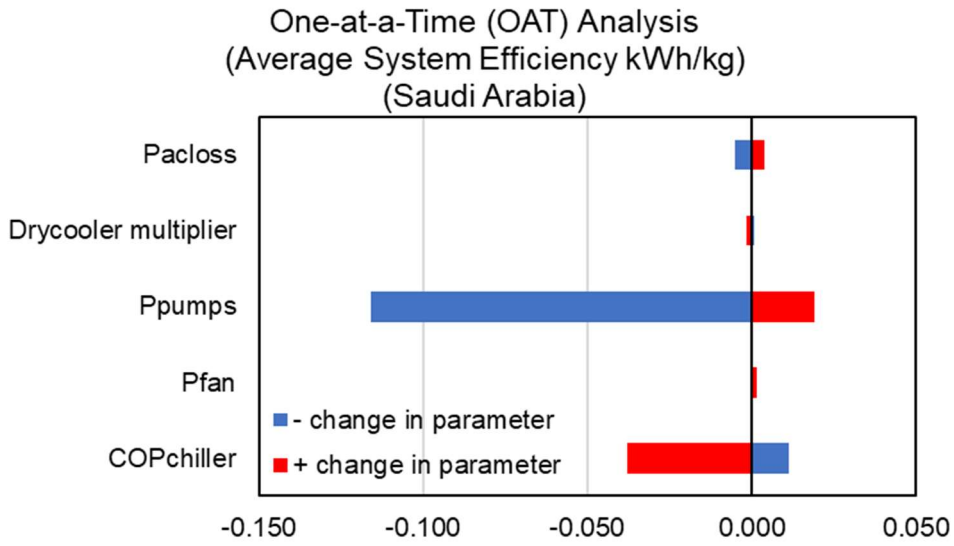

Figure 6.28 One at a time uncertainty analysis of average system efficiency of 100MW1.1 design for Saudi Arabia (zoomed)

It should be noted that the uncertainties of the model do not include the uncertainties regarding PV modeling and weather data files as it is not in the scope of this study. The model is to be a possible add-on to PV analysis.

6.3.3. Best and worst case scenarios

Taking the figures in to account, worst and best case scenarios are determined as shown in Table 6.7 and simulated for Saudi Arabia as a sample.

Table 6.7 Uncertainties arranged for best and worst case scenario of the PEM system

Model	Factor	BEST	WORST
PEM Stack	Tstack below 80°C	+5°C	-5°C
PEM Stack	Vstack	-0.5%	+0.5%
DC-DC Converter	Ploss/Pnom	-70%	+70%
AC-AC Transformer	Ploss/Pnom	-50%	+40%
Chiller	COPop	+60%	-10%
Dry Cooler	Mutlipier (Eq 5.18)	+1.5	-1.5
Pumps	Pop	-30%	+5%
Fans	Pop	-0%	+10%
Dryer	Dryer Losses	-1	+1

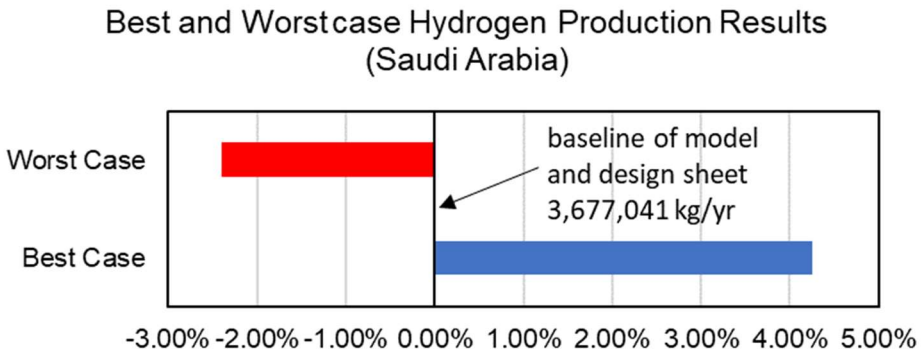

Figure 6.29 Best and worst case scenario analysis of annual hydrogen production of 100MW-1.1 design for Saudi Arabia

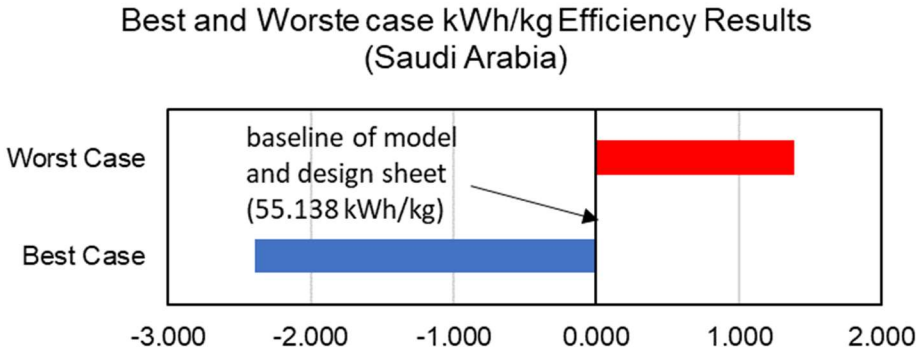

Figure 6.30 Best and worst case scenario analysis of average system efficiency of 100MW-1.1 design for Saudi Arabia

It can be seen that the performance of the system can vary significantly depending on design and equipment quality. The hydrogen production and the average system efficiency can vary between -2.5% and +4.5% and -2.5 and +1.5 kWh/kg respectively.

6.3.4. Simulations for selected locations worldwide

The best-worst case analysies were conducted for all the 15 locations. It was observed in Figures 6.31 and 6.32 that the effect of uncertainties are not sensitive to geographical location.

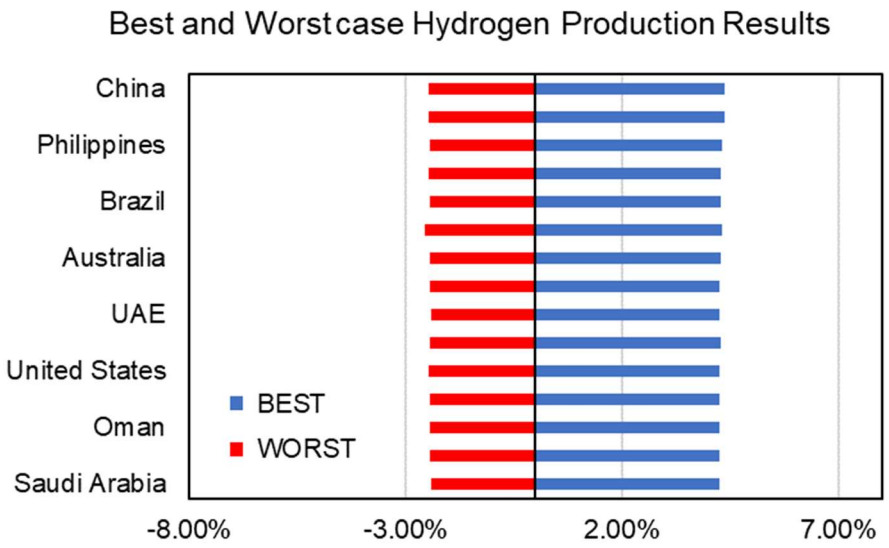

Figure 6.31 Best and worst case scenario analysis of annual hydrogen production of 100MW-1.1 design for locations worldwide

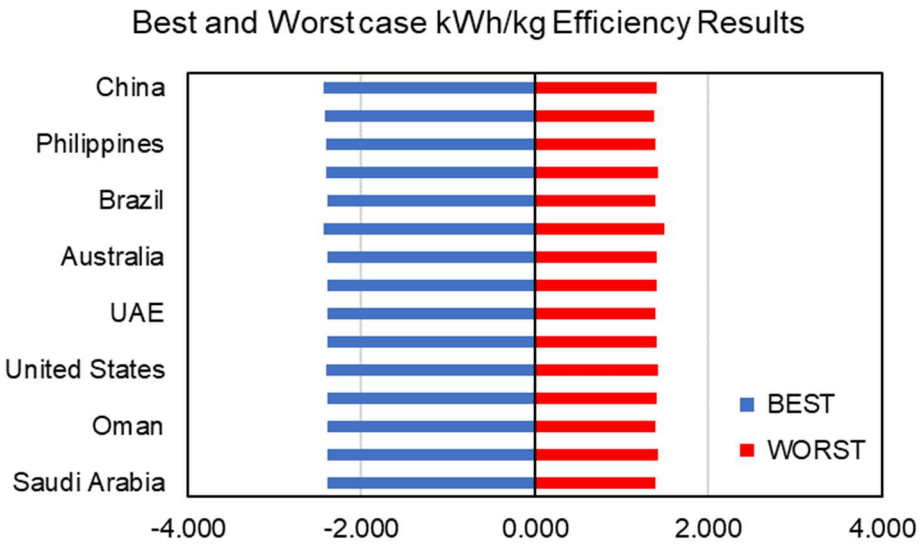

Figure 6.32 Best and worst case scenario analysis of average system efficiency of 100MW-1.1 design for locations worldwide

6.3.5. Simulations for selected locations worldwide

Results for simulations that were carried out for countries listed in Table 5.9 are shown in Table 6.8.

Table 6.8 Simulation results for fifteen locations worldwide

Location		Saudi Arabia	Tunisia	Oman	Egypt	United States	Kuwait	UAE	Namibia	Australia	India	Brazil	Morocco	Philippines	Indonesia	China
Plant Capacity	MW	100	100	100	100	100	100	100	100	100	100	100	100	100	100	100
Hours of Operation	hrs	3824	3686	3925	3764	3605	3840	3911	3677	3801	3342	3686	3309	3655	3662	3516
Capacity Factor	%	22.8%	22.9%	22.3%	22.2%	22.3%	22.1%	21.7%	21.7%	20.9%	20.3%	19.0%	17.9%	17.1%	14.5%	14.0%
Annual Solar DC Power Production	kWh	199468609	200384172	195299274	194768689	195349724	193456383	190305793	190072983	183064824	177967788	166363182	157090288	149435185	127239473	122888637
Annual Stack Consumption	kWh	190872405	191852015	186863272	186461026	187007252	185157111	182058606	181880053	175110220	170344026	159025545	150234746	142672014	121199253	116868584
Mechanical Consumption	kWh	2305323	2001100	2127715	2125988	2079067	2011245	2113107	2075263	2093526	1894836	2094669	1760394	2059370	1941414	1800017
Electrical Consumption	kWh	9565579	9498654	9403835	9275188	9310017	9265940	9214643	9161074	8922021	8579182	8304596	7820648	7727586	7004654	6984879
Annual BoP Consumption	kWh	11870902	11499754	11531550	11401176	11389084	11277185	11327750	11236337	11015548	10474018	10399266	9581042	9786955	8946068	8784896
Annual H2O Consumption	kg	45884317	45692188	45038962	44798923	44607148	44603528	44034227	43542294	42277729	40476003	38975749	36449224	35386913	30633099	29275776
Annual H2 Net Production	kg	3677042	3662817	3608444	3590001	3575330	3573536	3527131	3489649	3386418	3244638	3119118	2919343	2829514	2445478	2336529
Annual H2 Loss	kg	146651	144866	144803	143242	141932	143425	142388	138876	136726	128362	128861	118092	119396	107281	103119
Hydrogen Loss Percentage	%	3.99%	3.96%	4.01%	3.99%	3.97%	4.01%	4.04%	3.98%	4.04%	3.96%	4.13%	4.05%	4.22%	4.39%	4.41%
Stack Average Efficiency	kWh/kg	50.35	50.81	50.23	50.38	50.74	50.26	50.07	50.56	50.16	50.93	49.45	49.92	48.91	48.07	48.52
Mechanical Loss Average	kWh/kg	0.63	0.55	0.59	0.59	0.58	0.56	0.60	0.59	0.62	0.58	0.67	0.60	0.73	0.79	0.77
Electrical Loss Average	kWh/kg	2.60	2.59	2.61	2.58	2.60	2.59	2.61	2.63	2.63	2.64	2.66	2.68	2.73	2.86	2.99
Stack + BoP Average Efficiency	kWh/kg	55.14	55.52	54.98	55.11	55.49	54.97	54.83	55.34	54.96	55.73	54.32	54.74	53.88	53.22	53.78
Design Summer Dry Bulb Temperature	°C	36.1	44.0	44.0	38.3	35.3	48.9	46.0	32.0	40.0	22.7	37.2	38.9	32.9	33.7	35.3

If system efficiency values are plotted against their capacity factors, a slight increase with capacity factor can be observed as shown in Figure 6.33. the uncertainties of average system efficiency are also shown for each location.

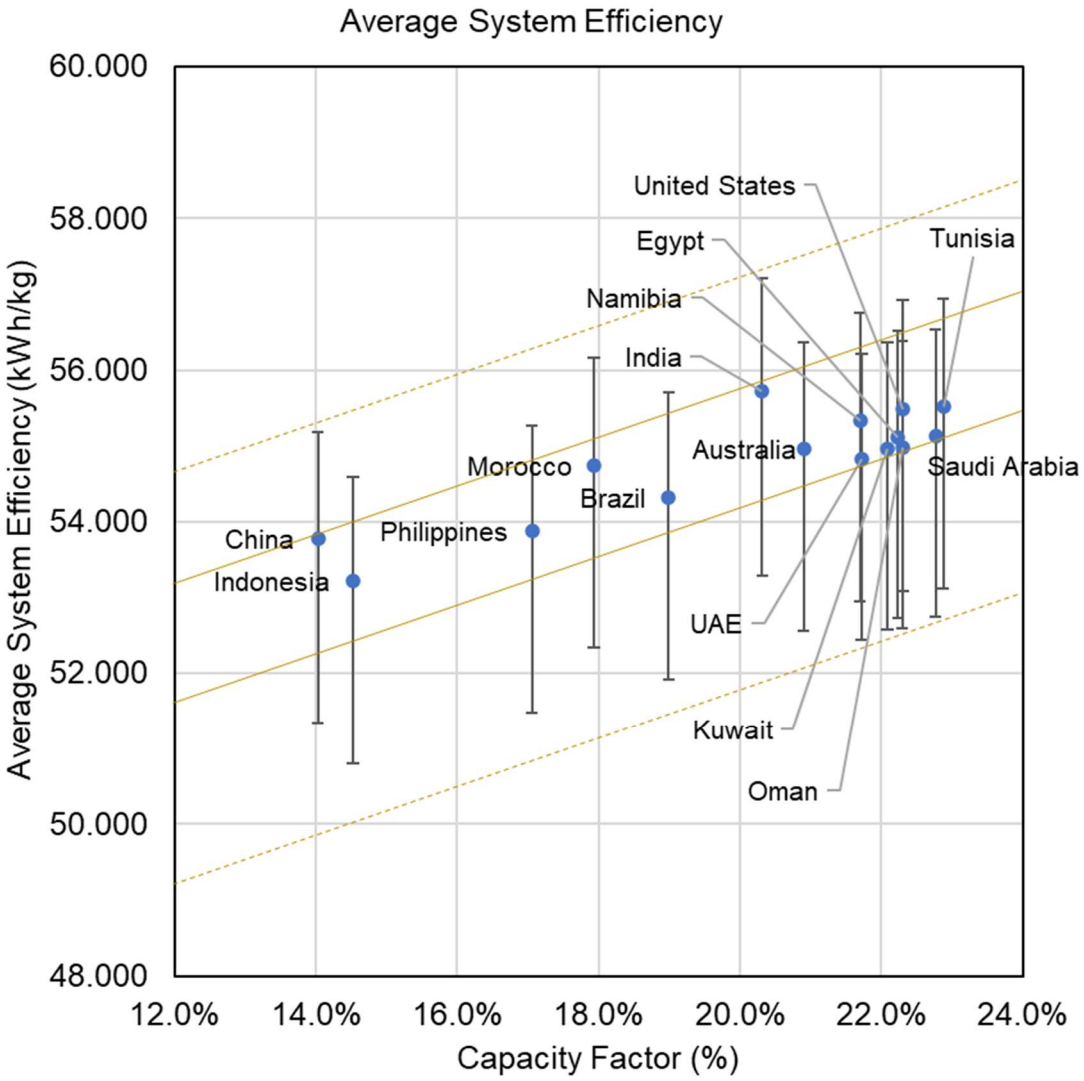

Figure 6.33 The variation of the average system efficiency with respect to capacity factor for different locations worldwide.

Although the tolerance of the curve seems to be large, the other effect of this is the energy distribution profile. For example, the location selected for India seems to have more operating hours at higher partial loads compared to its neighboring samples on the graph which is where the efficiency is the lowest as discussed in previous Section 6.1. This is why the system consumption of kWh/kg is higher for India.

This could be observed by comparing the two partial load graphs (Figure 6.34 and 6.35) of one belonging to India and the other belonging to Australia which has a similar capacity factor.

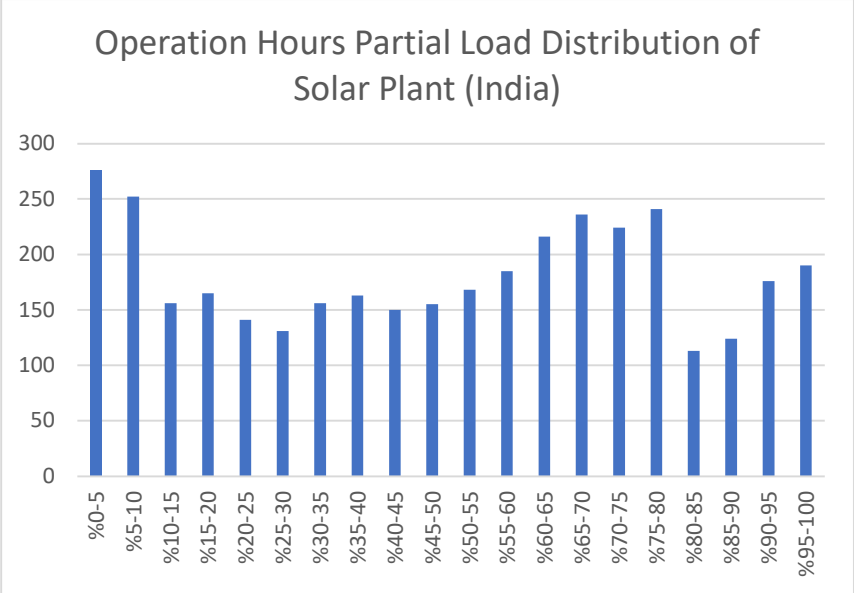

Figure 6.34 Operational hours partial load distribution of solar plant for India location.

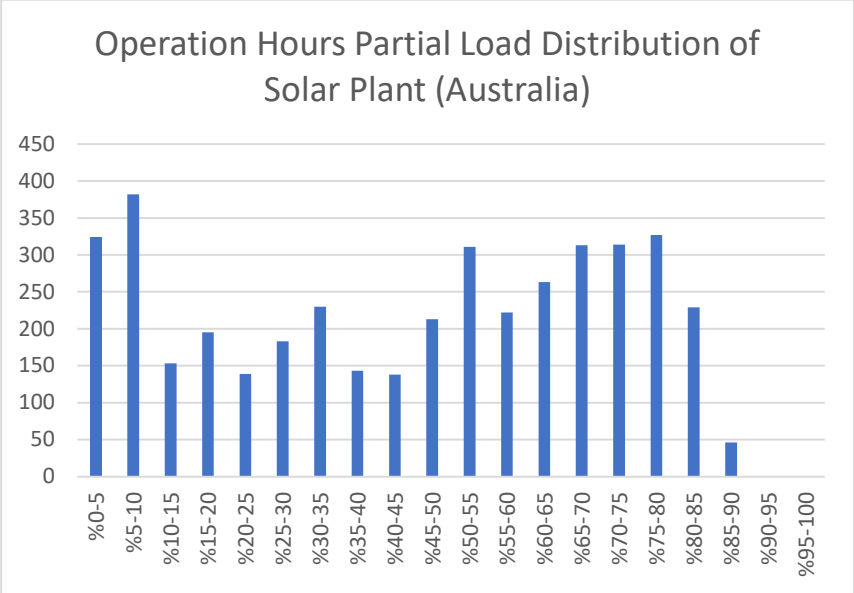

Figure 6.35 Operational hours partial load distribution of solar plant for India location.

As can be seen the effect of having more operation hours on the 90 – 100 % partial load range for India has resulted in more consumption and less efficiency although it has a close capacity factor to Australia.

The best and worst case scenarios were also reflected to Figure 6.33 which shows how much the system design and equipment quality can affect the average efficiency of the system.

It can also be deduced from Figure 6.36 that there is a closer correlation between the annual hydrogen production and capacity factor of the locations affecting a wide range of results where the highest point (Saudi Arabia) provides a 57% more yield than the lowest (China). The best and worst case scenario analysis is also presented on this figure and it has shown that the effect of design and equipment quality is not as much as the effect of the location.

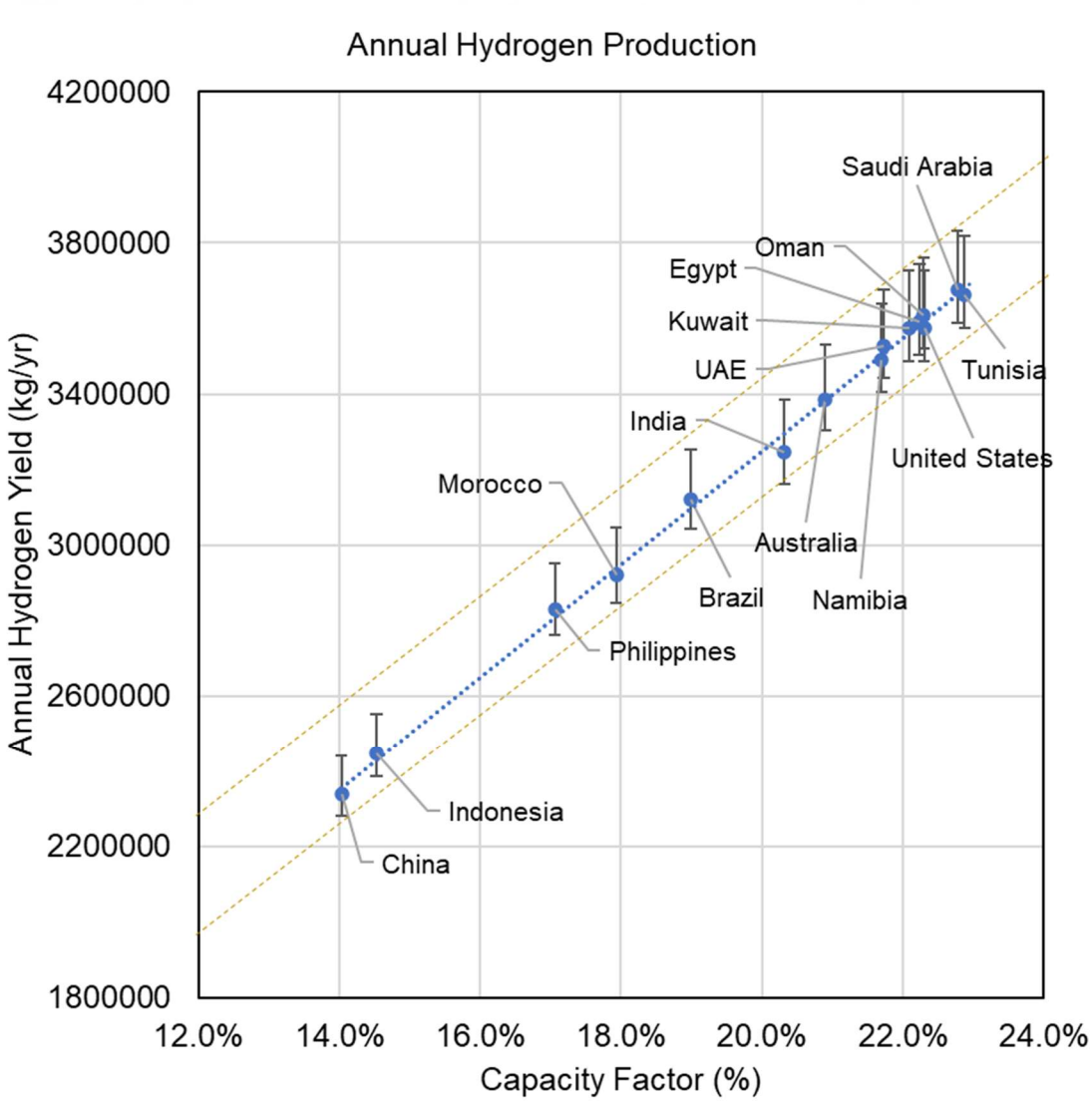

Figure 6.36 The variation of the annual hydrogen production with respect to capacity factor for different locations worldwide.

The efficiency and annual hydrogen production against summer design temperature of the locations has also been plotted in Figures 6.37 and 6.38 to observe any relationship.

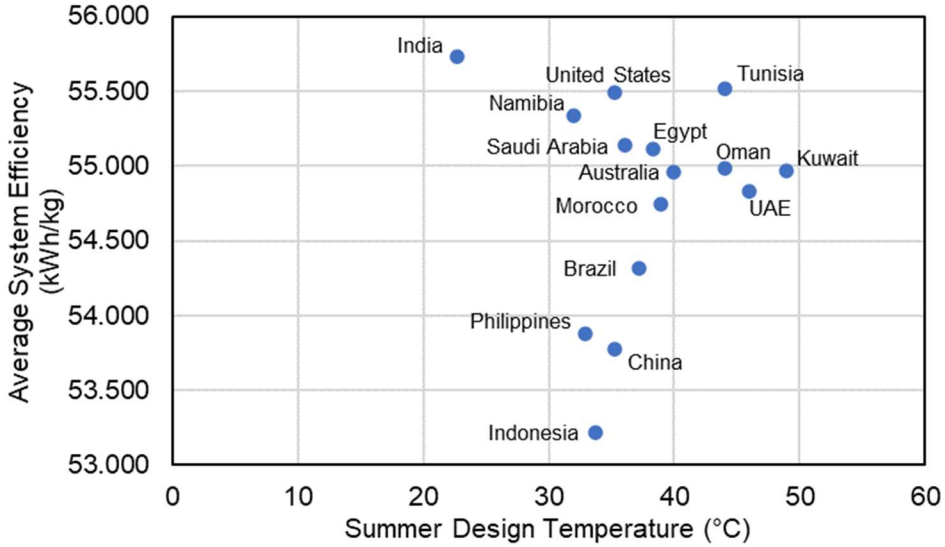

Figure 6.37 The variation of the average system efficiency with respect to summer dry-bulb temperature for different locations worldwide.

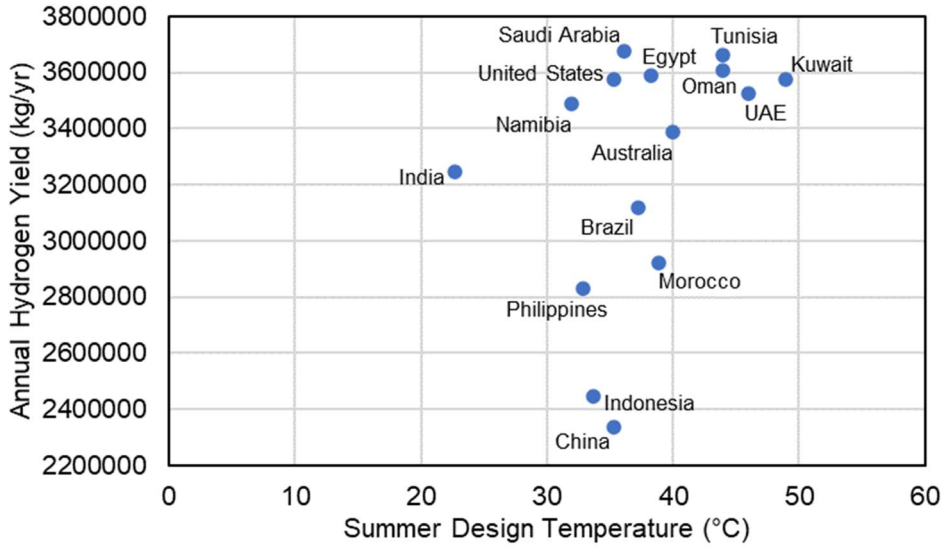

Figure 6.38 The variation of annual hydrogen production with respect to summer dry-bulb temperature for different locations worldwide.

As can be seen, there is no particular relationship between the summer design temperature and the efficiency of the system or the annual energy production. The ambient temperature would technically affect the performance of the PV modules which could affect the energy production and efficiency. Similarly, the

cooling system of the electrolysis is also affected by the ambient temperature which would only affect the efficiency of the system and would not have an impact on hydrogen production as BoP components are supplied power separately from the grid in order to operate consistently. Although the temperature has such effects, as mentioned earlier, it seems to be minimal and doesn't provide a correlation.

Figures 6.39 and 6.40 illustrate the total energy consumption and hydrogen production results for the location with highest production (Saudi Arabia) and the lowest production (China). These illustrations once again summarize what the model has to offer. Values like water consumption, AC power consumption and net hydrogen production can be used in decision making. It should be reminded that the system investment for both locations are to be very close as the only difference would be the sizing of the cooling system. Since the model performs simulations on hourly data, weekly summaries could also be obtained by hourly results to be used in a possible cash flow analysis to predict the expenses of water and AC energy as well as income from hydrogen production for any time frame throughout the year.

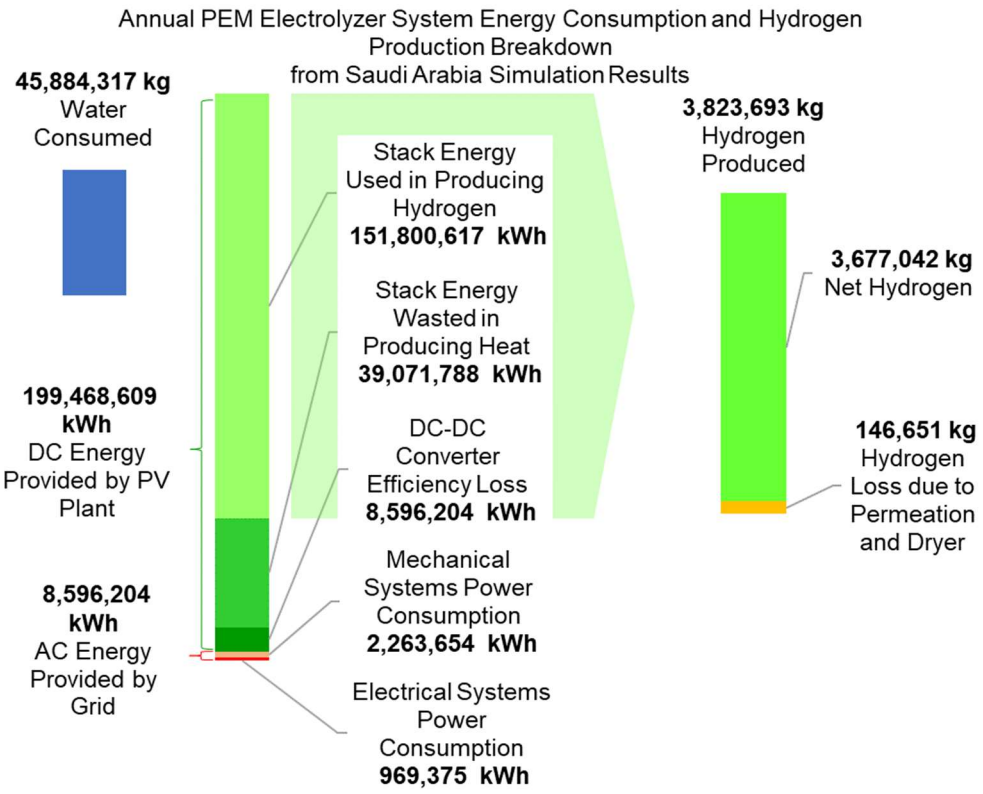

Figure 6.39 Annual PEM electrolyzer simulation data breakdown for Saudi Arabia.

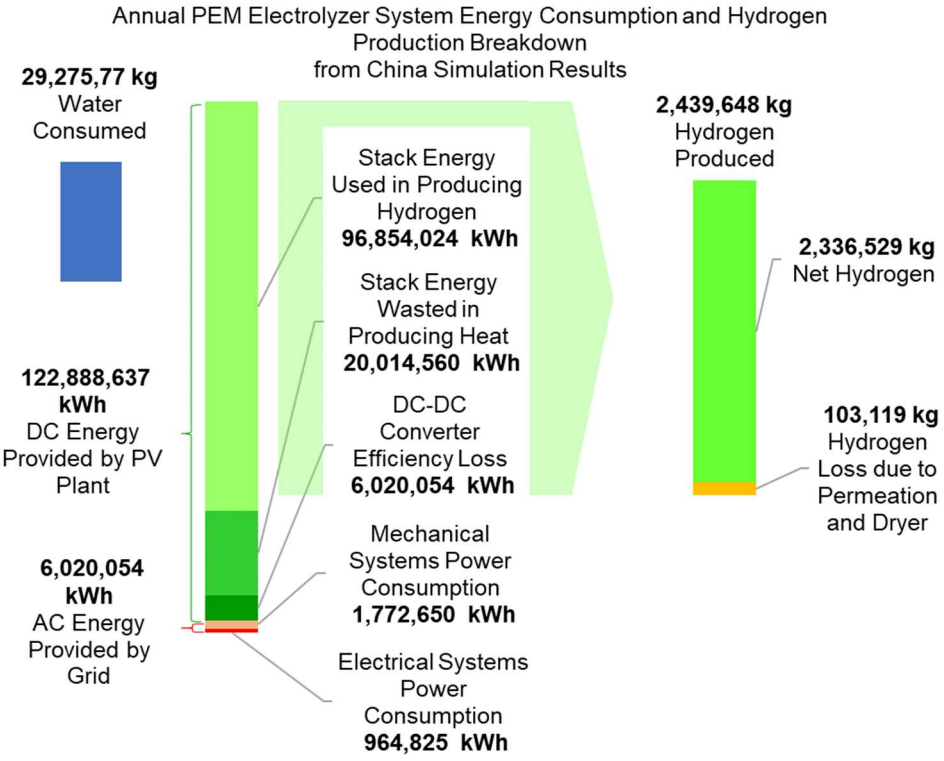

Figure 6.40 Annual PEM electrolyzer simulation data breakdown for China.

7. CONCLUSION

In this study, design and steady-state modeling of PEM electrolyzer system were performed to investigate the impact of balance of plant (BoP) components on the overall system efficiency under varying power supply conditions from renewable sources. The modeling of a PEM electrolyzer with available I-V curve test results of a commercial 1MW stack (Plug Power Allagash Electrolyzer) consisting of 129 cells producing hydrogen at 40 bars was performed. The balance of plant (BoP) components were also modeled according to baseline values suggested by certain standards such as ASHRAE and AHRI. The modeling of the electrolyzer and system components were performed in MATLAB and design parameters were fed by spreadsheets. Power supply data fed to the model were generated from solar PV plant modeling data performed in System Advisory Model (SAM). System capacities ranging from 1 MW to 1 GW were designed and simulated for different locations, allowing for the observation of the effects of capacity factor, weather conditions, system scale and design on overall system performance. Best and worst case scenarios for possible uncertainties due to system quality were also presented.

The results of this study are as follows:

- A PEM electrolysis stack model complying with performance curves provided by current literature was successfully carried out.
- System design and sizing of PEM system were performed complying to certain standards.
- The system modeling results show close compliance with limited number of studies on partial load system efficiency.
- Using cooling towers instead of dry coolers for stack cooling was found to have very low impact on the kWh/kgH_2 consumption of the system and also caused dramatic increase in water consumption of about four times more. Therefore, it was concluded that using cooling towers for this application is an insufficient way of cooling stacks and that the system design should be carried out by dry coolers.

- Performing simulations on a range of system sizes show that it has a negligible impact on system performance and therefore is not advantageous to install larger systems for the purpose of efficiency.
- Simulation results performed for different locations show a correlation between the system performance and the capacity factor of the solar plant. It is also observed that locations that provide close capacity factors can operate at different average system efficiencies. The systems with similar capacity factors operate at lower efficiency when the operation is carried out at high partial loads such as the 90 – 100 % range. The correlation of annual hydrogen production and capacity factor was also presented.
- The uncertainties of the system were also determined. The analysis show that three main factors had significantly more effect than others on system efficiency and also hydrogen production which are the PEM stack I-V curve, DC-DC converter losses and the hydrogen dryer/purifier losses.
- Best and worst case scenarios were analyzed and results show that effect of uncertainties are more on system efficiency but where significantly less for annual hydrogen production. Since the strong correlation between the hydrogen is still maintained in spite of uncertainties, and since the capacity factor is directly affected by chose of location, it is shown the location should be prioritized over the system design and equipment quality.
- Results show that different climate temperature conditions have impact on the cooling system, but it is also observed that the percentage of power consumption of the cooling system is significantly low. Therefore, it does not have a significant impact on the system performance showing no correlation between the summer design dry bulb temperature and average system efficiency as well as annual hydrogen production.

8. RECOMMENDATIONS

Several improvements and extensions can be made to the studied model.

- Investigating system performance with a more efficient stack can be carried out. The membrane thickness used in current commercial PEM stacks and also in this study are 127μm. As mentioned in this study, the membrane thickness is the primary factor that limits the stack to operate at higher densities. There is limited literature on experimenting with thinner membranes in laboratory scale stacks. The model can be used for experimenting the system analysis with thinner membranes for possible future commercial stacks to be developed.
- Investigating and including the building systems power consumptions for plant designs with building enclosers (HVAC systems, lighting and similar possible MEP equipment that consume power) can be done.
- An end use can be determined and compressors can be incorporated to supply required pressures to pipelines or various industry applications.
- Integrating other renewable energy sources such as wind power to observe difference in system efficiency and hydrogen production can be done.
- Adding cost analysis to the model to also provide cost per kg hydrogen results for green hydrogen investment decisions can be a future work.
- Integrating a fuel cell system model to simulate grid balancing by using hydrogen as a temporary storage as a cost-effective option to utility scale batteries is also an important topic that can be investigated.

REFERENCES

Abdin, Z., Webb, C.J., Gray, E.MacA., Modelling and simulation of a proton exchange membrane (PEM) electrolyser cell, International Journal of Hydrogen Energy 40, 13243–13257, 2015.

Al-Quraan, A., Al-Mahmodi, M., Alzaareer, K., El-Bayeh, C., Eicker, U., Minimizing the Utilized Area of PV Systems by Generating the Optimal Inter-Row Spacing Factor, Sustainability 14, 6077, 2022.

American Society of Heating, Refrigerating and Air-Conditioning Engineers, ASHRAE Handbook: Fundamentals, SI. ed. ASHRAE, Peachtree Corners, GA, 2021a.

American Society of Heating, Refrigerating and Air-Conditioning Engineers, ASHRAE Climatic Design Conditions 2009/2013/2017/2021, http://ashrae-meteo.info/v2.0/ (Accessed: 30 May 2023b).

American Society of Heating, Refrigerating and Air-Conditioning Engineers, ASHRAE Handbook: Heating, Ventilating, and Air-Conditioning Systems and Equipment., SI. ed. ASHRAE, Atlanta, GA, 2020.

Awasthi, A., Scott, K., Basu, S., Dynamic modeling and simulation of a proton exchange membrane electrolyzer for hydrogen production, International Journal of Hydrogen Energy 36, 14779–14786, 2011.

Ayers, K.E., Dalton, L., Roemer, A., Carter, B., Niedzwiecki, M., Manco, J., Anderson, E.B., Capuano, C., Wang, C., Zhao, W., High Performance, Low Cost Hydrogen Generation from Renewable Energy, National Renewable Energy Laboratory (NREL), 2014.

Baltimore Aircoil Company, Baltimore Aircoil Company—Evaporaative Cooling—Application Information, https://www.baltimoreaircoil.eu/en/knowledge-centre/evaporative-cooling (Accessed: 6 June 2023).

Bessarabov, D., Millet, P., PEM Water Electrolysis—Volume 1. Academic Press, 2018.

Bessarabov, D., Millet, P., Pollet, B.G., PEM Water Electrolysis—Volume 2. Academic Press, 2018.

Bessarabov, D., Wang, H., Li, H., Zhao, N. (Eds.), PEM Electrolysis for Hydrogen Production: Principles and Applications. CRC Press, 2016.

Biaku, C.Y., Dale, N.V., Mann, M.D., Salehfar, H., Peters, A.J., Han, T., A semiempirical study of the temperature dependence of the anode charge transfer coefficient of a 6 kW PEM electrolyzer, International Journal of Hydrogen Energy 33, 4247–4254, 2008.

Brown, T.M., Brouwer, J., Samuelsen, G.S., Holcomb, F.H., King, J., Dynamic first principles model of a complete reversible fuel cell system, Journal of Power Sources 182, 240–253, 2008.

Carmo, M., Fritz, D.L., Mergel, J., Stolten, D., A comprehensive review on PEM water electrolysis, International Journal of Hydrogen Energy 38, 4901–4934, 2013.

Carrier, Carrier Water Cooled Chillers, https://www.carrier.com/commercial/en/us/products/chillers-components/water-cooled-chillers/ (Accessed: 30 May 2023).

Choi, P., Bessarabov, D., Datta, R., A simple model for solid polymer electrolyte (SPE) water electrolysis, Solid State Ionics 175, 535–539, 2004.

Colella, W., James, B., Moton, J., Saur, G., Ramsden, T., Techno-economic Analysis of PEM Electrolysis for Hydrogen Production, Strategic Alanysis Inc. , National Renewable Energy Laboratory (NREL), 2014.

COMNET, Modeling Guidelines—Chillers, https://comnet.org/382-chillers (Accessed: 30 May 2023).

Crespi, E., Guandalini, G., Mastropasqua, L., Campanari, S., Brouwer, J., Experimental and theoretical evaluation of a 60 kW PEM electrolysis system for flexible dynamic operation, Energy Conversion and Management 277, 116622, 2023.

Cruz, J.C., Baglio, V., Siracusano, S., Ornelas, R., Ortiz-Frade, L., Arriaga, L.G., Antonucci, V., Aricò, A.S., Nanosized IrO2 electrocatalysts for oxygen evolution reaction in an SPE electrolyzer, Journal of Nanoparticle Research 13, 1639–1646, 2011.

Cummins Inc., Cummins HyLYZER 4000—Technical Specification, https://mart.cummins.com/imagelibrary/data/assetfiles/0070328.pdf (Accessed: 6 June 2023).

Daikin Airconditioning UK Limited, Applied catalogue Chillers & air side, https://www.daikin.co.uk/content/dam/dauk/document-library/catalogues/Applied/Applied%20Catalogue%20Chillers%20and%20Airside_Catalogue_English.pdf (Accessed: 30 May 2023).

Dale, N.V., Characterization of PEM Electrolyzer and PEM Fuel Cell Stacks Using Electrochemical Impedance Spectroscopy, Doctoral Thesis, University of North Dakota, North Dakota, 2009.

Davies, J., Dolci, F., Weidner, E., Historical Analysis of FCH 2 JU Electrolyser Projects: Evaluation of contributions towards advancing the State of the Art, Publications Office of the European Commission, 2021.

Debe, M.K., Hendricks, S.M., Vernstrom, G.D., Meyers, M., Brostrom, M., Stephens, M., Chan, Q., Willey, J., Hamden, M., Mittelsteadt, C.K., Capuano, C.B., Ayers, K.E., Anderson, E.B., Initial Performance and Durability of Ultra-Low Loaded NSTF Electrodes for PEM Electrolyzers, Journal of The Electrochemical Society 159, K165–K176, 2012.

Duffie, J.A., Beckman, W.A., Solar Engineering of Thermal Processes, John Wiley & Sons, Inc., 2013.

EATON, EATON - Ecodesign—What you need to know about the Tier 2 Directive for Transformers, https://www.eaton.com/content/dam/eaton/products/medium-voltage-power-distribution-control-systems/iec-assemblies-mv-switchgear/ulusoy-dry-type-transformers/eaton-transformers-ecodesign-directive-leaflet-en-us.pdf (Accessed: 6 July 2023).

Egeland-Eriksen, T., Jensen, J.F., Ulleberg, Ø., Sartori, S., Simulating offshore hydrogen production via PEM electrolysis using real power production data from a 2.3 MW floating offshore wind turbine, International Journal of Hydrogen Energy, 2023.

Elogen, Elogen—PEM Electrolyzers—Catalogue, https://elogenh2.com/wp-content/uploads/2021/04/Elogen_Product_sheet-Elyte10.pdf (Accessed: 6 June 2023).

EnergyPurse, EnergyPurse—Cooling Tower Approach, Most Important Term!!, https://www.energypurse.com/cooling-tower-approach-most-important-term/ (Accessed: 6 June 2023).

Evapco .Inc, Evapco Global Product Catalogue, https://www.evapco.com/sites/evapco.com/files/2023-05/Global%20Product%20Catalog.pdf (Accessed: 30 May 2023).

Falcão, D.S., Pinto, A.M.F.R., A review on PEM electrolyzer modelling: Guidelines for beginners, Journal of Cleaner Production 261, 121184, 2020.

García-Valverde, R., Espinosa, N., Urbina, A., Simple PEM water electrolyser model and experimental validation, International Journal of Hydrogen Energy 37, 1927–1938, 2012.

Georgilakis, P.S., Environmental cost of distribution transformer losses, Applied Energy 88, 3146–3155, 2011.

Global Energy Moniter, Global Solar Power Tracker, https://globalenergymonitor.org/projects/global-solar-power-tracker/tracker-map/ (Accessed: 30 May 2023).

Grigoriev, S.A., Fateev, V.N., Bessarabov, D.G., Millet, P., Current status, research trends, and challenges in water electrolysis science and technology, International Journal of Hydrogen Energy 45, 26036–26058, 2020.

Grigoriev, S.A., Khaliullin, M.M., Kuleshov, N.V., Fateev, V.N., Electrolysis of Water in a System with a Solid Polymer Electrolyte at Elevated Pressure, Russian Journal of Electrochemistry 37, 819–822, 2001.

Grigoriev, S.A., Porembskiy, V.I., Korobtsev, S.V., Fateev, V.N., Auprêtre, F., Millet, P., High-pressure PEM water electrolysis and corresponding safety issues, International Journal of Hydrogen Energy 36, 2721–2728, 2011.

Hamdan, M., PEM Electrolyzer Incorporating an Advanced Low Cost Membrane, U.S. Department of Energy, 2013.

Harrison, K., W-Scale PEM-Based Electrolyzers for RES Applications: Cooperative Research and Development Final Report, National Renewable Energy Laboratory (NREL), 2021.

Harrison, K., Design, Integration and Control of Proton Exchange Membrane Electrolyzer for Wind Based Renewable Energy Applications, Doctoral Thesis, University of North Dakota, North Dakota, 2006.

Harrison, K., Hernández-Pacheco, E., Mann, M.E., Salehfar, H., Semiempirical Model for Determining PEM Electrolyzer Stack Characteristics, Journal of Fuel Cell Science and Technology 3, 220–223, 2006.

Haynes, W.M., Lide, D.R., Bruno, T.J. (Eds.), CRC Handbook of Chemistry and Physics, 95th ed. CRC Press, 2014.

H-Tec, H-Tec Conatinerized PEM Electrolyzer, https://www.h-tec.com/en/products/detail/h-tec-pem-elektrolyseur-hcs/2-mw-hcs/ (Accessed: 30 May 2023).

Incropera, F.P. (Ed.), Fundamentals of heat and mass transfer, 6th ed. John Wiley, Hoboken, NJ, 2007.

Institute for Sustainable Process Technology, Final report—Integration of Hydrohub GigaWatt Electrolysis Facilities in Five Industrial Clusters in The Netherlands, ISPT, 2020.

International Renewable Energy Agency, Green Hydrogen Cost Reduction: Scaling up Electrolysers to Meet the 1.5^0C Climate Goal. IRENA, 2020a.

International Renewable Energy Agency, Green hydrogen: A guide to policy making. IRENA, 2020b.

Joseph, J.A., Optimisation of 100 MW PEM Electrolysis Systems considering Efficiency, Storage and Costs, 2022.

Kim, H., Park, M., Lee, K.S., One-dimensional dynamic modeling of a high-pressure water electrolysis system for hydrogen production, International Journal of Hydrogen Energy 38, 2596–2609, 2013.

Kumar, A., Review of PEM Electrolyser and Associated Balance of Plant System for Green Hydrogen Generation, International Journal of Current Advanced Research 10, 24409–24412, 2021.

Kumar, S.S., Himabindu, V., Hydrogen production by PEM water electrolysis – A review, Materials Science for Energy Technologies 2, 442–454, 2019.

Kumar, S.S., Lim, H., An overview of water electrolysis technologies for green hydrogen production, Energy Reports 8, 13793–13813, 2022.

Lamy, C., Millet, P., A critical review on the definitions used to calculate the energy efficiency coefficients of water electrolysis cells working under near ambient temperature conditions, Journal of Power Sources 447, 227350, 2020.

Lange, N.A., Lange's handbook of chemistry, 15th ed, McGraw-Hill handbooks. McGraw-Hill, New York, NY, 1999.

Lebbal, M.E., Lecœuche, S., Identification and monitoring of a PEM electrolyser based on dynamical modelling, International Journal of Hydrogen Energy 34, 5992–5999, 2009.

Liso, V., Savoia, G., Araya, S.S., Cinti, G., Kær, S.K., Modelling and Experimental Analysis of a Polymer Electrolyte Membrane Water Electrolysis Cell at Different Operating Temperatures, Energies 11, 3273, 2018.

Mancera, J.J.C., Manzano, F.S., Andújar, J.M., Vivas, F.J., Calderón, A.J., An Optimized Balance of Plant for a Medium-Size PEM Electrolyzer: Design, Control and Physical Implementation, Electronics 9, 871, 2020.

Marangio, F., Santarelli, M., Calì, M., Theoretical model and experimental analysis of a high pressure PEM water electrolyser for hydrogen production, International Journal of Hydrogen Energy 34, 1143–1158, 2009.

Marr, C., Li, X., An engineering model of proton exchange membrane fuel cell performance, ARI - An International Journal for Physical and Engineering Sciences 50, 190–200, 1998.

MEKSAN, MEKSAN - Transformer Catalogue, https://prokcssmedia.blob.core.windows.net/sys-master-images/h08/hae/8931368009758/MEKSAN%20KATALOG.pdf (Accessed: 6 July 2023).

National Renewable Energy Laboratory, System Advisory Model (SAM)—Weather Data, https://sam.nrel.gov/weather-data.html (Accessed: 30 May 2023).

National Renewable Energy Laboratory, H2A: Hydrogen Analysis Production Models, NREL, 2020.

National Research Council of the United States of America, International Critical Tables of Numerical Data, Physics, Chemistry and Technology. McGraw-Hill Book Company Inc., 1930.

Nel Hydrogen, Nel Hydrogen M-Series Containerized PEM Electrolyzer, Nel Hydrogen, https://nelhydrogen.com/product/m-series-containerized/ (Accessed: 30 May 2023).

Nel Hydrogen, Nel Hydrogen—M Series Containerized—Catalogue, https://nelhydrogen.com/wp-content/uploads/2021/01/M-Series-Containerized-Spec-Sheet-Rev-F.pdf (Accessed: 6 June 2023).

Ni, M., Leung, M.K.H., Leung, D.Y.C., Energy and exergy analysis of hydrogen production by a proton exchange membrane (PEM) electrolyzer plant, Energy Conversion and Management 49, 2748–2756, 2008.

Noordende, H. van't, Ripson, P., A One-GigaWatt Green-Hydrogen Plant—Advanced Design and Total Installed-Capital Costs, Institute for Sustainable Process Technology, 2022.

O'Hayre, R., Cha, S.-W., G. Colella, W., Prinz, F.B., Fuel Cell Fundamentals, 3rd ed. John Wiley & Sons, Inc, Hoboken, NJ, 2016.

Ojong, E.T., Characterization of the Performance of PEM Water Electrolysis Cells operating with and without Flow Channels, based on Experimentally Validated Semi-empirical Coupled-Physics Models, Doctoral Thesis, Brandenburgischen Technischen Universität Cottbus – Senftenberg, 2018.

Ojong, E.T., Kwan, J.T.H., Nouri-Khorasani, A., Bonakdarpour, A., Wilkinson, D.P., Smolinka, T., Development of an experimentally validated semi-empirical fully-coupled performance model of a PEM electrolysis cell with a 3-D structured porous transport layer, International Journal of Hydrogen Energy 42, 25831–25847, 2017.

Olivier, P., Bourasseau, C., Bouamama, B., Dynamic and multiphysic PEM electrolysis system modelling: A bond graph approach, International Journal of Hydrogen Energy 42, 14872–14904, 2017a.

Olivier, P., Bourasseau, C., Bouamama, Pr.B., Low-temperature electrolysis system modelling: A review, Renewable & Sustainable Energy Reviews 78, 280–300, 2017b.

Özgirgin, E., Devrim, Y., Albostan, A., Modeling and simulation of a hybrid photovoltaic (PV) module-electrolyzer-PEM fuel cell system for micro-cogeneration applications, International Journal of Hydrogen Energy 40, 15336–15342, 2015.

Pacific Northwest National Laboratory, ANSI/ASHRAE/IES Standard 90.1-2010 Performance Rating Method Reference Manual, PNNL, 2016.

Perry, R.H., Green, D.W., Maloney, J.O., Perry's Chemical Engineers' Handbook, 8th ed. The McGraw-Hill Companies Inc., 2007.

Petrovic, S., Electrochemistry Crash Course for Engineers. Springer Nature Switzerland AG, Cham, 2021.

Pivovar, B., Ruth, M., Ahluwalia, R., H2NEW: Hydrogen (H2) from Next-Generation Electrolyzers of Water LTE Task 3c: System and Techno-Economic Analysis, National Renewable Energy Laboratory (NREL), 2022.

Pivovar, B., Ruth, M., Ahluwalia, R., H2NEW: Hydrogen (H2) from Next-Generation Electrolyzers of Water LTE Task 3c: System and Technoeconomic Analysis, National Renewable Energy Laboratory (NREL), 2021.

Plug Power Inc., Electrolyzers and Water: Saving Water, Powering the World with Green Hydrogen, https://www.plugpower.com/water-electrolysis-powering-the-world-with-green-hydrogen/ (Accessed: 30 May 2023a).

Plug Power Inc., The Plug EX-425D - Catalogue, https://www.plugpower.com/wp-content/uploads/2022/04/EX-425D_042522.pdf (Accessed: 6 June 2023b).

Proton Onsite, Proton Onsite—M400 Technical Specification, https://protonenergy.com/sites/default/files/2017-06/PD-0600-0122%20REV%20A.pdf (Accessed: 6 June 2023).

Ragnhild Hancke, Thomas Holm, Øystein Ulleberg, The case for high-pressure PEM water electrolysis, Energy Conversion and Management 261, 115642, 2022.

REFTECO Srl, REFTECO - Dry cooler RDSD – RDLD, https://www.refteco.com/dry-coolers/dry-cooler-rdsd-rdld/ (Accessed: 6 June 2023).

Roy, A., Watson, S.J., Infield, D., Comparison of electrical energy efficiency of atmospheric and high-pressure electrolysers, International Journal of Hydrogen Energy 31, 1964–1979, 2006.

Rozain, C., Millet, P., Electrochemical characterization of Polymer Electrolyte Membrane Water Electrolysis Cells, Electrochimica Acta 131, 160–167, 2014.

Santarelli, M.G., Torchio, M.F., Experimental analysis of the effects of the operating variables on the performance of a single PEMFC, Energy Conversion and Management 48, 40–51, 2007.

Schiebahn, S., Grube, T., Robinius, M., Tietze, V., Kumar, B., Stolten, D., Power to gas: Technological overview, systems analysis and economic assessment for a case study in Germany, International Journal of Hydrogen Energy 40, 4285–4294, 2015.

Solagris, Global Solar Atlas Map, https://globalsolaratlas.info/map (Accessed: 30 May 2023).

Sood, S., Prakash, O., Boukerdja, M., Dieulot, J.-Y., Ould-Bouamama, B., Bressel, M., Gehin, A.-L., Generic Dynamical Model of PEM Electrolyser under Intermittent Sources, Energies 13, 6556, 2020.

Springer, T.E., Zawodzinski, T.A., Gottesfeld, S., Polymer Electrolyte Fuel Cell Model, Journal of The Electrochemical Society 138, 2334–2342, 1991.

Stansberry, J.M., Brouwer, J., Experimental dynamic dispatch of a 60 kW proton exchange membrane electrolyzer in power-to-gas application, International Journal of Hydrogen Energy 45, 9305–9316, 2020.

Steinbach, A., Ulsh, M., Xi, H., Low-Cost, High Performance Catalyst Coated Membranes for PEM Water Electrolyzers (Final Technical Report), U.S. Department of Energy, 2022.

T. Ohta, Veziroglu, T.N. (Eds.), Energy Carriers and Conversion Systems with Emphasis on Hydrogen. Encyclopedia of Life Support Systems (EOLSS), 2007.

Tiktak, J., Heat Management of PEM Electrolysis: A study on the potential of excess heat from medium- to large-scale PEM electrolysis and the performance analysis of a dedicated cooling system, Masters Thesis, Delft University of Technology, Amsterdam, 2019.

U.S. Department of Energy, Energy Plus Engineering Reference, USDOE, 2022.

Verkoeyen, G., Hydrogenics—REVIEW OF WORLD AND EUROPEAN HYDROGEN INITIATIVES IN TRANSPORT AND ENERGY SECTORS, Hydrogenics, 2018.

Villagra, A., Millet, P., An analysis of PEM water electrolysis cells operating at elevated current densities, International Journal of Hydrogen Energy 44, 9708–9717, 2019.

Vossos, V., Johnson, K., Kloss, M., Khattar, M., Daniel, G., Brown, R., Review of DC Power Distribution in Buildings: A Technology and Market Assessment, Lawrence Berkeley National Laboratory, 2017.

Xu, W., Scott, K., The effects of ionomer content on PEM water electrolyser membrane electrode assembly performance, International Journal of Hydrogen Energy 35, 12029–12037, 2010.

Yigit, T., Selamet, O.F., Mathematical modeling and dynamic Simulink simulation of high-pressure PEM electrolyzer system, International Journal of Hydrogen Energy 41, 13901–13914, 2016.

Zhang, H., Su, S., Chen, J., Efficiency Calculation and Configuration Design of a PEM Electrolyzer System for Hydrogen Production, International Journal of Electrochemical Science 7, 4143–4157, 2012.

APPENDIX

HyLYZER®
WATER ELECTROLYZERS

HyLYZER® is Cummins' globally proven modular water electrolyzer system designed for easy on-site installation inside or out, with simple interconnectivity to scale up, and an unrivaled record for reliability, low maintenance and on-site safety. Recommended for projects between 4,000 - 50,000 Nm^3/h.

- Proven technology, compliant with highest safety standards
- Exceptionally compact
- 30 bar pressurized stacks

FEATURES

	HyLYZER® - 4000
Technology	PEM water electrolysis
Hydrogen production	4000 Nm^3/h (8630 kg/day)
H_2 delivery pressure	30 bar_g (435 psig) without a compressor
H_2 quality max impurities	99.99% dry basis, gas is fully saturated with water O_2 < 100 ppm Optional > 99.998% with hydrogen purification system

cummins.com/hydrogen

Appendix 1. PEM Manufacturer Catalogues (Cummins Inc., 2021)

TECHNICAL SPECIFICATIONS

	HyLYZER® - 4000
Operating range	5-125%
DC power consumption at stack	40 to 50 kWh/kg, 48 at nominal load (3.6 to 4.5 kWh/Nm^3, 4.3 at nominal load)
System specific consumption*	≤ 51 kWh/kg
Utilities required to operate the plant	Electrical power, demineralized water, cooling water, HVAC, instrument air, nitrogen for purge
Rectifier specifications	4.1 to 30kV 50/60 Hz, 23 MVA 97% efficiency
Auxiliary installed power	150 kVA (estimated)
Demineralized Water Consumption and Recommended Water Quality	~0.8 L/Nm^3 of H_2 [9 L/kg of H_2] ASTM D1193 Type
Total footprint (including maintenance area)	Electrolyzer dimensions (estimated) = 10 m x 15 m (34 x 50 ft) Rectifier dimensions (estimated) = 10 x 15 m (34 x 50 ft)
Installation environment	Indoors 5°C to 40°C / 41°F to 104°F

*System specific consumption considers: the standard scope of supply (refer to BOS table); 100% Load capacity; Beginning Of Life; 1% increase per annum (at ≥8500 hours operation); Range for indoor setup

STACK AND BALANCE-OF-STACK (BOS)	Outdoor	Indoor
Cell stacks and gas generation system		■
Power rectifiers		■
Control panel		■
Water polishing system		■

BALANCE-OF-PLANT (BOP)	Outdoor	Indoor
Rectifier cooling		
Gas cooling		
Electrolysis cooling		
Water purification system		
Instrument air compressor		
Hydrogen purification system		**Optional**

Applicable Codes and Standards Pressure Equipment Directive 2014/68/EU, Low Voltage Directive 2014/35/EU, Machinery Directive 2006/42/EC, Electro-Magnetic Compatibility 2014/30/EU, ATEX Directive 2014/34/EU, IEC 61511, IEC 61508, IEC 60079-10-1, NFPA 2, NFPA 497, National Electrical Code (NEC), ANSI/NFPA 70, ASME B31.3-2016, ASME Boiler and Pressure Vessel Code 2017, CSA C22.1 and C22.2, CSA B51 2019, CAN/BNQ 1784-000/2007. Other jurisdictions available on request.

cummins.com

Bulletin 5676519 Produced in U.K. 9/21

Appendix 1. continued

Green Hydrogen at Work

The Plug EX-425D

Best-in-class PEM electrolysis based on nearly 50 years of experience

Appendix 1. continued (Plug Power Inc., 2022b)

Plug is the only company able to deliver on the entire hydrogen ecosystem.

Our portfolio includes products that produce, store, transport, dispense, and convert hydrogen to carbon-free electricity. Plug's turnkey, plug-and-play electrolyzers utilize proton exchange membrane (PEM) technology with decades of field experience and a track record of high performance and reliability.

Plug's electrolyzers are the safest, most efficient, and deliver the lowest total cost of ownership on the market today.

PEM electrolyzers generate hydrogen from water using electricity and a special membrane. No caustic chemical solutions required.

The Plug Gigafactory has the highest capacity in the industry (1GW), utilizing lean principals and cutting-edge technology.

EX-425D System Specifications

The Plug EX-425D provides up to 425 kg/day of high-quality on-site hydrogen.

Instant Load Following
Hydrogen production rate adjusts as electric capacity is available, making this a perfect product for use with grid or renewable energy resources.

Compact
Containerized solution is easy to site near point of use.

Modular and Scalable
Pair multiple units for high demand and availability.

Corporate Headquarters
968 Albany Shaker Rd,
Latham, NY 12110
518.782.4004

Input	
Stack Power Consumption	Up to 1MW
Voltage & Frequency	480VAC, 60HZ (USA) 400VAC, 50HZ (EU)
Water Consumption	13 liters per kg of H2 produced
Output (Hydrogen Gas)	
Volume	200 Nm^3 / hour
Mass	425 kg / day
Purity	Up to 99.999%
Pressure	40 barg / 580 psig (w/o compressor)
Operational	
Start Up Time	30 sec warm / < 5 min cold
Average Stack Efficiency	49.9 kWh / kg
Load Following	Instantaneous
Physical / Environment	
Installed Footprint	29.3m^2 / 320 ft^2
Ambient Temperature	-20°C to +40°C (wider temperature range optional)
Other	
Compliance / Certifications	ISO 22734, NFPA 2, CE

Appendix 1. continued

nel

M Series Containerized

Proton Exchange Membrane (PEM) Hydrogen Generation Systems

MC250 Power Supply Enclosure, Electrolyser Enclosure and optional Thermal Control System – installation may vary.

MODEL	MC250	MC500
Class	1.25 MW	2.5 MW
Description	Fully-automated MW-class on-site hydrogen generator utilizing a modular containerized design for ease of installation and integration Tri-mode operation (selectable): • Command mode allows operation based on customer input current command • Load following mode automatically adjusts output to match demand • Tank filling mode operates with power-conservation mode during standby	
Electrolyte	Proton Exchange Membrane (PEM) – caustic-free	
HYDROGEN PRODUCTION		
Net Production Rate Nm^3/h @ 0° C, 1 bar SCF/h @ 70° F, 1 atm kg/24 h	246 Nm^3/h 9,352 SCF/h 531 kg/24 h	492 Nm^3/h 18,704 SCF/h 1,062 kg/24 h
Delivery Pressure – Nominal	30 barg (435 psig); full differential pressure H_2 over O_2	
Average Power Consumption at Stack per Volume of H_2 Gas Produced[1]	4.5 kWh/Nm^3	
Average Power Consumption at Stack per Mass of H_2 Gas Produced[1]	50.4 kWh/kg	
Purity (concentration of impurities)	99.95% [H_2O < 500 ppm, N_2 < 2 ppm, O_2 < 1 ppm, all others undetectable]	
Purity (concentration of impurities with optional high purity dryer)	ISO 14687:2019(E) Type I, Type II Grade D and SAE J-2719 Type I Grade L 99.9995% [H_2O < 5 ppm, N_2 < 2 ppm, O_2 < 1 ppm, all others undetectable]	
Start-up Time (from off state)	< 8 min	
Ramp-up Time (minimum to full load)	< 15 sec	
Ramp Rate (% of full-scale)	≤ 15% per sec	
Production Capacity Dynamic Range	10 to 100%	
POTABLE WATER REQUIREMENTS		
Consumption Rate at Maximum Production	354 l/h (94 gal/h)	708 l/h (187 gal/h)
Temperature	5 to 40°C (41 to 104°F)	
Pressure	3.8 to 4.8 barg	
Input Water Quality	Potable, subject to site water quality analysis	
Water Purification System (included)	Reverse Osmosis/Electrodeionization (RO/EDI)	

Appendix 1. continued (Nel Hydrogen, 2021)

MODEL		MC250	MC500
ELECTRICAL SPECIFICATIONS			
Electrical Requirements		Typical installation: 6.6 to 35 kV, three phase 50 Hz/60 Hz Low voltage, three phase required for balance of plant and ancillary equipment Uninterruptible low voltage, three phase required for backup heating for freeze protection	
Power Quality (medium voltage)		Total harmonic distortion: < 5%, power factor: > 0.9 at normal power	
PHYSICAL CHARACTERISTICS			
Dimensions W x D x H	Power Supply Enclosure	6.1 m x 2.5 m x 2.6 m (20 ft x 8 ft x 8.5 ft)	12.2 m x 2.5 m x 3 m (40 ft x 8 ft x 9.9 ft)
	Electrolyser Enclosure[2]	12.2 m x 2.5 m x 3 m (40 ft x 8 ft x 9.9 ft)	12.2 m x 2.5 m x 3 m (40 ft x 8 ft x 9.9 ft)
Weight	Power Supply Enclosure	18,000 kg (39,700 lbs)	24,000 kg (53,000 lbs)
	Electrolyser Enclosure	17,300 kg (38,000 lbs)	18,600 kg (41,000 lbs)
ENVIRONMENTAL CONSIDERATIONS – DO NOT FREEZE			
Standard Siting Location		Outdoor, pad mounted Flatness 35/25 per ACI-117-10 Bottom access for AC and DC electrical connections, water and drains	
Storage/Transport Temperature		5 to 60°C (41 to 140°F)	
Ambient Temperature		-20 to 40°C (-4 to 104°F)	
Altitude Range – Sea Level		1,000 m (3,281 ft)	
OPTIONS			
• Medium voltage input 4.16 to 6.6 kV		• Thermal Control System	• High purity hydrogen dryer with dew point meter

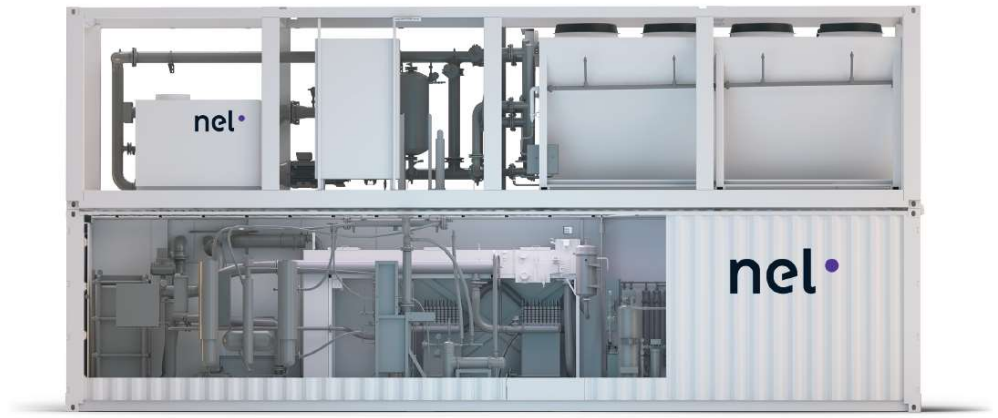

Side cutaway view of MC500 Electrolyser Enclosure and optional Thermal Control System – installation may vary.

Specifications are subject to change. Please contact Nel Hydrogen for solutions to best fit your needs.

[1] Dependent on configuration and operating conditions.
[2] Plus vent, ground mounted HVAC and rooftop equipment, site specific.

www.nelhydrogen.com | +1.203.949.8697 | info@nelhydrogen.com

Made in the USA

PD-0600-0136 Rev E

Appendix 1. continued

PROTON
THE LEADER IN ON SITE® GAS GENERATION.

Technical Specifications

M400

Hydrogen Generation System

MODEL	M400
Features	Fully-automated MW-class on-site hydrogen generator utilizing a modular skid-based design. Tri-mode operation (selectable): • Command-following mode allows operation based on available input power. • Load Following mode automatically adjusts output 0-100% to match demand. • Tank Filling mode operates with power-conservation mode during standby.
ELECTROLYTE	
	Proton Exchange Membrane (PEM) - caustic-free
HYDROGEN PRODUCTION	
Net Production Rate Nm^3/hr @ 0°C, 1 bar SCF/hr @ 70°F, 1 atm SLPM @ 70°F, 1 atm kg per 24 hours	 417 15882 7495 902
Delivery Pressure - Nominal	30 barg / 435 psig; Full Differential Pressure H_2 Over O_2
Hydrogen Purity With Optional High Purity Dryer	> 99.9% Water Vapor < 500 ppm, N2 < 2 ppm, O2 < 1 ppm, All others undetectable ISO 14687-1:1999 Type 1 Grade C / ISO 14687-2:2012 Type 1 grade D > 99.9995% Water Vapor < 2 ppm, N2 < 2 ppm, O2 < 1 ppm, All others undetectable
ELECTRICAL POWER CONSUMPTION	
MW's @ Cell Stack(s) MW's @ System	2.1 2.2
Power Consumed per Volume of H_2 Gas Produced[1] Mass of H_2 Gas	 5.3 kWh/Nm^3 59 kWh/kg
SYSTEM OPERATION	
Start-Up Time (from Off State)	<5 min
Turndown Range	10 to 100% (Input Power Mode); 0 to 100% (H_2 Demand Mode)
Ramp-Up Time (Minimum to Full Load)	<10 Sec
Ramp Rate (% of Full-Scale)	≥ 15% per sec (Power Input Mode)
DI WATER REQUIREMENT	
Consumption Rate at Maximum Production	373 L/hr 99 gal/hr
Maximum Inlet Flowrate	747 L/hr 197 gal/hr
Temperature	5°C to 40°C / 41°F to 104°F
Input Water Quality	ASTM Type II Deionized Water required, < 1 micro Siemen/cm (> 1 MegOhm-cm) ASTM Type I Deionized Water recommended, < 0.1 micro Siemen/cm (> 10 MegOhm-cm)

ProtonOnSite.com | 01.203.949.8697 | Info@ProtonOnSite.com

Appendix 1. continued (Proton Onsite, 2017)

MODEL	M400
PHYSICAL CHARACTERISTICS- MASS (KG)	
Classifed Area	
Water Circulation Skid (Operating)	10403
H2 Gas Management Skid	909
Unclassifed Area	
Power Conversion Assembly (each) (Includes Rectifiers, Transformer, and AC Distribution)	6500
Power Conversion Quantity	4
MCC	909
Controls	300
PHYSICAL CHARACTERISTICS -DIMENSIONS (MM)	
Classified Area	
Water Circulation Skid	9918 W x 820 D 2141 H
H2 Gas Management Skid	3317 W x 575 D x 2083 H
Unclassfied Area	
Power Conversion Assembly (each)	6200 W x 1200 D x 2850 H
MCC	2032 W x 549 D x 2210 H
Controls	1550 W x 382 D x 2190 H
ENVIRONMENTAL CONSIDERATIONS	
Standard Siting Location	Indoor, 10-90% RH non-condensing for Classified & Unclassified Equipment Outdoor Siting Options Available
Storage/Transport Temperature	5°C to 60°C / 41°F to 140°F
Ambient Temperature Range	10°C to 40°C / 50°F to 104°F
Altitude Range-Sea Level	1000 m /3281 ft
ELECTRICAL SPECIFICATIONS	
Electrical specification	Typical installation: 10 kV and 20 kV, 3 phase + Neutral, 50Hz/60Hz; For lower voltage connection, consult Proton Applications Engineering Department for specific requirements and options. Ancillary equipment powered by Customer or optionally powered by Proton OnSite
Power Quality	Designed to German TAB Specification
OPTIONS	

- Factory Matched RO/DI Water System
- Factory Matched Thermal Control Unit
- Dew Point Monitoring
- High Purity Hydrogen Dryer
- Air Compressor
- Containerization

Specifications are subject to change. Please contact Proton OnSite for solutions to best fit your needs.

PROTON THE LEADER IN ON SITE GAS GENERATION.

ProtonOnSite.com | 01.203.949.8697 | Info@ProtonOnSite.com

Certified to ISO 9001:2008

Appendix 1. continued

elogen | Empowering a sustainable world

PEM - Electrolysers

PROTON EXCHANGE MEMBRANE

Gas Production	Hydrogen	Oxygen
Max. output pressure	30 barg	9 barg
Purity without additional purification	>99.9 %	>99.8 %

Hydrogen Drying System

Industrial drying system with automatic regeneration. The hydrogen purity according to ISO 14687-2 for the use in fuel cell vehicles is met.	
Max. hydrogen purity	99.999 %

Feeding Water (Tap Water)

Water quality acc.	98/83/EG	Pressure	2 to 6 bar
PH	4 to 10	Temperature	+5 to +35 °C
Water treatment	Integrated Reverse Osmosis System (ROS) + electro de-ionisation system		

Power Input

Voltage	From 400 V AC to high voltage Alternatively a transformer can be included
Frequency	50 Hz, 60 Hz

Safety Norms and Regulations

Compliance	Machine directive 2006/42/CE Pressurised equipment directive 2014/68/UE Low voltage directive 2014/35/UE Electromagnetic compatibility directive 2014/30/UE ATEX directive 2014/34/UE CE Mark

8 Avenue du Parana | 91940 Les Ulis | France | Tel. +33 181 871 240
info@elogenh2.com

elogen

Eupener Straße 165 | 50933 Köln | Germany | Tel. +49 221 291 907 30
info@elogenh2.com

Appendix 1. continued (Elogen, 2021)

elogen | Empowering a sustainable world

Our solutions

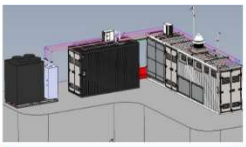

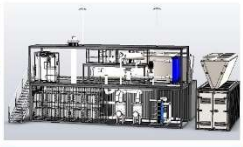

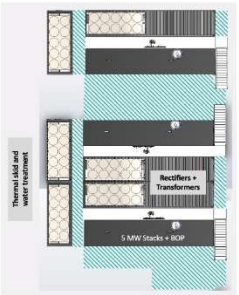

Specification	Containerized System			Semi-containerized Open Power System		Modular Open Power System
	E 50	E 100	E 200	E 500	E 1000	n x E 1000
Hydrogen Production						
H_2 flow rate [Nm^3/h]	50	100	200	500	1 000	< 4 000
Oxygen Production						
O_2 flow rate [Nm^3/h]	25	50	100	250	500	< 2 000
Operating range						
Hydrogen production [%]	5-100	5-100	5-100	5-100	5-100	5-100
Feeding Water						
Consumption [l/h]	<100	<160	<400	<1 000	<2 000	<8 000
Installed Power						
Electrolysis [kW]	250	500	1 000	2 500	5 000	< 20 000
Power [kVA]	350	620	1 240	3 200	6 500	< 25 000
Specific Energy						
Stack consumption [kWh/Nm^3H_2]	4.3	4.4	4.4	4.4	4.4	4.4
System consumption [kWh/Nm^3H_2]	4.9	4.9	4.9	4.9	4.85	4.85
Footprint						
Dimensions	20'	40'	40' + 20'	<30m²/MWel	<30m²/MWel	<30m²/MWel

More than 30 electrolysers delivered across Europe, Asia and US with project specific solutions

adaptation to other water quality on demand

waste heat recovery system

oxygen collection

8 Avenue du Parana | 91940 Les Ulis| France | Tel. +33 181 871 240
contact@elogenh2.com

elogen

Eupener Straße 165 | 50933 Köln | Germany | Tel. +49 221 291 907 30
info@elogenh2.com

Appendix 1. continued

Default capacity coefficients of air cooled chillers

Coefficient	Scroll	Screw
a	0.40070684	-0.09464899
b	0.01861548	0.03834070
c	0.00007199	-0.00009205
d	0.00177296	0.00378007
e	-0.00002014	-0.00001375
f	-0.00008273	-0.00015464

Default capacity coefficients of water cooled chillers

Coefficient	Scroll	Screw	Centrifugal
a	0.36131454	0.33269598	-0.29861976
b	0.01855477	0.00729116	0.02996076
c	0.00003011	-0.00049938	-0.00080125
d	0.00093592	0.01598983	0.01736268
e	-0.00001518	-0.00028254	-0.00032606
f	-0.00005481	0.00052346	0.00063139

Default efficiency EIR-FT coefficients of air cooled chillers

Coefficient	Scroll	Screw
a	0.99006553	0.13545636
b	-0.00584144	0.02292946
c	0.00016454	-0.00016107
d	-0.00661136	-0.00235396
e	0.00016808	0.00012991
f	-0.00022501	-0.00018685

Default efficiency EIR-FT coefficients of water cooled chillers

Coefficient	Scroll	Screw	Centrifugal
a	1.00121431	0.66625403	0.51777196
b	-0.01026981	0.00068584	-0.00400363
c	0.00016703	0.00028498	0.00002028
d	-0.00128136	-0.00341677	0.00698793
e	0.00014613	0.00025484	0.00008290
f	-0.00021959	-0.00048195	-0.00015467

Default efficiency EIR-FPLR coefficients of air cooled chillers

Coefficient	Scroll	Screw
a	0.06369119	0.03648722
b	0.58488832	0.73474298
c	0.35280274	0.21994748

Appendix 2. Chiller Model Coefficients (Pacific Northwest National Laboratory, 2016)

Default efficiency EIR-FPLR coefficients of water cooled chillers

Coefficient	Scroll	Screw	Centrifugal
a	0.04411957	0.33018833	0.17149273
b	0.64036703	0.23554291	0.58820208
c	0.31955532	0.46070828	0.23737257

Chiller minimum unloading ratios

Chiller Type	Default Unloading Ratio
Screw	0.15
Centrifugal	0.1
Scroll	0.25

Appendix 2. continued

SYSTEM DESIGN/ SIZING SHEET							
PEM Stack							
Cell Model Reference		harisson2021					
Cell Area		1250	cm2				
Vcell Max.		2.10	V				
Max. Current Density		3.5	A/cm2 @ 2.1V				
Max. Current		4375	A				
No. of Cells		129					
Max. Stack Capacity Est.		1.186	MW				
Stack Thermal Capacity		486.0	kJ/K				
Max H2 production rate		0.0058494	kg/s	21.05768	kg/h	234.288	Nm3/h
Max H2O consumption rate		0.0526442	kg/s	0.83441	GPM		
Stack Consumption at Max Poduction		56.3215	kWh/kg	0.000118			
No. of Stacks		1					
Max. System Capacity		1.186	MW				
Max System H2 production rate		0.0058494	kg/s	21.05768	kg/h	234.288	Nm3/h
Max System H2O consumption rate		0.0526442	kg/s	0.83441	GPM		
DC-DC Converter							
No of Converters		1					
Rated Capacity		1250	kW	Safety	0%		
Hydrogen Loss							
Hydrogen Permiation Loss		0.6%					
Hydrogen Sepration/Dryer Loss		3.0%					
Cooling							
Max. Stacks Cooling Load		350.2	kW				
Max. Dryer Cooling Load		7.6	kW				
Cooling System Design Option (1/2/3)		2					
Outdoor Design Condition							
Tdrybulb		44.3	°C	ASHRAE Fundametals 2021			
Twetbulb		30	°C	ASHRAE Fundametals 2021			
Chiller							
No. of Chillers		1					
Chiller Type		aircooled_scroll		aircooled_scroll_a			
Chiller Capacity		9	kW	10%	Safety		
COP Requirment	>=	2.985		ASHRAE 90.1 Standard			
IPLV Requirment	>=	4.048		ASHRAE 90.1 Standard			
Tevaporator leaving		5	°C				
ΔT		6	°C				
Tcondcold		44.3	°C				
Design water Maximum Flow		0.36	l/s				
Corrected COP Value		2.985		Calculated via Simulink			
Resulting IPLV		4.644		Calculated via Simulink			

Appendix 3. Sample System Design Sheet fed to the Matlab PEM System Model

Chiller Circulation Pump					
No. of Circulation Pump		1			
Pump Flowrate		0.36	l/s		
Circulation Pump Power for each		0.2	kW	(300 W·s/L) ASHRAE 90.1 Standard	
Chiller Cooling Tower					
No. of Cooling Towers		1			
Cooling Tower Design Capacity		0	kW	(1.25kW of tower cooling for every 1kW of chiller)	
ΔT		0	°C	ASHRAE Handbook - Systems and Equipments	
Tapproach		0	°C	Calculated via Simulink	
Tcondcold		0	°C	Calculated via Simulink	
Design Water Flow		0.00	l/s	constant	
Fan Power Criteria	>=	0	L/(s·kW)	water flow rate/fan power	ASHRAE 90.1 Standard
Fan Power	<=	0	kW		
No. of Circulation Pump		1			
Pump Flowrate		0	l/s		
Circulation Pump Power for each		0	kW	(300 W·s/L) ASHRAE 90.1 Standard	
Evaporative Water Loss		0	L/s	0.00175 1/°C	
Drift Water Loss		0	L/s	0.20%	
Cycles of Concentration		2.5			
Blowdown Loss		0	L/s		
Make-up Water		0	L/s		
Basin Heater Capacity		0.00	W/K		
Cooling Tower Water Thermal Capacitan		0.00	W/K		
Stack Dry Cooler/ Cooling Tower					
Type		Dry Cooler			
No. of Dry Cooler/ Cooling Tower		1			
Dry Cooler/ Cooling Tower Capacity		355	kW	0% Safety	
ΔT		15	°C		
Tcondcold setpoint		55	°C		
Design Water Flow for each		5.66	l/s	constant	
Cooling Tower FRwater		0		Calculated via Simulink 0.75<>1.25	
Cooling Tower Nominal Capacity		0	kW		
Evaporative Water Loss		0	L/s	0.00175 1/°C	
Drift Water Loss		0	L/s	0.2%	
Cycles of Concentration		2.5			
Blowdown Loss		0	L/s		
Make-up Water		0	L/s		
Basin Heater Capacity		0.00	W/K		
Cooling Tower Water Thermal Capacitan		0.00	W/K		
Dry Cooler Air Flow		89786	m3/h		
Dry Cooler UA factor		35303.6		Calculated via Simulink	
Fan Power Criteria	>=	0.38	L/(s·kW)	water flow rate/fan power	ASHRAE 90.1 Standard
Design/ Nominal Fan Power	<=	14.9	kW		

Appendix 3. continued

Stack Cooling Circulation Pump				
No. of Circulation Pump	1			
Pump Flowrate	5.66	l/s		
Circulation Pump Power for each	1.7	kW	(300 W·s/L) ASHRAE 90.1 Standard	
Anode Circulation Pump				
No. of Circulation Pump	1			
Pump Flowrate	5.66	l/s	(300 W·s/L) ASHRAE 90.1 Standard	
Circulation Pump Power for each	1.7	kW	(300 W·s/L) ASHRAE 90.1 Standard	
Reverse Osmosis System				
Capacity	5.7	m3/day	1500 GPD	
Recovery Rate	80%		2-stage recovery rate brackish water reverse osmosis	
Booster Pump				
Booster Pump Design Water Flow	0.3	m3/h		
Feed Pressure	10	bar	(10-17bar) for RO	
Theoretical Booster Pump Power	0.2	kW	50% efficiency	
Booster Pump Power	1.5	kW	min capcaity for commercial booster pumps around 1.5kW	
Control Cabinet (PLC/SCADA)				
Total Equipment Power Consumption	21.6	kW		
Cabinet Power Cunsumption	1.1	kW	Percent Load	5%
AC-AC Transformer				
No of Transformer	1			
Rated Capacity	50	kVA	Power Factor	0.8
No Load Losses	160	W		
Load Losses	1050	W		

Appendix 3. continued

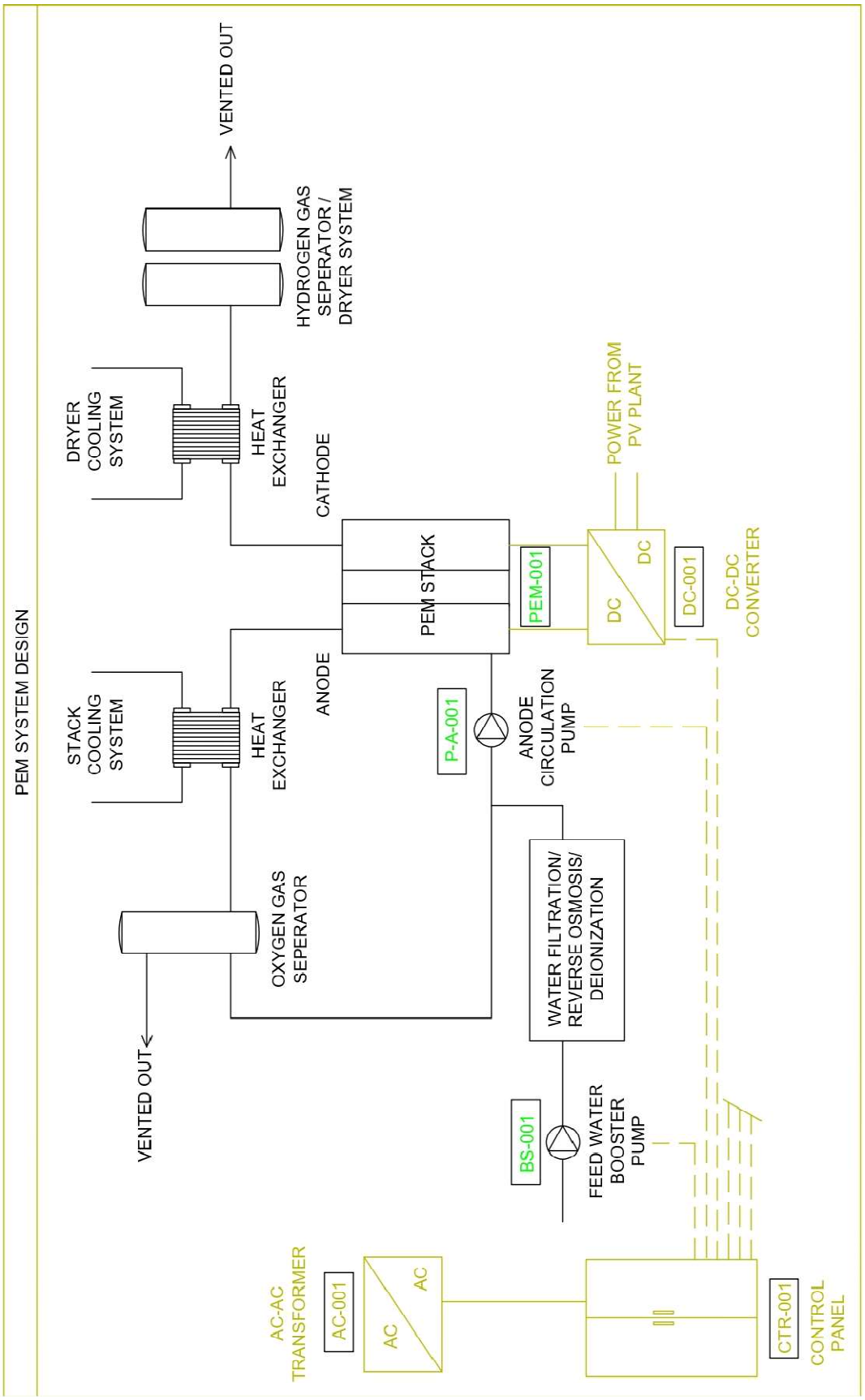

Appendix 4. PEM System Design Schematics

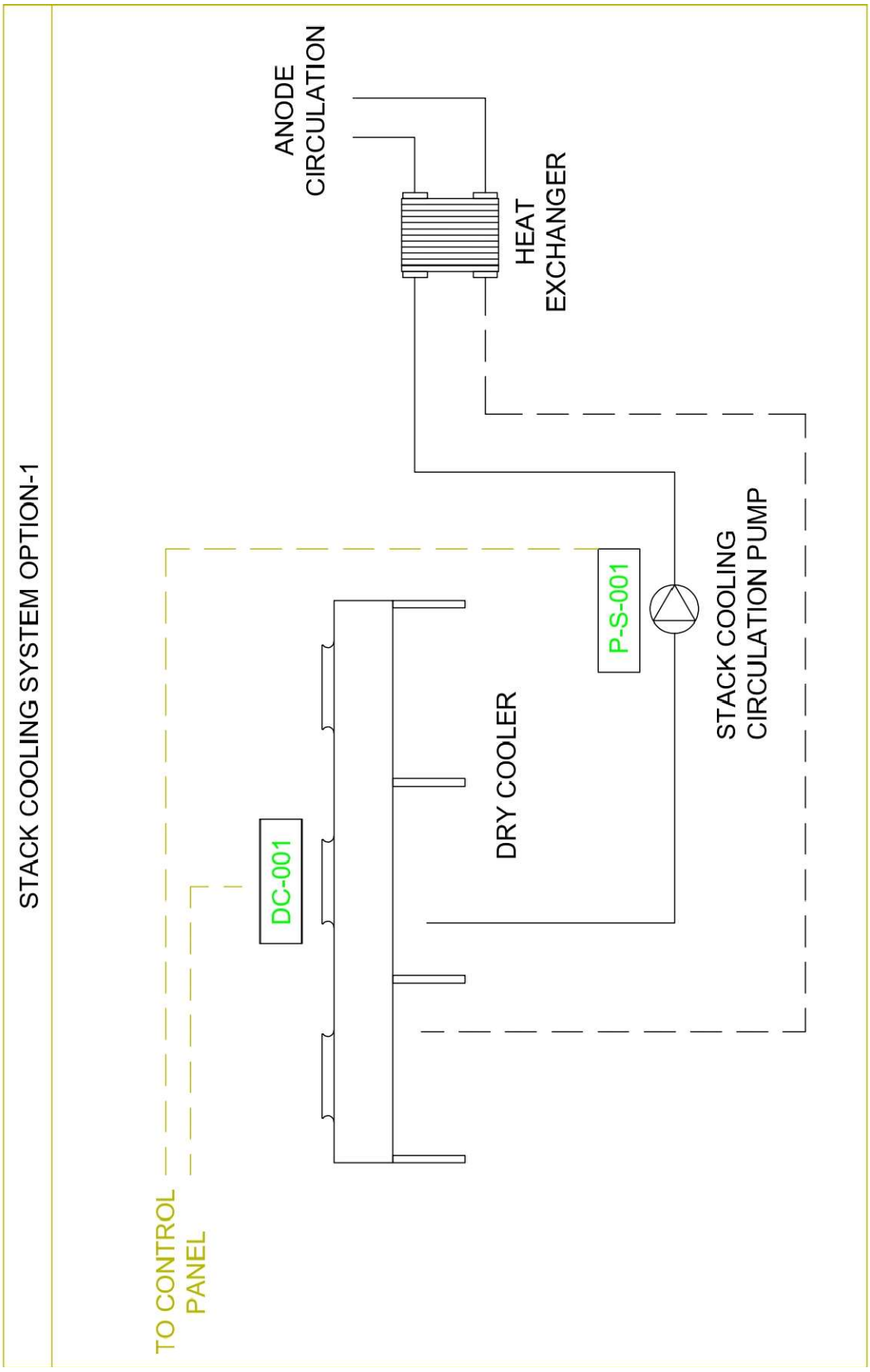

Appendix 4. continued

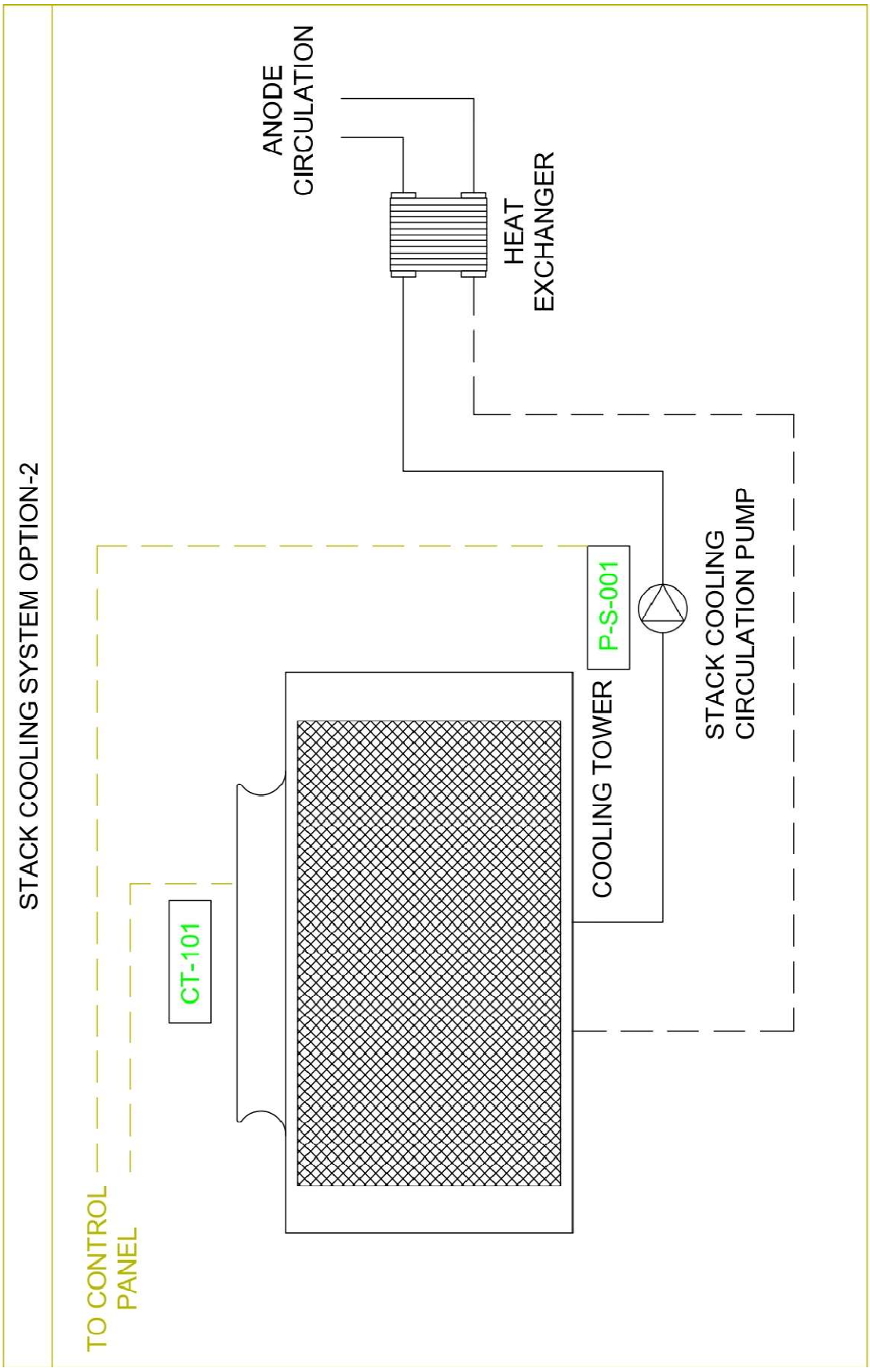

Appendix 4. continued

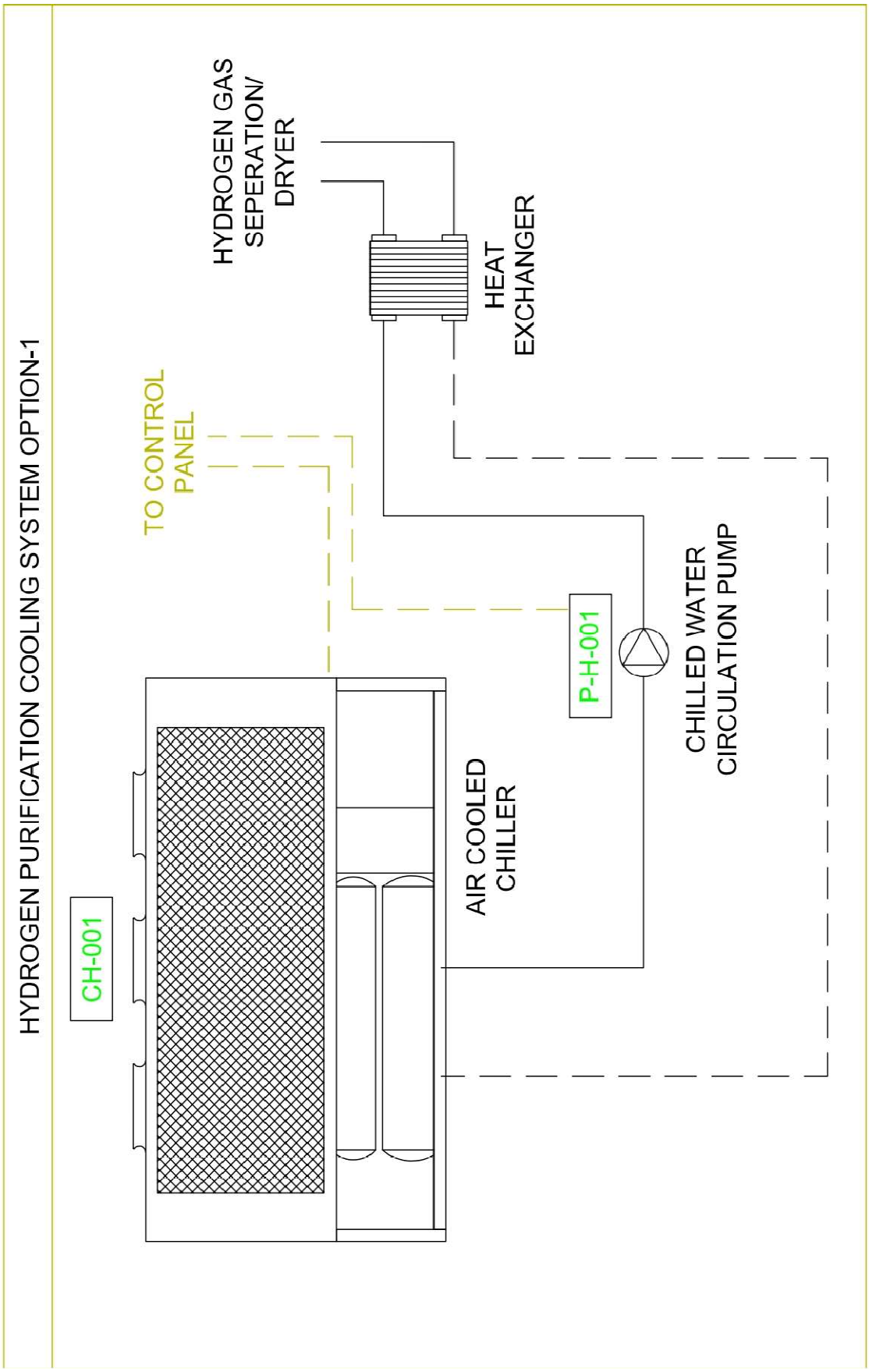

Appendix 4. continued

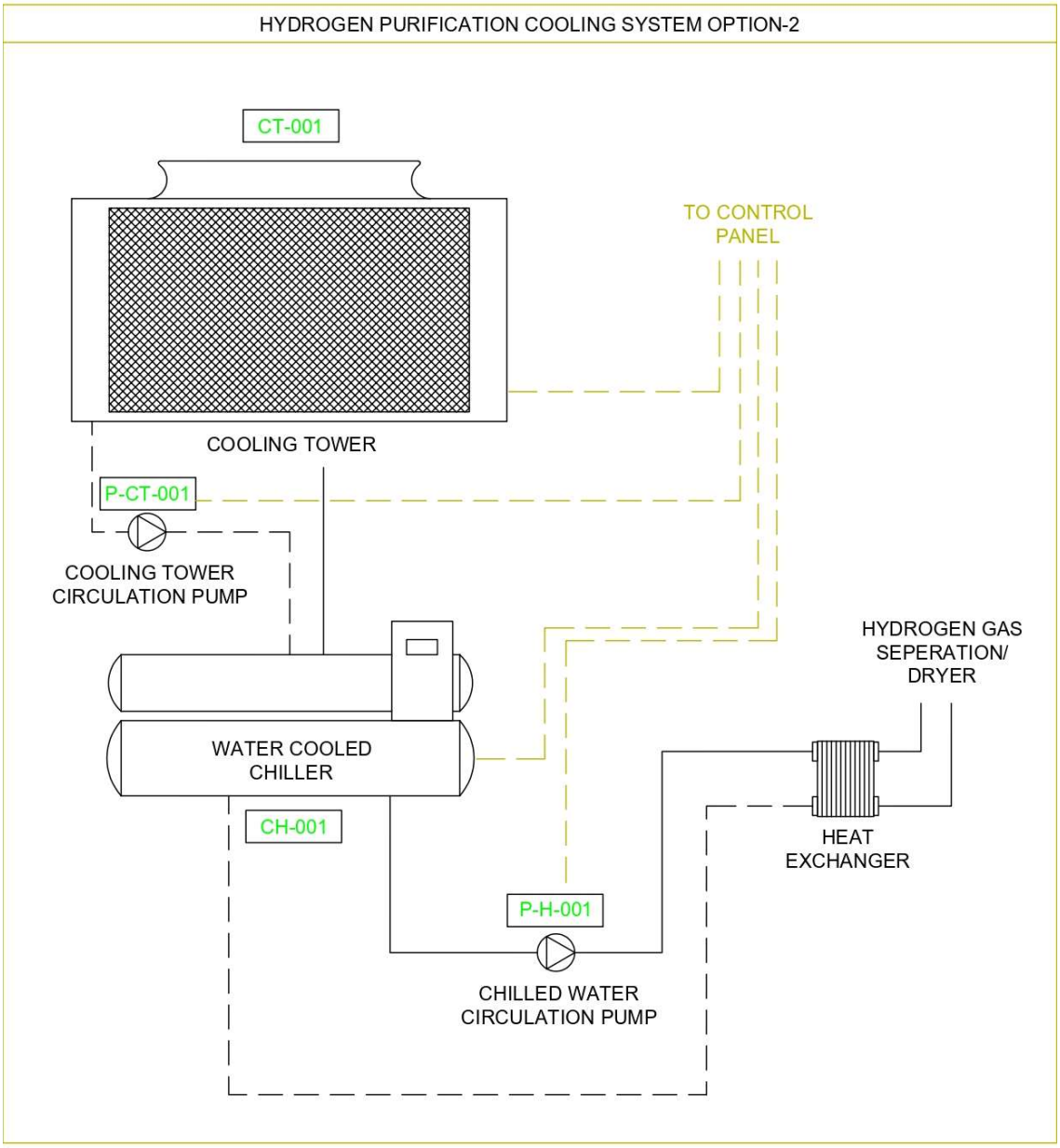

Appendix 4. continued

Simulation Result

Location	Turkey-Kocaeli	
System Design	100MW-1.1	
Plant Capacity	100000	kW
Hours of Operation	3907	hrs
Capacity Factor	15.1%	
Annual Solar DC Power Production	132496049	kWh
Annual Stack Consumption	126391710	kWh
Mechanical Consumption	1723824	kWh
Electrical Consumption	7062567	kWh
Annual BoP Consumption	8786391	kWh
Annual H2O Consumption	31324956	kg
Annual H2 Net Production	2503769	kg
Annual H2 Loss	106644	kg
Stack Average Efficiency	48.97	kWh/kg
Mechanical Loss Average	0.69	kWh/kg
Electrical Loss Average	2.82	kWh/kg
Stack + BoP Average Efficiency	53.99	kWh/kg

Permiation + %3 Dryer

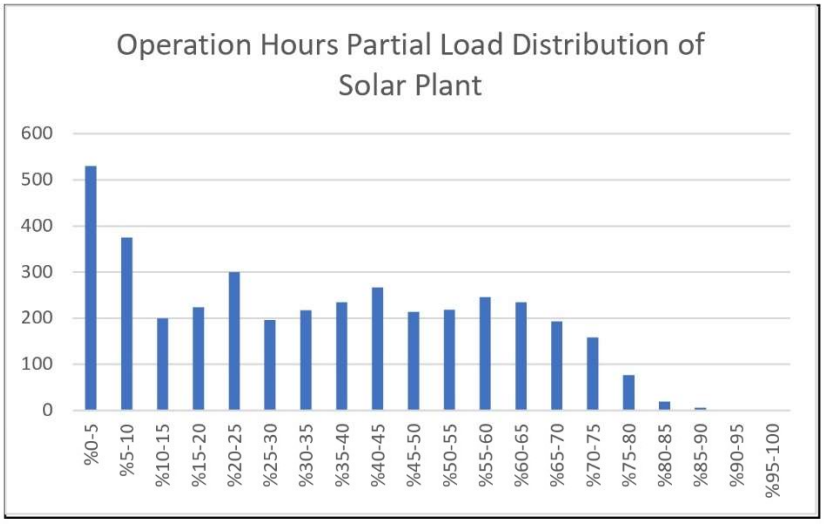

Simulation Results at Maximum Power

Max Solar DC Power	86896	kW
Stack Consumption	83421	kW
BoP Consumption	4220	kW
H2O Consumption	5.261325	kg/s
H2 Net Production	0.423053	kg/s
H2 Loss	0.002306	kg/s
Stack Efficiency	54.77	kWh/kg
Mechanical Loss	0.40	kWh/kg
Electrical Loss	2.36	kWh/kg
Stack + BoP Efficiency	57.55	kWh/kg

%0.6 Permiation + %3 Dryer

Appendix 5. Simulation Result Sheets for Three Locations in Turkey

Simulation Result

Location	Turkey-Antalya	
System Design	100MW-1.1	
Plant Capacity	100000 kW	
Hours of Operation	3867 hrs	
Capacity Factor	17.9%	
Annual Solar DC Power Production	156678076 kWh	
Annual Stack Consumption	149773303 kWh	
Mechanical Consumption	1834359 kWh	
Electrical Consumption	7870542 kWh	
Annual BoP Consumption	9704901 kWh	
Annual H2O Consumption	36565974 kg	
Annual H2 Net Production	2926909 kg	
Annual H2 Loss	120256 kg	Permiation + %3 Dryer
Stack Average Efficiency	49.64 kWh/kg	
Mechanical Loss Average	0.63 kWh/kg	
Electrical Loss Average	2.69 kWh/kg	
Stack + BoP Average Efficiency	54.49 kWh/kg	

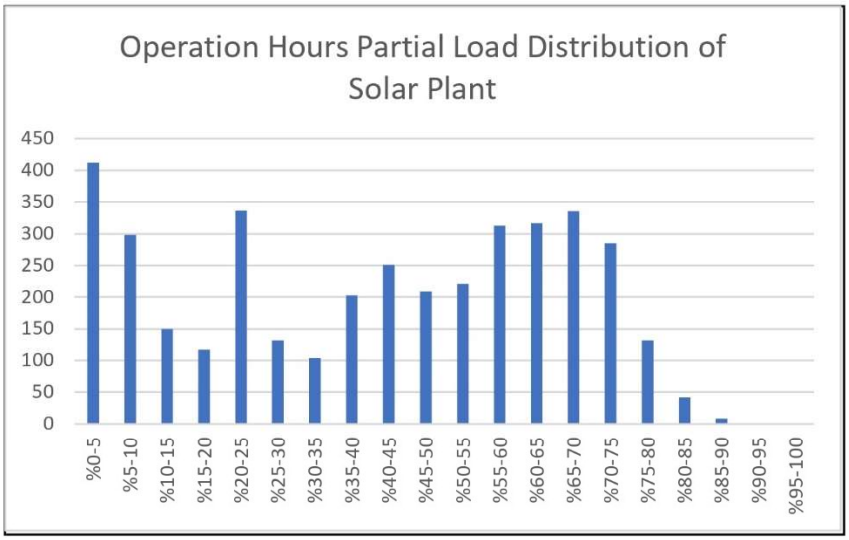

Simulation Results at Maximum Power

Max Solar DC Power	87725 kW	
Stack Consumption	84216 kW	
BoP Consumption	4242 kW	
H2O Consumption	5.303115 kg/s	
H2 Net Production	0.426431 kg/s	
H2 Loss	0.002306 kg/s	%0.6 Permiation + %3 Dryer
Stack Efficiency	54.86 kWh/kg	
Mechanical Loss	0.39 kWh/kg	
Electrical Loss	2.36 kWh/kg	
Stack + BoP Efficiency	57.62 kWh/kg	

Appendix 5. continued

Simulation Result

Location	Turkey-Sanliurfa	
System Design	100MW-1.1	
Plant Capacity	100000 kW	
Hours of Operation	4274 hrs	
Capacity Factor	19.8%	
Annual Solar DC Power Production	173558959 kWh	
Annual Stack Consumption	165901417 kWh	
Mechanical Consumption	1950277 kWh	
Electrical Consumption	8623467 kWh	
Annual BoP Consumption	10573744 kWh	
Annual H2O Consumption	40347079 kg	
Annual H2 Net Production	3230353 kg	
Annual H2 Loss	131903 kg	Permiation + %3 Dryer
Stack Average Efficiency	49.82 kWh/kg	
Mechanical Loss Average	0.60 kWh/kg	
Electrical Loss Average	2.67 kWh/kg	
Stack + BoP Average Efficiency	54.63 kWh/kg	

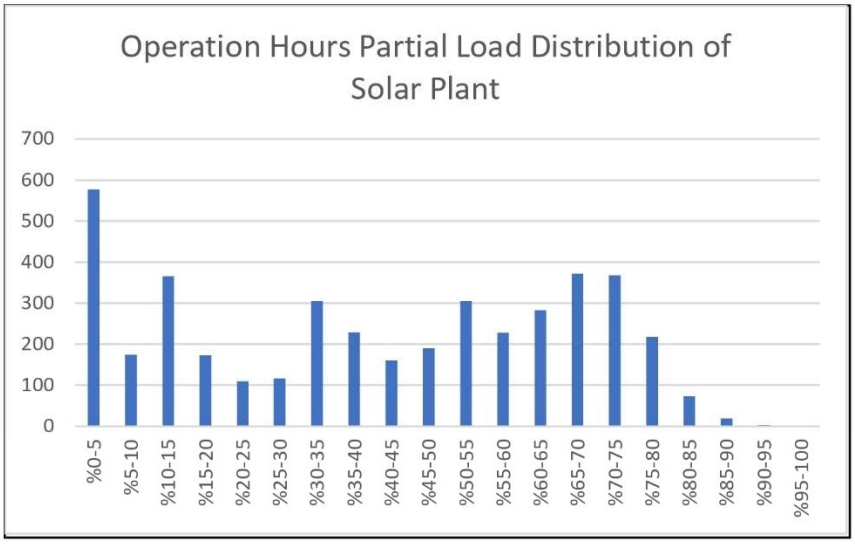

Simulation Results at Maximum Power

Max Solar DC Power	95158 kW	
Stack Consumption	91351 kW	
BoP Consumption	4501 kW	
H2O Consumption	5.673552 kg/s	
H2 Net Production	0.456375 kg/s	
H2 Loss	0.002306 kg/s	%0.6 Permiation + %3 Dryer
Stack Efficiency	55.60 kWh/kg	
Mechanical Loss	0.34 kWh/kg	
Electrical Loss	2.39 kWh/kg	
Stack + BoP Efficiency	58.34 kWh/kg	

Appendix 5. continued

Directive requirements

For medium power transformers

a) Liquid immersed

Maximum load and no-load losses (in W) for three-phase, liquid immersed, medium power transformers with one Um ≤24kV winding and another of Um ≤1.1kV.

	Tier 1 (July 1, 2015)		Tier 2 (July 1, 2021)	
Rated Power (kVA)	Maximum load losses Pk (W) *	Maximum noload losses Po (W)*	Maximum load losses Pk (W)*	Maximum noload losses Po (W)*
≤25	C_k (900)	A_o (70)	A_k (600)	A_o-10% (63)
50	C_k (1100)	A_o (90)	A_k (750)	A_o-10% (81)
100	C_k (1750)	A_o (145)	A_k (1250)	A_o-10% (130)
160	C_k (2350)	A_o (210)	A_k (1750)	A_o-10% (189)
250	C_k (3250)	A_o (300)	A_k (2350)	A_o-10% (270)
315	C_k (3900)	A_o (360)	A_k (2800)	A_o-10% (324)
400	C_k (4600)	A_o (430)	A_k (3250)	A_o-10% (387)
500	C_k (5500)	A_o (510)	Ak (3900)	A_o-10% (459)
630	C_k (6500)	A_o (600)	A_k (4600)	A_o-10% (540)
800	C_k (8400)	A_o (650)	A_k (6000)	A_o-10% (585)
1000	C_k (10500)	A_o (770)	A_k (7600)	A_o-10% (693)
1250	B_k (11000)	A_o (950)	A_k (9500)	A_o-10% (855)
1600	B_k(14000)	A_o (1200)	A_k (12000)	A_o-10% (1080)
2000	B_k (18000)	A_o (1450)	A_k (15000)	A_o-10% (1305)
2500	B_k (22000)	A_o (1750)	A_k (18500)	A_o-10% (1575)
3150	B_k (27500)	A_o (2200)	A_k (23000)	A_o-10% (1980)

b) Pole-mounted – 25 to 400 kVA

	Tier 1 (July 1, 2015)		Tier 2 (July 1, 2021)	
Rated Power (kVA)	Maximum load losses (in W)*	Maximum no-load losses (in W)*	Maximum load losses (in W)*	Maximum no-load losses (in W)*
25	C_k (900)	A_o (70)	B_k (725)	A_o (70)
50	C_k (1100)	A_o (90)	B_k (875)	A_o (90)
100	C_k (1750)	A_o (145)	B_k (1475)	A_o (145)
160	C_k+32% (3102)	C_o (300)	C_k+32% (3102)	C_o-10% (270)
200	C_k (2750)	C_o (356)	B_k (2333)	B_o (310)
250	C_k (3250)	C_o (425)	B_k (2750)	B_o (360)
315	C_k (3900)	C_o (520)	B_k (3250)	B_o (440)

c) Dry type

	Tier 1 (July 1, 2015)		Tier 2 (July 1, 2021)	
Rated Power (kVA)	Maximum load losses Pk (W)*	Maximum no-load losses Po (W)*	Maximum load losses Pk (W)*	Maximum no-load losses Po (W)*
≤50	B_k (1700)	A_o (200)	A_k (1500)	A_o-10% (180)
100	B_k (2050)	A_o (280)	A_k (1800)	A_o-10% (252)
160	B_k (2900)	A_o (400)	A_k (2600)	A_o-10% (360)
250	B_k (3800)	A_o (520)	A_k (3400)	A_o-10% (468)
400	B_k (5500)	A_o (750)	A_k (4500)	A_o-10% (675)
630	B_k (7600)	A_o (1100)	A_k (7100)	A_o-10% (990)
800	A_k (8000)	A_o (1300)	A_k (8000)	A_o-10% (1170)
1000	A_k (9000)	A_o (1550)	A_k (9000)	A_o-10% (1395)
1250	A_k (11000)	A_o (1800)	A_k (11000)	A_o-10% (1620)
1600	A_k (13000)	A_o (2200)	A_k (13000)	A_o-10% (1980)
2000	A_k (16000)	A_o (2600)	A_k (16000)	A_o-10% (2340)
2500	A_k (19000)	A_o (3100)	A_k (19000)	A_o-10% (2790)
3150	A_k (22000)	A_o (3800)	A_k (22000)	A_o-10% (3420)

d) Correction factors to be applied to the load and no-load losses indicated in Tables 1 to 3 for medium power transformers with special combinations of winding voltages (for rated power ≤ 3150 kVA)

Maximum permissible losses to be increased by factors as indicated tables below, based on individual product type.

Special combination of voltages in one winding		Load losses (Pk)	No load losses (Po)
For both liquid immersed (Table a) and dry type (Table c)		No correction	No correction
Primary highest voltage for equipment Um ≤ 24kV	Secondary highest voltage for equipment Um > 3,6kV		
For liquid immersed (Table a)		10%	15%
Primary highest voltage for equipment Um = 36kV	Secondary highest voltage for equipment Um ≤ 3,6kV		
Primary highest voltage for equipment Um = 36kV	Secondary highest voltage for equipment Um > 3,6kV	10%	15%
For dry type (Table c)		10%	15%
Primary highest voltage for equipment Um = 36kV	Secondary highest voltage for equipment Um ≤ 3,6kV		
Primary highest voltage for equipment Um = 36kV	Secondary highest voltage for equipment Um > 3,6kV	15%	20%

Appendix 6. AC-AC Transformer Data (EATON, 2021)

• Yağla Doldurulmuş Genleşme Depolu ve Hermetik Standard Meksan Dağıtım TransformatörleriTeknik Değerleri

Güç	Üst Gerilim	Boştaki Akım I_0	Bakır Kayıpları	Demir Kayıpları	Kısadevre Gerilimi	Cosϕ= 0,8		Cosϕ= 1	
						Tam Yük. Ger. Düş.	Tam Yükte Verim	Tam Yük. Ger. Düş.	Tam Yükte Verim
kVA	kV	%	W	W	%Uk	%	%	%	%
25	6,3-11 20 33	2,50 2,50 3,15	700 700 800	115 115 160	4 4 4,5	3,956 3,956 4.460	96,08 96,08 95,41	2,841 2,841 3,250	96,84 96,84 96,30
40	6,3-11 20 33	2,40 2,40 2,92	940 940 1070	160 160 200	4 4 4,5	3,829 3,829 4,319	96,67 96,67 96,18	2,402 2,402 2,740	97,32 97,32 96,92
50	6,3-11 20 33	2,30 2,30 2,76	1100 1110 1250	190 190 230	4 4 4,5	3,774 3,774 4,259	96,87 96,87 96,43	2,256 2,256 2,570	97,48 97,48 97,12
63	6,3-11 20 33	2,25 2,25 2,62	1270 1270 1430	225 225 270	4 4 4,5	3,698 3,698 4,162	97,11 97,11 96,73	2,076 2,076 2,345	97,68 97,68 97,37
80	6,3-11 20 33	2,20 2,20 2,50	1490 1490 1670	270 270 320	4 4 4,5	3,629 3,629 4.081	97,32 97,32 96,98	1,925 1,925 2,167	97,84 97,84 97,57
100	6,3-11 20 33	2,10 2,10 2,27	1750 1750 1950	320 320 380	4 4 4,5	3,575 3,575 4.015	97,47 97,47 97,16	1,815 1,815 2.035	97,97 97,97 97,72
125	6,3-11 20 33	2,00 2,00 2,14	2000 2000 2200	380 380 440	4 4 4,5	3,499 3,499 3,918	97,67 97,67 97,42	1,667 1,667 1,846	98,13 98,13 97,93
160	6,3-11 20 33	1,90 1,90 2,00	2350 2350 2550	460 460 520	4 4 4,5	3,429 3,429 3,629	97,85 97,85 97,65	1,538 1,538 1,682	98,27 98,27 98,11
200	6,3-11 20 33	1,90 1,90 1,90	2750 2750 2950	545 545 635	4 4 4,5	3,378 3378 3,768	97,98 97,98 97,79	1,446 1,446 1,575	98,37 98,37 98,22
250	6,3-11 20 33	1,60 1,60 1,80	3250 3250 3500	650 650 780	4 4 4,5	3,335 3,335 3,719	98,08 98,08 97,90	1,372 1,372 1,491	98,46 98,46 98,31

Güç	Üst Gerilim	Boştaki Akım I_0	Bakır Kayıpları	Demir Kayıpları	Kısadevre Gerilimi	Cosϕ= 0,8		Cosϕ= 1	
						Tam Yük. Ger. Düş.	Tam Yükte Verim	Tam Yük. Ger. Düş.	Tam Yükte Verim
kVA	kV	%	W	W	%Uk	%	%	%	%
315	6,3-11 20 33	1,50 1,50 1,70	3835 3835 4110	770 770 930	4 4 4,5	3,287 3,287 3,663	98,20 98,20 98,03	1,290 1,290 1,397	98,55 98,55 98,42
400	6,3-11 20 33	1,50 1,50 1,70	4600 4600 4900	930 930 1120	4 4 4,5	3,247 3,247 3,615	98,30 98,30 98,15	1,223 1,223 1,319	98,63 98,63 98,51
500	6,3-11 20 33	1,40 1,40 1,60	5425 5425 5700	1090 1090 1300	4 4 4,5	3,208 3,208 3,558	98,39 98,39 98,29	1,159 1,159 1,227	98,71 98,71 98,63
630	6,3-11 20 33	1,40 1,40 1,60	6500 6500 6650	1300 1300 1450	4 4 4,5	3,175 3,175 3,510	98,47 98,47 98,41	1,106 1,106 1,151	98,77 98,77 98,73
800	6,3-11 20 33	1,30 1,30 1,50	8500 8500 8700	1500 1500 1750	6 6 6	4,132 4,132 4,147	98,50 98,50 98,44	1,173 1,173 1,196	98,80 98,80 98,75
1000	6,3-11 20 33	1,20 1,20 1,40	10500 10500 10500	1700 1700 2000	6 6 6	4,468 4,468 4,468	98,49 98,49 98,46	1,224 1,224 1,224	98,79 98,79 98,76
1250	6,3-11 20 33	1,20 1,20 1,40	13000 13000 13000	2100 2100 2250	6 6 6	4,462 4,462 4,462	98,51 98,51 98,49	1,215 1,215 1,215	98,80 98,80 98,79
1600	6,3-11 20 33	1,10 1,10 1,30	17000 17000 17000	2600 2600 2800	6 6 6	4,477 4,477 4,477	98,49 98,49 98,47	1,237 1,237 1,237	98,78 98,78 98,77
2000	6,3-11 20 33	1,10 1,10 1,20	21000 21000 21000	3200 3200 3200	6 6 6	4,468 4,468 4,468	98,51 98,51 98,51	1,224 1,224 1,224	98,80 98,80 98,80
2500	6,3-11 20 33	1,0 1,0 1,1	24000 24000 24000	3800 3800 3800	6 6 6	4,408 4,408 4,408	98,62 98,62 98,62	1,135 1,135 1,135	98,90 98,90 98,90

Bağlantı Grubu : 25 - 200 kVA = Yzn 5-11 - Dyn 5-11 250-2500 kVA = Dyn 5-11

• Çeşitli Güçlerdeki Transformatörlerin AG Sigorta Ana Kablo ve Ölçü Karateristikleri

• Different Rated Power Transformers Fuse, Cable, And Current Table

ANMA AKIMLARI RATED CURRENT				YG SİGORTA HV FUSE			AG BARA LV BARS	AG ANA KABLO LV MAIN CABLE			TERMİK MANYETİK OTOMATİK ŞALTER T.M. AUTOMATIC SWICH		Akım Trf. Current Transformer	Ana Sayaç Main Counter	Amper Metre Ampere Meter
0.4 kV	10.5 kV	15 kV	30 kV	10.5 kV A	15 kV A	30 kV A	mm²	Toprak Altına Döşenirse Under Ground mm²	Direk Üzerine Döşenirse On the Pillar mm²	Kablo Cinsi Cable Type	Nominal Akım Current Raiting A	Termik Bobin T.M Winding A			
58	2.2	1.5	0.8	6	6	6	20x3	4x16	4x16	NYY	3x63	50-63	-	3x100	3x100
91	3.46	2.43	1.2	10	6	6	20x3	4x25	4x25	NYY	3x100	80-100	-	3x100	3x100
115	4.4	3.08	1.6	16	6	6	20x3	3x25+16	3x25+16	NYY	3x125	100-125	3x150/5	x/5	3x150/5
144	5.5	3.85	1.9	16	10	6	40x3	3x35+16	3x50+25	NYY	3x160	125-160	3x200/5	x/5	3x200/5
180	6.87	4.81	2.3	20	16	6	40x3	3x50+25	3x70+35	NYY	3x200	160-200	3x250/5	x/5	3x250/5
231	8.8	6.16	3.1	25	16	10	40x3	2(3x50/25) 3x70+35	3x95+50	NYY	3x250	200-250	3x250/5	x/5	3x250/5
289	11	7.7	3.8	25	16	10	40x3	3x120+70	3x150+70	NYY	3x300	250-300	3x400/5	x/5	3x400/5
361	13.75	9.63	4.8	30	20	10	40x3	3x150/70	2(3x70+35)	NYY	3x400	300-400	3x400/5	x/5	3x400/5
455	17.32	12.13	6.07	40	25	16	40x3	3x185/95	2(2x95+50)	NYY	3x500	400-500	3x600/5	x/5	3x600/5
578	22	15.41	7.7	40	30	16	40x5	3x240/120	2(3x150+70)	NYY	3x600	480-600	3x800/5	x/5	3x800/5
723	27.5	19.26	9.63	63	50	20	40x10	Bakır Bara Copper Bars 40x10	Alüminyum Bara Aluminium Bars 50x10		3x800	700-800	3x800/5	x/5	3x800/5
910	34.6	24.3	12.15	63	50	30	50x10	50x10	60x10		3x1000	800-1000	3x1000/5	x/5	3x1000/5
1156	44	30.82	15.4	80	63	30	60x10	60x10	80x10		3x1200	1000-1400	3x1200/5	x/5	3x1200/5
1445	55	38.53	19.2	100	80	40	80x10	80x10	100x10		3x1600	1400-1600	3x1600/5	x/5	3x1600/5
1804	68.73	48.15	24.08	125	100	50	100x10	100x10	2(80x10)		3x2000	1600-2150	3x2000/5	x/5	3x2000/5
2312	88	61.6	30.8	160	160	160	2x80x10	2x80x10	2(100x10)		3x2500	2150-2500	3x2500/5	x/5	3x2500/5

Appendix 6. continued (MEKSAN, 2023)

Unit Specifications			
Model	YKK9K2H95EWG	Gear Code	RP
Rated Net Capacity (kW)	3200	Specified Net Capacity (kW)	3200
NPLV.IP (COP.R)	8.852	Refrigerant Type/Charge (kg)	R-134a/886
Full Load (COP.R)	5.021	A-Weighted SPL (dBA)	84
Input Power (kW)	637.4	Max Motor Load (kW)	655.0
Voltage / Hz (Input)	400 / 50.0	Oil Cooler	Refrig clr
		Condenser Gas Inlet Type	Baffle
Job FLA (Amps)	1000	OptiSound Control	Y
		Isolation Valve	Y
LRA (Amps)	7487	Variable Orifice	VALVE:3
Min Circuit Ampacity	1250	Starter Type	VSD w/o Filter
Max Circuit Breaker Amps	2000	Starter Model	VSD914K-43
Heat Rejection Capacity (kW)	3796		

	Evaporator	Condenser
Fluid	Water*	Water*
Tube MTI No.	656	266 / 471
Passes	2*	2*
Fouling Factor ((m²-°C)/kW)	0.01761*	0.04403*
Entering Fluid Temp (°C)	12.00*	33.00*
Leaving Fluid Temp (°C)	6.00*	39.00*
Fluid Flow (L/s)	127.1	152.3
Fluid Pressure Drop (kPa H2O)	45.5	75.6

(*) Designates User Specified Input

Partload Data (Minimum Condenser Water Temperature)										
CEFT (°C)	% LOAD									
	100%	90%	80%	70%	60%	50%	40%	30%	20%	15%
33.00°	5.021	5.169	5.250	5.311	5.229	5.145	4.959	4.660	4.107	3.686
30.00°	5.582	5.796	5.869	5.927	5.919	5.881	5.729	5.352	4.706	4.223
27.00°	6.227	6.442	6.686	6.711	6.771	6.633	6.516	6.120	5.388	4.820
24.00°	6.957	7.271	7.531	7.689	7.738	7.732	7.473	7.124	6.272	5.591
21.00°	7.717	8.195	8.582	8.888	9.033	8.977	8.815	8.351	7.334	6.507
18.00°	8.654	9.274	9.812	10.26	10.63	10.69	10.45	9.736	8.675	7.641
17.50°	8.819	9.468	10.03	10.51	10.93	11.02	10.78	10.06	8.926	7.874
17.00°	8.987	9.665	10.25	10.78	11.25	11.36	11.13	10.39	9.213	8.107
16.50°	9.160	9.864	10.47	11.05	11.58	11.72	11.49	10.74	9.034	8.326
16.00°	9.337	10.06	10.70	11.34	11.92	12.09	11.93	11.07	9.312	8.531
15.50°	9.511	10.26	10.94	11.64	12.28	12.48	12.33	11.40	9.587	8.724
15.00°	9.687	10.46	11.18	11.96	12.65	12.89	12.70	11.71	9.850	8.905
14.50°	9.864	10.66	11.42	12.27	13.03	13.32	13.05	12.02	10.11	9.074
14.00°	10.04	10.86	11.68	12.60	13.38	13.68	13.40	12.32	10.35	8.849
13.50°	10.23	11.06	11.95	12.93	13.80	14.08	13.73	12.62	10.60	9.055
13.00°	10.41	11.27	12.23	13.29	14.24	14.44	14.06	12.91	10.84	9.258
12.50°	10.60	11.47	12.53	13.65	14.71	14.80	14.38	13.19	11.07	9.456
12.00°	10.79	11.67	12.83	14.01	14.89	15.14	14.69	13.46	11.30	9.652
11.50°	10.98	11.89	13.15	14.40	15.35	15.47	14.99	13.73	11.53	9.846
11.00°	11.18	12.12	13.47	14.81	15.73	15.79	15.28	14.00	11.76	10.04
*Values are in COP.R										
	Rated point is 60% or higher efficiency compared to design operation point.									
	Rated point is 70% or higher efficiency compared to design operation point.									
	Rated point is 80% or higher efficiency compared to design operation point.									

Appendix 7. Sample Commercial Water-Cooled Centrifugal Chiller Product Selection